Design and synthesis of ultra-bright organic nanoparticles (ONPs) for bioimaging

Paolo Pagano

université de BORDEAUX

THÈSE PRÉSENTÉE

POUR OBTENIR LE GRADE DE

DOCTEUR DE

L'UNIVERSITÉ DE BORDEAUX

ÉCOLE DOCTORALE DES SCIENCES CHIMIQUES

SPÉCIALITÉ: CHIMIE ORGANIQUE

Par Paolo PAGANO

Design and Synthesis of Ultra-Bright Organic Nanoparticles (ONPs) for Bioimaging

Sous la direction de: Mireille BLANCHARD-DESCE

Soutenue le 06/07/2017

Membres du jury:

Mme. FERY-FORGUES, Suzanne	Directeur de Recherce, CNRS	Rapporteur
M. GIERSCHNER, Johannes	Research Professor, IMDEA Madrid	Rapporteur
Mme. TERENZIANI, Francesca	Professeur des Université, Univ. Parma	Examinateur
M. LEMERCIER, Gilles	Professeur des Université, Univ. Reims	Examinateur
Mme. BLANCHARD-DESCE, Mireille	Directeur de Recherche, CNRS	Directrice de Thèse
M. VERLHAC, Jean-Baptiste	Professeur des Université, Univ. Bordeaux	Examinateur (President)

Elaboration et caractérisation de nanoparticules ultra-brillantes, fonctionnalisées et biocompatibles, pour applications en biologie et en médicine

L'utilisation de nano-objets luminescents en milieu biologique est devenue très répandue, notamment en vue d'applications biomédical est elles que l'imagerie, la thérapie et le diagnostic. Jusqu'à récemment, les principaux travaux réalisés dans ce domaine concernaient les nanoparticules de silice dopées ou fonctionnalisées avec des molécules organiques, les nanoparticules d'or et les nanoparticules semi-conductrices (quantum dots, i.e., QDs). Toutefois, un certain nombre de limitations demeurent pour les applications dans le domaine du vivant, en lien notamment avec des problèmes de stabilité, de biocompatibilité et de toxicité ou encore de biodégradabilité. En parallèle, un certain nombre de molécules organiques fluorescentes non-toxiques ont été utilisées comme sondes fluorescentes en milieu biologique, mais leur brillance demeure limitée. L'idée directrice de la thèse est de concevoir et synthétiser de nouveaux chromophores organiques présentant une émission modulable (du visible au proche infrarouge) et adaptés à la préparation de nanoparticules organiques fluorescentes (FONs) combinant à la fois une brillance extrêmement élevée, une excellente stabilité colloïdale et une photostabilité adaptée à leur utilisation en imagerie in vitro et in vivo. De tels nano-objets ultra-brillants pourraient alors représenter une alternative très intéressante aux nanoparticules actuellement les plus utilisées en imagerie de fluorescence du vivant (QDs). Le manuscrit décrit la synthèse et les propriétés de plusieurs classes de molécules fluorescentes spécifiquement conçues pour former des telles FONS par auto-assemblage dans l'eau. La préparation de ces FONs est présentée et leurs propriétés étudiées et discutées. Enfin des applications concrètes en bio-imagerie sont présentées.

Mots clés: Absorption à deux photons, fluorophores, nanoparticules organiques, imagerie biologique

Design and Synthesis of ultra-bright Organic Nanoparticles (ONPs) for bioimaging

Nowadays the use of bright luminescent nano-objects in biological environment is a topic that is gaining more and more importance, especially for biomedical applications such as imaging, therapy and diagnostic. So far, numerous studies have been conducted with gold nanoparticles, silica nanoparticles (doped or functionalized with organic molecules), as well as semiconductor nanoparticles (quantum dots, i.e., QDs). However, most of these nanoparticles suffer from drawbacks (in terms of stability, biocompatibility, eco-toxicity or degradability). On the other hand, several non-toxic fluorescent molecular probes have been widely used, but most of the time their brightness remain modest in biological environments compared to QDs. Our idea is to engineer new organic chromophores with tunable emission wavelength (from visible to near infrared) for further preparation of organic fluorescent nanoparticles (so called FONs) that display giant one-photon and two-photon brightness, as well as good colloidal and chemical stability, and suitable photostability for *in vitro* and *in vivo* imaging. As such, these FONs would represent interesting alternatives to QDs for use in bioimaging. This manuscript describes the synthesis and characterization of new classes of fluorescent molecules specifically engineered as building blocks for the fast preparation of such nanoparticles by self-aggregation in water. The FONs were fully characterized from both morphological and photophysical points of view and further used in bioimaging.

Keywords: Two-photon absorption, fluorophores, organic nanoparticles, bioimaging

UMR 5255

[ISM, équipe IPM, 351 Cours de la Libération, 33405 Talence, France]

Look wide, and even when you think you are looking wide, look wider still

(Sir Robert Baden-Powell)

AKNOWLEDGEMENTS

Here we are, also this overwhelming adventure is going to finish and with these few words I would like to thank all the people who have been sharing with me their time, their knowledge, their smiles…

First of all I would like to thank my supervisor Dr. Mireille Blanchard-Desce, thank you for giving me the chance to join your group during my Ph.D. internship, thanks for believing in me and giving me the opportunity to work autonomously and to learn many things in a great scientific environment. Thank you also for our productive discussions about science but not only.

I would thank all the jury members: Dr. Suzanne Fery-Forgues and Dr. Johannes Gierschner who accept to be referees and evaluate my manuscript; Prof. Francesca Terenziani, Prof. Gilles Lemercier and Prof. Jean-Baptiste Verlhac to evaluate my work.

A special acknowledgement is going to Nano2Fun (European Union's Seventh Framework Programme FP7/2007-2013/ under REA grant agreement n°607721) that gave me the opportunity to do this challenging experience. Thanks to the Nano2Funners, friendly people and bright scientists with whom I shared the project, travelling from the resort in Slupsk to the student's house in Bangalore (Antonio, Davide, Slava, Sergio, Laura, Cristiano, Valentina, Luca, Silvia, Antonio, Domna, Somananda, Siarhei, Dmitrii, Dzmitryi, Natascia and Maria). Within the network I would like to thank Dr. Rainer Kling, Prof. Wim Wenseleers and Prof. Francesca Terenziani for the fruitful discussions during my secondments. I would like to thank also Prof. Vincent Rodriguez, Flavie Bondu and Frederic Adamiez from GSM group for their help in HRS measurements, Prof. Jean-Christophe Baret and Laura Chacon from CRPP for the microfluidic experiments.

Of course I am extremely grateful to all the members of the IPM (was PHOENICS) group starting from Dr. Michel Vaultier and Prof. Jean-Baptiste Verlhac for the interesting discussions about

food and wine during the “social Friday” events, thanks Michel for the deer (it was tasteful!) and thanks Jean-Baptiste for the wine and the beer after-work. Thank you Guill for helping me since the beginning with laser stuff and many other things. Thanks to all the students, past and present, that passed through here: Talia, Ludo, Imanol, Adina, Judith, Danilo, Marine, Simon, Jessica, Victor, Petra, Jean-Baptiste, Melodie, Bastien and Jeanne. Thank you Catherine for being my mentor during my first year of experiments I wish you a successful future, thank you Séb for the music experience that I had here, good luck for your future building up your family with Fanny and the new baby, thank you Edü contributing with me and our “stupidity” to play and make funny even the most boring column give hugs to Chloe and Charlotte, thank you Nino for our Saturdays morning at the “Marché du Capucins” with our breakfast “Chez Jean-Mi” even if you are always late, thank you Max (MaximusMaximusMaximus…) for the good times spent together please remember to do not explode also because Max will NEVER DYE!

Thank you Cristiano, you are a fantastic travel companion, we started this adventure together and we will finish it together too. It was nice to share with you all the “missions”, having sumptuous meals all around the world. I wish you a great future with your family (don’t worry, you’ll find your permanent position!!). A special mention is for Jonathan “GrandeJ”. Well, what can I say: thank you for everything! It was great to spend my time with you, thanks for the scientific advices, thanks for our discussions about science and food indiscriminately, thanks for the help during my moving (and for the Ikea shopping…). I wish you an adventurous future with little Selene and Miriam, and the new baby that is arriving soon, enjoy always.

What would life be without friends? I would like to send a big hug to all the people that, despite the distance, were close to me: Veronica, Corrado, Fajo, Marta, Margherita, Dano, Bigi, Cami, Cami, Luisa my CFM staff (even though you didn’t come!!). Thank you Sergio, our “zii frusti” series should continue all around the World! A special thank to Fosca and Lollo to be always available since

ten years (almost), thanks for your advices and the great times spent together, you are very precious to me.

Together with the “old friends”, here in Bordeaux I found a wonderful group with whom I’m spending good times. Thanks to the “yoga-couple” Giulia and Igor, it is great to eat and drink together experimenting new flavors and testing new gastronomic combinations, I wish you a great future chasing your dreams. I am very grateful to Laura, a fantastic person, I will miss our beers at the beginning of the afternoon discussing about Life, the Universe and Everything. I wish you an adventurous future!

I would not be who I am without the roots, I would like to thank my parents because they are a constant in my life, I am here also because they transmitted me the passion to look forward. Thank you Carlo and Edoardo (Grill and Dudu) new great experiences are waiting for us.

Finally thank you Laura, thanks to support me, thanks to be always by my side, walking together since 7 years. Thank you for your patience, these three years (and half) were long but together we were able to arrive to the end we are ready to start a new future.

This manuscript is dedicated to you my Darling.

TABLE OF CONTENT

CHAPTER 1

INTRODUCTION

CHAPTER 1–INTRODUCTION

1. Basic principles of linear photophysical measurements[1,2]

Chromophore[3]: "Part of a molecular entity in which an electronic transition responsible for a given spectral band is approximately localized".

Luminophore[3]: "Part of a molecular entity in which electronic excitation associated with a given emission band is approximately localized".

In **Illustration I 1** is displayed the Perrin-Jablonski diagram that summarizes the main possible processes that occurs upon the interaction of a molecule with light: absorption, internal conversion, fluorescence emission, inter system crossing and phosphorescence emission.

Since in my manuscript I will discuss about molecules that are able to absorb and emit light, the goal of this first paragraph is to recall the basis of linear optical measurements used during my PhD internship.

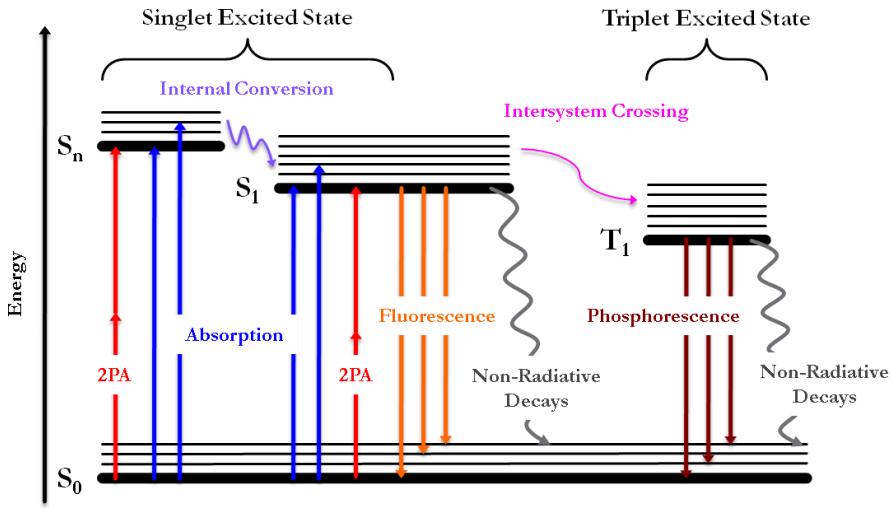

Illustration I 1. Perrin-Jablonski diagram

1.1. Absorption of ultraviolet and visible light

The absorption of one photon by a molecule induces an electronic transition from a lower electronic state (typically the ground state) to higher electronic states called excited states. Depending on the molecular structure, the absorption can promote electrons from σ, π and nonbonding (n) orbitals to an antibonding orbital (denoted as σ^* and π^*) with different energies. Here I will focus my attention on $n\rightarrow\pi^*$and $\pi\rightarrow\pi^*$transitions, since are those that I observed in measurements; I will not take into account in my manuscript the transitions that involve σ and σ^* orbitals because not interesting in terms of photophysical properties and, in addition, are located usually in the far UV. Concerning this manuscript the highest observed transition is the $n\rightarrow\pi^*$ where, upon excitation, an electron is promoted from an atom (here nitrogen) with nonbonding electrons to an antibonding π orbital. In my case the nitrogen is located in the "electron-releasing" moiety and the promoted electron goes into the lower energetic π^* orbital, expected to be located in the electron-withdrawing group (using the acceptor strength as driving force). The $n\rightarrow\pi^*$ transition is also important because it has a charge transfer character, necessary for both linear and non-linear optical applications.

One should consider that not all the transitions are allowed, indeed in absorption we have to take into account two main conditions:

- The transitions between states with different multiplicity are forbidden, while are allowed singlet→singlet and triplet→triplet transitions. Nevertheless, *via* spin-orbit coupling there is a weak interaction between the wavefunctions of the singlet and the triplet state, and sometimes, this transition can be observed i.e. the intersystem crossing from the first singlet-excited state to the first triplet excited state.
- Some transition can be forbidden for symmetrical reasons, for example in centrosymmetric molecules the one-photon absorption has to reach an antisymmetric state with respect to the ground state, while concerning non-centrosymmetric molecules the direct product of the irreducible representation of the ground state and

of the excited state must transform as the irreducible representation of the dipole moment operator.

Taking into account that the mass of the nuclei is bigger compared with the mass of the electrons one could consider that the electronic transition occurs without changes of the nuclei position because the transition is faster compared with the nuclear motion, this is called: Frank-Condon principle, thus one can consider that the electronic transition will occur vertically. Moreover, in addition to the pure electronic transition, one can observe also the vibrational structure that depends on the vibrational levels of the excited state. Because the electronic is a vertical transition, depending on the nuclear configuration during the excitation process, the most probable transition could be between two different vibrational states, as displayed in **Illustration I 2a** where the most probable transition occurs between the vibrational state 0 of the ground state and the vibrational state 2 of the excited state.

Most of the time, for molecules, the vibrational structure in not observable especially when the measurements are done in particular environment such as solution or colloidal suspension. In these cases, the bandwidth depends on two effects: homogeneous and inhomogeneous broadening. The first is mostly due to the finite lifetime associated to the excited state and the existence of a continuous set of vibrational sublevels in each electronic state, while the second is due to the fluctuation of the structure of the solvation shell surrounding the chromophore.

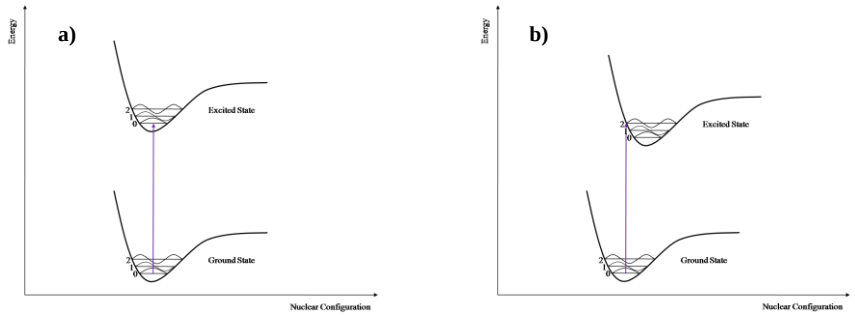

Illustration I 2. Potential energy diagram with vertical transition (Franck-Condon principle)

Another important feature to take into account when one speaks about absorption transition is the probability of the light absorption at a specific wavelength λ, in other words the probability that the transition occurs with a specific energy, given by the molar extinction coefficient ε(λ). This value is dependent from the electronic transition and the solvent in which is calculated from UV-visible absorption measurement using the Lambert-Beer law (**Eq. I 1**).

Eq I 1. $$A(\lambda) = \varepsilon(\lambda) \cdot l \cdot c$$

where the absorbance A(λ) measured at a specific wavelength is linearly dependent with the optical path of the light within the sample (l), with the concentration (c) and with the molar extinction coefficient (ε(λ)).

1.2. Emission of light upon one-photon excitation

Once a chromophore is excited, there are two main pathways that it can follow to return back to the ground state: radiative and non-radiative path. Between the two relaxation methods, the most interesting in terms of photophysical properties, for our purpose, is the radiative one since it involves the emission of photons. Depending on the spin multiplicity in the transition, one can call the phenomena fluorescence or phosphorescence.

As displayed in Perrin-Jablonski diagram in **Illustration I 1**, upon one-photon excitation the molecule can reach higher excited states (S_n) compared with the first excited state (S_1); but, except few cases[4], the emission of photons occurs from the lower excited state (called Kasha's Rule[5]). The relaxation from S_n to S_1 is a non-radiative process between electronic states with the same spin multiplicity called internal conversion. Thanks to the higher energy gap between S_1 and S_0 the internal conversion process is much less efficient, but indeed it can compete with the radiative decay.

Fluorescence emission band lies generally at lower energies compared with the relative absorption band, empirically observed by G.G. Stokes[6], thanks to energy losses between the excitation

and the emission combined with the Kasha's rule. There are many causes that can induces these phenomena such as fast decay to the lower vibrational level of the lower excited state, decay to higher vibrational levels of the ground state and solvent effects. Moreover, the vibrational level of the ground and the excited state are similar thus the fluorescence spectrum usually parallel the lower energetic absorption band, this is the "mirror image" rule, displayed as example in **Figure I 1**.

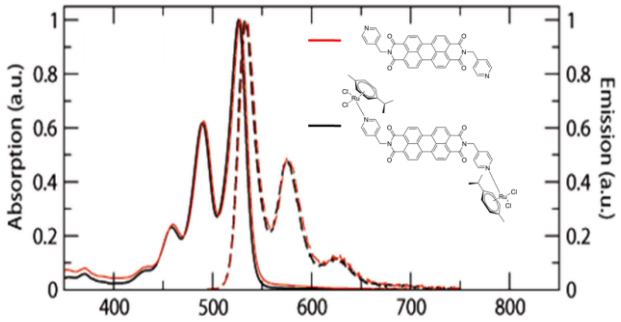

Figure I 1. Mirror image of perylene bis-imide ligand and relative complex[7]

Another possible deactivation of the excited state is displayed in **Illustration I 1** as intersystem crossing (ISC) (pink wavy line, right part of the illustration). Actually, this transition is forbidden since involves the passage between two states of different multiplicity: from the first singlet excited state to the triplet state. As I wrote previously, these forbidden transitions are observable thanks to the spin-orbit coupling and the presence of heavy atoms increases the spin-orbit coupling favoring the intersystem crossing. At room temperature non-radiative relaxation from the triplet state is favored compared with the radiative $T_1 \rightarrow S_0$ transition called phosphorescence. This deactivation pathway is very slow, therefore the collision with solvent, or oxygen, induces preferential vibrational relaxations. However, in some cases it is possible to observe phosphorescence that lies at higher wavelength compared with fluorescence emission. This fact is explained taken into account that the lowest vibrational level of T_1 is placed at lower energies compared with the first singlet excited state. The relaxation pathway that passes through the triplet state competes with the fluorescence, decreasing the efficiency of the radiative $S_1 \rightarrow S_0$ transition.

The ratio between the constant relative to both radiative and non-radiative relaxation is an important data in order to study the lifetime of the excited state and consequently the fluorescence quantum yield. Indicating with k^S_r the radiative decay constant and with k^S_{nr} the sum all non-radiative decays constant (which include the internal conversion as well as the intersystem crossing) of the singlet state, the excited state lifetime can be obtained with:

Eq I 2. $$\tau_s = \frac{1}{k_r^S + k_{nr}^S}$$

An important factor to take into account when one wants to compare the efficiency of different fluorophores is the fluorescence quantum yield (Φ_f), which is defined as the ratio of the number of emitted photons to the number of absorbed photons when the molecule is excited with a specific wavelength (**Eq I 3**).

Eq I 3. $$\Phi_f = \frac{N_{em}(\lambda_{exc})}{N_{abs}(\lambda_{exc})}$$

Eq I 4. $$\Phi_f = \frac{k_r^S}{k_r^S + k_{nr}^S} = \tau \cdot k_r^S$$

Since decay constants are complex to be measured by direct methods, the fluorescence quantum yield can be determined with various approaches including thermal and photoacoustic methods, but those considered in this manuscript are the optical methods. Φ_f can be measured in absolute way with an integrating sphere or relatively to a fluorescence standard[8,9]. Actually all the measurements that were done in this manuscript follow the relative determination of the fluorescence quantum yield using the **Eq I 5**.

Eq I 5. $$\Phi_{fS} = \Phi_{fR} \cdot \frac{n_S^2}{n_R^2} \cdot \frac{F_S}{F_R} \cdot \frac{f_R(\lambda_{exc})}{f_S(\lambda_{exc})}$$

with

Eq I 6. $$F = \int_{\lambda_1}^{\lambda_2} I_c(\lambda_{exc}, \lambda_{em}) \mathrm{d}\lambda_{em}$$

Eq I 7. $f = 1 - 10^{-A(\lambda_{exc})}$

Where the subscript "S" and "R" denote sample and reference respectively, Φ_f is the fluorescence quantum yield, n is the refractive index of the solvent, *F* is the spectrally integrated photon flux at the detector and $f(\lambda_{exc})$ is the absorption factor that provides the fraction of the excitation light absorbed by the chromophore.

To choose the right reference among different class of fluorophores one has to take into account that the fluorescence standard should absorb and emit within similar spectral region of the sample as well as the values of Φ_f of the reference and the sample should not be too different[9]. The well-established standards are three (Quinine Sulfate, Fluorescein and Rhodamine 6G) while there is a large amount of fluorophores used as references, which are less characterized or less reliable[10], unfortunately are still missing reliable fluorescence standard within the red/near infrared spectral region, which is the region that I mainly considered in my work, as well as robust reference with low fluorescence quantum yield.

1.3. Solvent effect on fluorescence emission

In order to understand the behavior of chromophores in complex systems such as nanoparticles, it is worth studying their character by tuning polarity of the local micro/nano-environment that surrounds the molecule.

Depending on their nature, the interaction chromophore-solvent can strongly affect both ground and excited state, stabilizing or destabilizing them. The shift that one can observe in absorption and emission, induced by the tuning of the polarity, is called solvatochromic shift.

A compound displays a solvatochromic behavior if its absorption and/or emission bands depend on the solvent polarity. Increasing the polarity one can observe a bathochromic shift or an hypsochromic shift indicating positive or negative solvatochromism respectively.

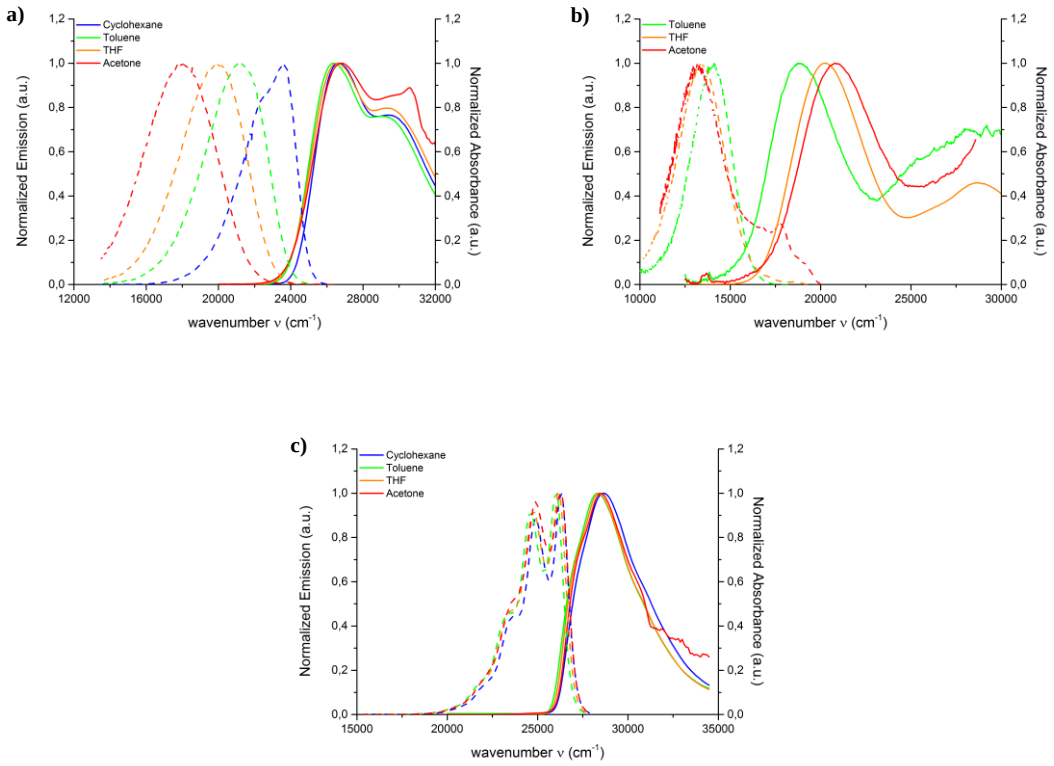

Figure I 2. Solvatochromic behavior of a) neutral dipole, b) charged dipole and c) quadrupole

In Figure I 2 are displayed the absorption and emission spectra measured for three different chromophores in solvent with different polarity. One can see that in **Figure I 2a-b** are displayed solvatochromic molecules with different behavior, while in **Figure I 2c** is displayed a non-solvatochromic chromophore (a more detailed discussion about solvatochromic behavior of different chromophores is given later in the manuscript).

2. Non-linear optical processes[11-14]

Non-linear optics (NLO) is the field of optics that studies the behavior of materials interacting with very high-intensity electric field (in the order of magnitude of 10^8 V/m). Indeed, non-linear optical phenomena were observed experimentally only after the development of lasers[15].

In linear optics the dipolar moment $\mu(t)$ is expressed in terms of permanent dipolar moment μ_0, external field $E(t)$ and the linear electric polarizability α.

Eq I 8. $\vec{\mu}(t) = \vec{\mu}_0 + \alpha\vec{E}(t)$

To generalize the dipolar moment it is necessary to expand the function with a Taylor series:

Eq I 9. $\vec{\mu}(t) = \vec{\mu}_0 + \alpha\vec{E}(t) + \beta\vec{E}\vec{E}(t) + \gamma\vec{E}\vec{E}\vec{E}(t) + \ldots$

with β first-order hyperpolarizability and γ second-order hyperpolarizability.

There are several non-linear phenomena that can be divided in second-order and third-order processes. Second-order processes, such as second-harmonic generation (SHG), sum-frequency generation (SFG) and difference-frequency generation (DFG), are observable in non-centrosymmetric systems and are directly related with β. There are two well-established ways to derive the second-order non-linear response: hyper-Rayleigh scattering (HRS) and electric-field-induced second-harmonic generation (EFISHG). I will not go in the description of these techniques since I did not use them in the work presented in this manuscript.

Among the numerous third-order non-linear processes, I would like to focus the attention on the two-photon absorption (2PA). Two-photon absorption is basically the simultaneous absorption of two photons, with same or different energy, by a single molecule. The phenomenon was theoretically predicted by Maria Göppert-Mayer during her doctoral dissertation[16,17] but the observation was possible only 30 years later with the development of lasers with the observation by Kaiser and Garret of the two-photon excitation of crystals of CaF_2:Eu^{2+} [18].

Even if the topic is gaining more and more interest, reliable absolute techniques to measure the 2PA cross section (σ_2) is still challenging. There are two well-established methods used for these measurements: the Z-scan[19] and the two-photon excited fluorescence (TPEF)[20].

Z-scan method is based on the non-linear transmittance of the sample. The transmittance is measured (in so-called open-aperture condition) as a function of the intensity by scanning the sample through the focal plane of a focused laser beam. σ_2 is determined with the decreasing of the

transmittance in non-resonant conditions. This technique usually needs higher energy compared with TPEF that can cause the observation of other non-linear optical processes as well as strong background signal. Moreover, the Z-scan needs high concentrated solution leading to aggregation phenomena that can affect the accuracy of the measurement. The advantage of this technique is that potentially all molecules can be measured.

TPEF method is based on the measure of the fluorescence emission induced by the simultaneous absorption of two photons. The measurement is done relatively to a 2PA reference[21], giving as a result the so-called two-photon action cross section ($\sigma_2(\omega)\Phi_f$). The value that is directly obtained from the measurement is F/P^2 for each wavelength measured, where F is the fluorescence signal induced by the two-photon excitation and P is the excitation power. This indicates that fluorescence signal must have a quadratic dependence with the power, then, to produce reliable data, this dependence has to be checked for each wavelength in order to prevent excited state absorption and/or saturation of the signal, overestimating the values of the two-photon cross section. When the measurement of the sample and the reference are done as a function of the excitation power, the $\sigma_2\Phi_f$ of the sample is given by the following equation (**Eq I 10**)

$$\text{Eq I 10.} \qquad \sigma_2\Phi_f = \frac{f_R}{f}\cdot\frac{n^2}{n_R^2}\cdot\frac{c_R}{c}\cdot\frac{F}{P^2}\cdot\left(\frac{F}{P^2}\right)_R^{-1}\cdot\left[\frac{n_R}{n}\right]\cdot\left(\sigma_2\Phi_f\right)_R$$

with the subscript R to indicate the reference chromophore, f is the correction factor taking into account the wavelength dispersion of the response function, n is the refractive index, c is the concentration, and the ratio in the squared brackets is the refractive index correction. From **Eq I 10** it is easy to derive the two-photon cross section knowing the fluorescence quantum yield of the sample, thus to obtain reliable values of σ_2, in addition to the check of quadraticity, it is necessary to have reliable value of Φ_f. This technique is limited to the use of fluorescent molecules but the higher sensitivity compared with Z-scan allows the measurement of low emissive chromophores unless the fluorescence quantum yield is measurable.

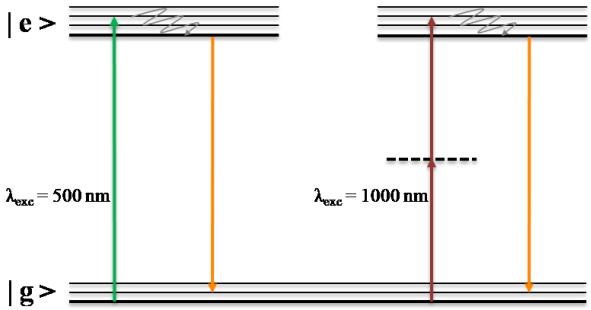

Illustration I 3. Two-photon excited fluorescence (right panel) compared with the one-photon excited fluorescence (left panel)

Since the process is not probable, the laser beam has to be focalized in order to enhance the two-photon absorption transition; therefore, the non-linear process occurs in the focal point. Moreover, in 2PA processes there is a quadratic proportion between the energy that is absorbed from the molecule and the intensity of the incident light, these two characters leads to improve the 3D spatial resolution as displayed in **Figure I 3**.

Figure I 3. Difference between the spatial resolution in one-photon (upper part, λ_{exc} = 405 nm) and two-photon (lower part, λ_{exc} = 1050 nm) process

The spatial resolution in addition with the possibility to use photons with half energy compared with the one-photon process, typically using wavelength that lies in the deep-red near infrared (NIR) spectral region, promote the two-photon absorption as suitable technique for a large variety of application in different fields such as optoelectronics[22,23], microfabrication[24-30], optical data storage[31,32], photodynamic therapy[33-41] and fluorescence microscopy.

3. Bioimaging: one-photon and two-photon microscopy[42-52]

Fluorescence-based imaging is a powerful tool for non-invasive study of biological processes, both *in vitro* and *in vivo*, as well as for the diagnosis of diseases.

One of the more important parameter to take into account in microscopy is the resolution, which is the minimum distance required between two objects to distinguish them. Usually in fluorescence microscopy the *x-y* resolution is approximately half of the excitation wavelength ranging from 200 to 400 nm for visible light, while the depth field, which is the thickness along the optical axis layer, depends on the microscopy technique that we consider. In wide-field fluorescence microscopy, the sample is all excited and the depth field is approximately 2-3 μm. In fact the detector collects also the out-of-focus fluorescence, thus generating blurred images (**Figure I 4**). To overcome this problem was developed another technique: the confocal microscopy. The main differences between wide-field and confocal microscopy are the light source (which is a laser) and the use of a pinhole that prevents the out-of-focus fluorescence detection. Contrarily to the wide-field, where the entire image is collected, in confocal microscopy the sample is scanned, therefore the first technique allows live images and videos while with the second does not. One important improvement of the confocal microscopy is the possibility to observe different slices of the sample with a resolution of about 500 nm, allowing the achievement of 3D images.

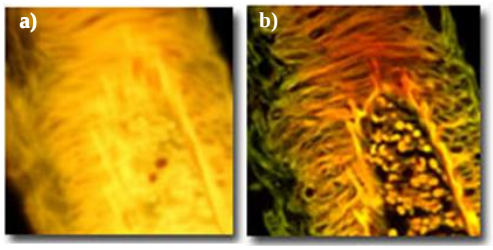

Figure I 4. Thick section of fluorescently stained human medulla observed in a) wide-field fluorescence and with b) confocal microscope (revised from ref.53)

In microscopy, since the fluorophores are excited with variably power for relatively long time, there is the possibility of irreversible destruction of the molecules that affects their luminescence

properties. This process is called photobleaching (displayed as example in **Figure I 5**). In confocal microscopy the excitation light is focused on the sample, therefore the probability of faster photobleaching is higher compared to the wide-field technique.

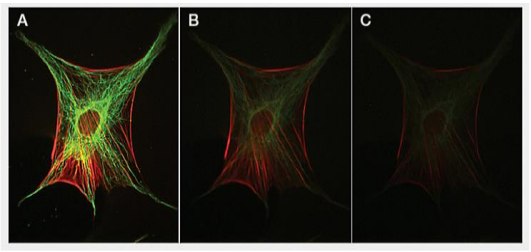

Figure I 5. Photobleaching of fluorescein and Texas Red dye in cells. Cytoskeleton of cells stained with fluorescein and Texas Red dye, excited with 488 or 594 nm lasers for A)t = 0 s B)t = 5 s and C)t = 15 s[54].

Imaging in biological environment is challenging because most of the endogenous chromophores naturally present, such as NADH, tyrosine, tryptophan and FMN, absorb in the UV-visible spectral range (**Table I 1**). Despite the low extinction coefficient, their concentration is high enough to limit the penetration of the excitation, inducing a loss of information. In addition to this, these chromophores are also able to emit fluorescence affecting the quality of the final image.

Table I 1. Photophysical properties of some endogenous chromophores[1,55]

Cpd	λ_{max}^{1PA} **[nm]**	ε_{max} **[$M^{-1}cm^{-1}$]**	λ_{max}^{em} **[nm]**	Φ_f	$\varepsilon_{max}\Phi_f$ **[$M^{-1}cm^{-1}$]**
Tyrosine	275	1500	303	0.14	210
Tryptophane	280	6300	348	0.13	820
NADH	340	6200	435	0.019	120
FMN[a)]	450	12200	530	0.25	3100

a) Flavin mononucleotide

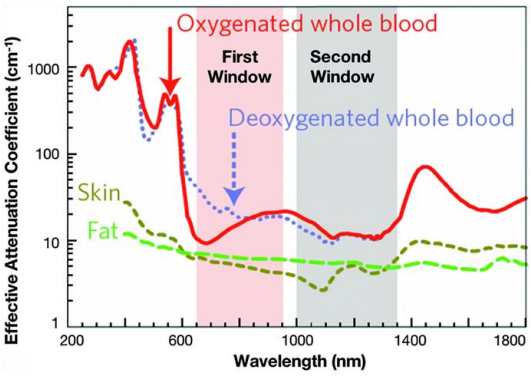

Figure I 6. Optical windows in biological tissues[56,57]

To go beyond the main limits displayed by confocal microscopy, the scientific community calls in action the "world of non-linear optics". There are several techniques of microscopy that are based on non-linear processes such as SHG microscopy[58,59], THG microscopy[60] and three-photon absorption microscopy[61], but I would like to focus the attention on the technique that exploits the two-photon excited fluorescence.

Two-photon absorption process displays an intrinsic 3D resolution since the laser beam has to be focused in order to observe the non-linear process, actually the excitation volume is approximately in the order of 0.1-1 fL (see **Figure I 3**). Two-photon excited fluorescence microscopy (2PM), firstly proposed by W.W. Webb and coworkers[62], displays interesting improvements compared with confocal microscopy. First of all it is important to say that the endogenous chromophores are not good two-photon absorbers as one can see in **Figure I 7** (σ_2 ranging from 0.04 GM of NAD(P)H to 0.45 GM of LipDH)[63,64], thus this technique allows high sensitivity thanks to very low background signal and thanks to the long-wavelength excitation it is possible to excite the sample in the "biological transparency window" (displayed in **Figure I 6**) reaching the depth of few hundreds of μm. Moreover, the excitation of the sample only in the focal point prevents the out-of-focus photobleaching. Concerning the photobleaching, one should think that in the focal point this phenomena occurs faster comparing with the confocal microscopy, since in two-photon microscopy higher photon flux are used in order to make the non-linear process allowed. Therefore, the goal is to obtain high brightness,

which is defined as the product of ε or σ_2 with the fluorescence quantum yield, in molecules and/or nanoobjects in order to use low power preventing the death of the cell and fast photobleaching.

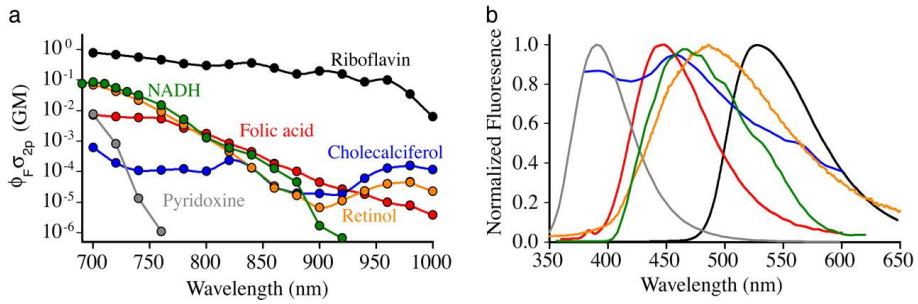

Figure I 7. Two-photon action cross sections and emission spectra from a basis set of biological molecules. (a) two-photon brightness of six molecules that contribute much of the intracellular 2PE intrinsic fluorescence. (b) Emission spectra of the compounds shown in (a)[65]

Since I did not use these techniques I will not go deep in the description but I guess that it is important to mention that the step further towards higher resolution is the development and the use of super-resolved fluorescence microscopies such as stimulated emission depletion (STED) microscopy[66], scanning near-field optical (SNOM) microscopy[67], photoactivated localized microscopy (PALM)[68], stochastic optical reconstruction microscopy (STORM)[69] only citing a few. Interestingly, this topic was awarded with the Nobel Prize in chemistry in 2014 in the person of Eric Betzig, Stefan W. Hell and William E. Moerner. The super-resolution techniques are aimed to break the diffraction resolution limit in order to obtain better images (**Figure I 8**).

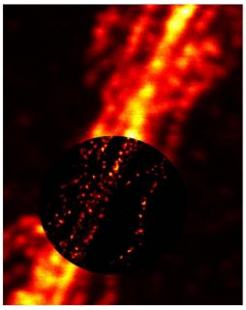

Figure I 8. STED microscopy (circular inset image) compared to a conventional light microscope (outer image) image of filament structures within a nerve cell. (G. Donnert, S. W. Hell; Max Planck Institute for Biophysical Chemistry[70])

4. From bioimaging to molecular engineering[13,14,55,71-76]

In order to fulfill all the requirements of bioimaging in the last decades a great deal of effort was made to understand the structure-properties relationship to prepare new classes of chromophores suitable to be used as bio-probes. In this paragraph, I will try to give a short overview of the properties that the chromophores should display for quality imaging in bioenvironment.

As I mentioned before, within cells and tissues there are several endogenous absorber that could hide the desired signals. To overcome this problem, the fluorophores used as probes in bioimaging should absorb and emit in the biological transparency window for preventing autofluorescence, allowing the deeper penetration as well as decreasing the cell damage. In the last decades a large work was done in order to understand the relationship between the molecular design and the bathochromic shift of the optical properties: generally an enhancement of the ICT character of the chromophore should induces a bathochromic shift of optical properties.

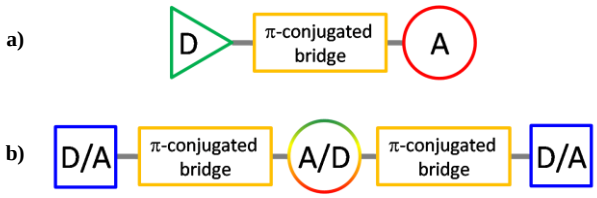

Illustration I 4. Representation of a) general dipolar chromophore and b) general quadrupolar chromophore. Indicating with A and D the electron acceptor and the electron donor moiety respectively.

Considering two main structures of chromophores, dipolar and quadrupolar (**Illustration I 4**), to improve the internal charge transfer character one can play with three particular parts of the molecule: the electron acceptor, the electron donor and the π-conjugated bridge. Specifically, enhancing the electron-withdrawing character of the acceptor group, strengthening the electron-releasing character of the donor group as well as improving the polarisability of the π bridge lead to a marked red-shift of both absorption and emission[77-80]. Interestingly, these three parts of the molecule play also an important role in the enhancement of the two-photon absorption process[13,14]. Indeed an

enhancement of the ICT character of the considered chromophore generally leads to an enhancement of the two-photon cross section.

For the preparation of new dyes for bioimaging, another difficulty that can be encountered is the possibility of re-absorption. This process occurs when the Stokes shift is short and the chromophore displays a large overlap between the absorption and the emission band. As one can observe in **Figure I 9**, that shows the overlap between absorption and emission spectra of two commercially available bioprobes (Alexa Fluor® 488 and Alexa Fluor® 700), the chromophores display a short Stokes shift associated with a large overlap between the absorption and the emission band.

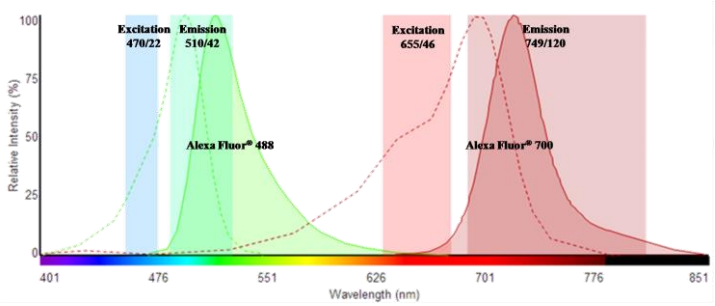

Figure I 9. Absorption (dashed line), emission (solid filled line) and excitation/emission filters (colored bars) of Alexa Fluor® 488 (green) and Alexa Fluor® 700 (red)[81]

In **Figure I 9** are displayed also the excitation and emission filter commercially available, as one can see, due to the short Stokes shift, the excitation filters do not include the maximum of absorption, lowering the intensity of the transition but preventing the re-absorption process. To overcome this issue the idea is to design fluorophores with large Stokes shift in order to reduce the re-absorption process. The extensive use in bioimaging of commercially available dyes such as Alexa Fluor®, DAPI, Texas Red®, Cy® 3/5/7 etc, induced the industry of microscopes to optimize filters for these molecules precluding the use of new class of probes for example with large Stokes shift. Therefore, to use new fluorophores in microscopy one has to choose the right compromise between the uses of filters and the photophysical properties of the dyes.

The chromophores, to be used as bio-probes, have to display high one-photon and two-photon brightness in bioenvironment, thus they should show good fluorescence quantum yield associated with large ε and/or σ_2 (depending on which kind of microscopy one would like to use). Unfortunately, driving the emission towards lower energies leads to a decreasing of the Φ_f that can be ascribed to a decreasing of the radiative decay rates in addition with an enhancement of non-radiative decay rates in the red/NIR spectral region[82]. Moreover, it is known that in biological media there is a large amount of fluorescence quenchers therefore the challenge is to prepare systems that can preserve their emissive properties in bioenvironment.

5. Fluorescent Organic Nanoparticles: a bottom-up approach toward hyper bright nanoobjects[83-87]

"Plenty of room at the bottom"[88] is the title of a talk presented by Richard P. Feynman in 1959 where he hypothesizes the advent of miniaturization; actually, he was the first who spoke about the "nano-world". Since then, this topic gained an overwhelming interest in the scientific community inducing the creation of a large amount of new journals that reached easily high impact factor[89] such as Nature nanotechnology (35.267), Nano letters (13.779), ACS nano (13.334) and Small (8.315).

Nano-objects are considered particles that have at least one dimension of the order of nanometer[90]. These nanoscale materials gained importance since the discovery of the so-called "nano-effect": when the particle size is in the nanometer domain, it displays changes in physico-chemical properties of the matter such as magnetic, electric or optical properties, compared with the bulk. This behavior can be easily observed in semiconductor-based nanoparticles (**Figure I 10a**) or in noble metal-based nanoparticles (**Figure I 10b**) where slight changes of the particle size and/or shape induces significant changes of photophysical properties.

Nanomaterials are suitable tools for a wide range of applications that go from optoelectronics[91,92] to solar cells[93-95], from photodynamic therapy[36,38,40,41,96-98] and drug delivery[39,99] to

bioimaging[100-105]. Among the numerous classes of nanomaterials used as bio-probes, a great effort was made in the study of semiconductor-based nanoparticles (quantum dots QDs)[101,102], silica-based nanoparticles[40,106,107], upconverting nanoparticles (UCNPs)[108,109] and noble metal-based nanoparticles[110]. In spite of their high photostability, tunability and brightness, these nanoparticles are known as potentially toxic nanomaterials[111-115], since they are constituted by heavy metals (i.e. Cd and Te for QDs) and/or rare hearth (i.e. Yb^{3+}, Eb^{3+} and Tm^{3+} for UCNPs). The biodegradability is still a limitation for these class of nanomaterials because they can induce serious damages to the environment.

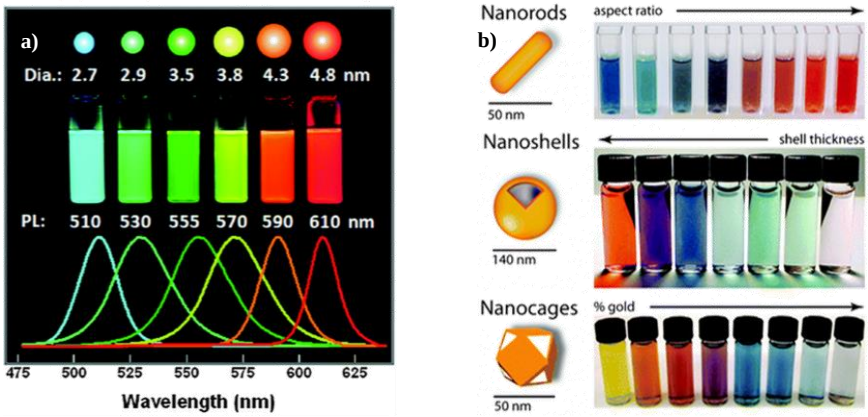

Figure I 10. a) Cartoon, photograph, and emission spectra showing the color changes of quantum dots (QDs) with increasing nanocrystal size[116], b) Gold nanoparticles (AuNPs) commonly applied in biomedical applications: gold nanorods, silica–gold core–shell nanoparticles and gold nanocages. The color of these nanoparticles varies with aspect ratio, shell thickness and/or galvanic displacement by gold[110].

In this perspective, organic nanoparticles (ONPs) present an encouraging alternative to overcome the problems that can be encountered with "inorganic" nanomaterials, and between them, molecular-based ONPs have nowadays attracted curiosity thanks to their versatility. Potentially it is possible to prepare organic nanoparticles with any molecule one can synthesize. Therefore, one can chose carefully non-toxic organic fluorophores in order to test their ability to form nanoparticles and thus to study their behaviors. Moreover, the adaptability of organic nanoparticles allows also surface functionalization towards high selectivity targeting of bio-receptors.

Contrarily to the engineering of molecules with expected photophysical behaviors, the design of ONPs is extremely challenging because one has to take into account several parameters that can strongly affect the properties of the obtained nanomaterials such as the preparation method, the size and the shape and the arrangement of chromophores upon nanoconfinement.

5.1. Preparation methods of organic nanoparticles: bottom-up and top-down approaches[117-119]

There are different methods used for the fabrication of molecular-based organic nanoparticles such as vapor deposition[120], confined crystallization[121], electrochemical deposition[122] but I would like to focus the attention on two other process of nanoparticles preparation: laser photofragmentation and reprecipitation.

Reprecipitation method, the easy and widely used process, can be considered as a bottom-up approach to prepare organic nanoparticles developed in the BASF laboratory[117] but firstly published by Nakanishi[123]. This process is based on fast solvent exchange producing nanoparticles under kinetic domain; basically, microliters of solution of the compound are quickly injected, usually under stirring or sonication, into a large amount of a solvent in which the compound is not soluble. There are several parameters to play with in order to control the morphology and the size of the obtained nanoobject such as the concentration of the injected solution, the use of stirring or sonication, the use of surfactants and the choice of the solvents, the good and the poor. Indeed the viscosity of the solvents and the respective diffusion have fundamental role in the reprecipitation method. Unfortunately, the nucleation/growth process is not fully understood and it is not predictable, in fact from similar compounds it is possible to obtain nanoparticles strongly different in terms of size (cf. **Chapter 3 Paragraph 2**, **Chapter 4 Paragraph 3** and **Chapter 5 Paragraph 4**). Since the nanoparticles are prepared under kinetic domain the probability to produce amorphous nanoobject is quite high. Nevertheless, depending on the intermolecular interactions, it is possible that the molecules within the nanoparticles are organized in a short range, forming small crystalline domains.

On the other hand, laser photofragmentation (LPF) is a top-down approach to prepare nanocolloids since the idea is to form nanoparticles starting from microcrystalline powder of the compound dispersed in a poor solvent. This method was proposed by Masuhara[124-126] with a work in which is displayed the dependence of nanoparticles formation by the laser fluence used. When microcrystals are suspended in a poor solvent and exposed to intense laser pulses, this induces the breakage of the powder and the ejected particles are caught by water and stabilized as nanocolloids. Several parameters can affect the fragmentation process leading to control both size and shape of ONPs: laser wavelength, pulse width, laser fluence, time of irradiation and total shot number. Contrarily to the reprecipitation method, with LPF the possibility to obtain organized nanocrystals is higher since the starting powder is microcrystalline, this can be interesting in order to study the optical properties of crystalline systems in both bulk and nano domains.

5.2. Intermolecular interaction in nano-environment[127-130]

The optical properties of organic nanoparticles do not show strong dependency on the size, as discussed previously for QDs and AuNPs, but they have the advantage that one nanoparticle is formed by 10^4-10^8 molecules which induces strong additive and/or cooperative effect within the nano-environment. Indeed, nanoparticles display an enhancement of absorption (both one- and two-photon) of several orders of magnitude with respect to the single chromophore.

The first studies about the behavior of molecules in confined environment were done independently in the late 1930s by Jelley[131] and by Scheibe[132]. They were the first who rationalized that molecular aggregates behave differently from the molecular solution. An extensive work was done trying to understand the effect of the intermolecular contributions on the photophysical properties, especially using distyrylbenzene derivatives[130], and the most comprehensive theory about molecular aggregation was proposed by Kasha and coworkers[133]: the exciton model (an exhaustive description of the exciton model will be done in **Chapter 3 Paragraph 1)**.

Upon molecular confinement especially of chromophores, which are molecules formed by more or less rigid π-conjugated systems, intermolecular π-π interactions have to be considered. Indeed, these contributions can strongly affect the emissive character of the resulting aggregates leading, most of the time, to a decrease of the luminescence properties. This phenomenon is known as "aggregation-caused quenching" (ACQ). To prevent this problem, we can call in action the molecular engineering trying to prepare chromophores with hindering groups that should increase the intermolecular distance, decreasing the probability of deleterious π-stacking interactions (several examples are discussed in the manuscript). Another way to overcome this problem was observed by Tang and coworkers[134] and the phenomenon was popularized with the name of "aggregation-induced emission" (AIE). AIE is referred to a process that exploits the decrease of the molecular motions in confined state that can lead to a decrease of non-radiative decay rate enhancing the luminescence. In fact, in the work of Tang they used methyl-pentaphenylsilole that in molecular solution display a twisted conformation while in aggregated state show a planar conformation. This phenomenon is not taking into account possible intermolecular contribution, thus is limited to the observation that a rigidification associated with a planarization of the system induce an improvement of the emissive character of the aggregates. Another phenomenon takes into account the synergic intra- and intermolecular contributions with respect to the photophysical properties: the phenomenon is known as "aggregation-induced enhanced emission" (AIEE). AIEE describes molecules that are already slightly emissive in solution but the molecular confinement induces an enhancement of the fluorescence properties thanks to the cooperative role of both intramolecular and intermolecular interactions.

Nowadays AIE or AIEE phenomena are widely exploited but, unfortunately, often wrongly claimed also due to the widespread confusion in this field.

BIBLIOGRAPHIC REFERENCES

(1) Lakowicz, J. R.: *Principles of Fluorescence Spectroscopy*; 3rd ed.; Springer US, 2006.

(2) Valeur, B.; Berberan-Santos, M. N.: *Molecular Fluorescence Principles and Applications*; Second Edition ed.; Wiley-VCH Verlag GmbH & Co. KGaA, 2012.

(3) Braslavsky, S. E. Glossary of terms used in photochemistry, 3rd edition (IUPAC Recommendations 2006). *Pure and Applied Chemistry* **2007**, *79*.

(4) Itoh, T. Fluorescence and Phosphorescence from Higher Excited States of Organic Molecules. *Chemical Reviews* **2012**, *112*, 4541-4568.

(5) Kasha, M. Characterization of electronic transitions in complex molecules. *Discussions of the Faraday Society* **1950**, *9*, 14-19.

(6) Stokes, G. G. On the change of refrangibility of light. *Philosophical Transactions of the Royal Society of London* **1852**.

(7) Pagano, P. Perylene bis-imide as covalent spacer in wheel and axle complexes of Ru(II): synthesis, spectroscopic characterization and adsorption of volatile aromatic compounds. Parma University, 2012.

(8) Würth, C.; Grabolle, M.; Pauli, J.; Spieles, M.; Resch-Genger, U. Relative and absolute determination of fluorescence quantum yields of transparent samples. *Nature Protocols* **2013**, *8*, 1535-1550.

(9) Resch-Genger, U.; Rurack, K. Determination of the photoluminescence quantum yield of dilute dye solutions (IUPAC Technical Report). *Pure and Applied Chemistry Pure Appl. Chem.* **2013**, *85*, 2005-2013.

(10) Brouwer, A. M. Standards for photoluminescence quantum yield measurements in solution (IUPAC Technical Report). *Pure and Applied Chemistry* **2011**, *83*, 2213-2228.

(11) Papadopoulos, M. G.; Sadlej, A. J.; Leszczynsk, J.: *Non-Linear Optical Properties of Matter: From molecules to condensed phases*; Springer Netherlands, 2006.

(12) Boyd, R. W.: In *Nonlinear Optics (Third Edition)*; Academic Press: Burlington, 2008.

(13) Terenziani, F.; Katan, C.; Badaeva, E.; Tretiak, S.; Blanchard‐Desce, M. Enhanced two‐photon absorption of organic chromophores: theoretical and experimental assessments. *Advanced Materials* **2008**, *20*, 4641-4678.

(14) Pawlicki, M.; Collins, H. A.; Denning, R. G.; Anderson, H. L. Two‐photon absorption and the design of two‐photon dyes. *Angewandte Chemie International Edition* **2009**, *48*, 3244-3266.

(15) Franken, P. A.; Hill, A. E.; Peters, C. W.; Weinreich, G. Generation of Optical Harmonics. *Physical Review Letters* **1961**, *7*, 118-119.

(16) Göppert-Mayer, M. Über elementarakte mit zwei quantensprüngen. *Annalen der Physik (Leipzig)* **1931**, *9*, 273-294.

(17) Göppert, M. Über die wahrscheinlichkeit des zusammenwirkens zweier lichtquanten in einem elementarakt *Die Naturwissenschaften* **1929**, *17*.

(18) Kaiser, W.; Garrett, C. G. B. Two-photon excitation in CaF_2:Eu^{2+}. *Physical Review Letters* **1961**, *7*, 229-231.

(19) Sheik-Bahae, M.; Said, A. A.; Wei, T. H.; Hagan, D. J.; Stryland, E. W. V. Sensitive measurement of optical nonlinearities using a single beam. *IEEE Journal of Quantum Electronics* **1990**, *26*, 760-769.

(20) Xu, C.; Webb, W. W. Measurement of two-photon excitation cross sections of molecular fluorophores with data from 690 to 1050 nm. *Journal of Optical Society of America B* **1996**, *13*.

(21) Makarov, N. S.; Drobizhev, M.; Rebane, A. Two-photon absorption standards in the 550-1600 nm excitation wavelength range. *Optics Express* **2008**, *16*, 4029.

(22) Entwistle, C. D.; Marder, T. B. Applications of three-coordinate organoboron compounds and polymers in optoelectronics. *Chemistry of Materials* **2004**, *16*, 4574-4585.

(23) Ta'eed, V. G.; Baker, N. J.; Fu, L.; Finsterbusch, K. Ultrafast all-optical chalcogenide glass photonic circuits. *Optics Express* **2007**.

(24) Maruo, S.; Nakamura, O.; Kawata, S. Three-dimensional microfabrication with two-photon-absorbed photopolymerization. *Optics letters* **1997**, *22*, 132-134.

(25) Joshi, M. P.; Pudavar, H. E.; Swiatkiewicz, J.; Prasad, P. N.; Reianhardt, B. A. Three-dimensional optical circuitry using two-photon-assisted polymerization. *Applied Physics Letters* **1999**, *74*, 170-172.

(26) Cumpston, B. H.; Ananthavel, S. P.; Barlow, S.; Dyer, D. L.; Ehrlich, J. E.; Erskine, L. L.; Heikal, A. A.; Kuebler, S. M.; Lee, I. Y. S.; McCord-Maughon, D.; Qin, J.; Rockel, H.; Rumi,

M.; Wu, X.-L.; Marder, S. R.; Perry, J. W. Two-photon polymerization initiators for three-dimensional optical data storage and microfabrication. *Nature* **1999**, *398*, 51-54.

(27) Zhou, W.; Kuebler, S. M.; Braun, K. L.; Yu, T.; Cammack, J. K.; Ober, C. K.; Perry, J. W.; Marder, S. R. An efficient two-photon-generated photoacid applied to positive-tone 3D microfabrication. *Science* **2002**, *296*, 1106-1109.

(28) Ovsianikov, A.; Viertl, J.; Chichkov, B.; Oubaha, M.; MacCraith, B.; Sakellari, I.; Giakoumaki, A.; Gray, D.; Vamvakaki, M.; Farsari, M.; Fotakis, C. Ultra-low shrinkage hybrid photosensitive material for two-photon polymerization microfabrication. *ACS Nano* **2008**, *2*, 2257-2262.

(29) Serbin, J.; Ovsianikov, A.; Chichkov, B. Fabrication of woodpile structures by two-photon polymerization and investigation of their optical properties. *Optics Express* **2004**.

(30) Serbin, J.; Egbert, A.; Ostendorf, A.; Chichkov, B. N. Femtosecond laser-induced two-photon polymerization of inorganic–organic hybrid materials for applications in photonics. *Optics Express* **2003**.

(31) Kawata, S.; Kawata, Y. Three-dimensional optical data storage using photochromic materials. *Chemical reviews* **2000**, *100*, 1777-1788.

(32) Parthenopoulos, D. A.; Rentzepis, P. M. Three-dimensional optical storage memory. *Science* **1989**, *245*, 843-845.

(33) Bhawalkar, J. D.; Kumar, N. D.; Zhao, C. F.; Prasad, P. N. Two-photon photodynamic therapy. *Journal of clinical laser medicine & surgery* **1997**, *15*, 201-204.

(34) Fisher, A. M. R.; Murphree, L. A.; Gomer, C. J. Clinical and preclinical photodynamic therapy. *Lasers in Surgery and Medicine* **1995**, *17*, 2-31.

(35) Pettit, D. L.; Wang, S. S.; Gee, K. R.; Augustine, G. J. Chemical two-photon uncaging: a novel approach to mapping glutamate receptors. *Neuron* **1997**, *19*, 465-471.

(36) Kim, S.; Ohulchanskyy, T. Y.; Pudavar, H. E.; Pandey, R. K.; Prasad, P. N. Organically modified silica nanoparticles co-encapsulating photosensitizing drug and aggregation-enhanced two-photon absorbing fluorescent dye aggregates for two-photon photodynamic therapy. *Journal of the American Chemical Society* **2007**, *129*, 2669-2675.

(37) Dichtel, W. R.; Serin, J. M.; Edder, C.; Fréchet, J. M.; Matuszewski, M.; Tan, L.-S. S.; Ohulchanskyy, T. Y.; Prasad, P. N. Singlet oxygen generation via two-photon excited FRET. *Journal of the American Chemical Society* **2004**, *126*, 5380-5381.

(38) Croissant, J. G.; Mauriello-Jimenez, C.; Maynadier, M.; Cattoën, X.; Man, M.; Raehm, L.; Mongin, O.; Blanchard-Desce, M.; Garcia, M.; Gary-Bobo, M.; Maillard, P.; Durand, J.-O. Synthesis of disulfide-based biodegradable bridged silsesquioxane nanoparticles for two-photon imaging and therapy of cancer cells. *Chemical Communications* **2015**, *51*, 12324-12327.

(39) Croissant, J. G.; Qi, C.; Mongin, O.; Hugues, V.; Blanchard-Desce, M.; Raehm, L.; Cattoën, X.; Man, M.; Maynadier, M.; Gary-Bobo, M.; Garcia, M.; Zink, J. I.; Durand, J.-O. Disulfide-gated mesoporous silica nanoparticles designed for two-photon-triggered drug release and imaging. *Journal of Materials Chemistry B* **2015**, *3*, 6456-6461.

(40) Croissant, J.; Salles, D.; Maynadier, M.; Mongin, O.; Hugues, V.; Blanchard-Desce, M.; Cattoën, X.; Man, M.; Gallud, A.; Garcia, M.; Gary-Bobo, M.; Raehm, L.; Durand, J.-O. Mixed periodic mesoporous organosilica nanoparticles and core–shell systems, application to in vitro two-photon imaging, therapy, and drug delivery. *Chemistry of Materials* **2014**, *26*, 7214-7220.

(41) Gary-Bobo, M.; Mir, Y.; Rouxel, C.; Brevet, D.; Hocine, O.; Maynadier, M.; Gallud, A.; Silva, A.; Mongin, O.; Blanchard-Desce, M.; Richeter, S.; Loock, B.; Maillard, P.; Morère, A.; Garcia, M.; Raehm, L.; Durand, J.-O. Multifunctionalized mesoporous silica nanoparticles for the in vitro treatment of retinoblastoma: Drug delivery, one and two-photon photodynamic therapy. *International journal of pharmaceutics* **2012**, *432*, 99-104.

(42) Pawley, J.: *Handbook of Biological Confocal Microscopy*; Springer US, 2006.

(43) Nwaneshiudu, A.; Kuschal, C.; Sakamoto, F. H.; Anderson, R. R.; Schwarzenberger, K.; Young, R. C. Introduction to confocal microscopy. *Journal of Investigative Dermatology* **2012**, *132*.

(44) Que, S. T.; Grant-Kels, J. M.; Longo, C.; Pellacani, G. Basics of confocal microscopy and the complexity of diagnosis skin tumors. *Dermatologic Clinics* **2016**, *34*, 367-375.

(45) Zipfel, W. R.; Williams, R. M.; Webb, W. W. Nonlinear magic: multiphoton microscopy in the biosciences. *Nature Biotechnology* **2003**, *21*, 1369-1377.

(46) Hell, S. W. Toward fluorescence nanoscopy. *Nature Biotechnology* **2003**, *21*, 1347-1355.

(47) Ntziachristos, V. Going deeper than microscopy: the optical imaging frontier in biology. *Nature Methods* **2010**, *7*, 603-614.

(48) Ustione, A.; Piston, D. W. A simple introduction to multiphoton microscopy. *Journal of Microscopy* **2011**, *243*, 221-226.

(49) Hoover, E. E.; Squier, J. A. Advances in multiphoton microscopy technology. *Nature Photonics* **2013**, *7*, 93-101.

(50) Helmchen, F.; Denk, W. Deep tissue two-photon microscopy. *Nature methods* **2005**, *2*, 932-940.

(51) Mazza, D.; Bianchini, P.; Caorsi, V.; Cella, F.; Mondal, P. P.; Ronzitti, E.; Testa, I.; Vicidomini, G.; Diaspro, A.: Non-Linear Microscopy. In *Biophotonics*; Pavesi, L., Fauchet, P. M., Eds.; Springer Berlin Heidelberg, 2008; pp pp 47-69.

(52) Leung, B. O.; Chou, K. C. Review of super-resolution fluorescence microscopy for biology. *Applied Spectroscopy* **2011**, *65*, 967-980.

(53) http://www.olympusmicro.com/primer/techniques/confocal/confocalintro.html.

(54) https://www.thermofisher.com/fr/en/home/life-science/cell-analysis/cell-analysis-learning-center/molecular-probes-school-of-fluorescence/fluorescence-basics/fluorescence-fundamentals/photobleaching-principles.html.

(55) Lavis, L. D.; Raines, R. T. Bright ideas for chemical biology. *ACS Chemical Biology* **2008**, *3*, 142-155.

(56) Smith, A. M.; Mancini, M. C.; Nie, S. Bioimaging: Second window for in vivo imaging. *Nature Nanotechnology* **2009**, *4*, 710-711.

(57) Hemmer, E.; Benayas, A.; Légaré, F.; Vetrone, F. Exploiting the biological windows: current perspectives on fluorescent bioprobes emitting above 1000 nm. *Nanoscale Horizons* **2016**, *1*, 168-184.

(58) Freund, I.; Deutsch, M. Second-harmonic microscopy of biological tissue. *Optics Letters* **1986**, *11*, 94-96.

(59) Campagnola, P. J.; Loew, L. M. Second-harmonic imaging microscopy for visualizing biomolecular arrays in cells, tissues and organisms. *Nature Biotechnology* **2003**, *21*, 1356-1360.

(60) Barad, Y.; Eisenberg, H.; Horowitz, M.; Silberberg, Y. Nonlinear scanning laser microscopy by third harmonic generation. *Applied Physics Letters* **1997**, *70*, 922-924.

(61) Gryczynski, I.; Malak, H.; Lakowicz, J. R. Three-photon induced fluorescence of 2,5-diphenyloxazole with a femtosecond Ti:sapphire laser. *Chemical Physics Letters* **1995**, *245*, 30-35.

(62) Denk, W.; Strickler, J. H.; Webb, W. W. Two-photon laser scanning fluorescence microscopy. *Science* **1990**, *248*, 73-76.

(63) Blab, G. A.; Lommerse, P.; Cognet, L.; Harms, G. S.; Schmidt, T. Two-photon excitation action cross-sections of the autofluorescent proteins. *Chemical Physics Letters* **2001**, *350*, 71-77.

(64) Huang, S.; Heikal, A. A.; Webb, W. W. Two-Photon Fluorescence Spectroscopy and Microscopy of NAD(P)H and Flavoprotein. *Biophysical Journal* **2002**, *82*, 2811-2825.

(65) Warren R. Zipfel, R. M. W., Richard Christie, Alexander Yu Nikitin, Bradley T. Hyman, and Watt W. Webb. Live tissue intrinsic emission microscopy using multiphoton-excited native fluorescence and second harmonic generation. *PNAS* **2003**, *100*, 7075-7080.

(66) Hell, S. W.; Wichmann, J. Breaking the diffraction resolution limit by stimulated emission: stimulated-emission-depletion fluorescence microscopy. *Optics letters* **1994**.

(67) Betzig, E.; Trautman, J. K. Near-field optics: microscopy, spectroscopy, and surface modification beyond the diffraction limit. *Science* **1992**.

(68) Betzig, E.; Patterson, G. H.; Sougrat, R. Imaging intracellular fluorescent proteins at nanometer resolution. *Science* **2006**, *313*, 1642-1645.

(69) Rust, M. J.; Bates, M.; Zhuang, X. Sub-diffraction-limit imaging by stochastic optical reconstruction microscopy (STORM). *Nature Methods* **2006**, *3*, 793-796.

(70) https://www.mpibpc.mpg.de/14734398/gallery_portraits.

(71) Albota, M. Design of organic molecules with large two-photon absorption cross sections. *Science* **1998**, *281*, 1653-1656.

(72) He, G. S.; Tan, L.-S.; Zheng, Q.; Prasad, P. N. Multiphoton absorbing materials: molecular designs, characterizations, and applications. *Chemical Reviews* **2008**, *108*, 1245-1330.

(73) Escobedo, J. O.; Rusin, O.; Lim, S.; Strongin, R. M. NIR dyes for bioimaging applications. *Current Opinion in Chemical Biology* **2010**, *14*, 64-70.

(74) Ptaszek, M.: Chapter Three - Rational design of fluorophores for in vivo applications. In *Progress in Molecular Biology and Translational Science*; May, C. M., Ed.; Academic Press, 2013; Vol. Volume 113; pp 59-108.

(75) Johnson, I.; Spence, M. T. Z.: *The Molecular Probes Handbook*; 11th ed.; Life Technologies, 2010.

(76) Kim, H. M.; Cho, B. R. Small-molecule two-photon probes for bioimaging applications. *Chemical Reviews* **2015**, *115*.

(77) Genin, E.; Hugues, V.; Clermont, G.; Herbivo, C.; Castro, M. C. R.; Comel, A.; Raposo, M. M. M.; Blanchard-Desce, M. Fluorescence and two-photon absorption of push–pull aryl (bi) thiophenes: structure–property relationships. *Photochemical & Photobiological Sciences* **2012**, *11*.

(78) Morales, A. R.; Frazer, A.; Woodward, A. W.; Ahn-White, H.-Y.; Fonari, A.; Tongwa, P.; Timofeeva, T.; Belfield, K. D. Design, synthesis, and structural and spectroscopic studies of push–pull two-photon absorbing chromophores with acceptor groups of varying strength. *The Journal of Organic Chemistry* **2013**, *78*, 1014-1025.

(79) Rouxel, C.; Charlot, M.; Mir, Y.; Frochot, C.; Mongin, O.; Blanchard-Desce, M. Banana-shaped biphotonic quadrupolar chromophores : from fluorophores to biphotonic photosensitizers. *New Journal of Chemistry* **2011**, *35*, 1771-1780.

(80) Mongin, O.; Porrès, L.; Charlot, M.; Katan, C.; Blanchard-Desce, M. Synthesis, fluorescence, and two-photon absorption of a series of elongated rodlike and banana-shaped quadrupolar fluorophores: a comprehensive study of structure-property relationships. *Chemistry - A European Journal* **2007**, *13*, 1481-1498.

(81) www.invitrogen.con/handbook/spectraviewer.

(82) Strickler, S. J.; Berg, R. A. Relationship between Absorption Intensity and Fluorescence Lifetime of Molecules. *The Journal of Chemical Physics* **1962**, *37*, 814.

(83) Zhao, Y.; Fu, H.; Peng, A.; Ma, Y.; Xiao, D.; Yao, J. Low‐dimensional nanomaterials based on small organic molecules: preparation and optoelectronic properties. *Advanced Materials* **2008**, *20*, 2859-2876.

(84) Patra, A.; Chandaluri, C. G.; Radhakrishnan, T. P. Optical materials based on molecular nanoparticles. *Nanoscale* **2011**, *4*, 343-359.

(85) Fery-Forgues, S. Fluorescent organic nanocrystals and non-doped nanoparticles for biological applications. *Nanoscale* **2013**, *5*, 8428-8442.

(86) Wolfbeis, O. S. An overview of nanoparticles commonly used in fluorescent bioimaging. *Chemical Society reviews* **2015**, *44*, 4743-4768.

(87) Battistelli, G.; Cantelli, A.; Guidetti, G.; Manzi, J.; Montalti, M. Ultra-bright and stimuli-responsive fluorescent nanoparticles for bioimaging. *Wiley Interdisciplinary Reviews: Nanomedicine and Nanobiotechnology* **2016**, *8*, 139-150.

(88) Feynman, R. P.: Plenty of room at the bottom. In *American Physical Society*: Pasadena, 1959.

(89) InCites Journal Citation Reports.

(90) IUPAC. Compendium of chemical terminology, 2nd ed. (the "Gold Book"). http://goldbook.iupac.org.

(91) Dmitri, T. V.; Jon-Soo, L.; Kovalenko, M. V.; Shevchenko, E. V. Prospects of colloidal nanocrystals for electronic and optoelectronic applications. *Chemical Reviews* **2010**, *110*.

(92) Zhai, X.; Li, J.; Liu, S.; Liu, X.; Zhao, D.; Wang, F.; Zhang, D.; Qin, G.; Qin, W. Enhancement of 153 μm emission band in $NaYF_4$:Er^{3+},Yb^{3+},Ce^{3+} nanocrystals for polymer-based optical waveguide amplifiers. *Optical Materials Express* **2013**, *3*, 270.

(93) Robel, I.; Subramanian, V.; Kuno, M.; Kamat, P. V. Quantum dot solar cells. harvesting light energy with CdSe nanocrystals molecularly linked to mesoscopic TiO_2 films. *Journal of the American Chemical Society* **2006**, *128*, 2385-2393.

(94) Mora-Seró, I.; Giménez, S.; Fabregat-Santiago, F.; Gómez, R.; Shen, Q.; Toyoda, T.; Bisquert, J. Recombination in quantum dot sensitized solar cells. *Accounts of chemical research* **2009**, *42*, 1848-1857.

(95) Lee, Y. L.; Lo, Y. S. Highly efficient quantum‐dot‐sensitized solar cell based on Co‐sensitization of CdS/CdSe. *Advanced Functional Materials* **2009**, *19*, 604-609.

(96) Croissant, J.; Maynadier, M.; Mongin, O.; Hugues, V.; Blanchard‐Desce, M.; Chaix, A.; Cattoën, X.; Man, M.; Gallud, A.; Gary‐Bobo, M.; Garcia, M.; Raehm, L.; Durand, J. O. Enhanced two‐photon fluorescence imaging and therapy of cancer cells via gold@bridged silsesquioxane nanoparticles. *Small* **2015**, *11*, 295-299.

(97) Secret, E.; Maynadier, M.; Gallud, A.; Chaix, A.; Bouffard, E.; Gary‐Bobo, M.; Marcotte, N.; Mongin, O.; Cheikh, K.; Hugues, V.; Auffan, M.; Frochot, C.; Morère, A.; Maillard, P.; Blanchard‐Desce, M.; Sailor, M. J.; Garcia, M.; Durand, J. O.; Cunin, F. Two‐photon excitation of porphyrin‐functionalized porous silicon nanoparticles for photodynamic therapy. *Advanced Materials* **2014**, *26*, 7643-7648.

(98) Gangopadhyay, M.; Mukhopadhyay, S. K.; Gayathri, S.; Biswas, S.; Barman, S.; Dey, S.; Singh, P. N. D. Fluorene–morpholine-based organic nanoparticles: lysosome-targeted pH-triggered two-photon photodynamic therapy with fluorescence switch on–off. *Journal of Materials Chemistry B* **2016**, *4*, 1862-1868.

(99) Park, W.; Na, K. Advances in the synthesis and application of nanoparticles for drug delivery. *Wiley Interdisciplinary Reviews: Nanomedicine and Nanobiotechnology* **2015**, *7*, 494-508.

(100) Sharma, P.; Brown, S.; Walter, G.; Santra; Moudgil, B. Nanoparticles for bioimaging. *Advances in Colloid and Interface Science* **2006**, *123*.

(101) Petryayeva, E.; Algar, W. R.; Medintz, I. L. Quantum dots in bioanalysis: a review of applications across various platforms for fluorescence spectroscopy and imaging. *Applied spectroscopy* **2013**, *67*, 215-252.

(102) Larson, D. R.; Zipfel, W. R.; Williams, R. M.; Clark, S. W.; Bruchez, M. P.; Wise, F. W.; Webb, W. W. Water-soluble quantum dots for multiphoton fluorescence imaging in vivo. *Science* **2003**, *300*, 1434-1436.

(103) Michalet, X.; Pinaud, F. F.; Bentolila, L. A.; Tsay, J. M.; Doose, S.; Li, J. J.; Sundaresan, G.; Wu, A. M.; Gambhir, S. S.; Weiss, S. Quantum dots for live cells, in vivo imaging, and diagnostics. *Science* **2005**, *307*, 538-544.

(104) He, X.; Wang, K.; Cheng, Z. In vivo near‐infrared fluorescence imaging of cancer with nanoparticle‐based probes. *Wiley Interdisciplinary Reviews: Nanomedicine and Nanobiotechnology* **2010**, *2*, 349-366.

(105) Parthasarathy, V.; Fery-Forgues, S.; Campioli, E.; Recher, G.; Terenziani, F.; Blanchard-Desce, M. Dipolar versus octupolar triphenylamine-based fluorescent organic nanoparticles as brilliant one- and two-photon emitters for (bio)imaging. *Small* **2011**, *7*, 3219-3229.

(106) Vivero-Escoto, J. L.; Huxford-Phillips, R. C.; Lin, W. Silica-based nanoprobes for biomedical imaging and theranostic applications. *Chemical Society Reviews* **2012**, *41*, 2673-2685.

(107) Rampazzo, E.; Boschi, F.; Bonacchi, S.; Juris, R.; Montalti, M.; Zaccheroni, N.; Prodi, L.; Calderan, L.; Rossi, B.; Becchi, S.; Sbarbati, A. Multicolor core/shell silica nanoparticles for in vivo and ex vivo imaging. *Nanoscale* **2011**, *4*, 824-830.

(108) Haase, M.; Shafer, H. Upconverting Nanoparticles. *Angewandte Chemie International Edition* **2011**, *50*.

(109) Chen, J.; Zhao, J. Upconversion nanomaterials: synthesis, mechanism, and applications in sensing. *Sensors* **2012**, *12*, 2414-2435.

(110) Dreaden, E. C.; Alkilany, A. M.; Huang, X.; Murphy, C. J.; El-Sayed, M. A. The golden age: gold nanoparticles for biomedicine. *Chemical Society Reviews* **2012**, *41*, 2740-2779.

(111) Nel, A.; Xia, T.; Mädler, L.; Li, N. Toxic potential of materials at the nanolevel. *Science* **2006**, *311*, 622-627.

(112) Murphy, C. J.; Gole, A. M.; Stone, J. W.; Sisco, P. N.; Alkilany, A. M.; Goldsmith, E. C.; Baxter, S. C. Gold nanoparticles in biology: beyond toxicity to cellular imaging. *Accounts of Chemical Research* **2008**, *41*, 1721-1730.

(113) Lewinski, N.; Colvin, V.; Drezek, R. Cytotoxicity of nanoparticles. *Small* **2008**, *4*, 26-49.

(114) Maurer-Jones, M. A.; Bantz, K. C.; Love, S. A.; Marquis, B. J. Toxicity of therapeutic nanoparticles. *Nanomedicine* **2009**, *4*, 219-241.

(115) Sharifi, S.; Behzadi, S.; Laurent, S.; Forrest, L. M.; Stroeve, P.; Mahmoudi, M. Toxicity of nanomaterials. *Chemical Society Reviews* **2011**, *41*, 2323-2343.

(116) Algar, R. W.; Susumu, K.; Delehanty, J. B.; Medintz, I. L. Semiconductor quantum dots in bioanalysis: crossing the valley of death. *Analytical Chemistry* **2011**, *83*, 8826-8837.

(117) Horn, D.; Rieger, J. Organic nanoparticles in the aqueous phase—theory, experiment, and use. *Angewandte Chemie International Edition* **2001**, *40*, 4330-4361.

(118) Asahi, T.; Sugiyama, T.; Masuhara, H. Laser fabrication and spectroscopy of organic nanoparticles. *Accounts of Chemical Research* **2008**.

(119) Masuhara, H.; Nakanishi, H.; Sasaki, K.: *Single Organic Nanoparticles*; Springer-Verlag Berlin Heidelberg, 2003. pp. XLIX, 402.

(120) Zhao, Y.; Xiao, D.; Yang, W.; Peng, A.; Yao, J. 2,4,5-Triphenylimidazole nanowires with fluorescence narrowing spectra prepared through the adsorbent-assisted physical vapor deposition method. *Chemistry of Materials* **2006**, *18*, 2302-2306.

(121) Cui, S.; Liu, H.; Gan, L.; Li, Y.; Zhu, D. Fabrication of low-dimension nanostructures based on organic conjugated molecules. *Advanced Materials* **2008**, *20*, 2918-2925.

(122) Mas-Torrent, M.; Hadley, P. Electrochemical growth of organic conducting microcrystals of tetrathiafulvalene bromide. *Small* **2005**, *1*, 806-808.

(123) Kasai, H.; Nalwa, H.; Oikawa, H.; Okada, S.; Matsuda, H.; Minami, N.; Kakuta, A.; Ono, K.; Mukoh, A.; Nakanishi, H. A novel preparation method of organic microcrystals. *Japanese Journal of Applied Physics* **1992**, *31*.

(124) Sugiyama, T.; Asahi, T.; Takeuchi, H.; Masuhara, H. Size and phase control in quinacridone nanoparticle formation by laser ablation in water. *Japanese Journal of Applied Physics* **2006**, *45*, 384-388.

(125) Tamaki, Y.; Asahi, T.; Masuhara, H. Solvent-dependent size and phase of vanadyl phthalocyanine nanoparticles formed by laser ablation of VOPc crystal-dispersed solution. *Japanese Journal of Applied Physics* **2003**, *42*, 2725-2729.

(126) Tamaki, Y.; Asahi, T.; Masuhara, H. Nanoparticle formation of vanadyl phthalocyanine by laser ablation of its crystalline powder in a poor solvent. *The Journal of Physical Chemistry A* **2002**, *106*, 2135-2139.

(127) Hong, Y.; Lam, J. W. Y.; Tang, B. Aggregation-induced emission. *Chemical Society Reviews* **2011**, *40*, 5361-5388.

(128) Würthner, F.; Kaiser, T. E.; Saha-Möller, C. R. J-aggregates: from serendipitous discovery to supra- molecular engineering of functional dye materials. *Angewandte Chemie International Edition* **2011**, *50*.

(129) Hong, Y.; Lam, J. W. Y.; Tang, B. Z. Aggregation-induced emission: phenomenon, mechanism and applications. *Chemical Communications* **2009**, 4332-4353.

(130) Gierschner, J.; Park, S. Y. Luminescent distyrylbenzenes: tailoring molecular structure and crystalline morphology. *Journal of Materials Chemistry C* **2013**, *1*, 5818-5832.

(131) Jelley, E. E. Spectral absorption and fluorescence of dyes in the molecular state. *Nature* **1936**, 1009-1010.

(132) Scheibe, G. Über die Veränderlichkeit der absorptionsspektren in lösungen und die nebenvalenzen als ihre ursache. *Angewandte Chemie* **1937**, *50*, 212-219.

(133) Kasha, M.; Rawls, H. R.; El-Bayoumi, M. A. The exciton model in molecular spectroscopy. *Pure Applied Chemistry* **1965**, *11*.

(134) Luo, J.; Xie, Z.; Lam, J. W. Y.; Cheng, L.; Chen, H.; Qiu, C.; Kwok, H.; Zhan, X.; Liu, Y.; Zhu, D.; Tang, B. Aggregation-induced emission of 1-methyl-1,2,3,4,5-pentaphenylsilole. *Chemical Communications* **2001**, *0*, 1740-1741.

CHAPTER 2

DIPOLAR CHROMOPHORES

IN MOLECULAR SOLUTION

CHAPTER 2 –DIPOLAR CHROMOPHORES

IN MOLECULAR SOLUTION

1. Introduction

As discussed in **Chapter 1**, the design and synthesis of new organic chromophores with a large π-conjugated system is a very active topic thanks to the non-linear optical properties that can be exploited in a large number of different areas. In this field, great effort was dedicated to the study of dipolar "push-pull" chromophores[1-9]. These dyes gather in the same molecule an electron-donor and an electron-acceptor moiety, connected through a π-conjugated bridge. To tune the photophysical properties of these chromophores we can play with the degree of the charge separation in the ground state choosing appropriately the electron withdrawing and the electron-donating groups, adapting the strength of the dipole[8,10-13]. Moreover, lengthening and/or rigidifying the π-conjugated bridge can affect the charge transfer behavior influencing consequently the photophysical properties of the chromophores[11,12,14].

In this chapter are displayed the results of the studies that were done on push-pull dipolar chromophores bearing a triphenylamine moiety as electron-donating group (**Figure II 1**), which is a well known motif capable to an easy delocalization of the free doublet on the nitrogen. Moreover, triphenylamine-like compounds are known to be good 2PA systems[15]. Here will be discussed the changes of the photophysical properties that occur playing on the strength of the acceptor group; tuning the substituent on the triphenylamine part; lengthening and/or rigidifying the π-connector bridge. Concerning the para-substituent on the triphenylamine the idea was to increase the donor character but mainly to introduce bulky groups that play an important role when the molecules are confined in nanoparticles (cf. **Chapter 3**). Since we wanted to play in the dipolar strength tuning the acceptor moiety is another way to improve the charge transfer. In fact, electron-withdrawing groups with increase acceptor character from aldehyde to cyanoamide, cyanoester dicyano and DETB were

investigated. In the following **Figure II 1** are gathered all the chromophores that will be the subject of study in this chapter.

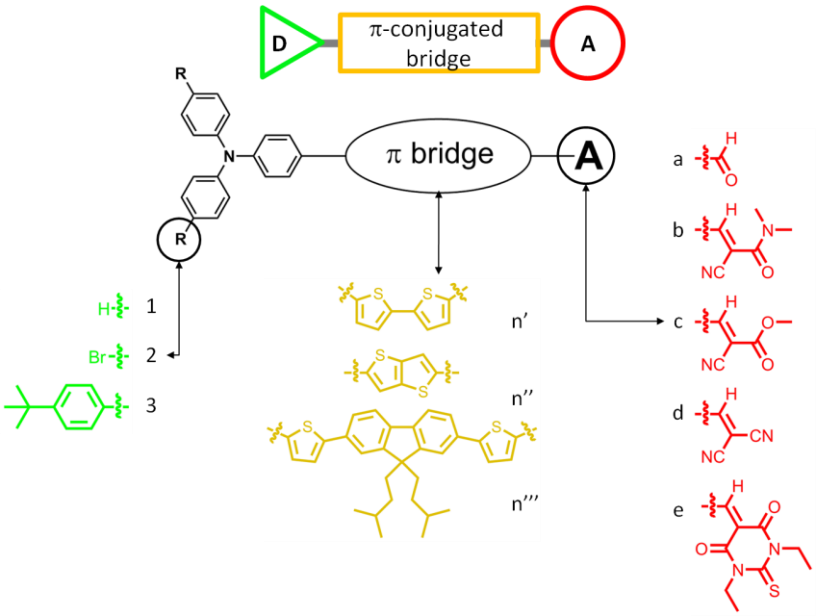

Figure II 1. Dipolar push-pull chromophores (n = **1**, **2** or **3**)

As it will be shown, the changes on the dipolar molecule will affect strongly the photophysical behavior of the chromophore as monomer, in organic solvents, as well as when confined in nano-environment.

2. Synthesis and structural characterization of dipolar chromophores

Here will be described the synthetic route that was followed to synthesize the chromophores that are the subject of study in this chapter. Since the chromophores with thienothiophene were synthesized by Cristiano Matteo Mastrodonato [CMM], I will not describe here the synthesis; I will focus the attention on the "linear thiophenes" chromophores.

2.1. Playing on the dipolar strength

To synthesize the three series of complementary chromophores, I started with the preparation of the triphenylamine precursor using a Ullmann reaction, following a procedure reported in literature[16] as shown in the **Scheme II 1**.

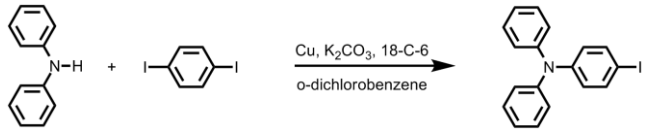

Scheme II 1. Synthesis of triphenylamine monoiodo

A Suzuki cross coupling was used to synthesize the first aldehyde, which is the starting compound to prepare all the other chromophores of the three series. To reach the same molecule were used two different pathways displayed in the **Scheme II 2** adapted from literature[17], in both cases the compound was isolated in good yield (>75%). Because the second pathway is less expensive in terms of reagent, it was chosen to prepare the compound **D1'a** in large amount.

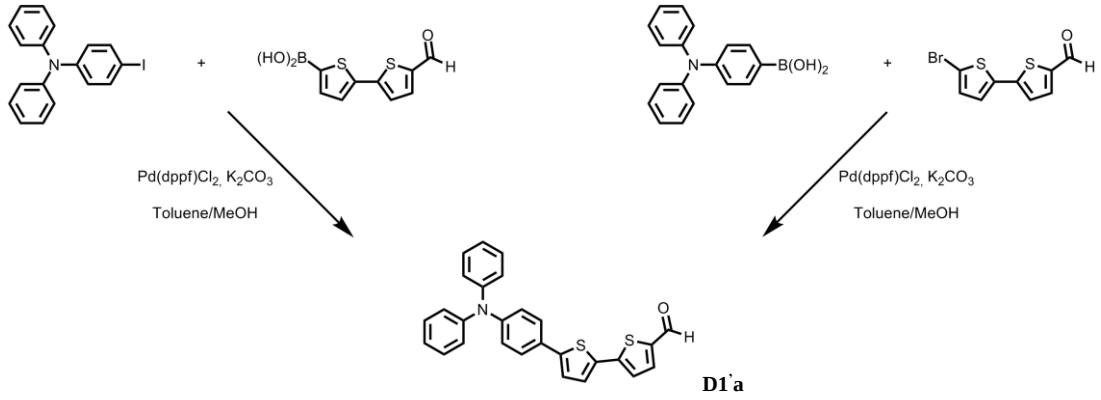

Scheme II 2. Synthesis of the chromophore **D1'a** through Suzuki cross coupling

Once the precursor chromophore of the three series was obtained, was prepared by a bromination using NBS (**Scheme II 3a**) the aldehyde of the second series; with a Suzuki coupling from this aldehyde, was obtained the compound **D3'a** as displayed in the **Scheme II 3b**. The procedures followed were reported in a previous work in our lab[10,11].

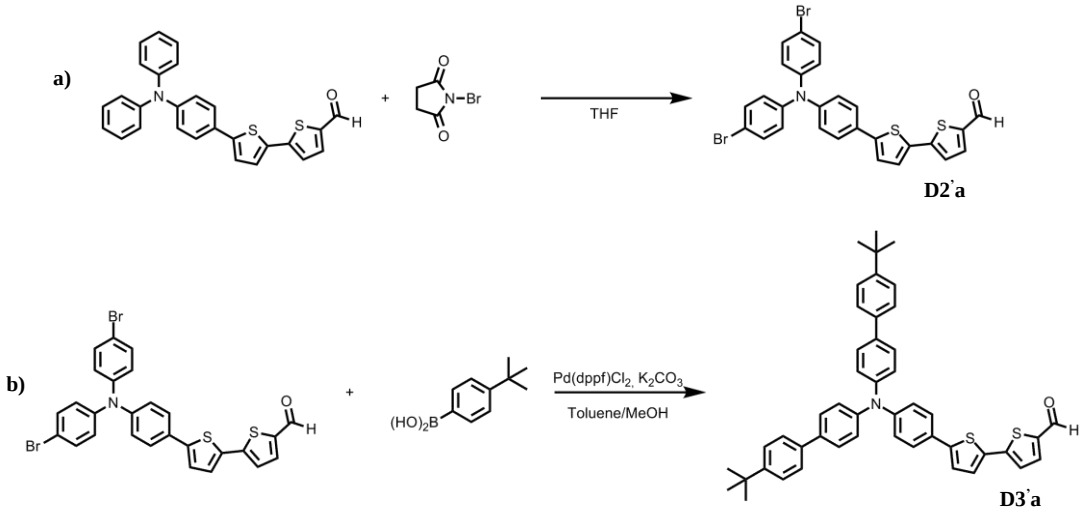

Scheme II 3. a) Bromination of the para position of the diphenylamine (compound **D2'a**); b) Suzuki cross coupling to achieve the chromophore **D3'a**.

From both the reactions were isolated the compounds in good yields (>70%).

Through a Knoevenagel condensation using absolute ethanol or dry CH_3CN (depending on the α-acid derivative) I synthesized the different members of each series starting from the respective aldehyde (**1'a**, **2'a** or **3'a**).The reaction condition were optimized in order to obtain the direct precipitation of the final chromophores which is not soluble in the solvent used for the synthesis, therefore the compound was isolated without further purification (for the scheme of the reaction see the **Scheme II 4**). To accelerate the reaction, a catalytic amount of β-alanine was used to facilitate the deprotonation of the α-position of the carbonyl. I was not able to isolate the pure chromophore D3'b and it was not possible to purified it easily.

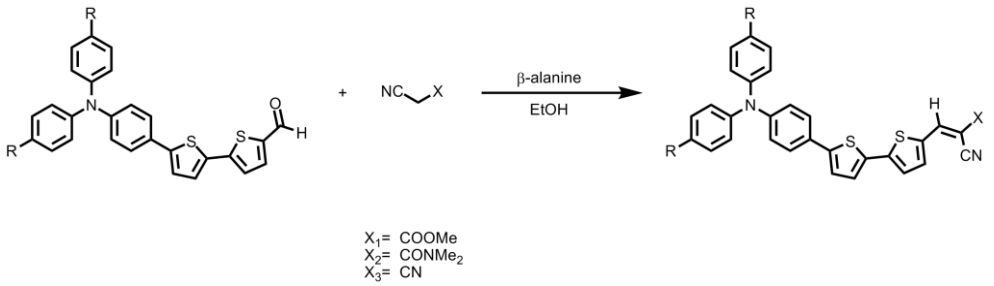

Scheme II 4. Knoevenagel condensation used to synthesize the members of the three series.

2.2. Elongating the π-conjugated bridge (synthesis of the chromophore D1‴a)

The π-conjugated bridge of the compound **D1‴a** was synthesized starting from the commercially available fluorene in three steps. The first one is the bis-iodination of the fluorene in position 2 and 7 using strong conditions shown in **Scheme II 5**.

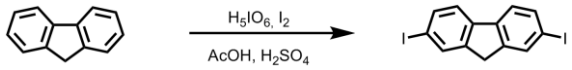

Scheme II 5. Preparation of the 2,7-diiodofluorene

To increase the solubility of the synthon and to prevent the strong intermolecular interaction that can occur in the target molecule upon aggregation, two branched iso-pentyl chain were added in the methylene bridge *via* alkylation as described in **Scheme II 6**.

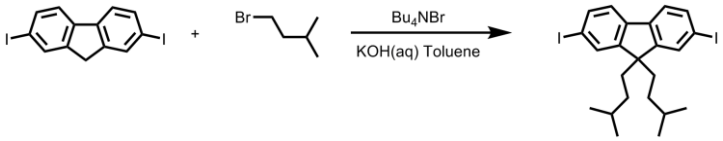

Scheme II 6. Alkylation on the methylene bridge of the fluorene

Once alkylated the bridge of the fluorene, the step further was a Kumada cross coupling to elongate the π-bridge with two thiophenes, one on each side (**Scheme II 7**).

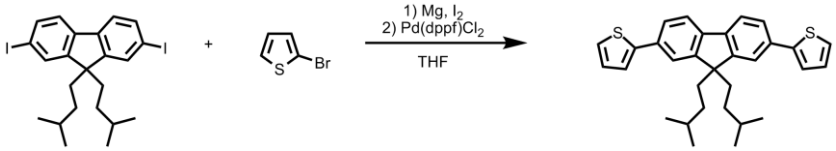

Scheme II 7. Kumada cross coupling

After the Kumada coupling the π-connector of the push-pull chromophore is completed, the next step was the mono-formylation on one thiophene of the bridge, *via* Vilsmeier-Haack reaction as displayed in the **Scheme II 8**. The introduction of CHO group in one thiophene strongly deactivates the position on the second thiophene and prevents the bis-formylation.

Scheme II 8. Mono-formylation via Vilsmeier-Haack reaction

In the last step, the thiophene was iodinated as drawn in **Scheme II 9a**, Suzuki coupling was then used to form the C-C bond between the thiophene and the triphenylamine to achieve the target molecule (**Scheme II 9b**).

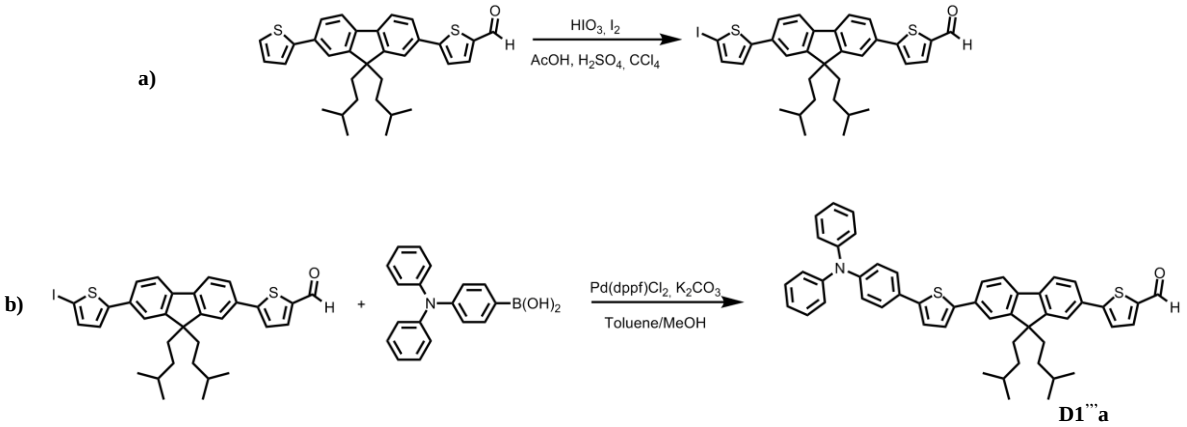

Scheme II 9. a) Iodination and b) Suzuki coupling to obtain the target molecule **D1‴a**

2.3. Crystal characterization

*2.3.1. Compound **D1ʹb***

Single crystals of chromophore **D1ʹb** were grown by slow evaporation of an oversaturated toluene solution. The compound crystallizes in a centrosymmetric monoclinic $P2_1/c$ space group. As it can be observed in **Figure II 2a**, the two thiophenes of the π-conjugated bridge are in anti conformation. Between the main plane of the bridge and the phenyl ring linked to the electron-donor moiety there is a torsion angle of 9°.

The molecules within the crystal lattice are organized in parallel and oblique (62°) planes with short contacts: 3.26 Å and 3.38 Å respectively (see **Figure II 2b-d**).

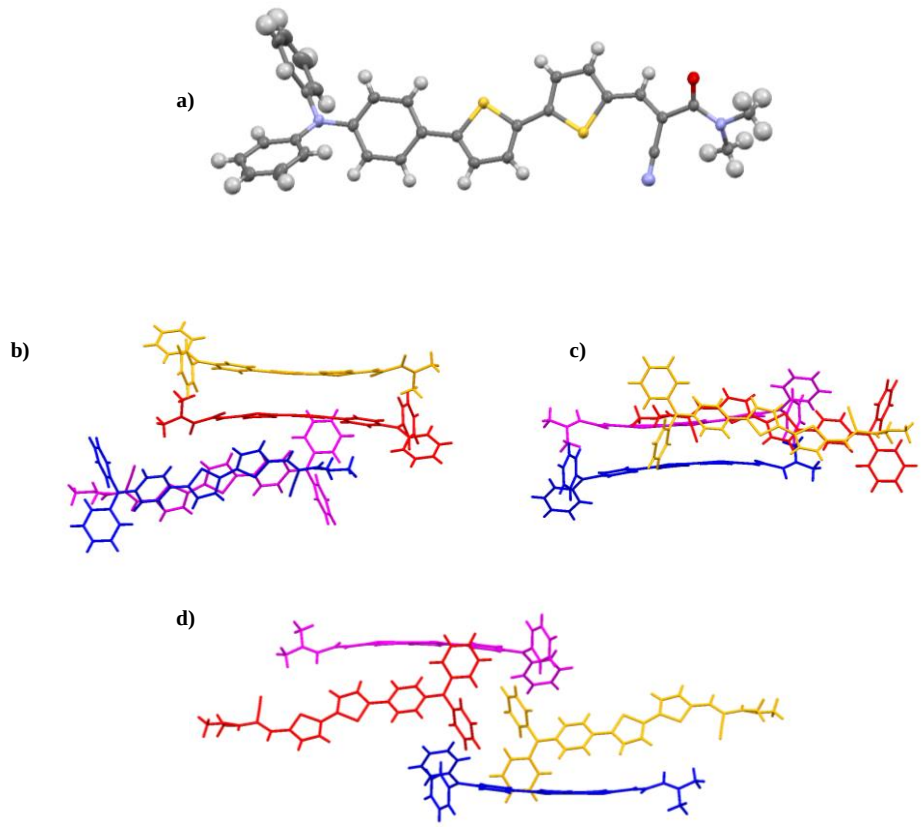

Figure II 2. a) **D1'b** in general position and different view of the packing b) and c) π-π interaction between the π-conjugated bridge, d) edge-to-edge dimer between two triphenylamine

*2.3.2. Compound **D1'c***

Chromophore **D1'c** crystallizes in a monoclinic enantiomorphic C2 space group and single crystals for XRD were obtained by slow evaporation of a supersaturated solution of THF. Additional disordered solvent molecules were found in the crystal lattice, but unfortunately they could not be refined and thus the SQUEEZE command was applied during the structural resolution. As can be observed in the **Figure II 3a** the two thiophene rings of the π-bridge adopt a syn-conformation, which induces a significant torsion angle of 20° between the phenyl ring and the thienyl group, while between the two thiophenes along the π-conjugation the twisting angle is 22°.

The molecules within the crystal lattice are organized in antiparallel configuration forming dimers with a short π-π distance between the bridges (3.52 Å) as displayed in **Figure II 3b-c**.

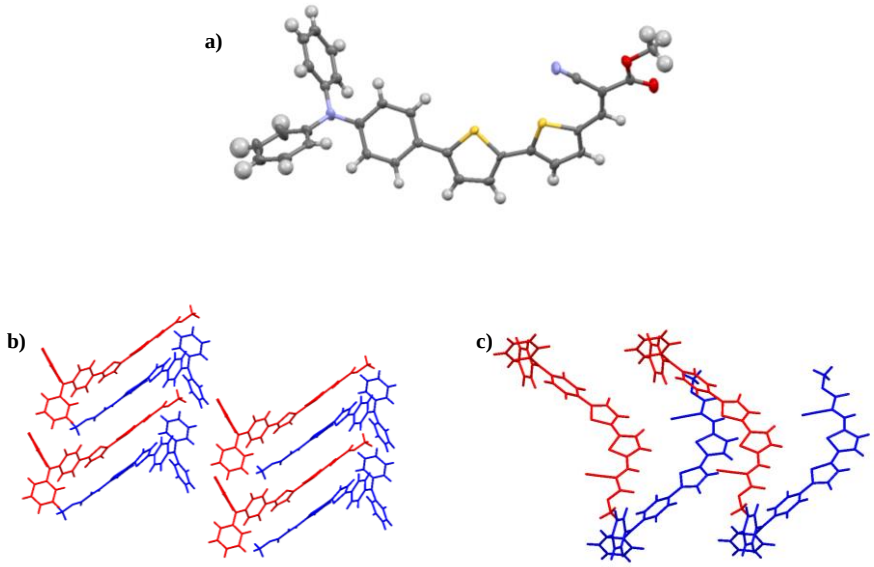

Figure II 3. a) **D1'c** in general position; , b) view of the crystal packing along the b axis c) view of the crystal packing along the a axis

*2.3.3. Compound **D2'b***

Single crystals of chromophore **D2'b** were obtained by slow evaporation of an oversaturated solution of CH_2Cl_2. The compound crystallizes in a centrosymmetric monoclinic $P2_1/c$ space group with one molecule of solvent each molecule of dye (see **Figure II 4a**).

Like compound **D1'c** also this chromophore shows a syn-conformation of the thiophenes in the crystalline state. The torsion angle between the two thienyl groups of the bridge is 18°, while the twisting between the phenyl ring linked to the donor moiety and the thiophene is 32°.

As it can be observed in **Figure II 4b**, thanks to a medium-weak hydrogen bonding interaction (CH•••O 3.33 Å)[18] a linear dimer is formed. The packing is completed with two short Van der Waals interactions: π-π between two bridges 3.29 Å (blue dashed line in **Figure II 4c**) and CH-π between two triphenylamine moieties of two neighbor molecules (3.48-3.63 Å) (green dashed line in **Figure II 4c**).

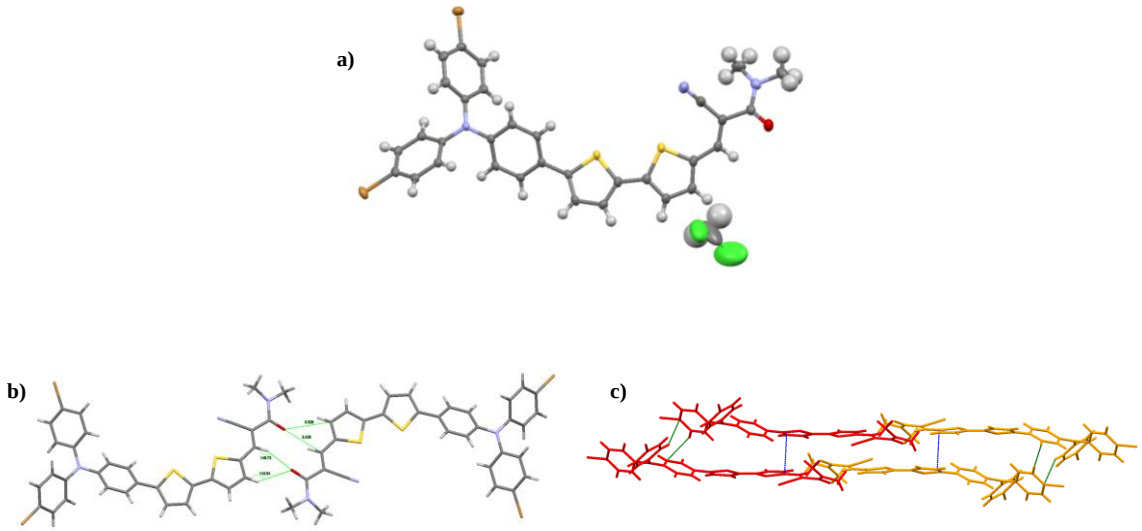

Figure II 4. a) **D2'b** in general position with the solvent of crystallization in the crystal lattice b) Dimerization of the chromophores through weak hydrogen bond c) Interaction between two parallel layers

*2.3.4. Compound **D1'''a***

Single crystals of **D1'''a** were grown by slow diffusion of pentane layered over a supersaturated solution of the compound in dichloromethane. The chromophore crystallizes in a centrosymmetric monoclinic space group ($P2_1/c$).

The π-conjugated bridge can be divided in two parts distinguishing the torsion angle between the thiophenes and the fluorene core. The thienyl group linked with the donor moiety (NPh_3) is placed on the same plane as fluorene (0.6° of torsion angle), while the thiophene linked to the electron-acceptor group displays a significant torsion of 41° with the main plane of the fluorene unit (**Figure II 5a**). Moreover, the branched alkyl chains on the core form a cross-like structure with the fluorene (89°), and this is consistent with what is found in literature[19].

It is interesting to highlight the packing of this chromophore. The molecules are arranged in head-to-tail configuration forming a rod, as it can be observed in the **Figure II 5b**. The layers are

formed thanks to short π-π (3.40 Å) and CH-π (3.58 Å) interaction in parallel and obliquely (63° between the molecular planes), despite the hindering groups on the fluorene moiety (**Figure II 5c**).

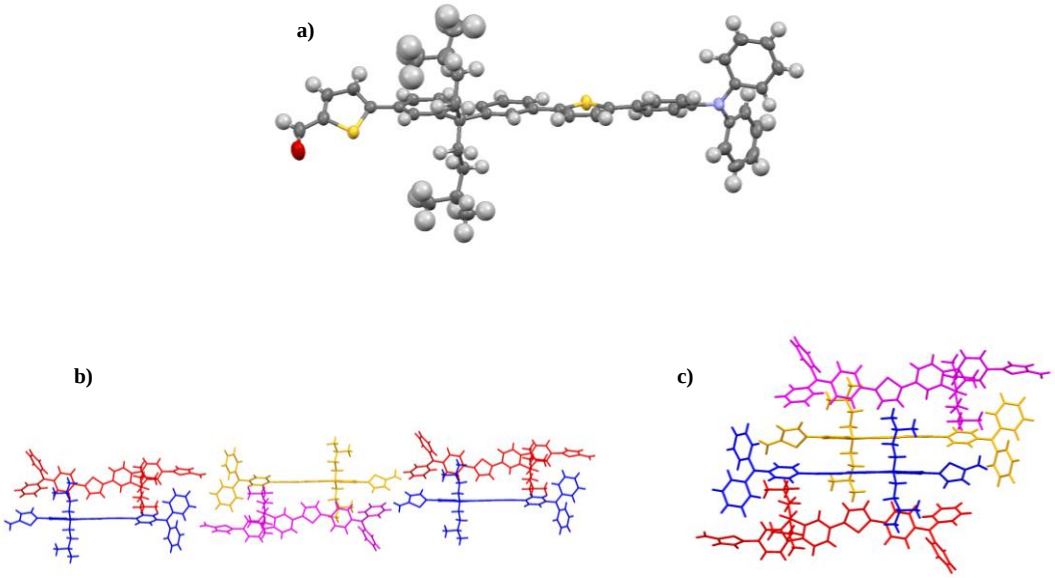

Figure II 5. a) **D1'''a** in a general position b) Packing between two layers c) Pile of chromophores

3. Linear optical properties of chromophores in organic solvents

For the dipolar chromophores, subject of this chapter, the linear and non-linear optical properties in molecular solutions were studied. For an easy comprehension, because of the large amount of compounds, the chromophores are compared under three different viewpoints: the effect of the acceptor, the effect of the para-substituent and the effect of the π-conjugated bridge.

3.1. Effect of the environment

The influence of the environment on the photophysical properties was investigated by studying both absorption and emission in organic solvents, tuning the solvent polarity.

In **Figure II 6** is displayed the comparison between the absorption spectra measured for two chromophores of the series **D3'** (**a** and **d**) increasing the solvent polarity from cyclohexane to

dimethylsulfoxide. As one can see the ICT transition is not affected by the environment suggesting that the main contribution to the ground state is given by the neutral form of the molecule. It is important to notice that the chromophore with the dicyanovinyl moiety as acceptor (**D3'd**) in DMSO displays a behavior that is attributable to the retro-Knoevenagel reaction that occurs in polar solvents, which can contains traces of water that favor the hydrolysis.

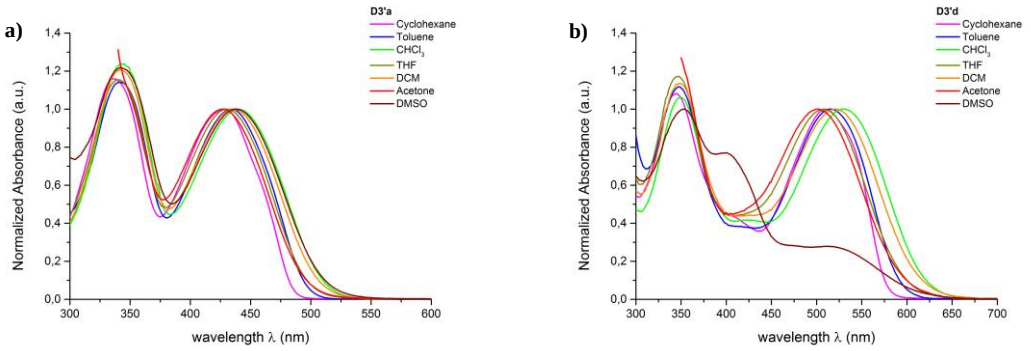

Figure II 6. Comparison between the absorption spectra measured for the chromophores a) **D3'a** and b) **D3'd**, increasing the solvent polarity

Contrarily to what we observed for absorption, the increase of the solvent polarity strongly affects the luminescence properties. In fact, the tuning of the solvents from cyclohexane to DMSO induces a marked bathochromic shift of the transition with a consequent broadening of the emission band (see **Figure II 7**) and a quenching of the fluorescence quantum yield, due to competitive non-radiative decay[20]. The positive solvatochromic behavior is coherent with an ICT transition that is associated with a large enhancement of the dipolar moment upon excitation, suggesting that the main contribution to the excited state is given by the zwitterionic form, which is stabilized by the interactions with polar solvents, therefore the excited state lies to lower energy.

The hydrolysis also strongly affects the emission. As it can be observed in **Figure II 7c,e,f**, the chromophores bearing strong acceptor such as cyanoester (**c**), dicyanovinyl (**d**) and DETB (**e**) display different properties compared to the expectations. This is an important issue that will be discussed in **Chapter 3**.

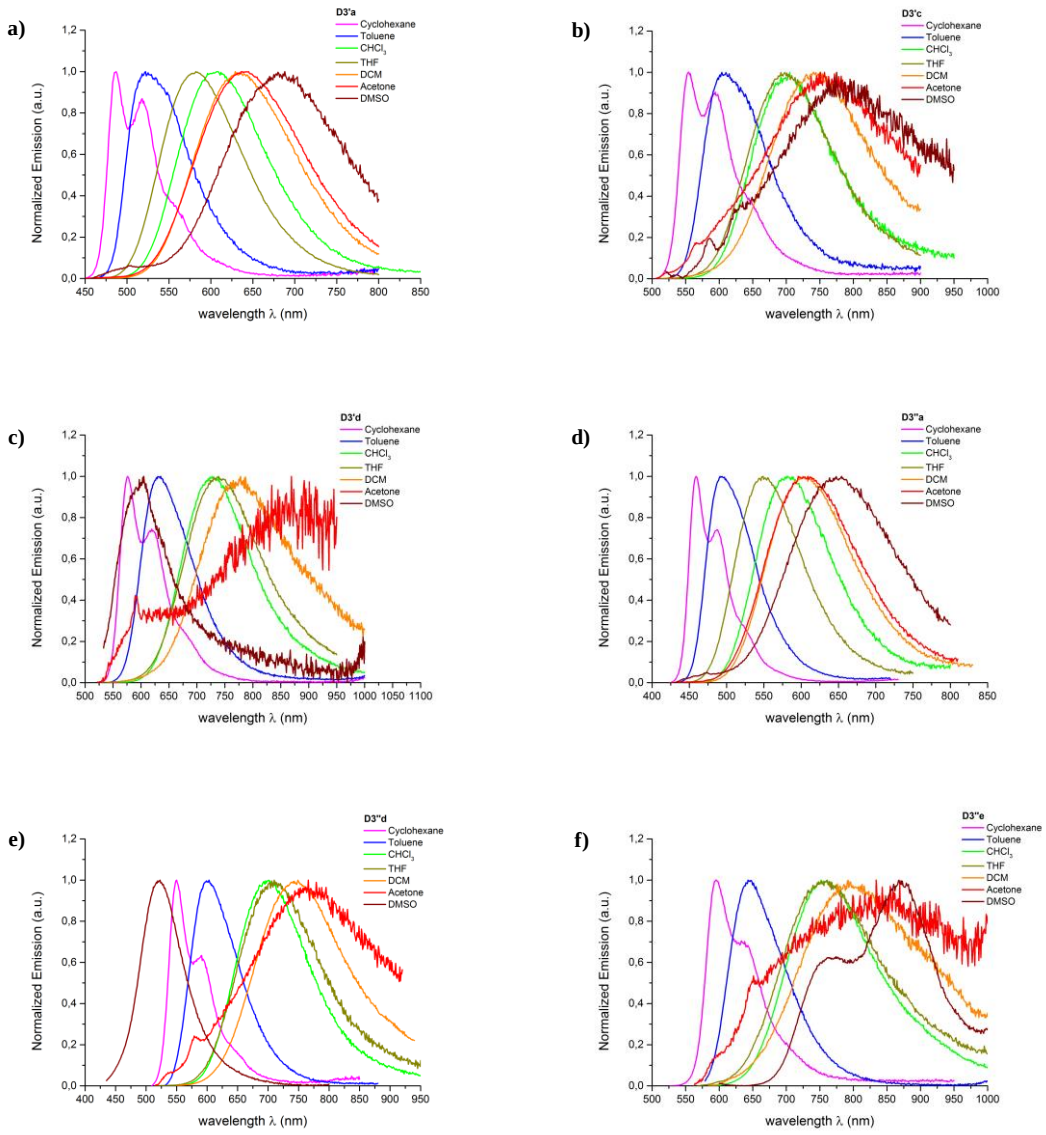

Figure II 7. Comparison between the emission spectra measured increasing the solvent polarity for the chromophores a) **D3'a;** b) **D3'c;** c) **D3'd;** d) **D3''a,** e) **D3''d** and f) **D3''e**.

Interestingly, the solvatochromic behavior can be fitted with a Lippert-Mataga correlation[21-23] as the Stokes shift are found linearly dependent on the polarity-polarisability parameter of the solvent Δf:

Eq II 1. $$\nu_{abs} - \nu_{em} = 2\left(\Delta\mu^2/_{hca^3}\right)\Delta f + const$$

Where ν_{abs} (ν_{em}) is the energy of the absorption (emission) maximum given in wavenumber, *h* is the Planck constant, *c* is the light velocity, *a* is the radius of the Onsager cavity (assumed to be spherical), $\Delta\mu$ is the change of the dipole moment of the solute upon excitation and

Eq II 2. $$\Delta f = \left(\varepsilon - a/2\varepsilon + 1\right) - \left(n^2 - 1/2n^2 + 1\right)$$

where ε is the dielectric constant, *n* is the refractive index of the solvent.

We can estimate the value of the photo-induced change of the dipole moment of the chromophores by deriving $\Delta\mu$ from the Lippert-Mataga correlation (**Eq II 1**) using the Perrin equation[23,24]

Eq II 3. $$2\left(\Delta\mu^2/hca^3\right) = Specific\ solvatochromic\ shift$$ (derived from the slope of the Lippert-Mataga correlation)

Eq II 4. $$a = \sqrt[3]{v}$$

Eq II 5. $$v = kT\theta/\eta$$

Eq II 6. $$\theta = \tau/\frac{0.4}{<r>} - 1$$

Table II 1. Solvatochromism and anisotropy measurements on the chromophores of the **D3'** series measured in triacetin solution at 20°C.

Cpd	Specific Solvatochromic Shift [cm^{-1}]	$<r>^{a)}$	$\tau^{b)}$ [ns]	$\theta^{c)}$ [ns]	$v^{d)}$ [$Å^3$]	$a^{e)}$ [Å]	$\Delta\mu$ [D]
D3'a	$17.8 \cdot 10^3$	0.22	3.5	4.3	1018	6.2	20.7
D3'c	$15.6 \cdot 10^3$	0.35	1.1	7.1	1697	7.4	25.1
D3'd	$17.0 \cdot 10^3$	0.36	0.8	6.9	1650	7.3	25.8

a) medium value of anisotropy measured in triacetin solution at 20°C, b) lifetime measured in triacetin at 20°C, c) longitudinal rotational correlation time, d) volume of the molecule, e) Onsager cavity radius (approximated to be spherical)

The large slope values obtained underline an expected large increase of the dipolar moment in the excited state for the chromophores. Comparing the values of $\Delta\mu$ in the same series (as displayed in the **Table II 1**), it can be noticed a marked enhancement of the photo-induced change of dipole moment passing from the aldehyde to the cyanoester (**D3'a** → **D3'c**) as acceptor group. This behavior is consistent with an increase of the dipolar strength that generates a highly polarized molecule in the excited state. On the other hand, replacing the acceptor group from **c** to **d** does not affect strongly the $\Delta\mu$.

3.2. Effect induced by the tuning of the acceptor group

In this paragraph are reported the results obtained in the photophysical properties by tuning the acceptor group (from aldehyde to DETB)[25] in order to study the dependence of the properties from the dipolar strength. For an easy overview here are compared the members of three different series: **D1'**, **D3'**, **D3"**. In **Table II 2** are gathered the relevant data measured for the three families of chromophores in $CHCl_3$ solution. Chloroform was chosen as common solvent thanks to its medium-low polarity character for further comparison with the molecules confined in nano-environment.

The chromophores of these three families display an absorption band located in the visible spectral region ranging from blue to orange, depending on the acceptor. The intense band is ascribed to an intramolecular charge transfer (ICT) transition that could be associated with a combination of n-π^* and π-π^* transitions, while the band located in the UV spectral region can be attributed to the higher energetic π-π^* transition. As one can notice, in **Figure II 8**, this transition is emphasized in the families **D3'** and **D3"** thanks to the presence of the tertbutyl-phenyl as para-substituent in the triphenylamine moiety. From the **Figure II 8** one can clearly observe that an enhancement of the dipolar strength induces a marked bathochromic shift of the ICT band, associated with a narrowing of the absorption band (**Table II 2**), which indicates an increase of polarization of the ground state, enhancing the contribution of the zwitterionic state. One can expect that, after an increase of the electron-withdrawing strength, with a consequent enhancement of the dipolar moment, the ICT transition is

more probable, leading to higher molar extinction coefficients[12]. This is not what we can observe from the **Table II 2** and from the **Figure II 8**. While the trend of the family **D3**" follows the expectations increasing the molar extinction coefficient from 3.9 to 5.5 · 10^4 M^{-1} cm^{-1} passing from the aldehyde (CHO) to the 1,3-diethyl-thiobarbiturate (DETB), in the other two families this behavior is not observable, the ε_{max} measured in chloroform are comparable, ranging from 3.1 and 3.7 · 10^4 M^{-1} cm^{-1} for **D1**' and between 3.3 and 3.7 · 10^4 M^{-1} cm^{-1} for **D3**'.

Table II 2. One-photon photophysical data measured in $CHCl_3$ solution for the chromophores of the families **D1'a-d**, **D3'a-d**, **D3"a-e**.

Cpd	λ_{max}^{1PA} [nm]	FWHM [10^3 cm^{-1}]	ε_{max} [10^4 $M^{-1}cm^{-1}$]	λ_{max}^{em} [nm]	Stokes shift [10^3 cm^{-1}]	Φ_f	τ_1/τ_2 [ns]	k_r [$10^9 s^{-1}$]	k_{nr} [$10^9 s^{-1}$]
D1'a	432	4.6	3.1	586	6.1	0.80	3.1	0.26	0.06
D1'b	469	4.7	3.7	648	5.9	0.50	1.3 (0.2)/2.7 (0.8)	0.23	0.23
D1'c	495	4.4	3.7	680	5.5	0.60	3.1	0.19	0.13
D1'd	521	4.0	3.3	706	5.0	0.55	3.0	0.18	0.15
D3'a	441	4.7	3.3	607	6.2	0.80	3.4	0.24	0.06
D3'c	503	4.6	3.7	705	5.7	0.40	2.5	0.16	0.24
D3'd	530	4.2	3.5	748	5.5	0.25	1.5	0.17	0.50
D3"a	429	4.2	3.9	582	6.1	0.70	3.3	0.21	0.09
D3"d	525	3.7	4.5	700	4.8	0.25	1.9	0.13	0.39
D3"e	576	3.4	5.5	755	4.1	0.06	0.6	0.10	1.57

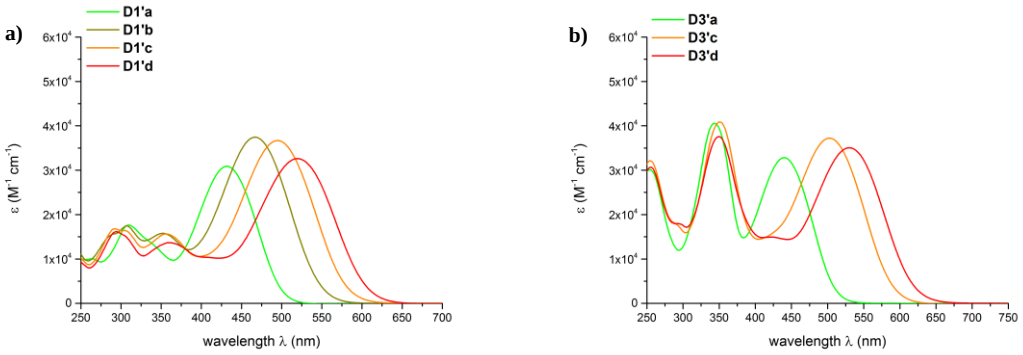

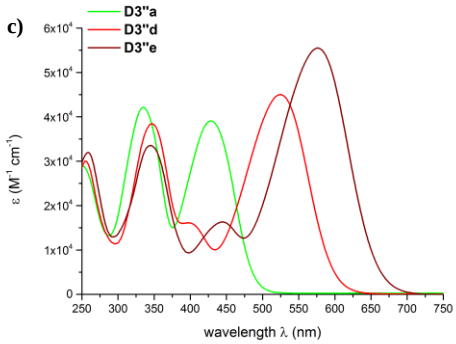

Figure II 8. Comparison between the one-photon absorption spectra measured for the different members of the dye family a) **D1**'; b) **D3**' and c) **D3**'' in $CHCl_3$ solution.

As observed for the absorption properties, the luminescent properties of these families of dyes are strongly affected by the nature of the acceptor moiety, as shown in **Figure II 9.** An increase of the dipolar strength induces a marked bathochromic shift in the emission band. Tuning the acceptor group towards higher electron-withdrawing moiety, we were able to cover the visible range from yellow to near infrared (NIR). Concerning the fluorescence quantum yields (Φ_f) for these chromophores in $CHCl_3$ solution, one can observe from the **Table II 2** that pushing the emission towards red or NIR spectral region leads to a decreasing of the Φ_f associated with a reduction of the fluorescence lifetime. This behavior can be ascribed to a decrease of the radiative decay rates in addition with an enhancement of non-radiative decay rates in the red/NIR spectral region[20]. It is important to underline that there is one exception among the chromophores that I presented here, in fact the chromophore **D1'b** displays an unexpected decreasing of the fluorescence quantum yield associated with a lifetime fitted with a biexponential decay. This behavior can be attributed to the presence of two different conformations of the vinyl-amide system in solution in the excited state.

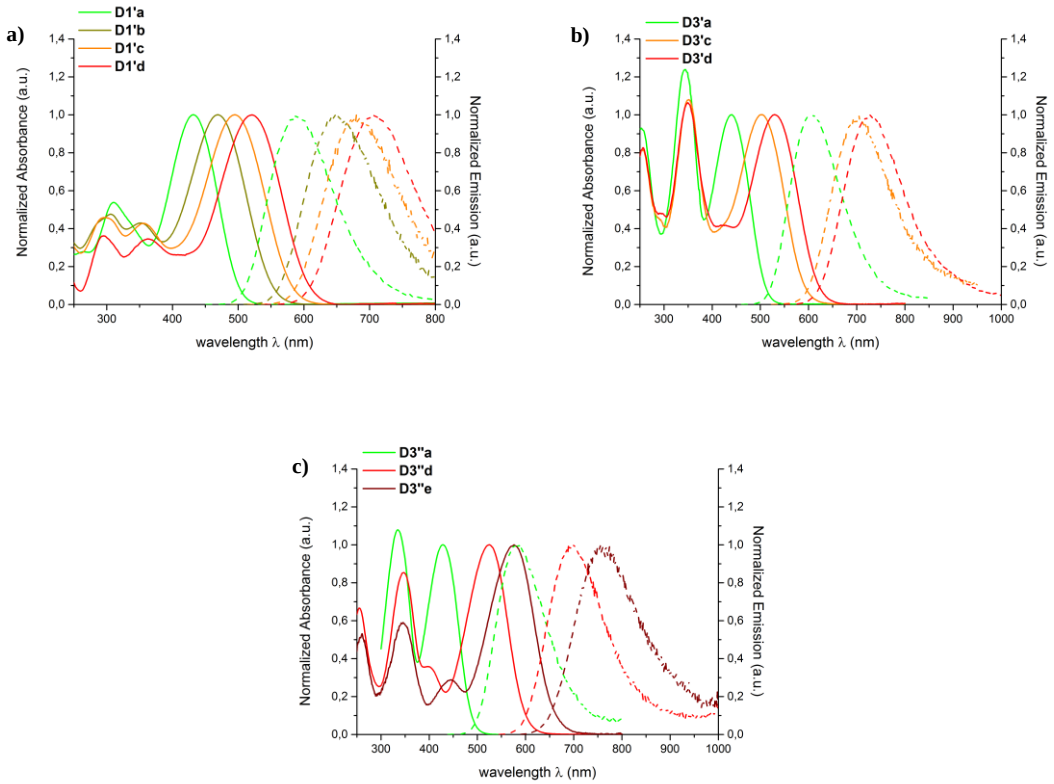

Figure II 9. Comparison between normalized absorption (solid line) and emission (dashed line) spectra measured for the different members of the dye family a) **D1**'; b) **D3**' and c) **D3**'' in $CHCl_3$ solution (*consistent color code between the figures of the paragraph*)

3.3. Effect induced by the "para-substituent" on the triphenylamine

For an easy comparison of the effect on the photophysical properties upon the replacement of the substituent on the triphenylamine, I chose to compare two different series of compounds keeping constant the acceptor moiety: **D1**'**-D3**'**c** (cyanoester) and **D1**''**-D3**''**d** (dicyano), which could help me to give a complete overview of the behavior.

In **Table II 3** are gathered the relevant data measured for the two series of chromophores in $CHCl_3$ solution.

Both families display an intense ICT band placed in the cyano-green spectral region and as already discussed beforehand, this transition is associated with a large molar extinction coefficient up to $5.4 \cdot 10^4$ M^{-1} cm^{-1}, as it can be observed in **Figure II 10** and in **Table II 3**.

Basically the idea is similar to the one explained previously, an enhancement of the push-pull effect by increasing the strength of the dipole, induces a bathochromic shift of the absorption transition. Indeed, as one can observe in **Figure II 10**, the addition of two bromine atoms in para-position on the triphenylamine donor moiety induces an hypsochromic shift related to the slight electron-withdrawing inductive effect. On the other hand, the replacement of the hydrogen with a *tert*-butylphenyl group leads to a bathochromic shift of the ICT transition thanks to the slight electron-releasing behavior. As one could expect, an enhancement of the dipolar strength should induce an hyperchromic effect of the absorption band although is not what was observed (**see Figure II 10**). In both series, the higher molar extinction coefficient is displayed by the chromophore bearing bromines as substituent, while the other two end groups lead to comparable ε_{max}.

Table II 3. One-photon photophysical data measured in $CHCl_3$ solution for the chromophores **D1'-D3'c** and **D1''-D3''d**.

Cpd	λ_{max}^{1PA} [nm]	ε_{max} [10^4 $M^{-1}cm^{-1}$]	λ_{max}^{em} [nm]	Stokes shift [10^3 cm^{-1}]	Φ_f	τ_1 [ns]	k_r [$10^9 s^{-1}$]	k_{nr} [$10^9 s^{-1}$]
D1'c	495	3.7	680	5.5	0.60	3.1	0.19	0.13
D2'c	483	3.9	652	5.4	0.75	2.8	0.27	0.09
D3'c	503	3.7	705	5.7	0.40	2.5	0.16	0.24
D1''d	511	4.2	652	4.2	0.47	2.6	0.18	0.20
D2''d	495	5.4	629	4.3	0.31	1.5	0.21	0.46
D3''d	525	4.5	700	4.8	0.34	1.9	0.18	0.35

Concerning the luminescence properties, as can be observed in **Figure II 11**, the behavior follows the one discussed for the absorption band. Tuning from –H to –Br is observable a blue-shift, while the substitution of –H with –*tert*-butylphenyl induces a bathochromic shift. However, the shift of the bands is not large indicating that the dipolar strength is only slightly affected by the replacement on the triphenylamine donor group. The bromine substituent also seem to promote efficient non-radiative decay processes (most probably intersystem crossing due to spin-orbit coupling effect) in the

case of **D2"d**, which is not observable for the chromophore **D2'c**, leading to smaller fluorescence quantum yields and shorter lifetimes.

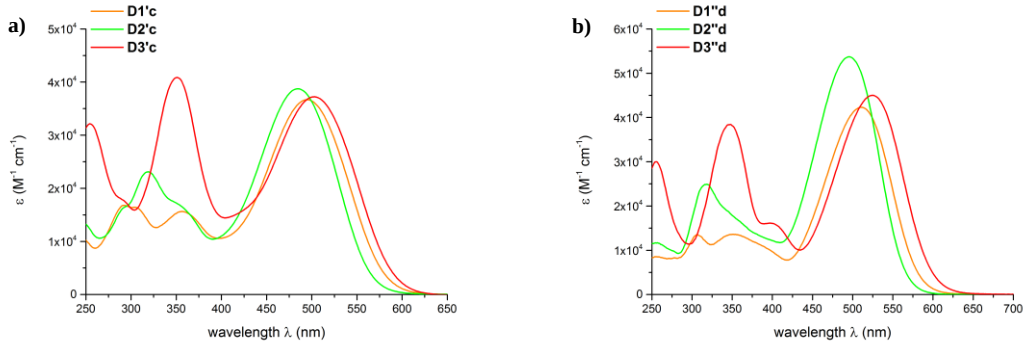

Figure II 10. Comparison between the one-photon absorption spectra measured for the different members of the series a) **D1'-D3'c**; b) **D1"-D3"d** in $CHCl_3$ solution.

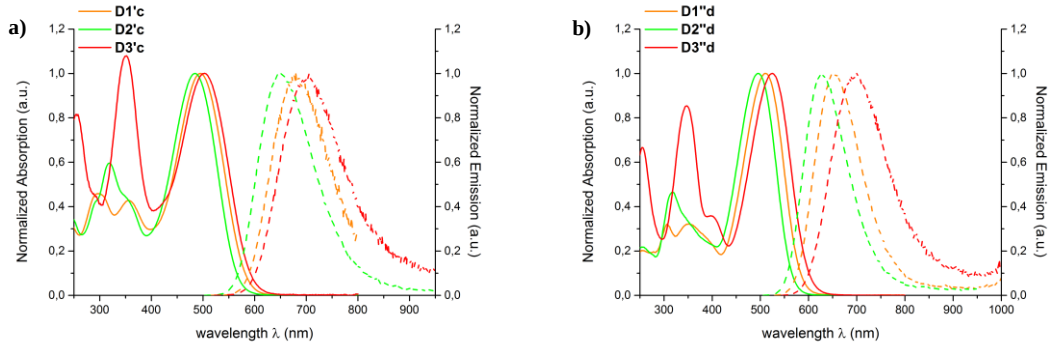

Figure II 11. Comparison between the normalized absorption (solid line) and emission (dashed line) spectra measured for chromophores a) **D1'-D3'c**; b) **D1"-D3"d** in $CHCl_3$ solution (*consistent color code between the figures of the paragraph*)

3.4. Effect of the tuning of the π-conjugated connector

In this paragraph is discussed the influence of the changes of the π bridge on the linear photophysical properties of the chromophores. As could be expected the nature of the connector can strongly affect the behavior of the compound. Here are compared three dipolar dyes **D1'a**, **D1"a** and **D1"'a** in order to display a complete overview of the behaviors. The important parameters to take into account when we want to compare the π bridge are the donor/acceptor character, the number of π

electrons and the rigidity/flexibility. The studied conjugated connectors n', n'' and n''' are displayed in **Figure II 12**.

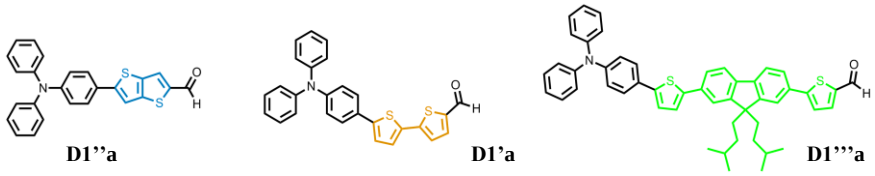

Figure II 12. Dipolar push-pull chromophores changing the π-conjugated bridge between the end-groups.

As you can observe in **Figure II 12** above, the main common constituent of the π-conjugated bridge used for the comparison is the thienyl group, which is known as good charge transmitter with a slight electron-donor character. We played on both the flexibility of the connector by replacing bis-thiophenes with a thienothiophene group, and on the length of the bridge by inserting a substituted fluorene core between the bis-thiophene π systems. This is aimed to enhance the linear and non-linear response of the chromophore.

In the **Table II 4** are gathered the relevant photophysical data measured in organic solution using chloroform as common solvent.

Table II 4. One-photon photophysical data measured in $CHCl_3$ solution for the chromophores **D1'-D1'''a**.

Cpd	λ_{max}^{1PA} [nm]	ε_{max} [10^4 $M^{-1}cm^{-1}$]	λ_{max}^{em} [nm]	Stokes shift [10^3 cm^{-1}]	Φ_f	τ_1 [ns]	k_r [$10^9 s^{-1}$]	k_{nr} [$10^9 s^{-1}$]
D1'a	432	3.1	586	6.1	0.80	3.1	0.26	0.06
D1''a	417	3.9	534	5.2	0.84	2.8	0.30	0.06
D1'''a	415	5.1	609	7.7	0.20	1.2	0.17	0.68

As displayed in **Figure II 13a** the rigidification of the connector induces a hypsochromic shift associated with a slight hyperchromic effect due to a higher transmission character. The shift towards lower wavelength can be due to the lower delocalization of the charge in the thienothiophene π-

conjugated bridge compared with the bis-thiophene. On the other hand the addition of the fluorene core within the two thiophenes provokes a marked enhancement of the molar extinction coefficient (from $3.1 \cdot 10^4$ **D1'a** to $5.1 \cdot 10^4$ **D1'''a**) associated with a blue-shift of the ICT band.

Concerning the fluorescence properties, interestingly, by tuning the bridge towards higher rigidity, one can observed a marked blue-shift of the emission band associated with a slight increasing of the fluorescence quantum yield. As displayed in **Table II 4** this structural change does not affect strongly the fluorescence lifetime as well as the radiative decay rate. While, the elongation of the conjugation by adding the fluorene induces a broadening of the emission band. The elongation induces also a marked decrease of the fluorescence quantum yield associated with an enhancement of the non-radiative decay rate compared with the chromophore **D1'a**.

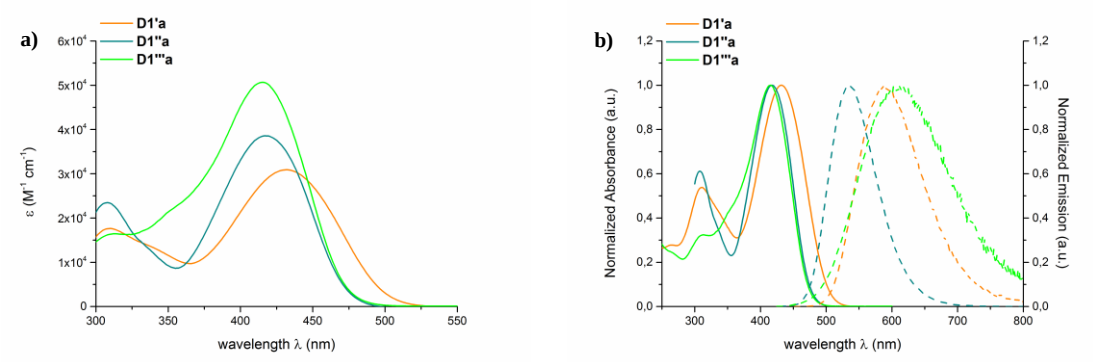

Figure II 13. a) Comparison between the one-photon absorption spectra measured for the chromophores **D1'-D1'''a** in $CHCl_3$ solution b) Normalized absorption and emission spectra measured for the chromophores **D1'-D1'''a** in $CHCl_3$ solution.

4. Non-linear optical properties of chromophores in organic solvents

Thanks to the emissive properties of these dipolar chromophores, we were able to estimate the two-photon cross section (σ_2) by measuring the two-photon brightness ($\sigma_2\Phi_f$) with the two-photon excited fluorescence (TPEF) technique widely discussed in the introductive chapter.

The measurements were done in a range between 680 nm and 1160 nm using as references Fluorescein (from 680 nm to 1000 nm) or Nile Red (from 1000 nm to 1160 nm). The range of detection was chosen depending on the λ_{max}^{1PA} as well as the range of emission.

For an easy comprehension, this section will be divided in the same paragraphs that were used in the previous section: effect of the acceptor part, effect of the "para-substituent" and effect of the π-connector. To simplify and make a complete overview, here will be displayed the non-linear optical properties of the chromophores used for the linear characterization. Since the chromophores are solvatochromic, to have a good comparison with the results obtained upon one-photon excitation, the 2PA measurements were done in chloroform.

4.1. Effect induced by the tuning of the acceptor group

As is displayed in **Figure II 14** (one member for each series was taken as an example) and in **Table II 5**, the dipolar chromophores show an intense and structured two-photon absorption band in which the maximum wavelength is almost twice the λ_{max}^{1PA} suggesting that the ICT transition is symmetrically allowed upon both one-photon and two-photon excitation. This behavior is expected for non-centrosymmetric "push-pull" chromophores.

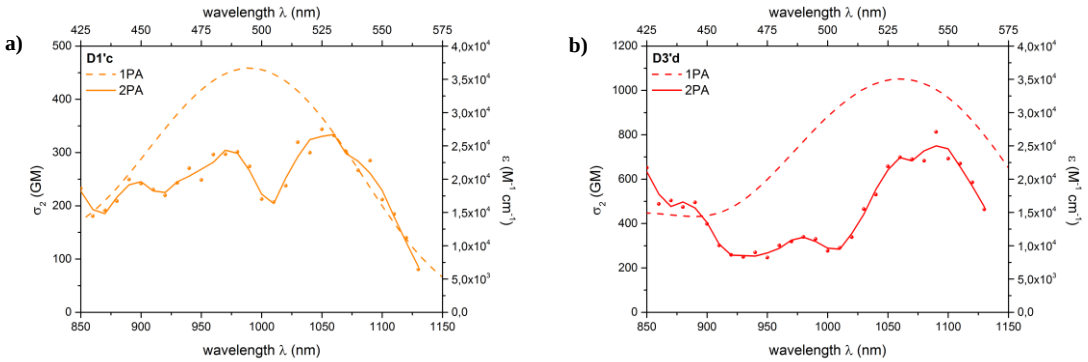

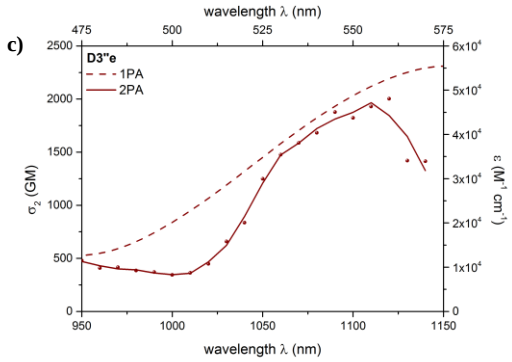

Figure II 14. Superimposition between one-photon (dashed line) and two-photon (colored point and solid line) absorption spectra of chromophores a) **D1'c**; b) **D3'd** and c) **D3"e** in $CHCl_3$ solution.

Since the one-photon absorption band is affected by the dipolar strength, you can see a parallel behavior upon excitation with two-photon. Increasing the electron-withdrawing character of the acceptor end-group leads to a marked bathochromic shift, which is associated with an enhancement of the two-photon cross section, as it can be seen in **Figure II 15**. Interestingly, the hyperchromic effect is much more pronounced for the two-photon process compared with the linear absorption, suggesting that the charge separation upon two-photon excitation is more affected by the strength of the dipole compared with the 1PA process.

Table II 5. Two-photon photophysical data measured in $CHCl_3$ solution for the chromophores of the families **D1'a-d**, **D3'a-d**, **D3"a-e**.

Cpd	$2\lambda_{max}^{1PA}$ [nm]	λ_{max}^{2PA} [nm]	σ_2 [GM]	λ_{max2}^{2PA} [nm]	σ_2 [GM]
D1'a	864	910	302	850	246
D1'b	938	940	277	890	273
D1'c	990	1050	343	980	301
D1'd	1042	1090	492	980	268
D3'a	882	940	422	850	280
D3'c	1006	1050	647	980	490
D3'd	1060	1090	813	980	340
D3"a	858	890	479	850	428
D3"d	1050	1060	1402	980	813
D3"e	1152	1120	2002	/	/

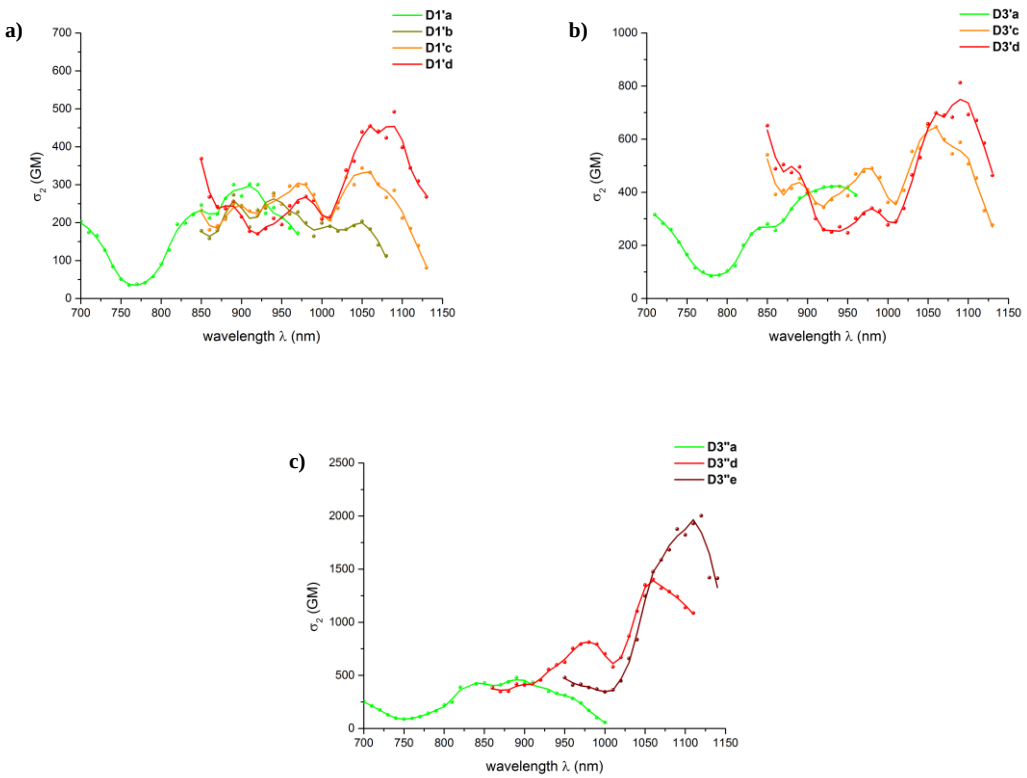

Figure II 15. Comparison between the two-photon absorption spectra measured for the different members of the family a) **D1'**; b) **D3'** and c) **D3"** in $CHCl_3$ solution.

4.2. Effect induced by the "para-substituent" on the triphenylamine

As observed in the previous paragraph, the chromophores display an intense two-photon absorption band related to the same transition observed in the linear process (**Table II 6**).

Table II 6. Two-photon photophysical data measured in $CHCl_3$ solution for the chromophores of the families **D1'a-d**, **D3'a-d**, **D3"a-e**.

Cpd	$2\lambda_{max}^{1PA}$ [nm]	λ_{max}^{2PA} [nm]	σ_2 [GM]	λ_{max2}^{2PA} [nm]	σ_2 [GM]	λ_{max3}^{2PA} [nm]	σ_2 [GM]
D3'a	990	1050	344	980	301	890	250
D3'c	966	1030	254	960	280	890	262
D3'd	1006	1050	647	980	490	890	451
D3"a	1022	1050	1164	970	951	/	/
D3"d	990	1050	778	960	933	/	/
D3"e	1050	1060	1402	980	813	/	/

The trend observed parallel the one already discussed in the previous paragraph, an increase of the dipolar strength induces an enhancement of the σ_2 associated with a bathochromic shift. As observed for the linear process, the shift caused by the replacing of the para-substituent on the donor moiety is not marked, as you can observe in **Figure II 16**. Interestingly, the 2PA spectrum displays a structured band in which the relative intensity of each sub-band depends on the electron-releasing character of the substituent on the triphenylamine. While for chromophore **D2'c** the more intense band is placed at 960 nm, in **Figure II 16a** one can see that the most red-shifted band (1050 nm) is more pronounced for the chromophore **D3'c**. The same trend is followed by the chromophores displayed in **Figure II 16b**, the higher and more shifted band belongs to the chromophore bearing the *tert*-butylphenyl group as para substituent.

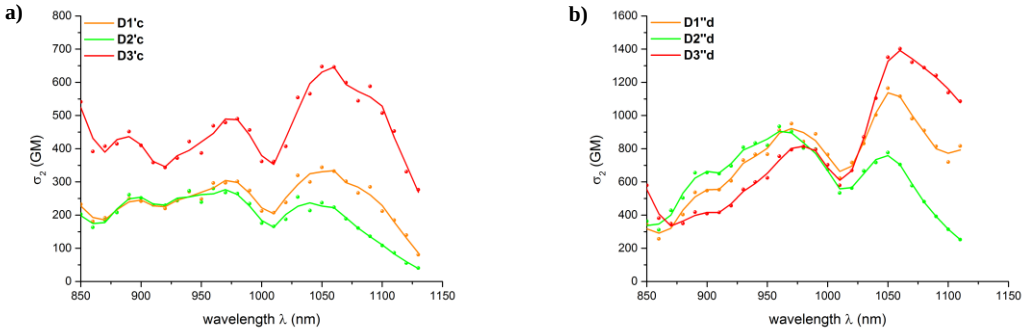

Figure II 16. Comparison between the two-photon absorption spectra measured for the different chromophores bearing the same acceptor moiety a) **c** (cyanoester); b) **d** (dicyanovinyl) in $CHCl_3$ solution.

4.3. Effect of the tuning of the π-conjugated connector

In the **Table II 7** are gathered the relevant data measured for the series of chromophores **D1a** in $CHCl_3$ solution.

Interestingly, as you can observe in **Figure II 17c**, chromophore **D1'''a** display a structured absorption in which the most allowed transition band is markedly blue-shifted compared with twice the wavelength of the ICT band upon one-photon process. A band can be also observed at 840 nm,

which is almost twice the λ_{max}^{1PA}. This was not expected for a dipolar "push-pull" chromophore, because it is a typical character for centrosymmetric dyes. Actually, this behavior can be due to another electronic transition that is more allowed upon one-photon absorption than upon two-photon absorption, thanks to the presence of the fluorene core. On the other hand, **D1'a** and **D1''a** display the expected behavior.

It is worthy to underline the fact that comparing **D1'a** and **D1'''a**, each chromophore displays a broad structured 2PA band in which the sub-bands are superimposable with different relative intensity. Moreover, the addition of the fluorene induces a strong enhancement of the two-photon cross section, paralleling the behavior observed upon one-photon excitation. This hyperchromic effect is associated to a marked blue shift due to the higher energetic most allowed two-photon transition. The rigidification of the π-conjugated bridge, passing from thienothiophene to bis-thiophene, induces a hypsochromic shift. Contrarily to what was observed for the linear process, this effect is now associated with a hypochromic effect.

Table II 7. Two-photon photophysical data measured in $CHCl_3$ solution for the chromophores of the series **D1a**.

Cpd	$2\lambda_{max}^{1PA}$ [nm]	λ_{max}^{2PA} [nm]	σ_2 [GM]	λ_{max2}^{2PA} [nm]	σ_2 [GM]	λ_{max3}^{2PA} [nm]	σ_2 [GM]
D1'a	864	910	302	850	246	/	/
D1''a	834	830	238	/	/	/	/
D1'''a	828	890	467	830	526	720	814

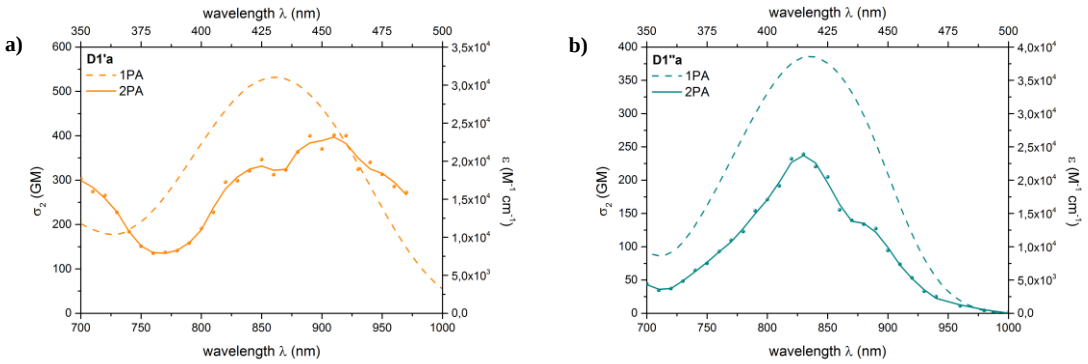

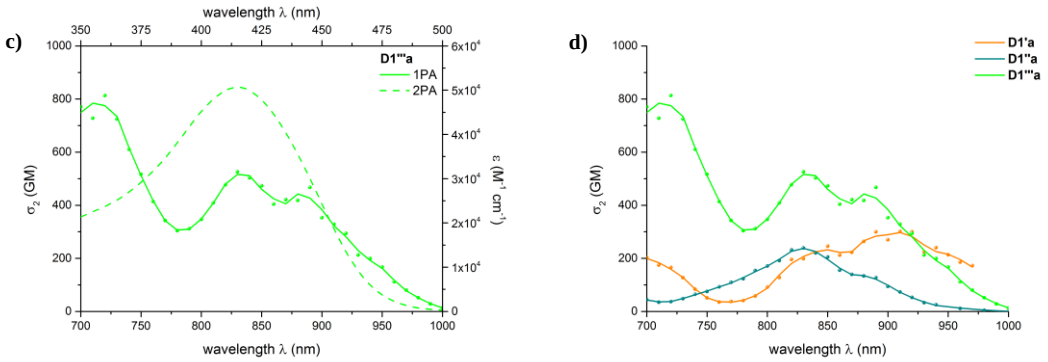

Figure II 17. Superimposition between one-photon (dashed line) and two-photon (colored point and solid line) absorption spectra of chromophores a) **D1'a**; b) **D1'''a**; c) **D1'''a** in $CHCl_3$ solution and d) comparison between the 2PA spectra measured for the different members of the series **D1a**.

5. Conclusion

In this chapter were discussed the changes of both linear and non-linear optical properties in a series of complementary "push-pull" chromophores, by tuning the chemical structure playing on the electron-withdrawing or electron-releasing strength of the end groups, as well as the properties of the π-conjugated bridge.

All dyes display an intense one-photon absorption band associated with a strong ICT transition with high molar extinction coefficient, up to $5.5 \cdot 10^4$ M^{-1} cm^{-1}. Moreover, the studied molecules show a tunable emission band ranging from green (i.e. **D1''a**) to red (i.e. **D1'c** and **D1''d**) or even NIR (i.e. **D3'd** and **D3''e**) associated with a high fluorescence quantum yield, even for the NIR dyes (i.e Φ_f = 0.55 **D1'd** and Φ_f = 0.24 **D3'd**).

The changes of the structure allowed us also to tune the two-photon absorption band in the range between 700 nm to 1150 nm enhancing the two-photon cross section up to 2000 GM in molecular solution.

In **Figure II 18** is displayed a flowchart that would resume the results obtained in $CHCl_3$ solution for the chromophores taken into account in this chapter.

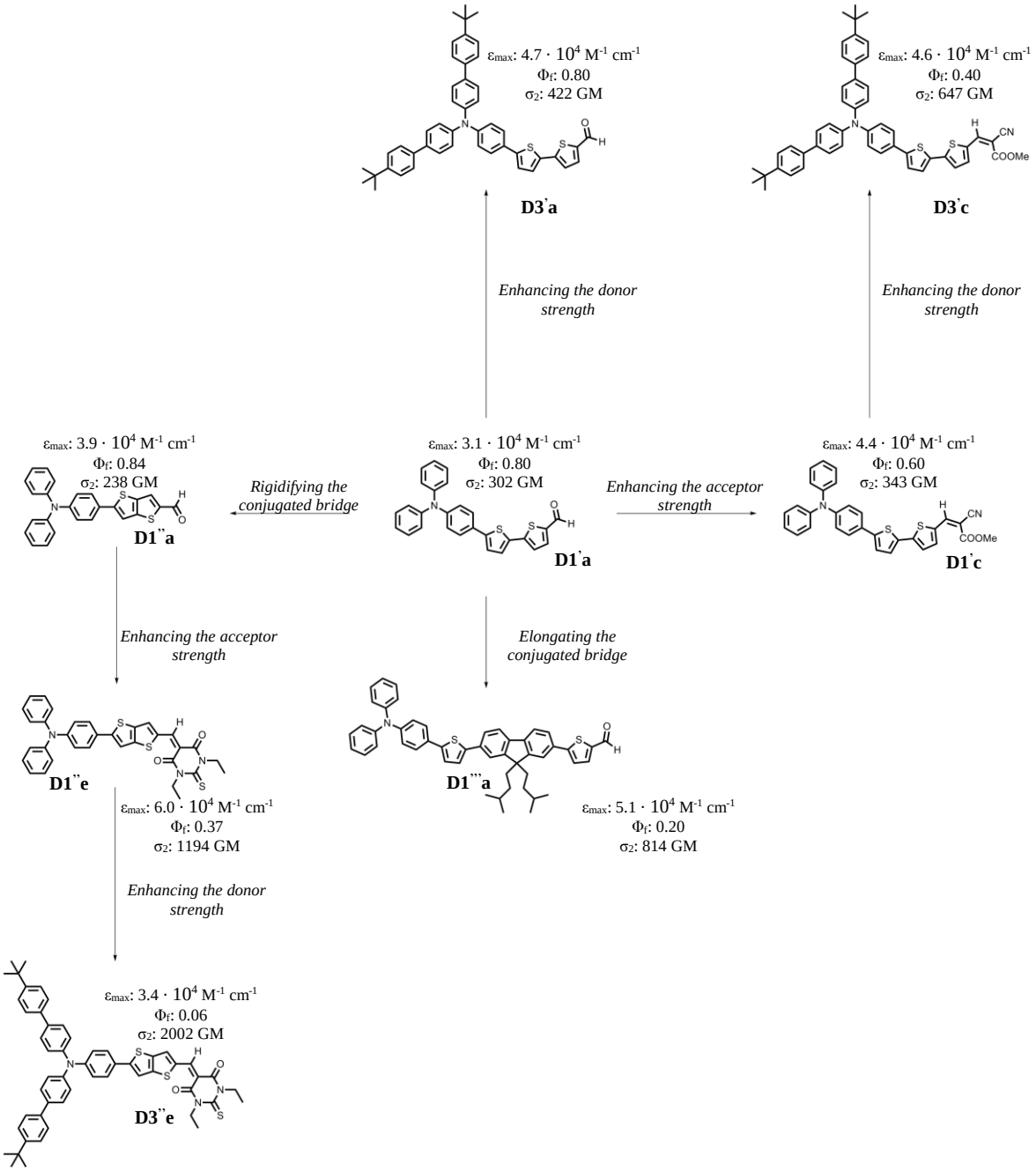

Figure II 18. Resuming flowchart of chromophores in $CHCl_3$ solution studied in this chapter

BIBLIOGRAPHIC REFERENCES

(1) Braga, D.; Grepioni, F.; GuyOrpen, A.: *Crystal Engineering: From Molecules and Crystals to Materials*; Springer Science, 1999.

(2) Papadopoulos, M. G.; Sadlej, A. J.; Leszczynski, J.: *Non-Linear Optical Properties of Matter From Molecules to Condensed Phases*; Springer, 2006.

(3) Steybe, F.; Effenberger, F.; Gubler, U.; Bosshard, C.; Günter, P. Highly polarizable chromophores for nonlinear optics: syntheses, structures and properties of donor-acceptor substituted thiophenes and oligothiophenes. *Tetrahedron* **1998**, *54*, 8469-8480.

(4) Alain, V.; Thouin, L.; Blanchard‐Desce, M. Molecular engineering of push‐pull phenylpolyenes for nonlinear optics: improved solubility, stability, and nonlinearities. *Molecular engineering of push‐pull phenylpolyenes for nonlinear optics: improved solubility, stability, and nonlinearities* **1999**.

(5) Blanchard‐Desce, M.; Alain, V.; Bedworth, P. V.; Marder, S. R.; Fort, A.; Runser, C.; Barzoukas, M.; Lebus, S.; Wortmann, R. Large quadratic hyperpolarizabilities with donor‐acceptor polyenes exhibiting optimum bond length alternation: correlation between structure and hyperpolarizability. *Chemistry - A European Journal* **1997**, *3*, 1091-1104.

(6) Painelli, A. Amplification of NLO responses: vibronic and solvent effects in push–pull polyenes. *Chemical Physics* **1999**, *245*, 185-197.

(7) Laage, D.; Thompson, W. H.; Blanchard-Desce, M.; Hynes, J. T. charged push−pull polyenes in solution: anomalous solvatochromism and nonlinear optical properties. *The Journal of Physical Chemistry A* **2003**, *107*, 6032-6046.

(8) Katan, C.; Terenziani, F.; Mongin, O.; Werts, M. H. V.; Porrès, L.; Pons, T.; Mertz, J.; Tretiak, S.; Blanchard-Desce, M. Effects of (multi)branching of dipolar chromophores on photophysical properties and two-photon absorption. *The Journal of Physical Chemistry A* **2005**, *109*, 3024-3037.

(9) Akemann, W.; Laage, D.; Plaza, P.; Martin, M. M.; Blanchard-Desce, M. Photoinduced intramolecular charge transfer in push−pull polyenes: effects of solvation, electron-donor group, and polyenic chain length. *The Journal of Physical Chemistry B* **2008**, *112*, 358-368.

(10) Genin, E.; Gao, Z.; Varela, J. A.; Daniel, J.; Bsaibess, T.; Gosse, I.; Groc, L.; Cognet, L.; Blanchard‐Desce, M. "Hyper‐bright" near‐infrared emitting fluorescent organic nanoparticles for single particle tracking. *Advanced Materials* **2014**, *26*, 2258-2261.

(11) Amro, K.; Daniel, J.; Clermont, G.; Bsaibess, T.; Pucheault, M.; Genin, E.; Vaultier, M.; Blanchard-Desce, M. A new route towards fluorescent organic nanoparticles with red-shifted emission and increased colloidal stability. *Tetrahedron* **2014**, *70*, 1903-1909.

(12) Genin, E.; Hugues, V.; Clermont, G.; Herbivo, C.; Castro, M. C. R.; Comel, A.; Raposo, M. M. M.; Blanchard-Desce, M. Fluorescence and two-photon absorption of push–pull aryl (bi) thiophenes: structure–property relationships. *Photochemical & Photobiological Sciences* **2012**, *11*.

(13) Morales, A. R.; Frazer, A.; Woodward, A. W.; Ahn-White, H.-Y.; Fonari, A.; Tongwa, P.; Timofeeva, T.; Belfield, K. D. Design, synthesis, and structural and spectroscopic studies of push–pull two-photon absorbing chromophores with acceptor groups of varying strength. *The Journal of Organic Chemistry* **2013**, *78*, 1014-1025.

(14) Mastrodonato, C.; Pagano, P.; Daniel, J.; Vaultier, M.; Blanchard-Desce, M. Molecular-based fluorescent nanoparticles built from dedicated dipolar thienothiophene dyes as ultra-bright green to nir nanoemitters. *Molecules* **2016**, *21*, 1227.

(15) Terenziani, F.; Katan, C.; Badaeva, E.; Tretiak, S.; Blanchard‐Desce, M. Enhanced two‐photon absorption of organic chromophores: theoretical and experimental assessments. *Advanced Materials* **2008**, *20*, 4641-4678.

(16) Sissa, C.; Werts, H. V.; Blanchard-Desce, M.; Terenziani, F. The effectiveness of essential-state models in the description of optical properties of branched push–pull chromophores. *Physical Chemistry Chemical Physics* **2010**, *12*.

(17) Khanasa, T.; Jantasing, N.; Morada, S.; Leesakul, N.; Tarsang, R.; Namuangruk, S.; Kaewin, T.; Jungsuttiwong, S.; Sudyoadsuk, T.; Promarak, V. Synthesis and characterization of 2d‐d‐π‐a‐type organic dyes bearing bis (3,6‐di‐tert‐butylcarbazol‐9‐ylphenyl) aniline as donor moiety for dye‐sensitized solar cells. *European Journal of Organic Chemistry* **2013**, *2013*, 2608-2620.

(18) Desiraju, G. R. Hydrogen bridges in crystal engineering: interactions without borders. *Accounts of chemical research* **2002**, *35*, 565-573.

(19) Destri, S.; Pasini, M.; Botta, C.; Porzio, W.; Bertini, F.; Marchiò, L. Synthesis and crystal structure and optical properties of fluorenic-core oligomers. *Journal of Materials Chemistry* **2002**, *12*, 924-933.

(20) Strickler, S. J.; Berg, R. A. Relationship between absorption intensity and fluorescence lifetime of molecules. *The Journal of Chemical Physics* **1962**, *37*, 814.

(21) Lippert, E. Dipolmoment und Elektronenstruktur von angeregten Molekülen. *Zeitschrift für Naturforschung A* **1955**, *10*, 541-545.

(22) Mataga, N.; Kaifu, Y.; Koizumi, M. The solvent effect on fluorescence spectrum, change of solute-solvent interaction during the lifetime of excited solute molecule. *Bulletin of the Chemical Society of Japan* **1955**, *28*, 690-691.

(23) Lakowicz, J. R.: *Principles of Fluorescence Spectroscopy*; 3rd ed.; Springer US, 2006.

(24) Perrin, F. Polarisation de la lumière de fluorescence. Vie moyenne des molécules dans l'etat excité. *J. Phys. Radium* **1926**, *7*, 390-401.

(25) Hansch, C.; Leo, A.; Taft, R. W. A survey of Hammett substituent constants and resonance and field parameters. *Chemical Reviews* **1991**, *91*, 165-195.

CHAPTER 3

DIPOLAR CHROMOPHORES

IN CONFINED ENVIRONMENT

CHAPTER 3–DIPOLAR CHROMOPHORES IN CONFINED ENVIRONMENT

1. Introduction

The "nano-world" is gaining an overwhelming role thanks to the versatility of the nanoobjects, especially when we speak about organic nanoparticles with which we can synthesize molecules with expected properties in order to obtain nanoaggregates with specific behaviors. In this chapter will be described the morphological and both linear and non-linear optical properties of fluorescent organic nanoparticles, so called FONs, prepared starting from dipolar chromophores discussed in **Chapter 2**.

The main peculiarity of dipolar molecules is their tendency to form dipole-dipole interaction in aggregated state, which can include highly concentrated solution, nanoparticles and solid state. The normal arrangement for dipoles is the so-called antiparallel configuration as displayed in **Illustration III 1**; this distribution of chromophores leads to strong intermolecular interaction. This antiparallel arrangement of the molecules decreases strongly the overall polarization of the system, moreover it can also cause an enhancement of intermolecular charge transfer transition.

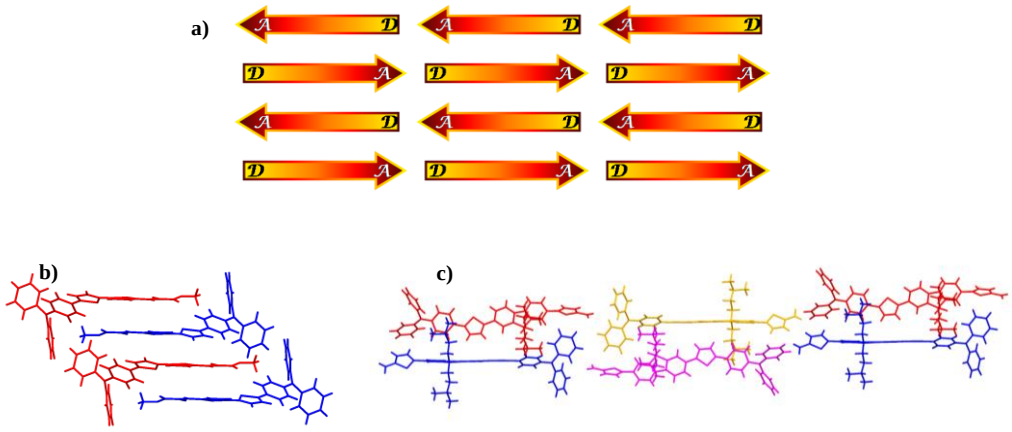

Illustration III 1. a) Antiparallel configuration of dipolar molecules represented by arrows, b) crystal packing of **D1'c** and c) crystal packing of **D1'''a**

Antiparallel configuration usually affects strongly the photophysical properties of the molecular aggregates, therefore including nanoparticles. This behavior is well explained by the theory of molecular exciton[1,2].

Once you approach two molecules they start to interact, therefore you have a system with four combined states in which two of them are degenerate.

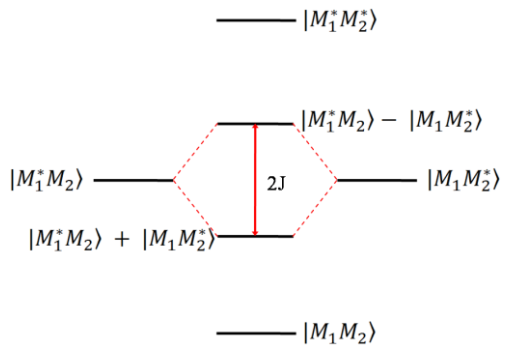

Scheme III 1. Schematic representation of the excitonic splitting in a dimer where M1 and M2 are the two dipoles that form the dimer, * represent the excited molecules and 2J is the energetic difference between the two splitted states

The combinations between the two degenerate states provoke the excitonic splitting, depending on the arrangement of the molecules; there is a state at higher or lower energy compared with the starting state.

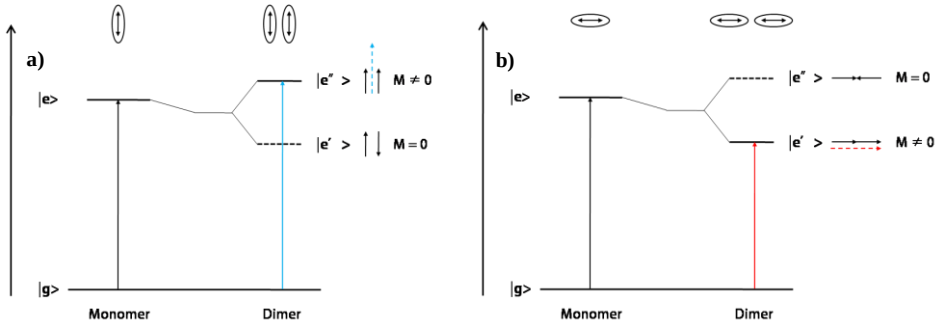

Scheme III 2. Schematic representation of the exciton band energy diagram for a molecular dimer with a) parallel transition dipoles and b) in-line transition dipoles. Where |**g**› and |**e**› are the ground and the excited states, ↔ represent the dipolar moment of the molecule and M is the transition moment of the dimer. Revised from Ref. 2

The transition moment is given by the vector that is the sum of each transition dipole moment of the dimer, therefore when we have the limit "parallel" form, so-called H-aggregates (**Scheme III 2a**), the allowed state will be the one at higher energy, thus we should observe a hypsochromic shift of the ICT band associated with no luminescent properties. When we have the limit "in-line" form, so-called J-aggregates (**Scheme III 2b**), the allowed state will be the one at lower energy, thus we should observe a bathochromic shift of the ICT band, with respect to the monomer absorption, associated with an enhancement and a red shift of the emissive properties[1-4].

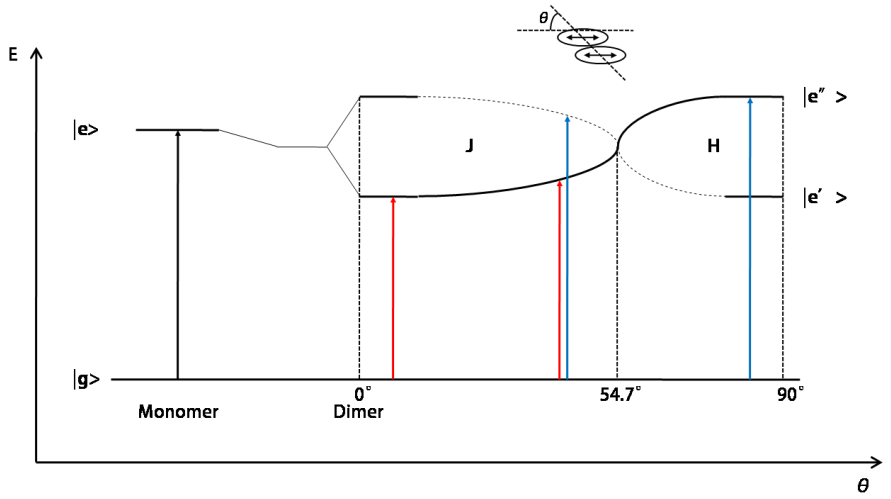

Scheme III 3. Schematic representation of the exciton band energy diagram for a molecular dimer considering the angle θ between the single transition moments, where |**g**› and |**e**› are the ground and the excited states

As it can be observed in **Scheme III 3**, depending on the angle between the two dipole moments is allowed either the lower |**e**'› or the higher |**e**"› state, influencing the photophysical properties. Experimentally, it was observed that both states are reached, indicating a more complex aggregate in which the molecules are arranged with different relative angles between them.

The dipolar chromophores studied in this chapter are molecules based on triphenylamine as electron releasing group. This moiety was chosen, in addition to what was discusses in the previous chapter, also because of the typical propeller shape that could prevent close π-stacking interactions between neighbor chromophores. Moreover, the replacing of the para-substituent on the donor group,

in addition to the changing of the donating strength already discussed, allow us to study the behavior of the chromophores with bulky groups within the nanoparticle, preventing the interchromophoric interaction, which are deleterious for emissive properties, and increasing the colloidal and chemical stability[5-7].

The starting idea was to prepare full organic, biocompatible fluorescent nanoparticles (FONs) with an emission range that lies in the biological transparency window (cf. **Chapter 1**), with high one-photon and two-photon brightness in order to use them as fluorescent probes in bioimaging.

2. Preparation of nanoparticles with their structural and morphological characterization

To prepare organic nanoparticles (ONPs) was used the easy and fast method of nanoprecipitation, a process based on solvent exchange. A stock solution of chromophore, with mM concentration, was prepared in a solvent fully miscible with water (such as THF, Acetone or DMSO) and a small amount of the stock solution was injected in a large amount of water (typically 1% of stock solution), in which the compound is not soluble. This process induces a fast nanoaggregation of molecules depending mainly on the nucleation/aggregation process but also on the diffusion of the solvent in water[8,9].

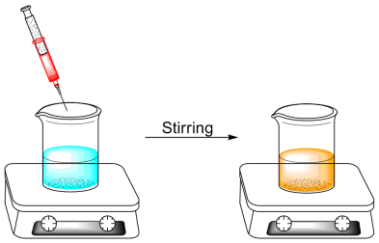

Scheme III 4. Schematic representation of the nanoprecipitation process

After the preparation, the FONs were characterized by transmission electron microscopy (TEM) to study the size distribution and the shape, as well as by zetametry to study the surface potential, important parameter to predict the colloidal stability overtime (that will be discussed later in

the chapter). In **Table III 1** are gathered the relevant data concerning the morphological properties of the ONPs.

Table III 1. Morphological and structural data

Cpd	d_{TEM} [nm]	N[a)] [10^4]	ζ-potential [mV]
D1'a	36	4.0	-40
D1'b	27	1.2	-62
D1'c	40	3.9	-61
D1'd	41	4.5	-68
D2'a	38	2.9	-73
D2'b	66	13.1	-63
D2'c	38	2.6	-69
D2'd	21	0.4	-68
D3'a	40	0.9	-81
D3'c	32	1.3	-73
D3'd	45	3.9	-75
D1''a	42	5.7	-70
D1''d	21	0.6	-74
D1''e	30	1.4	-67
D2''a	37	2.8	-85
D2''d	39	3.0	-75
D2''e	29	1.0	-75
D3''a	27	0.9	-72
D3''d	32	1.5	-79
D3''e	32	1.2	-72
D1'''a	34	1.7	-73

a) Estimated number of dyes subunits *per* ONPs based on their size

The evolution of nucleation/growth is of main importance in the nanoaggregation process, and is not predictable. As displayed in **Figure III 1**, three chromophores of the same family bearing the same para-substituent but different acceptor groups (**D2'b**, **D2'c** and **D2'd**) are compared in terms of size distribution.

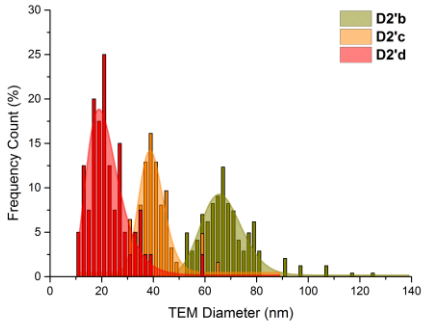

Figure III 1. Comparison between size distribution of nanoparticles prepared with chromophores **D2'b** (dark yellow), **D2'c** (orange) and **D2'd** (red)

These nanoparticles were considered as example because they display an emblematic behavior: a slight change of the chemical structure strongly affects the size. As said before, this behavior is not predictable, therefore is not possible to generalize this property. From these data we can deduce that in the process of nanoparticles formation for the chromophore **D2'd**, the nucleation is the faster process compared to the growth; on the other hand for the chromophore **D2'b** the growing of nanoparticles is the prevalent step. Evidently, this behavior affects also the number of chromophores *per* nanoparticle (see in **Table III 1**) there are two orders of magnitude among the number of molecules of nanoparticles prepared with **D2'b** and **D2'd**: $13.1 \cdot 10^4$ and $0.4 \cdot 10^4$ respectively.

As one can see from TEM images in **Figure III 2**, the shape of the obtained nanoparticles is spherical; therefore, we could assume that the nanoobjects prepared are not crystalline. This was expected since the solvent exchange is a kinetic process and the chromophores do not have enough time to the full thermodynamic organization within the object. Anyway, the ONPs are not completely amorphous, indeed a previous work of the lab[10] has shown that on the surface of the nanoparticle, which is in contact with water, the chromophores are organized in a short range while going deeper in the bulk the molecules increase their disorder.

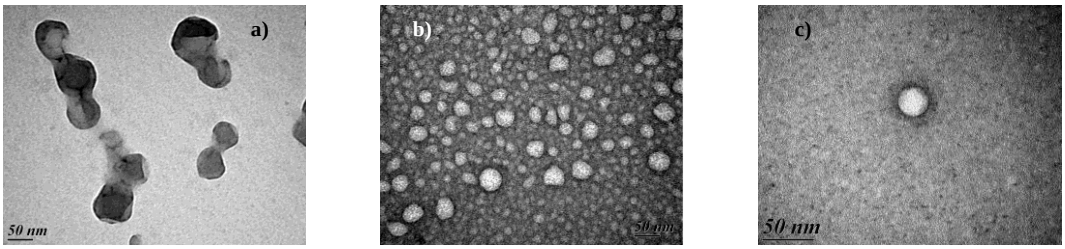

Figure III 2. TEM images of a) **D2'b**, b) **D2'c**, c) **D2'd**

3. Linear and non-linear optical properties of FONs in water

After the confirmation of the nanoparticles formation, it was possible to go further and characterize the obtained nanoobjects under the viewpoint of optical properties. Thanks to the luminescent properties of the prepared ONPs, it was also possible to estimate the two-photon cross section of the chromophores upon nano-confinement.

Due to the large number of samples, for an easy and clear comparison the FONs will be compared in the same way used as for the chromophores dissolved in organic solvents.

To have a good comparison about the behavior of the molecule in both solution and nanoparticle, the molar extinction coefficient of the chromophore within the nanoobject was measured for the samples taken into account in this chapter. Furthermore, to confirm the value measured, I evaluate the Lambert-Beer dependency of the dye in FONs and in **Figure III 3** are gathered the results obtained for few molecules.

One can observe that the FONs follow the Lambert-Beer law, indicating that the size of the nanoaggregates is independent from the number of chromophores used to prepare the nanoparticles.

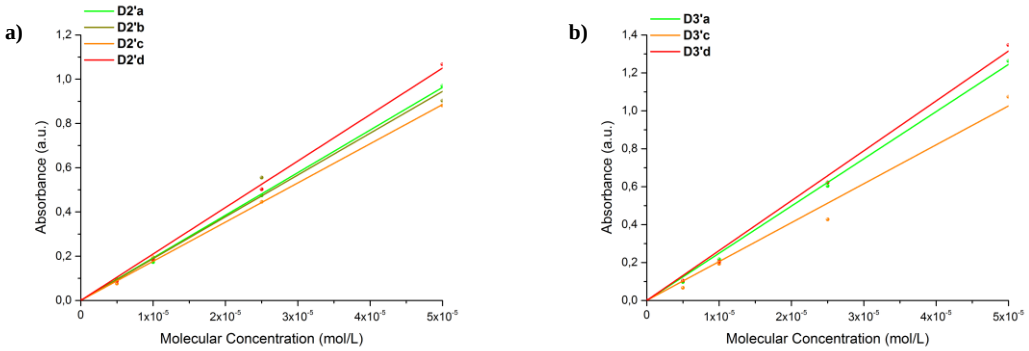

Figure III 3. Lambert-Beer dependency of nanoparticles prepared with chromophores of the series a) **D2'a-d** and b) **D3'a-d**

3.1. Effect induced by the tuning of the acceptor group

3.1.1. One-photon characterization

In order to study the changes in the photophysical properties by increasing the dipolar strength, in this paragraph are compared three different series of FONs (**D1'**, **D3'**, **D3''**) prepared with chromophores bearing different acceptor group, from aldehyde (**a**) to DETB (**e**) passing through cyanoamide (**b**), cyanoester (**c**) and dicyano (**d**)[11].

In **Table III 2** are gathered the relevant data measured for the members of the three families of chromophores upon nanoaggregation.

The FONs of these three series display a broad and intense absorption band that lies from the violet to the green visible spectral region depending on the acceptor group. As already discussed in the previous chapter, the intense band located at lower energies is ascribed to an ICT transition, while the high energetic band is attributed to π-π^* transition. The ICT band is associated with a large molar extinction coefficient ranging from 2.3 to 5.0 $\cdot$ 10^4 M^{-1} cm^{-1}, but a more exhaustive discussion, which include also the comparison with the results obtained for the chromophores in solution, will be found later in the chapter (**Paragraph 4**: Molecular Confinement).

Table III 2. Photophysical data measured for the chromophores of the series **D1'a-d**, **D3'a-d**, **D3''a-e** in FONs in water.

Cpd	λ_{max}^{1PA} [nm]	ε_{max} [10^4 $M^{-1}cm^{-1}$]	λ_{max}^{em} [nm]	Stokes shift [10^3 cm^{-1}]	Φ_f	τ_1/τ_2 [ns]	λ_{max}^{2PA} [nm]	σ_{2max} [GM]
D1'a	422	2.3	597	6.9	0.07	1.1 (0.6) / 3.5 (0.4)	970	114
D1'b	458	2.6	673	7.0	0.06	1.6 (0.7) / 4.2 (0.3)	890	159
D1'c	481	2.5	721	6.9	0.02	1.4 (0.8) / 4.1 (0.2)	1070	207
D1'd	513	3.6	770	6.5	0.01	1.5 (0.8) / 4.9 (0.2)	1110	460
D3'a	441	3.1	587	5.6	0.12	1.3 (0.5) / 4.2 (0.5)	970	245
D3'c	499	2.7	702	5.8	0.04	1.5 (0.4) / 3.8 (0.6)	1050	336
D3'd	525	3.0	747	5.7	0.01	nd	1050	1150
D3''a	424	3.3	570	6.0	0.06	0.9 (0.6)/3.8 (0.4)	910	182
D3''d	507	5.0	714	5.7	0.02	1.5 (0.5)/4.6 (0.5)	1080	726
D3''e	541	4.9	749	5.1	0.005	1.0 (0.8)/3.0 (0.2)	/	/

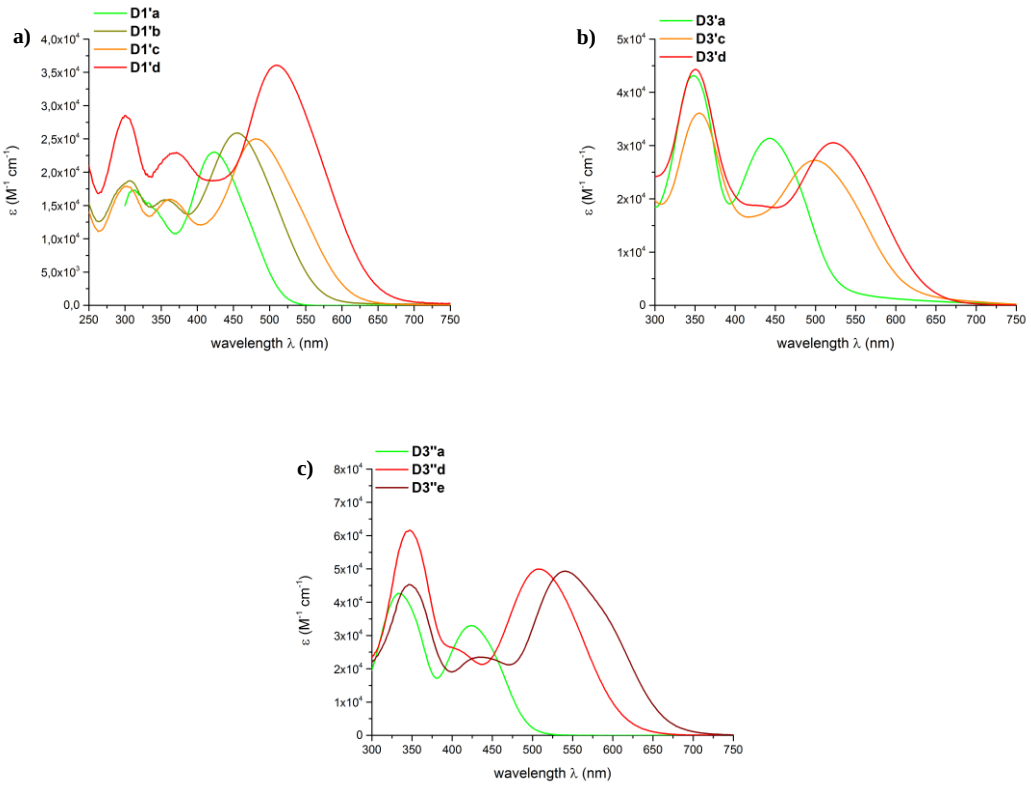

Figure III 4. Comparison between the one-photon absorption spectra measured for the different members of the family a) **D1'**; b) **D3'** and c) **D3''** upon nano-confinement.

In **Figure III 4** it can be observed a bathochromic shift induced by the increase of the dipolar strength due to the enhancement of the electron-withdrawing character of the acceptor end-group. As discussed for solution, the red-shift measured is not associated with the expected hyperchromic effect.

The luminescent properties of these nanoparticles parallel the trend observed in absorption, an enhancement of dipolar strength induces a marked shift towards lower energies, see **Figure III 5**. Indeed, tuning the acceptor group it was possible to obtain nanoobjects that cover the spectral range from yellow to NIR.

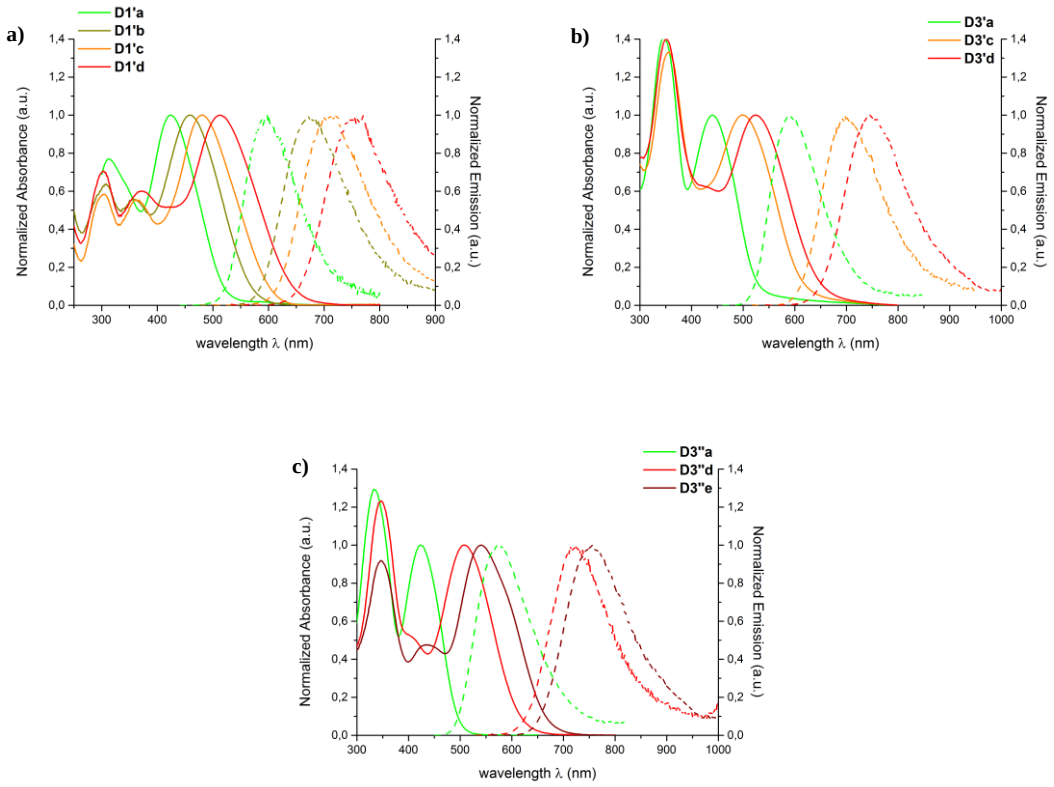

Figure III 5. Comparison between normalized absorption (solid line) and emission (dashed line) spectra measured for the FONs prepared with the family a) **D1**'; b) **D3**' and c) **D3**" (*consistent color code between the figures of the paragraph*)

It can be clearly noticed that, upon aggregation, the FONs undergo a quenching of fluorescence but are still luminescent nanoparticles with a fluorescence quantum yield Φ_f ranging from 0.005 to 0.12, which is very important for the brightness, fundamental data for bioimaging.

Concerning the fluorescence lifetime, one can see in **Table III 2**, that all the FONs display two lifetimes; the shorter lifetime, ranging from 0.9 (**D3"a**) to 1.6 nm (**D1'b**) is dominant with respect to the other one, which is longer (from 3.0 to 4.9 nm). In each sample, the short lifetime can be attributed to the "shell", the surface, which is in contact with water and where it is possible to have competitive non-radiative decays; on the other hand, the long lifetime can be attributed to the bulk of the particle.

3.1.2. Two-photon characterization

The behavior observed in FONs parallels the one observed in solution, all the dipolar chromophores confined in nano-environment show a structured 2PA band in which $\lambda_{max}^{2PA} \approx 2\ \lambda_{max}^{1PA}$ indicating that the transition is allowed in both processes (see **Figure III 6**).

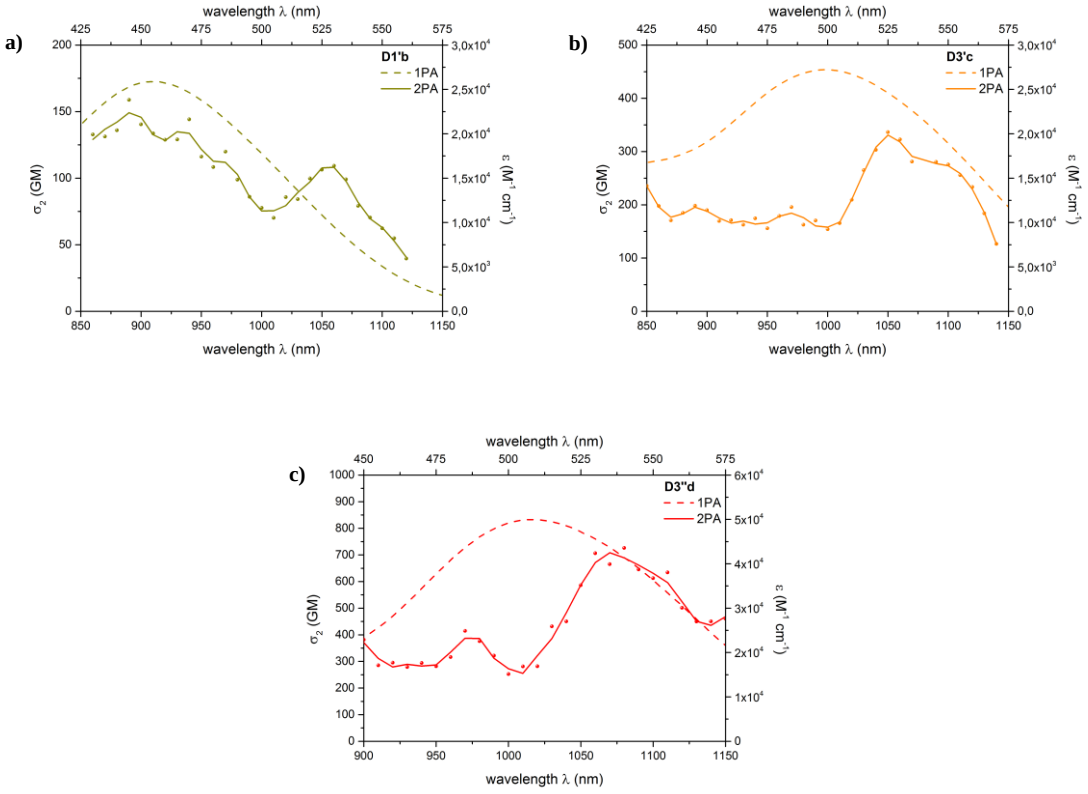

Figure III 6. Superimposition between one-photon (dashed line) and two-photon (colored point and solid line) absorption spectra of chromophores a) **D1'b**; b) **D3'c** and c) **D3"d** in confined environment.

In these three series of FONs, it can be observed that increasing the electron-withdrawing character of the acceptor end-group leads to a bathochromic shift, as observed upon one-photon excitation, associated with a marked enhancement of the two-photon cross section. An interesting behavior is displayed by FONs prepared with chromophore **D1'b**. Actually this sample does not follow the general trend, because the λ_{max}^{2PA} is blue-shifted compared with FONs made from the aldehyde (**D1'a**). One can observe, in **Figure III 7**, that there is a sub-band placed at 1060 nm, whose relative intensity of it is much lower than that of the main absorption band (109 GM and 159 GM respectively).

It is also worth underlining that FONs bearing DETB as acceptor group (**D1-3"e**) show too low fluorescence quantum yield to perform reliable 2PEF measurements, therefore the data are omitted.

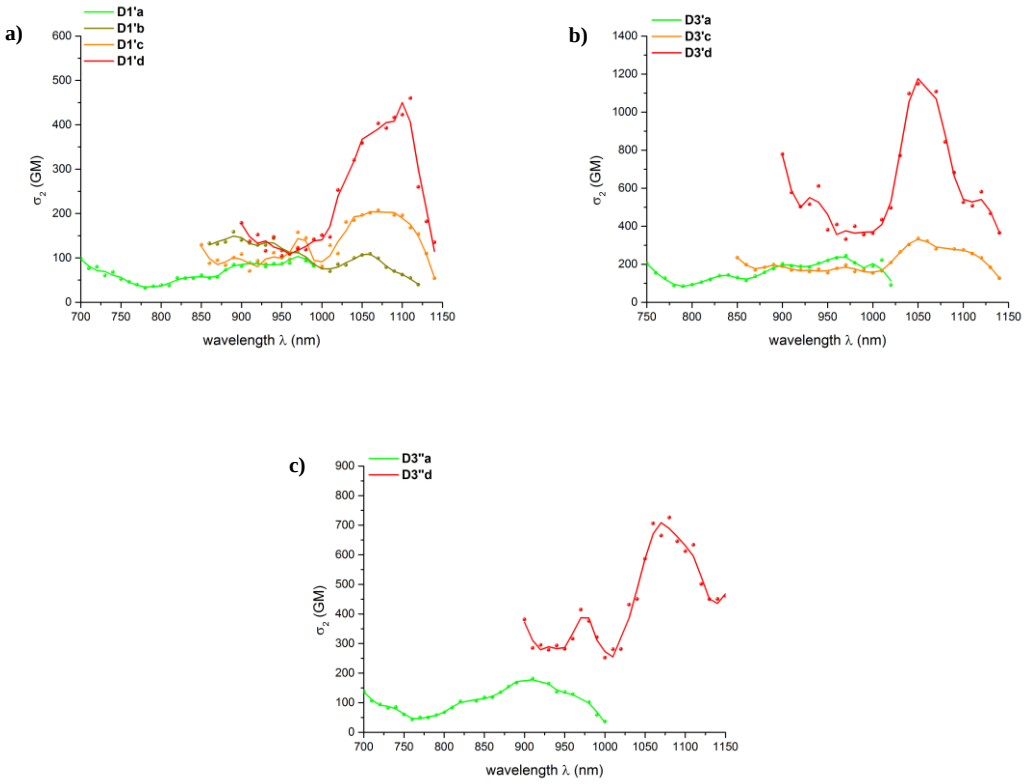

Figure III 7. Comparison between the two-photon absorption spectra measured for the different members of the family a) **D1'**; b) **D3'** and c) **D3"** in FONs in water.

3.2. Effect induced by the "para-substituent" on the triphenylamine

3.2.1. One-photon characterization

Like the chromophores in solution, the molecules confined in nano-environment display a similar trend upon one-photon excitation: by replacing –H with –Br, a slight hypsochromic shift is observed, while the addition of *tert*-butylphenyl as para-substituent increases the electron-releasing character of the donor group, thus inducing a weak shift towards lower energies. The ICT band measured for these FONs is placed in the cyano-green spectral region and it is associated with a large molar extinction coefficient up to $6.1 \cdot 10^4$ M^{-1} cm^{-1} as reported in **Table III 3** (see also **Figure III 8**).

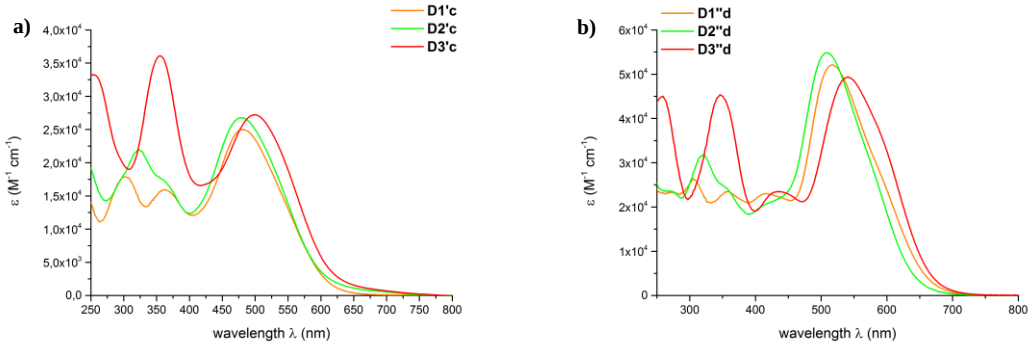

Figure III 8. Comparison between the one-photon absorption spectra measured for the different members of the series a) **D1'-D3'c**; b) **D1"-D3"d** in confined environment.

Table III 3. Photophysical data measured for the FONs prepared with chromophores **D1'-D3'c** and **D1"-D3"d**.

Cpd	λ_{max}^{1PA} [nm]	ε_{max} [10^4 $M^{-1}cm^{-1}$]	λ_{max}^{em} [nm]	Stokes shift [10^3 cm^{-1}]	Φ_f	τ_1/τ_2 [ns]	λ_{max}^{2PA} [nm]	σ_{2max} [GM]
D1'c	481	2.5	721	6.9	0.02	1.4 (0.8)/4.1 (0.2)	1070	204
D2'c	476	2.7	688	6.5	0.04	1.4 (0.8)/3.8 (0.2)	1060	141
D3'c	499	2.7	702	5.8	0.04	1.5 (0.4)/3.8 (0.6)	1050	336
D1"d	476	3.5	719	7.1	0.01	1.5 (0.6)/4.0 (0.4)	1070	300
D2"d	478	6.1	711	6.9	0.01	1.1 (0.7)/3.5 (0.3)	1060	921
D3"d	507	5.0	714	5.7	0.02	1.5 (0.5)/4.6 (0.5)	1080	726

Concerning the luminescent properties, it is worth to highlight the behavior of these FONs: as expected, replacing the hydrogen with bromine induces a hypsochromic shift of the emission band but, strikingly, no bathochromic shift was observed by adding the bulky *tert*-butylphenyl group. Indeed, as reported in **Table III 3** as well as in **Figure III 9**, FONs prepared with chromophores **D3'c** and **D3"d** are blue-shifted compared with the respective **D1**. This interesting behavior indicates that the *tert*-butylphenyl group within the nanoparticle does not work as donor, as observed in solution, but only as hindering group limiting interchromophoric interactions. Moreover, this property induces a slight enhancement of the fluorescence quantum yield, underlying our initial idea to prevent the π-π interaction in confined environment by adding bulky groups.

Also in this case, as observed in the previous paragraph, the fluorescence decay can be fitted with a biexponential decay giving two fluorescence lifetimes. The shorter and dominant lifetime is attributable to the chromophores that form the surface, while the longer one can be ascribed to the bulk of the nanoparticle.

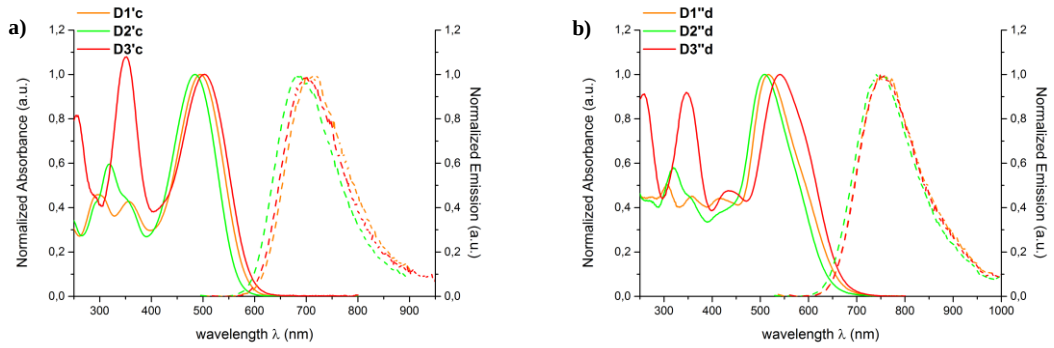

Figure III 9. Comparison between the normalized absorption (solid line) and emission (dashed line) spectra measured for chromophores a) **D1'-D3'c**; b) **D1"-D3"d** in nanoparticles (*consistent color code between the figures of the paragraph*)

3.2.2. Two-photon characterization

As could be expected, the properties of the chromophores upon nano-confinement in water are comparable with the behaviors observed for the chromophores in solution. As displayed in **Figure III**

6 as example, also FONs displayed in this paragraph show that the position of the 2PA maximum is comparable or slightly red-shifted compared with twice λ_{max}^{1PA} indicating that the occurring transition is symmetrically allowed upon both excitation one-photon and two-photon.

Contrarily to what was observed for solution, the chromophores in FONs display a structured band but the intensity does not depend on the strength on the electron-releasing character (cf. **Figure II 16**). The trend of the series **D'c** in FONs follows the expectation; the compounds display a hyperchromic effect passing from –Br to –H and to –*tert*-butylphenyl. On the other hand, in series **D"d**, the FONs prepared with chromophore **D2"d** show the highest two-photon response, indicating an arrangement of the molecules within the nanoparticles that promote the 2PA enhancement.

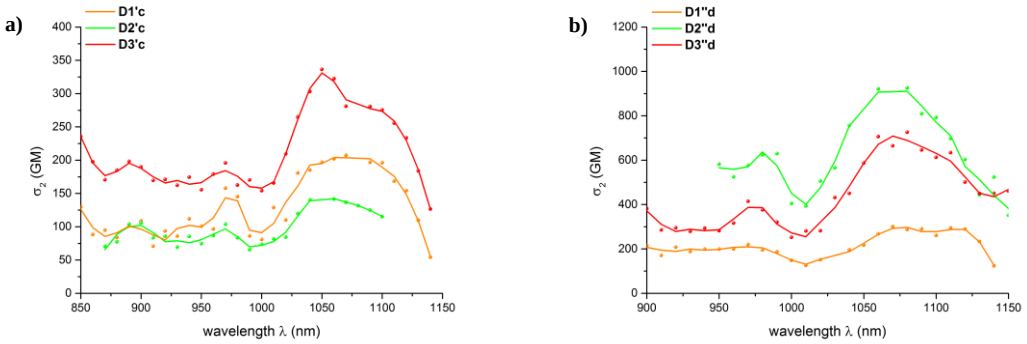

Figure III 10. Comparison between the two-photon absorption spectra measured for the different chromophores bearing the same acceptor moiety a) **c** (cyanoester); b) **d** (dicyanovinyl) in FONs.

3.3. Effect of the tuning of the π-conjugated connector

3.3.1. One-photon characterization

In this paragraph FONs prepared with chromophores **D1'a**, **D1"a** and **D1'"a** are compared. Since the connectors between the end-groups are not similar here I cannot generalize the properties, I will just give an overview of the different behaviors that can be induced by the change of the π-bridge.

As reported in **Table III 4** and displayed in **Figure III 11a**, the FONs prepared with a more rigid system (**D1'a** → **D1"a**) show a hypsochromic shift in the ICT band associated with a slight

enhancement of the molar extinction coefficient. Strikingly the same behavior is observable also by adding a fluorene core between two thiophenes, this structural change promotes, in FONs prepared with **D1'''a**, a marked enhancement of the molar extinction coefficient with a slight blue shift of the absorption band.

A parallel behavior can be observed in emission. The substitution of a bis-thiophene as conjugated bridge with both thienothiophene and bis-thiophene-fluorene induces a blue shift of the band. As could be expected, in FONs the close interaction between neighbor molecules leads to a decreasing of the fluorescence quantum yield, and as it is reported in **Table III 4** this quenching is more pronounced in nanoparticles prepared with **D1''a** and **D1'''a**.

Table III 4. Linear and *non*-linear optical characterization for chromophores **D1'-D1'''a** in FONs in water.

Cpd	λ_{max}^{1PA} [nm]	ε_{max} [10^4 $M^{-1}cm^{-1}$]	λ_{max}^{em} [nm]	Stokes shift [10^3 cm^{-1}]	Φ_f	τ_1 [ns]	λ_{max}^{2PA} [nm]	σ_{2max} [GM]
D1'a	422	2.3	597	6.9	0.070	1.1 (0.6)/3.5 (0.4)	970	114
D1''a	410	3.4	557	6.4	0.050	1.2 (0.5)/3.9 (0.5)	910	395
D1'''a	409	4.8	557	6.5	0.035	2.9 (0.5)/0.8 (0.5)	730 890	634 323

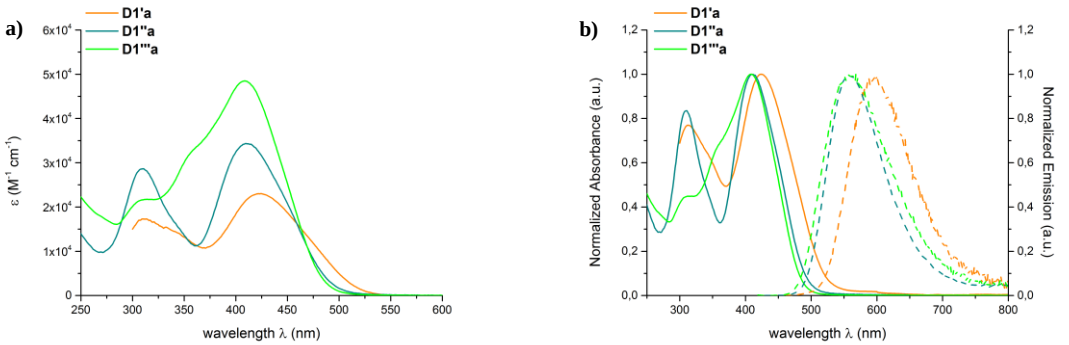

Figure III 11. a) Comparison between the one-photon absorption spectra measured for the chromophores **D1'-D1'''a** in confined environment b) Normalized absorption and emission spectra measured for the chromophores **D1'-D1'''a** in FONs in water.

3.3.2. Two-photon characterization

Similar to what was observed for the chromophores in solution, when the molecules are confined in nano-environment it can be noticed that in FONs prepared with **D1'a** and **D1''a** the same transition is allowed in both one-photon and two-photon process, as displayed in **Figure III 12a-b**. However, contrarily to solutions, FONs prepared with **D1''a** show higher two photon cross section, suggesting an arrangement of chromophores within the nanoparticles that improve the non-linear response.

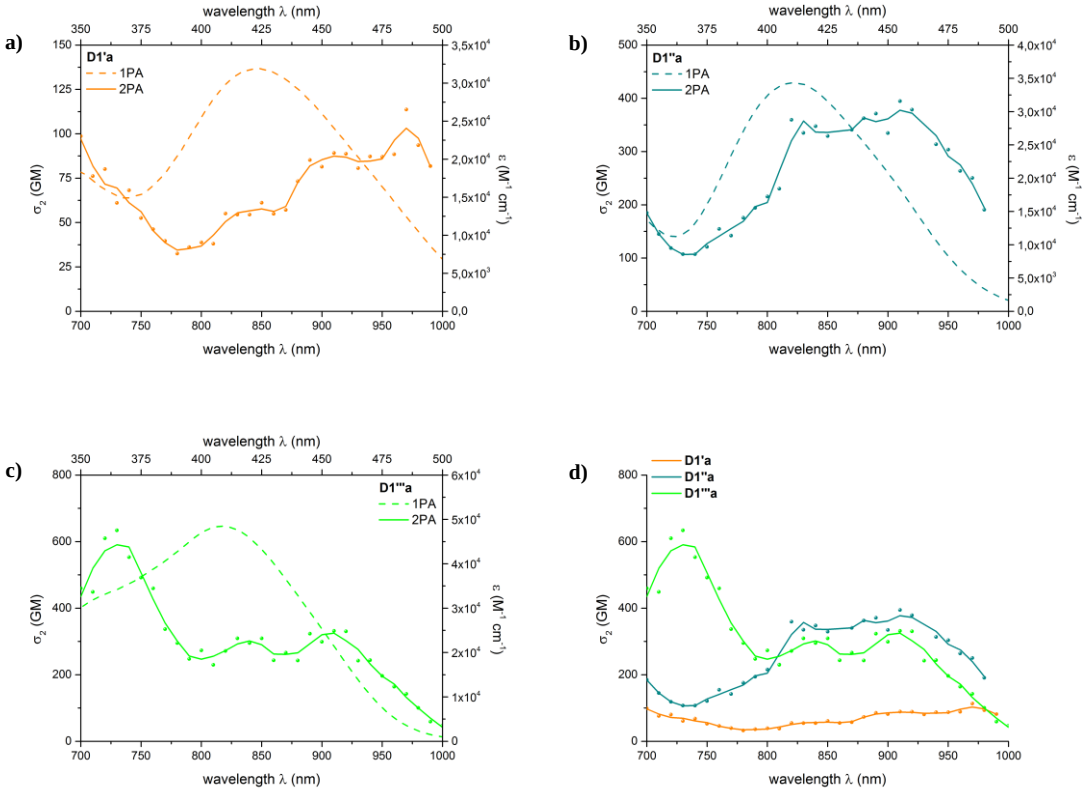

Figure III 12. Superimposition between one-photon (dashed line) and two-photon (colored point and solid line) absorption spectra of chromophores a) **D1'a**; b) **D1''a**; c) **D1'''a** in $CHCl_3$ solution and d) comparison between the two-photon absorption spectra measured for the different members of the series **D1a**.

On the other hand, as displayed in **Figure III 11c**, FONs **D1'''a** show a broad two-photon absorption spectra in which are present two allowed states reachable upon two-photon excitation. The

most allowed band is markedly blue-shifted compared with twice the wavelength of the ICT band of the linear process, paralleling the behavior observed in $CHCl_3$ solution.

Furthermore, it can be observed in **Figure III 11d** that within FONs the rigidification of the π-conjugated bridge as well as the addition of a hindered fluorene core in the connector, induce an improving of the 2P response.

4. Molecular confinement

In this paragraph will be discussed the differences of the optical properties of chromophores in both molecular solution and organic nanoparticles. So far, intensive studies were done to understand the behavior of one-photon processes of molecules upon nano-confinement inducing either aggregation caused quenching (ACQ) or aggregation induced enhanced emission (AIEE)[12,13], however the "world" of NLO is still to be fully discovered. As discussed previously (cf. **Paragraph 1:** Introduction), the arrangement of molecules within nanoparticles can strongly affect the photophysical properties.

Here I would like to display a complete overview of the behaviors of dipolar chromophores before and after the nanoaggregation process. Due to the big amount of dipolar dyes, I chose few emblematic samples to give an exhaustive review of the observations done.

4.1. Linear optical properties

4.1.1. Emission in solid state and upon nanoaggregation

As I wrote earlier in the chapter (cf. **Paragraph 2**), the nanoparticles are formed under a kinetic domain and I guess that it is worth to compare the photophysical behavior of the molecules in solid state (smeared powders, microcrystalline when it was possible) and in nanoparticle. It is interesting to highlight the fact that these chromophores, even in solid state, maintain their luminescent properties without undergoing any quenching of fluorescence due to close intermolecular interactions.

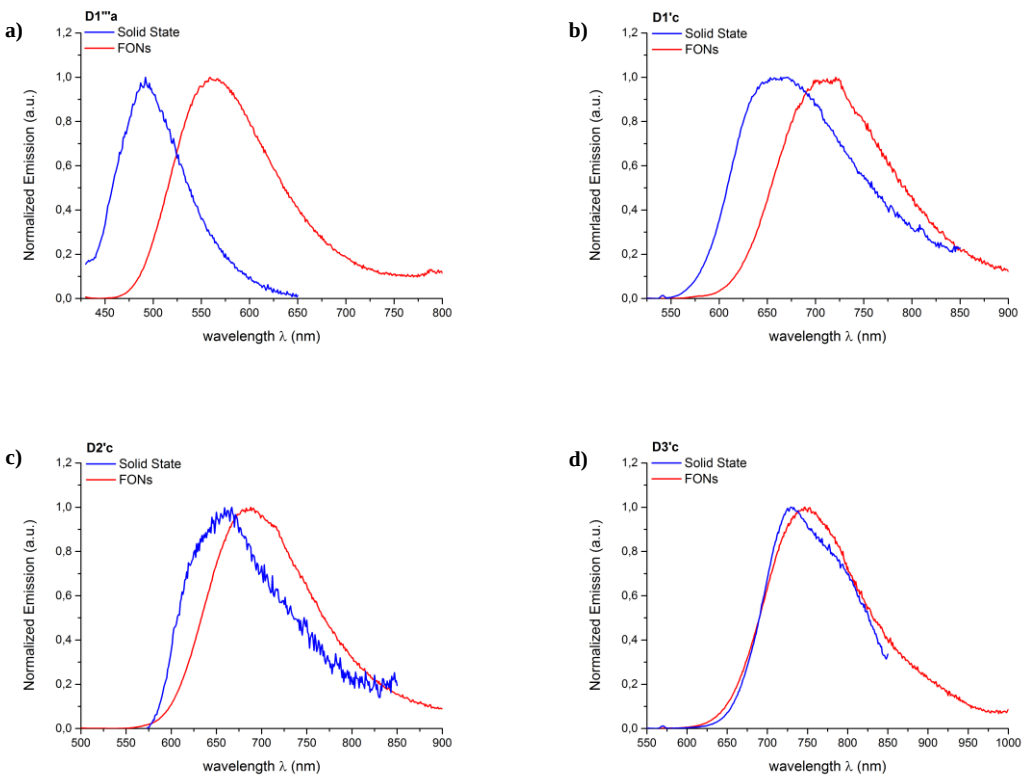

Figure III 13. Comparison between the normalized emission measured in solid state (blue line) and the FONs (red line) for the chromophores a) **D1'''a** (smeared microcrystalline powder), b) **D1'c** (smeared microcrystalline powder), c) **D2'c** (smeared amorphous powder) and d) **D3'c** (smeared amorphous powder).

As one can observe in **Figure III 13**, the trend followed by the different molecules in solid state as well as in nanoparticles is not the same for all the samples. Indeed, it can be noticed that tuning the chemical structure we have the emission of FONs similar (as in the case of **D3'c**), or red-shifted (as in the case of **D1'''a**, **D1'c** and **D2'c**) compared with the solid state, suggesting the different arrangement of the molecules in both states.

4.1.2. Behavior of the chromophores in solution and nano-environment

It is interesting to compare the behavior of the chromophores in both solution and nanoparticle in order to study the influence of aggregation on the photophysical properties. Since these chromophores are solvatochromic, I will not discuss precisely the shift of both absorption and emission band. I can say that for all chromophores we observed an hypsochromic shift of the

absorption band associated with a bathochromic shift (or comparable emission i.e. **D3'c**, **D3'd** and **D3''e**) of the emission band, with respect to the measurement of the molecules in $CHCl_3$ solution. This behavior suggests that the dye part of the bulk in the nanoparticle has a more polar environment compared with the chromophore in chloroform solution.

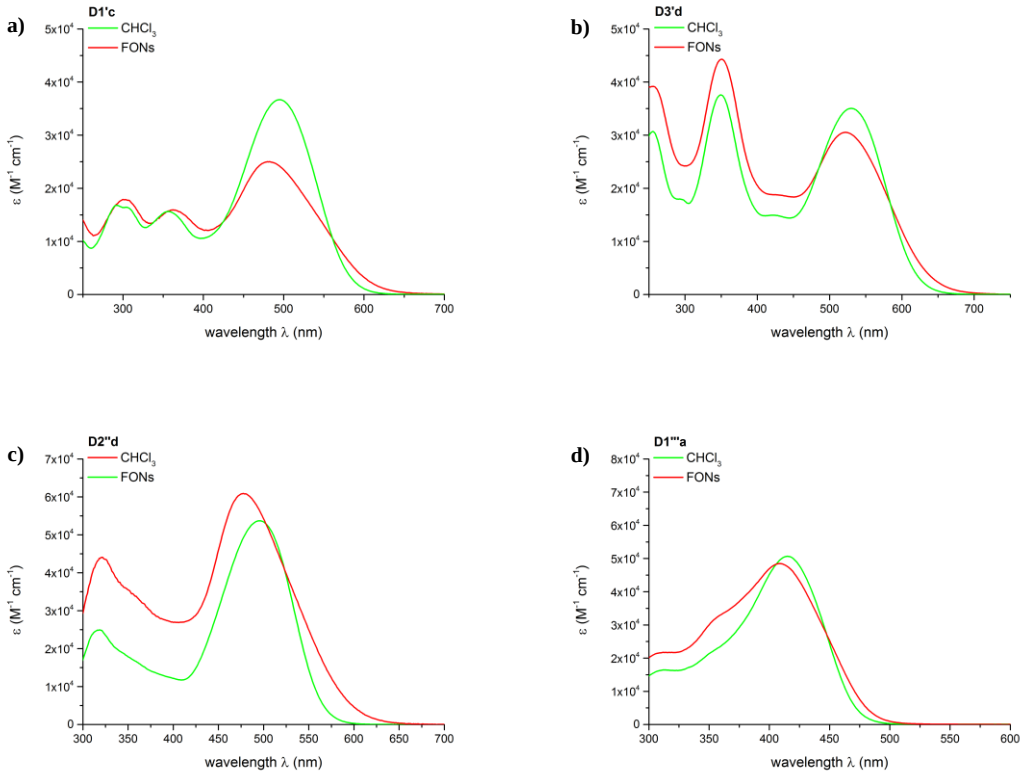

Figure III 14. Comparison between the one-photon absorption spectra measured in both $CHCl_3$ solution (green line) and FONs (red line) for chromophores a) **D1'c**, b) **D3'd**, c) **D2''d** and d) **D1'''a**

Comparing the absorption spectra of the molecules in both organic solution and FONs in water, one can observe in **Figure III 14a-b** that most of the chromophores upon aggregation undergo a marked decrease of the molecular response as can be expected[6,7,14,15]. Interestingly, some of the molecules (see **Figure III 14c-d**) display comparable or even higher response in nano-environment compared to the solution. This behavior can be due to a cooperative effect due to the arrangement of the chromophores within the FONs.

Moreover, it can be observed either a broadening or an asymmetric shape of the absorption band when the molecules are confined in FONs compared with the molecule in solution. This effect can be ascribed to excitonic coupling, which is favored by the interchromophoric interactions between neighbor molecules within the nanoparticle. As you can notice, the hyperchromic or hypochromic effect upon nanoaggregation depends on the structure of the chromophore, therefore is not possible to generalize the behavior.

4.2. Non-linear optical properties

As can be expected, the molecular confinement of two-photon responsive chromophores strongly affects their 2PA behavior. Indeed, dipolar interactions and consequent arrangement of molecules when confined in nano-environment influence the two-photon response of polar and polarizable chromophores[16,17]. As expected, the confinement of dyes within a nanoparticle induces a marked decrease of the two-photon cross section per chromophore subunit, as discussed for the linear process (see **Figure III 15a/d**). On the other hand, the molecular arrangements as well as the interchromophoric interactions in FONs prepared with dye **D3'd** can lead to an hyperchromic effect in the 2PA response (**Figure III 15b**) or can induce a modification in the vibronic structure as displayed for chromophore **D2"d** in **Figure III 15c**.

As one can notice, the trend followed upon two-photon excitation does not parallel the one observed in one-photon absorption. This underlines the fact that predicting the behavior of chromophores in nanoparticles is not easy.

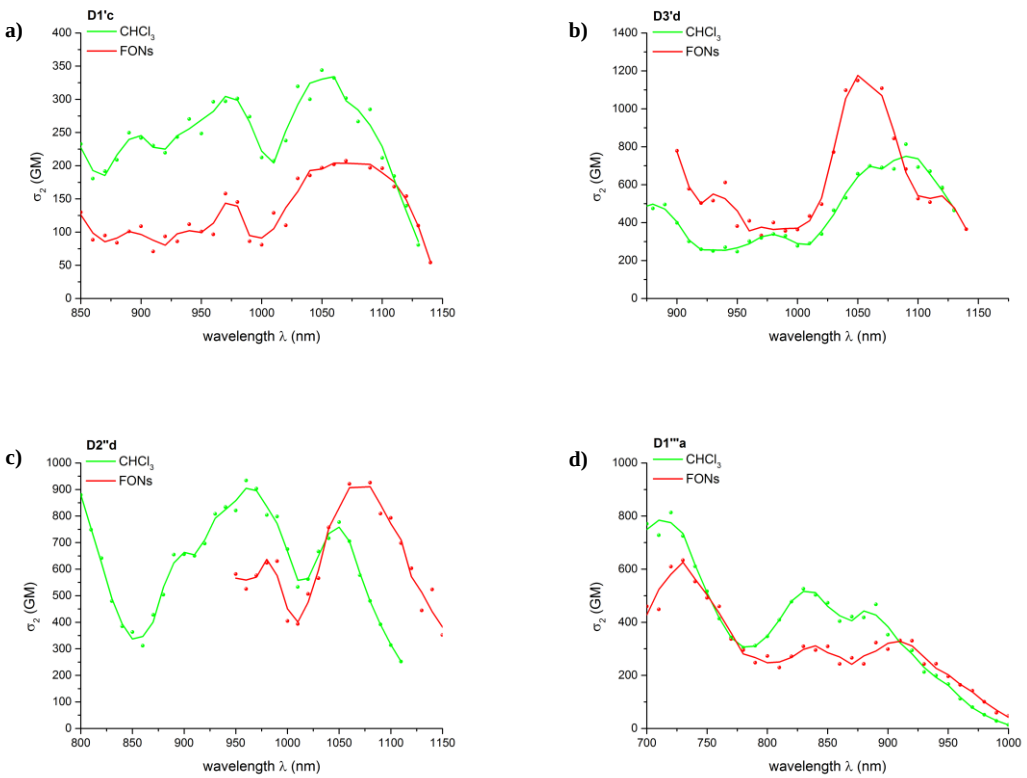

Figure III 15. Comparison between the two-photon absorption spectra measured in both $CHCl_3$ solution (green line) and FONs (red line) for chromophores a) **D1'c**, b) **D3'd**, c) **D2"d** and d) **D1'"a**

4.3. One-photon and two-photon brightness

As widely discussed in the introductive chapter, to have hyper-bright nanoobject is a great issue, especially if we would like to use our systems as bio-probe in confocal and/or multiphoton microscopy. The brightness of nanoparticle takes into account the number of chromophoric subunits that form the object, therefore the molar extinction coefficient and the two-photon cross section for FONs were estimated taken into account the concentration of nanoparticles, and not the moles of chromophore in nanoparticles.

In spite of the low fluorescence quantum yield of the nanoparticles due to the aggregation caused quenching process, one can observe in **Table III 5**, that our FONs display huge one-photon (up to $2.5 \cdot 10^8$ M^{-1} cm^{-1}) and two-photon brightness (ranging from 0.02 to $1.4 \cdot 10^6$ GM) surpassing all

other types of nanoparticles including QDs[18-20], depending also on the cooperative/additive effect due to the number of chromophores per nanoparticle (See **Table III 1**). Since the brightness is strictly dependent of the size of the nanoparticle, and so far it is not possible to predict the size and the shape of the FONs, the brightness of the nanoobjects is not predictable either.

Table III 5. Luminescence properties including one-photon and two-photon brightness of FONs in water

Cpd	λ_{max}^{1PA} [nm]	λ_{max}^{em} [nm]	$FWHM^{em}$ [10^3 cm^{-1}]	Φ_f	$\varepsilon_{max}\Phi_f$ a) [10^8 M^{-1} cm^{-1}]	λ_{max}^{2PA} [10^4]	$\sigma_2\Phi_f$ a) [10^6 GM]
D1'a	422	597	3.0	0.07	0.7	970	0.3
D1'b	458	673	2.8	0.06	0.2	890	0.1
D1'c	481	721	2.6	0.02	0.2	1070	0.2
D1'd	513	770	2.4	0.01	0.2	1110	0.2
D2'a	424	575	3.1	0.14	1.1	970	0.4
D2'b	451	653	3.0	0.06	2.5	900	1.4
D2'c	476	688	2.7	0.04	0.3	1060	0.3
D2'd	500	732	2.6	0.02	0.03	1060	0.02
D3'a	441	587	3.1	0.12	0.3	970	0.8
D3'c	499	702	2.6	0.04	0.1	1050	0.2
D3'd	525	747	2.5	0.01	0.1	1050	0.2
D1''a	410	557	3.1	0.05	1.0	910	1.1
D1''d	476	719	2.5	0.01	0.02	1070	0.02
D1''e	517	754	2.5	0.004	0.03	/	/
D2''a	407	541	3.0	0.05	0.5	890	0.8
D2''d	478	711	2.5	0.01	0.2	1060	0.3
D2''e	509	752	2.6	0.007	0.04	/	/
D3''a	424	570	3.6	0.06	0.4	910	0.2
D3''d	507	714	2.5	0.02	0.4	1080	0.5
D3''e	541	749	2.5	0.005	0.02	/	/
D1'''a	409	557	3.7	0.035	0.3	730	0.4

a) the values of one-photon and two-photon brightness are reported taking into account the concentration of nanoparticles

Our systems are strongly bright with a tunable emission ranging from green to NIR, therefore they could be nice tools for further applications in both one-photon or two-photon microscopy.

5. Colloidal and chemical stability of FONs overtime

Another important behavior that we should consider when we speak about FONs is the stability of the colloidal suspension overtime. This property can affect strongly the possibility of nanoparticles application in bio-environment.

This behavior is connected with the value of the surface potential, the more the nanoparticle displays a negative surface potential, the less is the probability of nanoparticles aggregation overtime. As reported in **Table III 1**, all FONs prepared show a very negative surface potential up to -85 mV. This indicates that the nanoaggregates could have a great colloidal stability; indeed, this is what was observed.

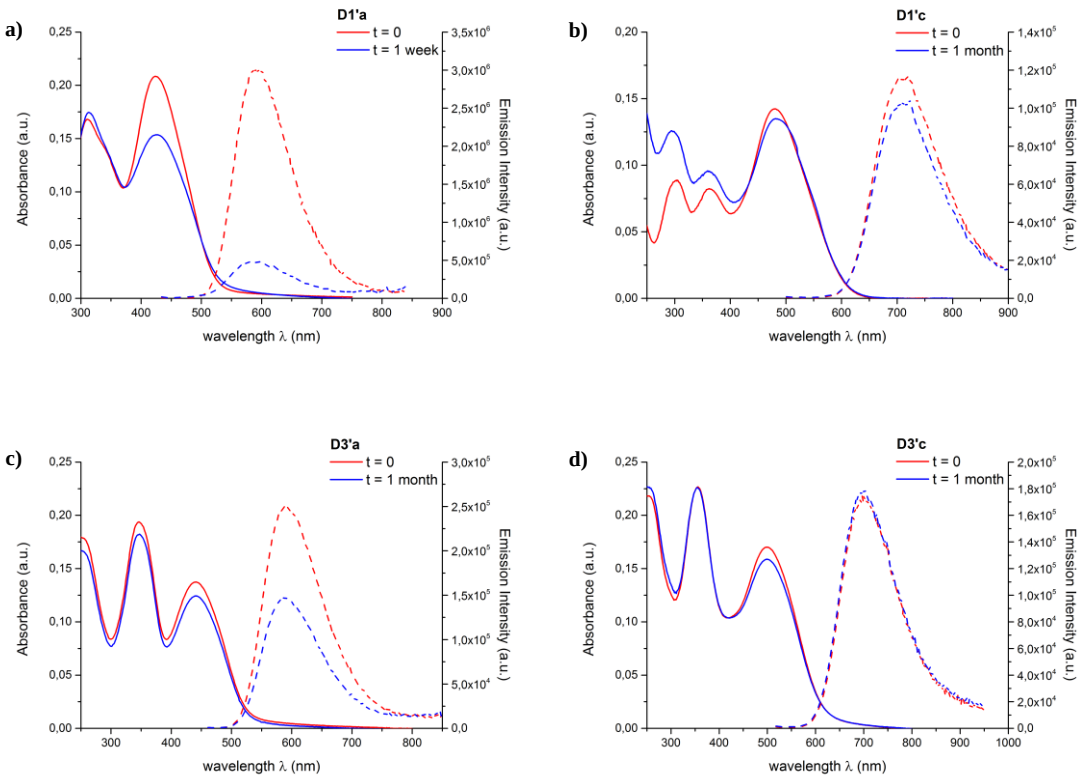

Figure III 16. Comparison between absorption (solid line) and emission (dashed line) spectra measured overtime for FONs prepared with chromophores: a) **D1'a**, b) **D1'c**, c) **D3'a** and d) **D3'c**

To study the colloidal stability, the evolution of both absorption and emission spectra was monitored overtime.

As one can observe in **Figure III 16** that passing from **D'a** → **c**, so increasing the electron withdrawing character of the acceptor group, there is an enhancement of the colloidal stability. In fact **D1'a** display a marked decrease of the absorption band and a quenching of the luminescent properties after one week, while **D1'c** after one month only shows a slight decrease of both absorption and emission spectra indicating the improvement of the stability. Parallel behavior can be observed adding the *tert*-butylphenyl groups in the available para position of the triphenylamine (**D1'a** → **D3'a**), these bulky groups improve considerably the overtime stability as expected[6].

This observation suggests that the stability is dependent from the chemical structure of the chromophores. Strong electron withdrawing as well as bulky substituent lead to an improvement of the stability.

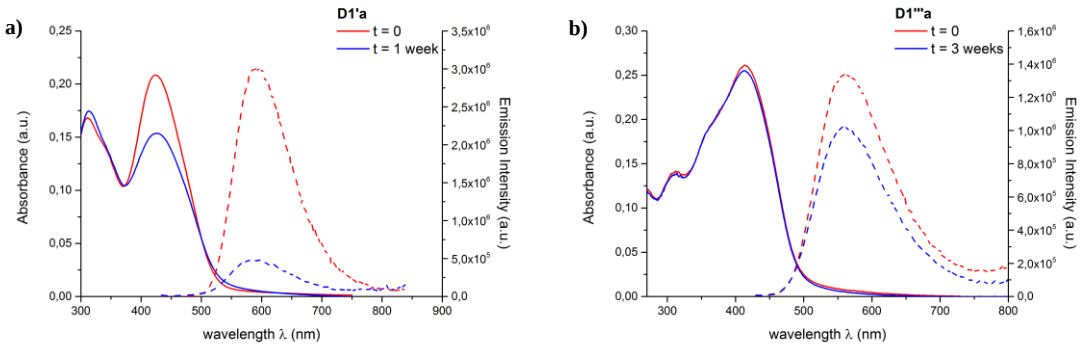

Figure III 17. Comparison between absorption (solid line) and emission (dashed line) spectra measured overtime for FONs prepared with chromophores: a) **D1'a** and b) **D1'''a**

Moreover, it is worth to notice that by addition of a hindered fluorene in the π-conjugated bridge leads to an enhancement of the colloidal stability of the FONs, indeed as can be observed in **Figure III 17** with passing from **D1'a** to **D1'''a**. After three weeks, the absorption spectra of FONs **D1'''a** does not change while only a slight decrease of the emissive properties is observed due to a slow rearrangement of the molecules within the nanoparticle.

In **Chapter II Paragraph 3.1** (Effect of the environment) it was mentioned that chromophores with strong acceptor group could undergo hydrolysis. Since the condensation reaction is an equilibrium, if the product molecule is surrounded by water, the reaction could return back towards the reagents. Actually, a retro-Knoevenagel reaction was observed for some chromophores in polar solvents, such as acetone, acetonitrile or DMSO (cf. **Figure II 6-7**). After these observations, one could think that a chromophore that could undergo a retro-condensation in a water environment like that of FONs, should not be stable at all, therefore we should not be able to obtain nanoparticles of these chromophores. Strikingly, a very interesting behavior was observed, as displayed in **Figure III 18**. We were able to obtain nanoparticles and, indeed, FONs were very stable in comparison with the chromophore in DMSO after addition of a drop of water.

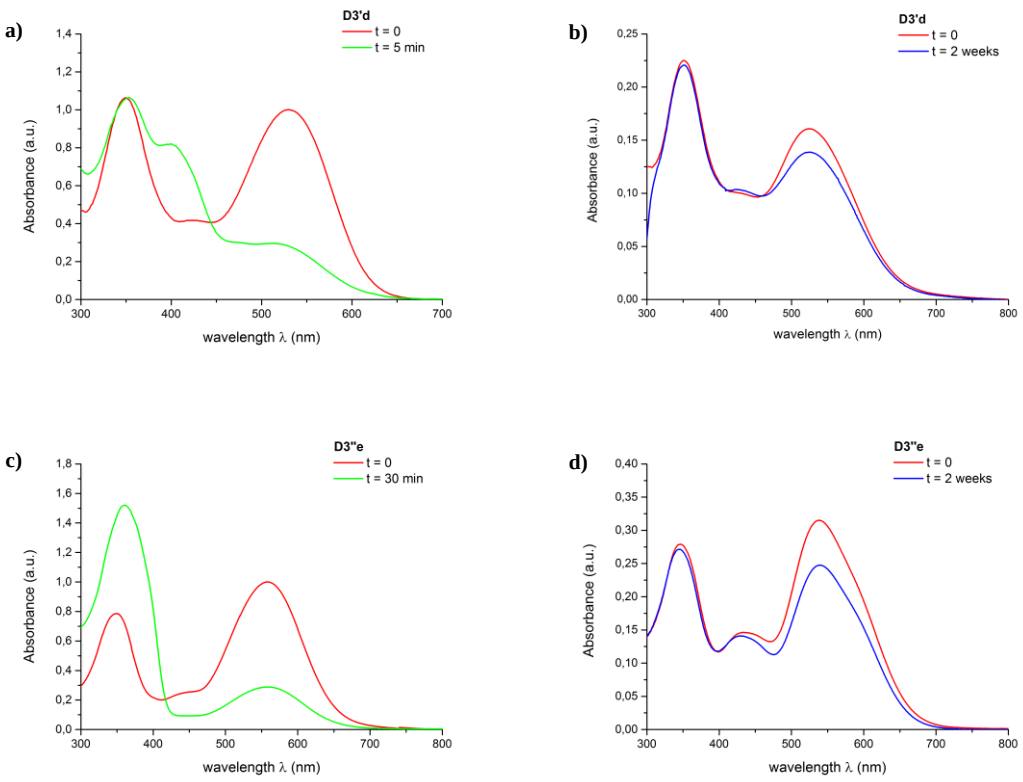

Figure III 18. Absorption spectra measured overtime for chromophores **D3'd** and **D3"e** in DMSO solution adding one drop of water (a and c respectively) and confined in nanoparticles in water (b and d respectively)

The stability of these nanoaggregates suggests us a cooperative shielding effect that protect the chromophores within the nanoparticle from the “aggressive” water environment that could induce the retro-Knoevenagel reaction.

6. Conclusion

In this chapter were displayed the preparation and the morphological characterization of fluorescent organic nanoparticles prepared starting from dipolar chromophores. We were able to obtain colloidally stable spherical nanoparticles with an average size ranging from 21 nm to 66 nm.

On these FONs were studied the optical properties upon one-photon and two-photon excitation. By tuning the chemical structure, it was possible to tune the photophysical properties, as already observed for the chromophores in organic solution. We were able to obtain nanoparticles with a tunable emission from green to deep red or even near infrared, associated with an aggregation-caused quenching phenomenon, indeed the fluorescence quantum yield of FONs is low compared with that measured in $CHCl_3$ solution. In spite of the low Φ_f (up to 0.14 for green-yellow emitter **D2'a**), all FONs display a huge one-photon (ranging from $0.02 \cdot 10^8$ to $2.5 \cdot 10^8$ M^{-1} cm^{-1}) and two-photon (ranging from $0.02 \cdot 10^6$ to $1.1 \cdot 10^6$ GM) brightness, which associated with the two-photon excitation and the emission range in the biological transparency window, suggesting these nanoparticles suitable to be used for both confocal and multiphoton microscopy.

Moreover, an interesting cooperative shielding effect was observed in FONs that prevent the hydrolysis for chromophores bearing strong acceptor groups.

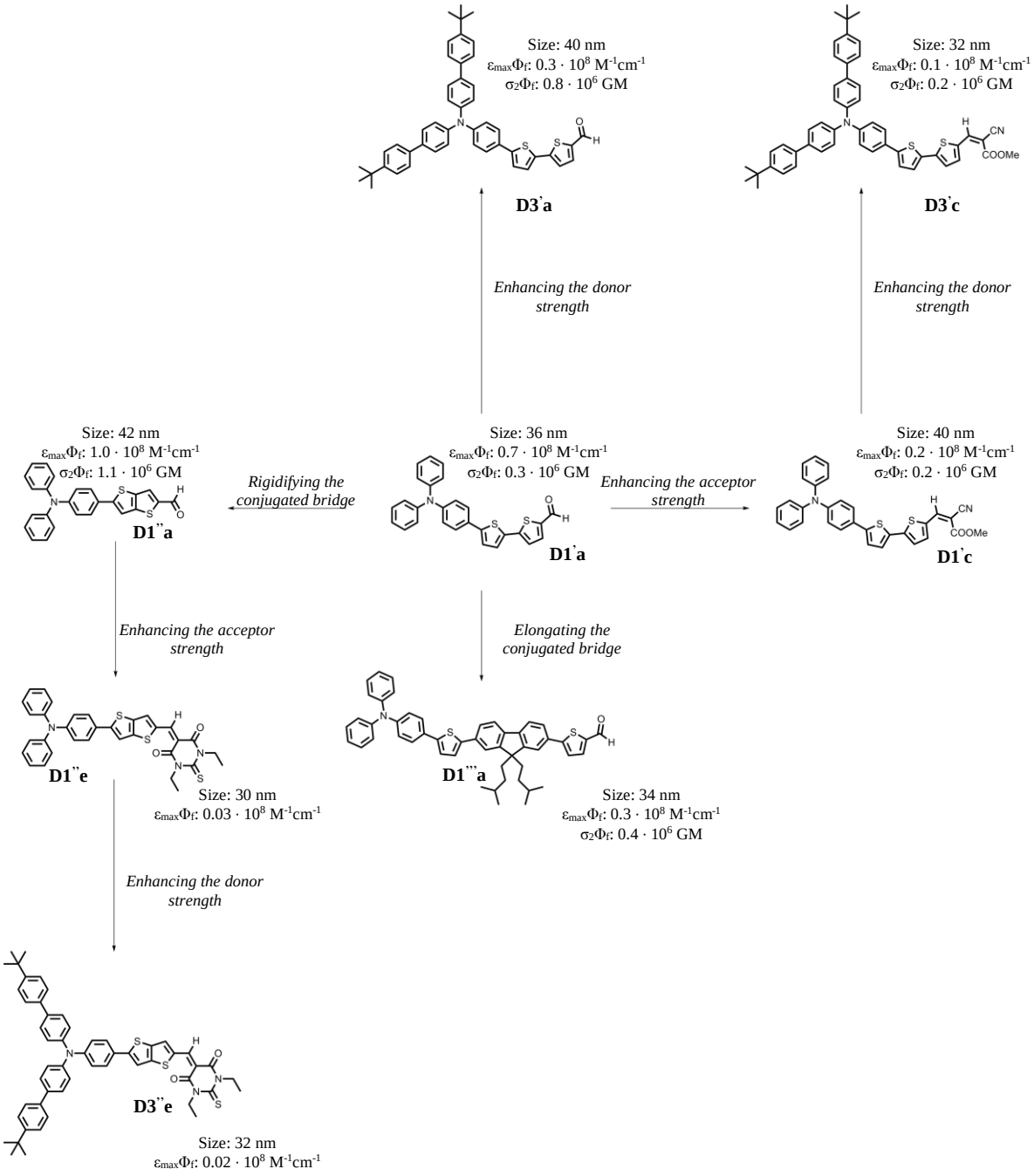

Figure III 19. Resuming flowchart of chromophores in confined environment studied in this chapter

BIBLIOGRAPHIC REFERENCES

(1) Davydov, A. S. The theory of molecular exciton. *Soviet Physics Uspekhi* **1964**, *82*.

(2) Kasha, M.; Rawls, H. R.; El-Bayoumi, M. A. The exciton model in molecular spectroscopy. *Pure Applied Chemistry* **1965**, *11*.

(3) Würthner, F.; Kaiser, T. E.; Saha-Möller, C. R. J-aggregates: from serendipitous discovery to supra- molecular engineering of functional dye materials. *Angewandte Chemie International Edition* **2011**, *50*.

(4) Mishra, A.; Behera, R. K.; Behera, P. K.; Mishra, B. K.; Behera, G. B. Cyanines during the 1990s: A Review. *Chemical Reviews* **2000**, *100*.

(5) Mastrodonato, C.; Pagano, P.; Daniel, J.; Vaultier, M.; Blanchard-Desce, M. Molecular-based fluorescent nanoparticles built from dedicated dipolar thienothiophene dyes as ultra-bright green to NIR nanoemitters. *Molecules* **2016**, *21*, 1227.

(6) Genin, E.; Gao, Z.; Varela, J. A.; Daniel, J.; Bsaibess, T.; Gosse, I.; Groc, L.; Cognet, L.; Blanchard‐Desce, M. "Hyper‐bright" near‐infrared emitting fluorescent organic nanoparticles for single particle tracking. *Advanced Materials* **2014**, *26*, 2258-2261.

(7) Amro, K.; Daniel, J.; Clermont, G.; Bsaibess, T.; Pucheault, M.; Genin, E.; Vaultier, M.; Blanchard-Desce, M. A new route towards fluorescent organic nanoparticles with red-shifted emission and increased colloidal stability. *Tetrahedron* **2014**, *70*, 1903-1909.

(8) Masuhara, H.; Nakanishi, H.; Sasaki, K.: *Single Organic Nanoparticles*; Springer-Verlag Berlin Heidelberg, 2003. pp. XLIX, 402.

(9) Horn, D.; Rieger, J. Organic nanoparticles in the aqueous phase—theory, experiment, and use. *Angewandte Chemie International Edition* **2001**, *40*, 4330-4361.

(10) Daniel, J.; Bondu, F.; Adamietz, F.; Blanchard-Desce, M.; Rodriguez, V. Interfacial organization in dipolar dye-based organic nanoparticles probed by second-harmonic scattering. *ACS Photonics* **2015**, *2*, 1209-1216.

(11) Hansch, C.; Leo, A.; Taft, R. W. A survey of Hammett substituent constants and resonance and field parameters. *Chemical Reviews* **1991**, *91*, 165-195.

(12) Hong, Y.; Lam, J. W. Y.; Tang, B. Aggregation-induced emission. *Chemical Society Reviews* **2011**, *40*, 5361-5388.

(13) Yuan, W.; Lu, P.; Chen, S.; Lam, J. W. Y.; Wang, Z.; Liu, Y.; Kwok, H.; Ma, Y.; Tang, B. Changing the behavior of chromophores from aggregation-caused quenching to aggregation-induced emission: development of highly efficient light emitters in the solid state. *Advanced materials* **2010**, *22*, 2159-2163.

(14) Parthasarathy, V.; Fery-Forgues, S.; Campioli, E.; Recher, G.; Terenziani, F.; Blanchard-Desce, M. Dipolar versus octupolar triphenylamine-based fluorescent organic nanoparticles as brilliant one- and two-photon emitters for (bio)imaging. *Small* **2011**, *7*, 3219-3229.

(15) Daniel, J. Nano outils moléculaires biphotoniques pour le vivant. Université de Bordeaux, 2015.

(16) Terenziani, F.; Parthasarathy, V.; Pla‐Quintana, A.; Maishal, T.; Caminade, A. M.; Majoral, J. P.; Blanchard‐Desce, M. Cooperative two‐photon absorption enhancement by through‐space interactions in multichromophoric compounds. *Angewandte Chemie International Edition* **2009**, *48*, 8691-8694.

(17) Robin, A.-C.; Parthasarathy, V.; Pla-Quintana, A.; Mongin, O.; Terenziani, F.; Caminade, A.-M.; Majoral, J.-P.; Blanchard-Desce, M. In *Tilte*2010.

(18) Larson, D. R.; Zipfel, W. R.; Williams, R. M.; Clark, S. W.; Bruchez, M. P.; Wise, F. W.; Webb, W. W. Water-soluble quantum dots for multiphoton fluorescence imaging in vivo. *Science* **2003**, *300*, 1434-1436.

(19) Lim, S.; Zahid, M. U.; Le, P.; Ma, L.; Entenberg, D.; Harney, A. S.; Condeelis, J.; Smith, A. M. Brightness-equalized quantum dots. *Nature Communications* **2015**, *6*, 8210.

(20) Johnson, I.; Spence, M. T. Z.: *The Molecular Probes Handbook*; 11th ed.; Life Technologies, 2010.

CHAPTER 4

CHARGED DIPOLES

CHAPTER 4–CHARGED DIPOLES

1. Introduction

In the last decade, a large effort was made to understand the cellular internalization of nanoobjects[1-10], while the knowledge is still limited concerning the distribution of nanoparticles within the bio-environment in relation with their morphological and structural properties. Indeed, the interaction of nanoparticles with cells *in vitro* and *in vivo* is known to be strongly affected by their size and their shape[11-19] and numerous studies shown that the surface potential plays a significant role in cellular internalization[20-24]. For instance, positively charged nanoparticles are usually internalized faster than the neutral and negative one. Moreover, it is interesting to explore this way because the membrane of cancer cells are mostly negatively charged thanks to anionic biomolecules in the double layer.

So far, the surface potential of FONs prepared in the hosting lab was always negative[25-32]. Therefore, our challenge was to try to prepare organic nanoparticles with a positive surface potential in order to compare the behaviors in bio-environment. In literature, there are few examples of organic nanoparticles prepared with organic salts[33,34], between them the most known class of nanomaterials are the so-called nanoGUMBOS (Group of Uniform Materials Based on Organic Salts) proposed by the group of Warner[35-40].

To prepare positively charged nanoparticles our idea was to use methyl-pyridinium and methyl-quinolinium as acceptor group in dipolar chromophores with a similar structure compare to the dyes displayed in **Chapter 2** and **3**, with a triphenylamine as donor moiety and thienyl group in the π-conjugated path, using a lipophilic and hindering counterion (**Scheme IV 1**). Heteroaromatic salt-type acceptor moieties display large electron-withdrawing character that leads to interesting optical properties. Moreover, methyl-pyridinium and methyl-quinolinium salts are gaining more and more

interest in recent years thanks to their potential application in medical fields[41-43] and in optoelectronics materials[44].

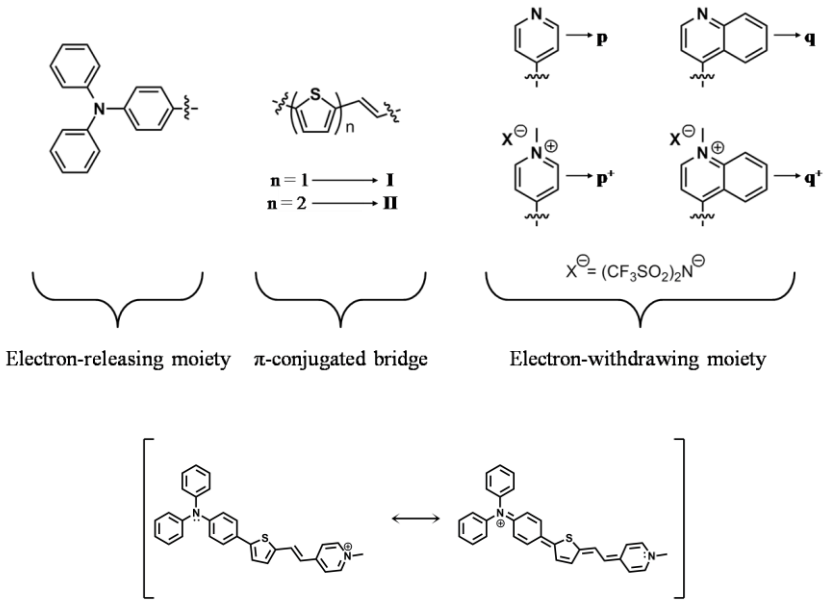

Scheme IV 1. Dipolar pyridine, quinoline, methyl-pyridinium and methyl-quinolinium derivatives subjects of this chapter with the resonance structure of the hemicyanine species (**DIp**$^+$ specifically)

2. Optical properties of chromophores in organic solvents

The photophysical properties of **p**$^+$ and **q**$^+$ chromophores in solution are compared with the respective neutral precursors in order to have terms of comparison.

2.1. Effect of the environment

Solvent polarity can strongly affect the photophysical response of chromophores and that is why also for this new series of compound the solvatochromic behavior was studied. Toluene, THF, DCM and acetone were chosen as common solvents in order to dissolve the dyes as well as preventing protonation of the pyridine and quinoline moiety, which influences the optical properties.

It is interesting to notice the different behavior of the chromophores of the two classes of the series: the neutral dipoles and the hemicyanine. In **Figure IV 1a-b** one can see that **DIp** and **DIIp**

show a non-solvatochromic absorption band and a positive solvatochromism in emission, associated with a broadening of the band, as expected for classical push-pull chromophores; this behavior is explained by a marked ICT transition upon excitation that leads to an enhancement of the dipole moment. On the other hand, dyes **DIp**$^{+}$ and **DIIp**$^{+}$ (**Figure IV 1c-d**) display a negative solvatochromism in absorption with the exception of DCM in which is observable a red-shift of the ICT band, this behavior is known in literature[45,46]. Concerning the emission one can observe that a tuning of the solvent polarity does not affect strongly the fluorescence, non-solvatochromic emission is typical for this class of compounds[46,47].

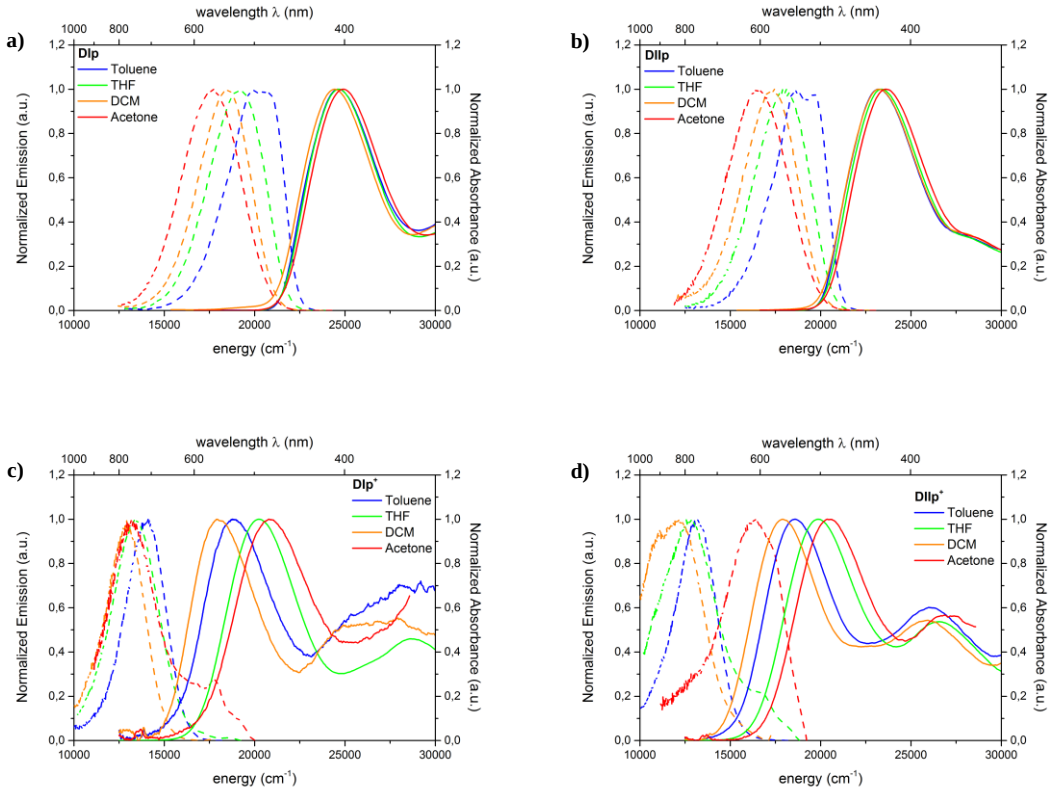

Figure IV 1. Comparison between absorption (solid line) and emission (dashed line) measured in solvent of increasing polarity for chromophores a) **DIp**, b)**DIIp**, c) **DIp**$^{+}$ and d) **DIIp**$^{+}$

It is worth to highlight the emission band of **DIp**$^{+}$ and **DIIp**$^{+}$ measured in acetone, one can see that in chromophore **DIIp**$^{+}$ the band is markedly shifted towards higher energies (**Figure IV 1d**) while for **DIp**$^{+}$ it can be observed a shoulder blue-shifted with respect to the main band (**Figure IV 1c**); this

can be explained by the separation of the ion pair in polar solvent, actually this behavior can be seen also in THF for the compound **DIIp**$^+$.

2.2. Photophysical characterization in THF solution

As common solvent, was chosen THF for the full photophysical characterization of these chromophores. The relevant data are gathered in **Table IV 1**.

Table IV 1. Linear photophysical data for chromophores in THF solution

Cpd	λ_{max}^{1PA} [nm]	ε_{max} [10^4 $M^{-1}cm^{-1}$]	λ_{max}^{em} [nm]	Φ_f	τ_1 [ns]	k_r [10^9 s^{-1}]	k_{nr} [10^9 s^{-1}]
DIp	404	4.1	519	0.55	1.98	0.28	0.23
DIq	406	2.7	558	0.11	1.18	0.09	0.75
DIIp	426	4.7	554	0.26	0.73	0.36	1.01
DIIq	433	4.2	588	0.28	1.05	0.28	0.69
DIp$^+$	500	3.1	745	0.03	0.48 (0.8)/2.17 (0.2)	0.05	1.76
DIq$^+$	555	2.7	835	0.004	/		
DIIp$^+$	506	3.3	779	0.005	0.51 (0.8)/3.28 (0.2)	0.01	1.62
DIIq$^+$	557	3.1	/	/	/		

All chromophores display a broad absorption band that lies between the violet and the green-yellow visible range depending on the dipolar strength of the dyes. The band can be ascribed to a strong ICT band associated with a large molar extinction coefficient ranging from 2.7 to 4.7 $\cdot$ 10^4 M^{-1} cm^{-1}. An elongation of the π-conjugated path by adding one thiophene in the bridge (**I** → **II**) induces a bathochromic shift (**Figure IV 2a**) of the ICT band associated with the expected hyperchromic effect[32,48], while the enhancement of the electron withdrawing character by changing the acceptor group from **p** to **p**$^+$ leads to a marked shift towards longer wavelengths with a decrease of the molar extinction coefficient, contrarily to what was expected[27,48] (see also **Chapter 2**). Anyway, increasing both the electron withdrawing character of the acceptor and the elongation of the π-conjugated path induces a broadening of the absorption band.

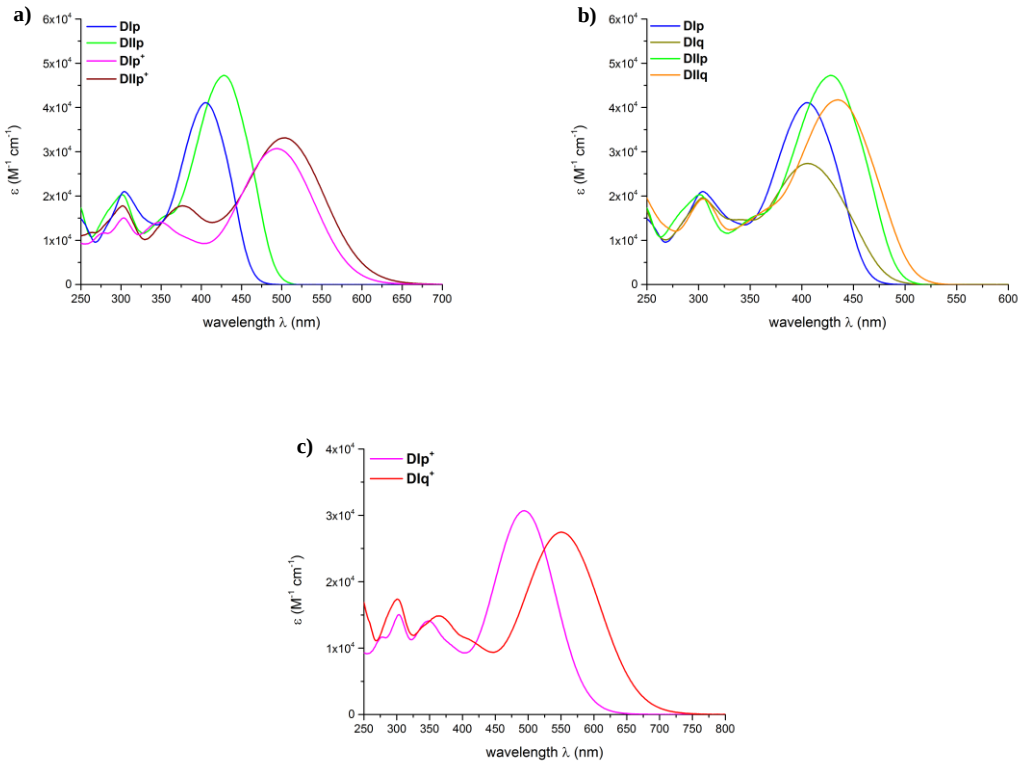

Figure IV 2. Comparison between absorption band of different chromophores studied in this chapter (*consistent color code between the figures of the chapter*)

It is interesting to underline the different behavior displayed by chromophores after the replacement of **p** with **q** and $\mathbf{p}^+$ with $\mathbf{q}^+$ (**Figure IV 2b-c**). The elongation of the conjugation leads to a shift of the ICT band towards lower energies, it can be observed that this behavior is more pronounced in hemicyanine chromophores thanks to the presence of a formal charge on the acceptor group. Moreover, it can be observed a decreasing of the ε_{max} after substitution $\mathbf{p} \rightarrow \mathbf{q}$ and $\mathbf{p}^+ \rightarrow \mathbf{q}^+$.

The luminescent properties generally parallel the behavior observed in absorption, the elongation of the bridge by adding a second thienyl group induces a bathochromic shift; passing from **DIp** to **DIIp** we have a decrease of the fluorescence quantum yield, while going from **DIq** to **DIIq** induces a slight enhancement of Φ_f. Enhancing the strength of the acceptor group after alkylation of the nitrogen in the heteroaromatic rings ($\mathbf{p} \rightarrow \mathbf{p}^+$ and $\mathbf{q} \rightarrow \mathbf{q}^+$) leads to a marked red-shift associated with a broadening of the band. Moreover, it is interesting to highlight that the hemicyanine

chromophores synthesized are near infrared emitters; unfortunately, these chromophores display also a marked quenching of the luminescent properties (**Table IV 1**) indicating that the relaxation mainly follows non-radiative pathways. As it can be seen in **Figure IV 2b-c**, the extra ring in the electron acceptor moiety (**p** → **q** and $\mathbf{p}^+ \rightarrow \mathbf{q}^+$) induces a shift towards longer wavelengths as observed for the absorption band.

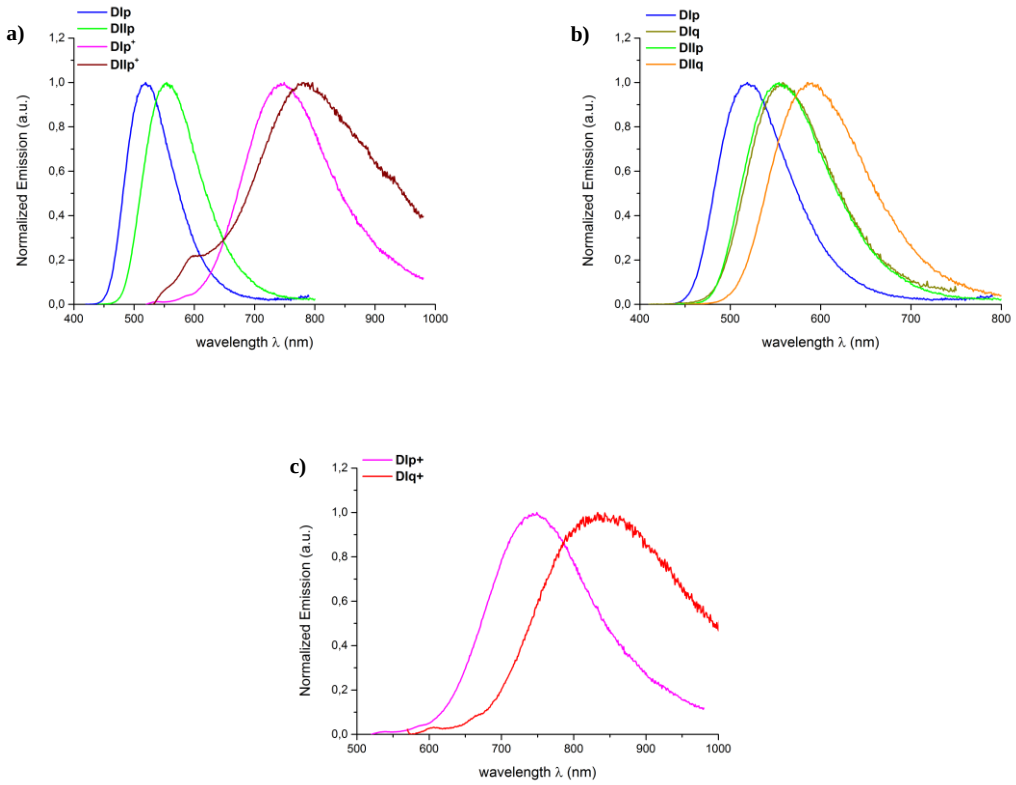

Figure IV 3. Comparison between emission spectra of different chromophores studied in this chapter

Concerning the fluorescence lifetime, it is worth to underline that the neutral dipolar chromophores display a mono-exponential decay with a lifetime between 0.73 and 1.98 ns, while charged compounds show bi-exponential fluorescence decay.

2.3. Photophysical characterization of hemicyanine dyes in SDS micellar solution

Since the idea is to use these chromophores in bio-environment, one of the fundamental requirements is water solubility. Unfortunately, these dyes are not soluble in water, thus I tried to use a

micellar solution of SDS in order to study their optical properties in this medium for further comparison with the molecule confined in nanoparticles.

Table IV 2. Comparison between photophysical data of chromophores in THF and SDS solution

Cpd	λ_{max}^{1PA} [nm]	ε_{max} [10^4 $M^{-1}cm^{-1}$]	λ_{max}^{em} [nm]	Φ_f	τ_1 [ns]
DIp$^+$ (THF)	500	3.1	745	0.03	0.48 (0.8)/2.17 (0.2)
DIp$^+$ (SDS)	477	3.9	650	0.14	0.90 (0.9)/2.04 (0.1)
DIq$^+$ (THF)	555	2.7	835	0.004	/
DIq$^+$ (SDS)	530	1.8	710	0.07	0.80
DIIp$^+$ (THF)	506	3.3	779	0.005	0.51 (0.8)/3.28 (0.2)
DIIp$^+$ (SDS)	484	1.2	680	0.11	0.95
DIIq$^+$ (THF)	557	3.1	/	/	/
DIIq$^+$ (SDS)	534	2.4	754	0.03	0.51

The inner pocket of the micelles formed with SDS has a hydrophobic character therefore the chromophores dissolved in SDS display an hypsochromic shift compared with THF solution, even though the environment is water (**Figure IV 4a-b**). This blue shift is more pronounced for the emission band, which is associated with a large enhancement of the luminescent properties, for example one can see in **Table IV 2** that the Φ_f of compound **DIIp$^+$**, from THF to SDS, displays an increase of more than 20 times (from 0.005 to 0.11) in the NIR region.

Strikingly, contrarily to what was observed in THF solution, an elongation of the π bridge does not affect the ICT transition band, which is strongly affected by the change of the acceptor group from the methyl-pyridinium to the methyl-quinolinium. On the other hand, both structural changes induce a shift of the emission band towards lower energies, as observed for the chromophores dissolved in THF solution.

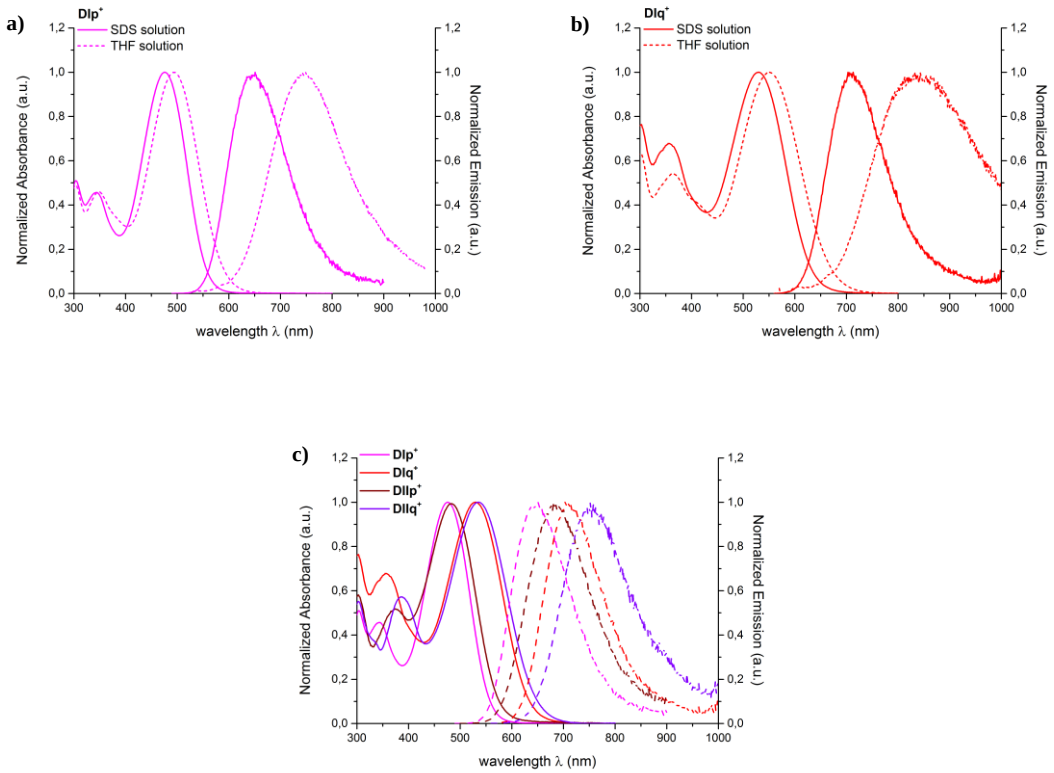

Figure IV 4. Comparison between absorption and emission measured for chromophore a) **DIp**$^+$ and b) **DIq**$^+$ in both SDS and THF solution; absorption and emission measured for the hemicyanine chromophores in SDS solution

3. Optical properties of chromophores when confined in nano-environment

The step further was the preparation of nanoparticles with these classes of chromophores to study the behavior of the molecules upon nanoaggregation. The preparation method used was the same as used and described before: the nanoprecipitation.

3.1. Morphological and structural characterization of FONs

After their preparation, the nanoobjects obtained were characterized by transmission electron microscopy, for the size and the shape, and by zetametry to have an idea of the surface potential of these nanoparticles. Unfortunately, as one can see in **Table IV 3**, it was not possible to obtain ONPs with chromophore **DIp**$^+$.

Table IV 3. Morphological and structural data of FONs

Cpd	d_{TEM} [nm]	N[a)] [10^4]	ζ-potential [mV]
DIp	104	82.4	-46
DIq	23	0.8	-64
DIIp	29	1.5	-49
DIIq	41	3.9	-70
DIp$^+$	/	/	/
DIq$^+$	82	22.4	+54
DIIp$^+$	55	6.5	+50
DIIq$^+$	46	3.6	+53

a) Estimated number of dyes subunit *per* ONPs based on their size

As discussed earlier in the manuscript, since the number of dyes per nanoparticles depends strongly on the size of the object, we can have various orders of magnitude for FONs prepared with different chromophores. For example, as displayed in **Figure IV 5**, ONPs prepared with **DIp** display an average diameters of 104 nm with an estimated number of molecules per nanoparticles of $82.4 \cdot 10^4$, while replacing the pyridine with the quinoline (**DIq**) one can observe an average diameter of 23 nm with a number of chromophores of $0.8 \cdot 10^4$.

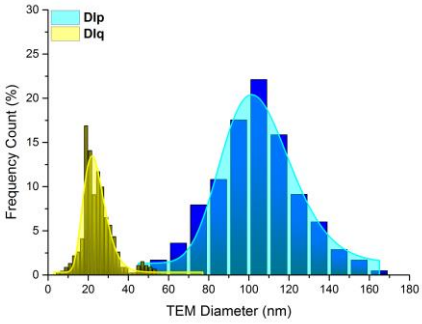

Figure IV 5. Comparison between size distribution of nanoparticles prepared with chromophores **DIp** (dark yellow) and **DIq** (blue)

Strikingly, the alkylation of the nitrogen on the heteroaromatic ring induces an interesting behavior: the nanoparticles prepared display a positively charged surface, so far observed only in few

cases; moreover, from the magnitude of the ζ-potential one could expect good colloidal stability overtime.

As displayed in **Figure IV 6**, the shape of FONs prepared with the hemicyanine dyes is spherical with a broad size distribution, especially for **DIq**$^{+}$,

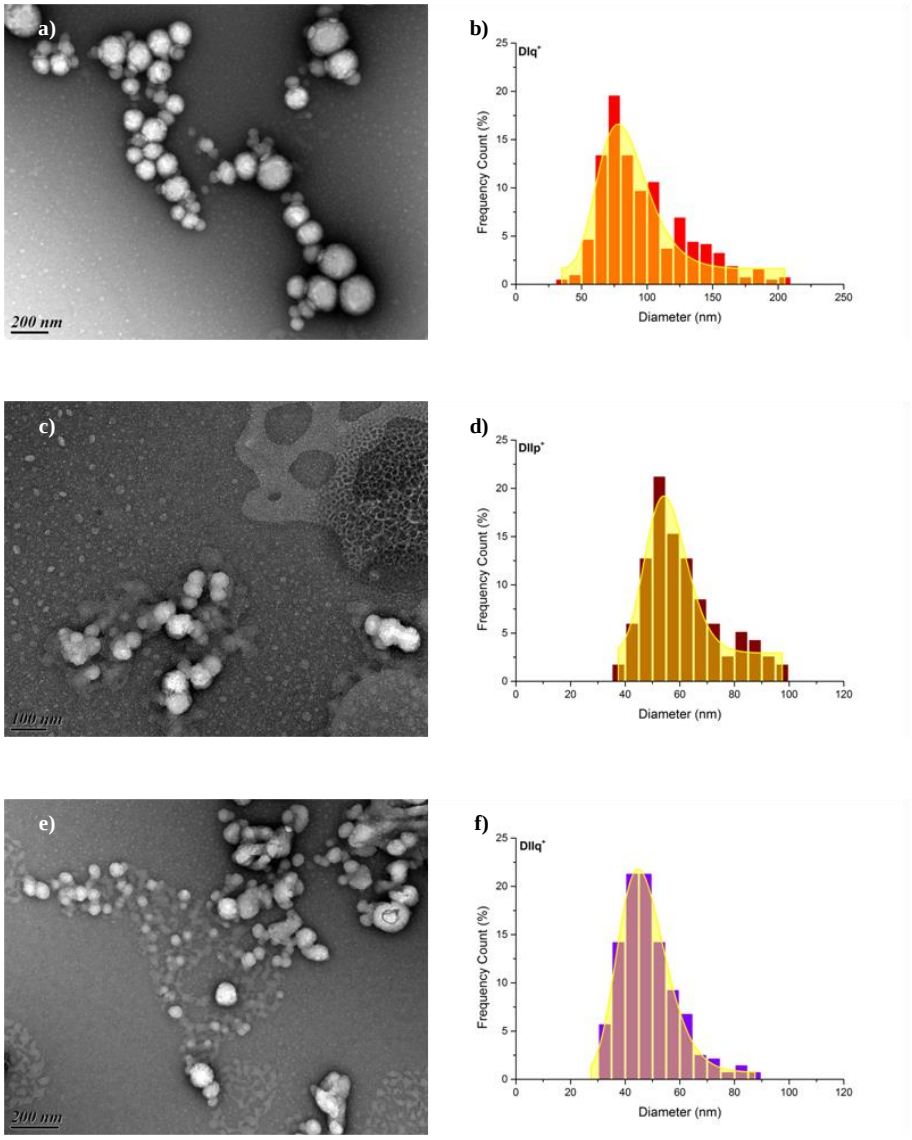

Figure IV 6. TEM images and size distribution of ONPs prepared with chromophore a-b) **DIq**$^{+}$, c-d) **DIIp**$^{+}$ and e-f) **DIIq**$^{+}$.

3.2. Photophysical characterization of hemicyanine dyes upon nanoconfinement

The FONs prepared with methyl-pyridinium and methyl-quinolinium as acceptor group display an intense and broad absorption band that lies in the blue-green visible spectral region. The molar extinction coefficient (gathered with the relevant photophysical data in **Table IV 4**) of the chromophores after nanoaggregation is comparable to, or even higher than the one measured in THF solution. This behavior can be due to a cooperative effect induced by the packing of the molecules in confined environment.

It is worth to notice the absorption band of FONs **DIIp$^+$**, whose unusual shape may be due to the arrangement of chromophores and counter ions within the nanoparticle.

Table IV 4. Photophysical data measured for the hemicyanine chromophores upon nanoaggregation

Cpd	λ_{max}^{1PA} [nm]	$\varepsilon_{max}^{Chrom\ b)}$ [10^4 $M^{-1}cm^{-1}$]	$\varepsilon_{max}^{FONs\ c)}$ [10^9 $M^{-1}cm^{-1}$]	λ_{max}^{em} [nm]	Φ_f	$\varepsilon_{max}^{FONs}\Phi_f$ [10^6 $M^{-1}cm^{-1}$]
DIp$^+$	/	/	/	/	/	/
DIq$^+$	553	4.8	11	830	0.002	22.0
DIIp$^+$	468	3.2	2.1	771	0.002	4.2
DIIq$^+$	545	3.7	1.2	889	0.0005[a)]	0.6

a) Because of the low fluorescence quantum yield this data is an average between 5 independent measurements, b) estimated value taking into account the total concentration of chromophores in nanoparticles, c) estimated value taking into account the concentration of FONs

As observed for the chromophores dissolved in THF or SDS, the ICT band is not affected by the change of the electron-withdrawing moiety, while it can be observed a bathochromic shift of the emission band passing from **DIIp$^+$** to **DIIq$^+$**. The shift towards low energies is observed also with elongating the π-conjugated pathway.

Despite their low luminescent properties, it is worth to underline the fact that these FONs display strikingly high one-photon brightness (up to $2.2 \cdot 10^7$ M^{-1} cm^{-1}), thanks to the high molar extinction coefficient estimated *per* nanoparticle, that associated with the NIR emission make these object suitable for confocal microscopy.

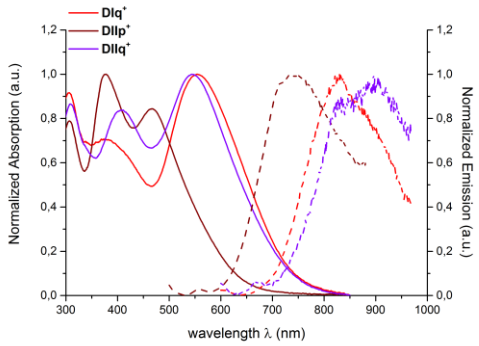

Figure IV 7. Comparison between normalized absorption and emission of FONs prepared with hemicyanine dyes.

Moreover, from the comparison of the emission spectra of chromophores in THF solution, in SDS micellar environment and in FONs, one can observe that depending on the dye we have different behaviors indicating different local environment seen by the molecule in confined environment. FONs prepared with **DIq**$^+$ display an emission similar to the one measured in THF, **DIIp**$^+$ within nanoparticles have an environment slightly more polar than SDS, and it is also the case for **DIIq**$^+$ (**Figure IV 8**).

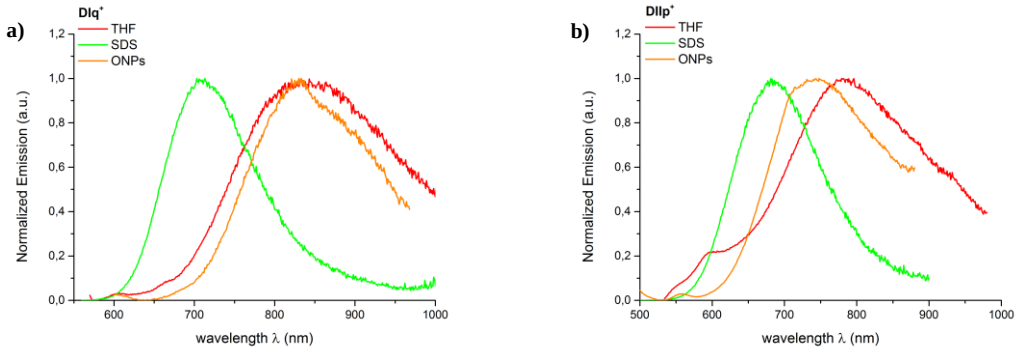

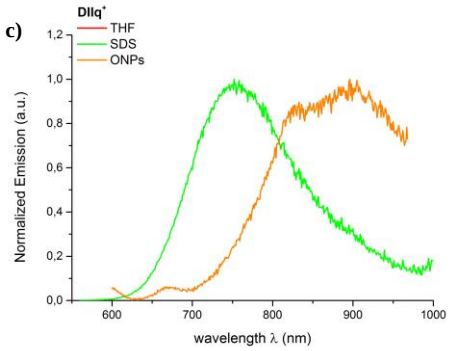

Figure IV 8. Comparison between the emission spectra measured for chromophores a) **DIq**$^+$, b) **DIIp**$^+$ and c) **DIIq**$^+$ in THF solution (red line), SDS solution (green line) and FONs (orange line)

3.3. Monitoring of colloidal and structural stability of FONs overtime

An important requirement that nanoparticles should satisfy to be used in bio-environment is the colloidal stability. As discussed earlier, this property is related to the surface potential and since these nanoparticles display a large absolute value of ζ-potential, thus one could expect a good stability of the colloidal suspension overtime.

As displayed in **Figure IV 9**, this expectation was disregarded; indeed one can see that even after one day there is a marked decrease of the absorption band. It is also worth to point out the evolution of the absorption band measured on FONs prepared with chromophore **DIIp**$^+$. After one day it displays a broadening associated with a slight bathochromic shift that may indicate, in addition with an aggregation process, a rearrangement of the chromophores within the nanoparticles towards a more emissive structure. In fact, after one day the structural change induces a marked enhancement of the luminescent properties. As a consequence, also the fluorescence quantum yield displays an enhancement from 0.002 measured at t = 0 to 0.01 measured at t = 1 day, going from kinetic to thermodynamic equilibrium. Contrarily to what was observed for FONs **DIIp**$^+$, the hypochromic effect observed in absorption is associated with a quenching of luminescence, marked for FONs **DIq**$^+$ with respect to FONs **DIIq**$^+$.

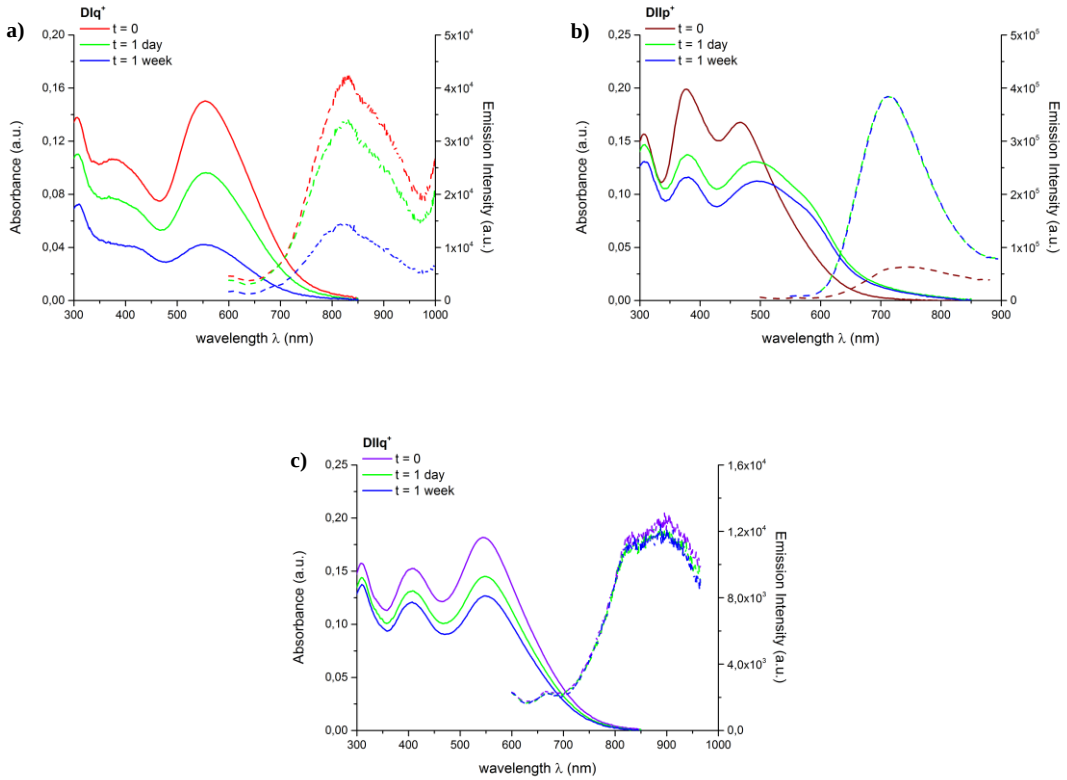

Figure IV 9. Monitoring of absorption and emission overtime of FONs prepared with a) **DIq**$^+$, b) **DIIp**$^+$ and c) **DIIq**$^+$

4. Conclusion

In this chapter, the photophysical properties of hemicyanine chromophore in organic solution and in SDS micellar solution were discussed. It was shown that the methylation of the nitrogen of the heteroaromatic rings induces a large bathochromic shift of the emission band yielding deep red to NIR emissive chromophores. This behavior is associated with a marked quenching of the fluorescence quantum yield.

We were able to prepare spherical organic nanoparticles, ranging between 46 and 82 nm size, with a positive surface potential. Despite their low Φ_f and their poor stability overtime, they show an interesting large one-photon brightness, up to $2.2 \cdot 10^7$ M^{-1} cm^{-1}, in the NIR spectral region; the step further will be to study these nanoobjects in bioenvironment as fluorescent probes.

BIBLIOGRAPHIC REFERENCES

(1) Rejman, J.; Oberle, V.; Zuho, I. S.; Hoekstra, D. Size-dependent internalization of particles via the pathways of clathrin- and caveolae-mediated endocytosis. *Biochemical Journal* **2004**, *377*, 159-169.

(2) Decuzzi, P.; Ferrari, M. The role of specific and non-specific interactions in receptor-mediated endocytosis of nanoparticles. *Biomaterials* **2007**, *28*, 2915-2922.

(3) Reynwar, B. J.; Illya, G.; Harmandaris, V. A.; Müller, M. M.; Kremer, K.; Deserno, M. Aggregation and vesiculation of membrane proteins by curvature-mediated interactions. *Nature* **2007**, *447*, 461-464.

(4) Verma, A.; Uzun, O.; Hu, Y.; Hu, Y.; Han, H.-S.; Watson, N.; Chen, S.; Irvine, D. J.; Stellacci, F. Surface-structure-regulated cell-membrane penetration by monolayer-protected nanoparticles. *Nature Materials* **2008**, *7*, 588-595.

(5) Feng, D.; Zhao, W. L.; Ye, Y. Y.; Bai, X. C.; Liu, R. Q.; Chang, L. F.; Zhou, Q.; Sui, S. F. Cellular internalization of exosomes occurs through phagocytosis. *Traffic* **2010**, *11*, 675-687.

(6) Shi, X.; von dem Bussche, A.; Hurt, R. H.; Kane, A. B.; Gao, H. Cell entry of one-dimensional nanomaterials occurs by tip recognition and rotation. *Nature Nanotechnology* **2011**, *6*, 714-719.

(7) Pogodin, S.; Werner, M.; Sommer, J.-U.; Baulin, V. A. Nanoparticle-induced permeability of lipid membranes. *ACS Nano* **2012**, *6*, 10555-10561.

(8) Kim, A.; Shin, T.-H.; Shin, S.-M.; Pham, C. D.; Choi, D.-K.; Kwon, M.-H.; Kim, Y.-S. Cellular internalization mechanism and intracellular trafficking of filamentous m13 phages displaying a cell-penetrating transbody and TAT peptide. *PLoS ONE* **2012**, *7*.

(9) Li, Y.; Zhang, X.; Cao, D. Nanoparticle hardness controls the internalization pathway for drug delivery. *Nanoscale* **2015**.

(10) Li, Y.; Shang, L.; Nienhaus, U. G. Super-resolution imaging-based single particle tracking reveals dynamics of nanoparticle internalization by live cells. *Nanoscale* **2016**, *8*, 7423-7429.

(11) Miller, C. R.; Bondurant, B.; McLean, S. D.; McGovern, K. A.; O'Brien, D. F. Liposome-cell interactions in vitro: effect of liposome surface charge on the binding and endocytosis of conventional and sterically stabilized liposomes. *Biochemistry* **1998**, *37*, 12875-12883.

(12) Win, K.; Feng, S.-S. Effects of particle size and surface coating on cellular uptake of polymeric nanoparticles for oral delivery of anticancer drugs. *Biomaterials* **2005**, *26*, 2713-2722.

(13) Foged, C.; Brodin, B.; Frokjaer, S.; Sundblad, A. Particle size and surface charge affect particle uptake by human dendritic cells in an in vitro model. *International Journal of Pharmaceutics* **2005**, *298*, 315-322.

(14) Euliss, L. E.; DuPont, J. A.; Gratton, S.; DeSimone, J. Imparting size, shape, and composition control of materials for nanomedicine. *Chemical Society Reviews* **2006**, *35*, 1095-1104.

(15) Gratton, S. E. A.; Ropp, P. A.; Pohlhaus, P. D.; Luft, C. J.; Madden, V. J.; Napier, M. E.; DeSimone, J. M. The effect of particle design on cellular internalization pathways. *Proceedings of the National Academy of Sciences* **2008**, *105*, 11613-11618.

(16) Yang, K.; Ma, Y. Q. Computer simulation of the translocation of nanoparticles with different shapes across a lipid bilayer. *Nature Nanotechnology* **2010**.

(17) Chithrani, D. B.; Ghazani, A. A.; Chan, W. C. W. Determining the size and shape dependence of gold nanoparticle uptake into mammalian cells. *Nano Letters* **2006**, *6*, 662-668.

(18) Chithrani, D. B.; Chan, W. C. W. Elucidating the mechanism of cellular uptake and removal of protein-coated gold nanoparticles of different sizes and shapes. *Nano Letters* **2007**, *7*, 1542-1550.

(19) Jiang, W.; Kim, B. Y. S.; Rutka, J. T.; Chan, W. C. W. Nanoparticle-mediated cellular response is size-dependent. *Nature Nanotechnology* **2008**, *3*, 145-150.

(20) Slowing, I.; Trewyn, B. G.; Lin, V. Effect of surface functionalization of MCM-41-type mesoporous silica nanoparticles on the endocytosis by human cancer cells. *Journal of the American Chemical Society* **2006**, *128*, 14792-14793.

(21) Harush-Frenkel, O.; Rozentur, E.; Benita, S.; Altschuler, Y. Surface charge of nanoparticles determines their endocytic and transcytotic pathway in polarized MDCK cells. *Biomacromolecules* **2008**, *9*, 435-443.

(22) Cho, E.; Xie, J.; Wurm, P. A.; Xia, Y. understanding the role of surface charges in cellular adsorption versus internalization by selectively removing gold nanoparticles on the cell surface with a I2/KI etchant. *Nano Letters* **2009**, *9*, 1080-1084.

(23) Villanueva, A.; Cañete, M.; Roca, A. G.; Calero, M.; Veintemillas-Verdaguer, S.; Serna, C. J.; del Morales, M.; Miranda, R. The influence of surface functionalization on the enhanced internalization of magnetic nanoparticles in cancer cells. *Nanotechnology* **2009**, *20*, 115103.

(24) Shin, E. H.; Li, Y.; Kumar, U.; Sureka, H. V.; Zhang, X.; Payne, C. K. Membrane potential mediates the cellular binding of nanoparticles. *Nanoscale* **2013**, *5*, 5879-5886.

(25) Daniel, J.; Godin, A. G.; Palayret, M.; Lounis, B.; Cognet, L.; Blanchard-Desce, M. Innovative molecular-based fluorescent nanoparticles for multicolor single particle tracking in cells. *Journal of Physics D: Applied Physics* **2016**, *49*, 84002.

(26) Verlhac, J.-B.; Daniel, J.; Pagano, P.; Clermont, G.; Blanchard-Desce, M. Enhanced two-photon brightness in molecular-based organic nanoparticles built from articulated-dipoles. *Comptes Rendus Chimie* **2016**, *19*, 28-38.

(27) Mastrodonato, C.; Pagano, P.; Daniel, J.; Vaultier, M.; Blanchard-Desce, M. Molecular-based fluorescent nanoparticles built from dedicated dipolar thienothiophene dyes as ultra-bright green to NIR nanoemitters. *Molecules* **2016**, *21*, 1227.

(28) Li, H.; Daniel, J.; Verlhac, J. B.; Blanchard‐Desce, M.; Sojic, N. Bright electrogenerated chemiluminescence of a bis‐donor quadrupolar spirofluorene dye and its nanoparticles. *Chemistry - A European Journal* **2016**, *22*, 12702-12714.

(29) Daniel, J.; Godin, A. G.; Clermont, G.; Lounis, B.; Cognet, L.; Blanchard-Desce, M. NIR-emitting molecular-based nanoparticles as new two-photon absorbing nanotools for single particle tracking. *SPIE* **2015**.

(30) Daniel, J.; Bondu, F.; Adamietz, F.; Blanchard-Desce, M.; Rodriguez, V. Interfacial organization in dipolar dye-based organic nanoparticles probed by second-harmonic scattering. *ACS Photonics* **2015**, *2*, 1209-1216.

(31) Genin, E.; Gao, Z.; Varela, J. A.; Daniel, J.; Bsaibess, T.; Gosse, I.; Groc, L.; Cognet, L.; Blanchard‐Desce, M. "Hyper‐bright" near‐infrared emitting fluorescent organic nanoparticles for single particle tracking. *Advanced Materials* **2014**, *26*, 2258-2261.

(32) Amro, K.; Daniel, J.; Clermont, G.; Bsaibess, T.; Pucheault, M.; Genin, E.; Vaultier, M.; Blanchard-Desce, M. A new route towards fluorescent organic nanoparticles with red-shifted emission and increased colloidal stability. *Tetrahedron* **2014**, *70*, 1903-1909.

(33) Huang, Y.; Zhang, G.; Hu, F.; Jin, Y.; Zhao, R.; Zhang, D. Emissive nanoparticles from pyridinium-substituted tetraphenylethylene salts: imaging and selective cytotoxicity towards cancer cells in vitro and in vivo by varying counter anions. *Chemical Science* **2016**, *7*, 7013-7019.

(34) Shulov, I.; Arntz, Y.; Mély, Y.; Pivovarenko, V. G.; Klymchenko, A. S. Non-coordinating anions assemble cyanine amphiphiles into ultra-small fluorescent nanoparticles. *Chemical Communications (Cambridge, England)* **2016**, *52*, 7962-7965.

(35) Dumke, J. C.; Qureshi, A.; Hamdan, S.; El-Zahab, B.; Das, S.; Hayes, D. J.; Boldor, D.; Rupnik, K.; Warner, I. M. Photothermal response of near-infrared-absorbing NanoGUMBOS. *Applied Spectroscopy* **2014**, *68*, 340-352.

(36) Jordan, A. N.; Siraj, N.; Das, S.; Warner, I. M. Tunable near-infrared emission of binary nano- and mesoscale GUMBOS. *RSC Advances* **2014**, *4*, 28471.

(37) Dumke, J. C.; Qureshi, A.; Hamdan, S.; Rupnik, K.; El-Zahab, B.; Hayes, D. J.; Warner, I. M. In vitro activity studies of hyperthermal near-infrared nanoGUMBOS in MDA-MB-231 breast cancer cells. *Photochemical & Photobiological Sciences* **2014**, *13*, 1270.

(38) Das, S.; Bwambok, D.; El-Zahab, B.; Monk, J.; de Rooy, S. L.; Challa, S.; Li, M.; Hung, F. R.; Baker, G. A.; Warner, I. M. Nontemplated approach to tuning the spectral properties of cyanine-based fluorescent NanoGUMBOS. *Langmuir* **2010**, *26*, 12867-12876.

(39) Bwambok, D. K.; El-Zahab, B.; Challa, S. K.; Li, M.; Chandler, L.; Baker, G. A.; Warner, I. M. Near-infrared fluorescent nanoGUMBOS for biomedical imaging. *ACS nano* **2009**, *3*, 3854-3860.

(40) Tesfai, A.; El-Zahab, B.; Kelley, A. T.; Li, M.; Garno, J. C.; Baker, G. A.; Warner, I. M. Magnetic and nonmagnetic nanoparticles from a group of uniform materials based on organic salts. *ACS nano* **2009**, *3*, 3244-3250.

(41) Mazzoli, A.; Carlotti, B.; Consiglio, G.; Fortuna, C. G.; Miolo, G.; Spalletti, A. Photobehaviour of methyl-pyridinium and quinolinium iodide derivatives, free and complexed with DNA. A case of bisintercalation. *Photochemical & Photobiological Sciences* **2014**, *13*, 939-950.

(42) Fortuna, C. G.; Barresi, V.; Bonaccorso, C.; Consiglio, G.; Failla, S.; Trovato-Salinaro, A.; Musumarra, G. Design, synthesis and in vitro antitumour activity of new heteroaryl ethylenes. *European Journal of Medicinal Chemistry* **2012**, *47*, 221-227.

(43) Fortuna, C. G.; Forte, G.; Pittalà, V.; Giuffrida, A.; Consiglio, G. Could 2,6-bis((E)-2-(furan-2-yl)vinyl)-1-methylpyridinium iodide and analog compounds intercalate DNA? A first principle prediction based on structural and electronic properties. *Computational and Theoretical Chemistry* **2012**, *985*, 8-13.

(44) Jeong, J.-H.; Kim, J.-S.; Campo, J.; Lee, S.-H.; Jeon, W.-Y.; Wenseleers, W.; Jazbinsek, M.; Yun, H.; Kwon, O. P. N-Methylquinolinium derivatives for photonic applications:

Enhancement of electron-withdrawing character beyond that of the widely-used N-methylpyridinium. *Dyes and Pigments* **2015**, *113*, 8-17.

(45) Zhan, C.-L.; Wang, D.-Y. Nonlinear dependence of solvent polarity effects on twisted intramolecular charge-transfer states and linear relation for electronic spectra in a stilbazolium-like dye. *Journal of Photochemistry and Photobiology A: Chemistry* **2002**, *147*, 93-101.

(46) Carlotti, B.; Cesaretti, A.; Fortuna, C. G.; Spalletti, A.; Elisei, F. Experimental evidence of dual emission in a negatively solvatochromic push–pull pyridinium derivative. *Physical Chemistry Chemical Physics* **2014**, *17*, 1877-1882.

(47) Carlotti, B.; Consiglio, G.; Elisei, F.; Fortuna, C. G.; Mazzucato, U.; Spalletti, A. Intramolecular charge transfer of push–pull pyridinium salts in the singlet manifold. *The Journal of Physical Chemistry A* **2014**, *118*, 3580-3592.

(48) Genin, E.; Hugues, V.; Clermont, G.; Herbivo, C.; Castro, M. C. R.; Comel, A.; Raposo, M. M. M.; Blanchard-Desce, M. Fluorescence and two-photon absorption of push–pull aryl (bi) thiophenes: structure–property relationships. *Photochemical & Photobiological Sciences* **2012**, *11*.

CHAPTER 5

ARTICULATED DIPOLES

CHAPTER 5–ARTICULATED DIPOLES

1. Introduction

Molecular confinement of a large number of chromophores generates strong intermolecular interactions that can induce the so-called aggregation caused quenching[1]. As already discussed in **Chapter 3**, to prevent this problem one can use the molecular engineering, designing molecules with hindering groups that limit the deleterious π-π stacking responsible of competitive non-radiative decay. The purpose is to prepare chromophores that are able to display AIE or AIEE and to do this we should take into account molecules that in solution are free to rotate while in confined environment some degrees of freedom are blocked in order to decrease the non-radiative decay rate, thus enhancing the emissive properties[2-4].

When one considers classical dipolar "push-pull" chromophores D-π-A, which usually display large intramolecular charge transfer (ICT) transition, a strong dipole-dipole interaction is expected hence an anti-parallel packing of molecules. This molecular arrangement can markedly affect both linear and non-linear optical properties[5] (cf. **Chapter 3**).

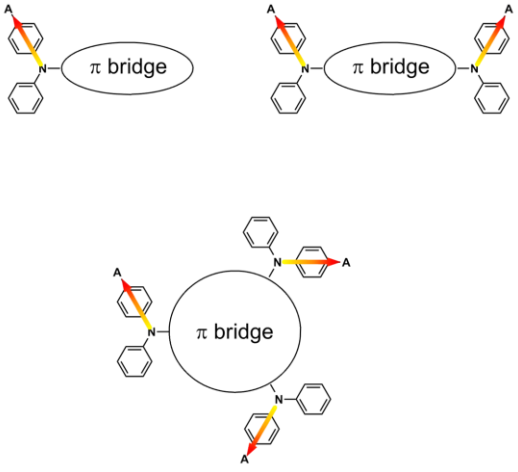

Illustration V 1. Schematic representation of multidipolar chromophores studied in this chapter. The dipoles are represented by arrows

To decrease the probability of close interactions between neighbor dipoles, the idea was to synthesize multi-dipolar chromophores in which the active subunits are connected by a rigid π-conjugated bridge, as displayed in **Illustration V 1**. The propeller shape of the diphenylamine associated with the rotational motion of the different part of the molecules give us the opportunity to study these chromophores upon nano-confinement hoping an AIE/AIEE phenomenon.

The short dipoles were prepared using a substituted phenylamine as donor moiety and either aldehyde (CHO) or dicyanovinyl (DCV) as electron-withdrawing end-groups. The dipolar subunits were linked together by a fluorene or a biphenyl core in a quadrupolar-like arrangement, or with a truxene core in a octupolar-like configuration. It was used as monomer a push-pull dipole linked simply with a fluorenyl moiety. In **Figure V 1** are displayed the chromophores presented in this chapter.

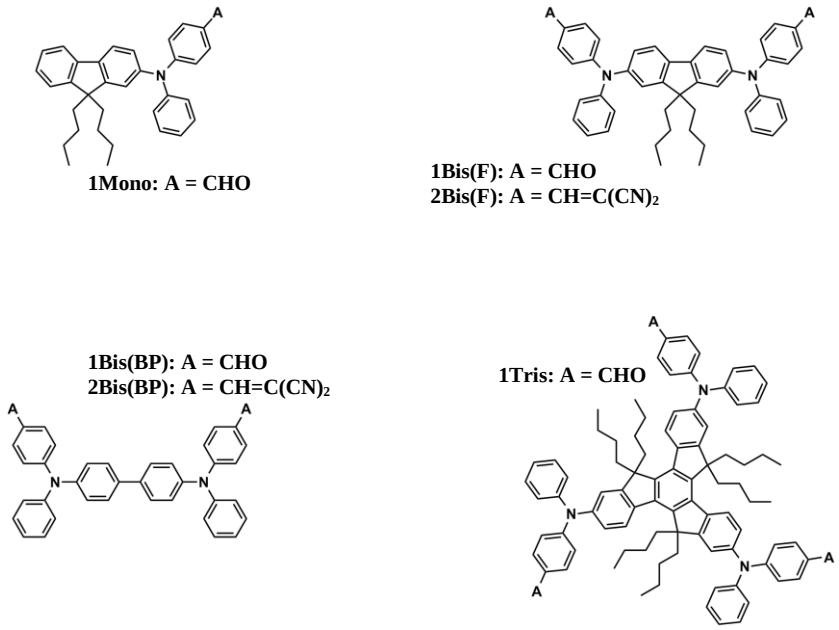

Figure V 1. Articulated dipoles chromophores studied in this chapter

On these chromophores was investigated the influence of the number of dipolar subunits, regarding both linear and non-linear optical properties when the molecules are both in organic solution and confined in nano-environment.

2. Structural characterization of the articulated dipoles

The chromophores studied in this chapter were synthesized by Prof. Jean-Baptiste Verlhac (JBV), thus the chemical synthesis will not be explained in detail here. In **Scheme V 1** you can find the general synthetic route followed.

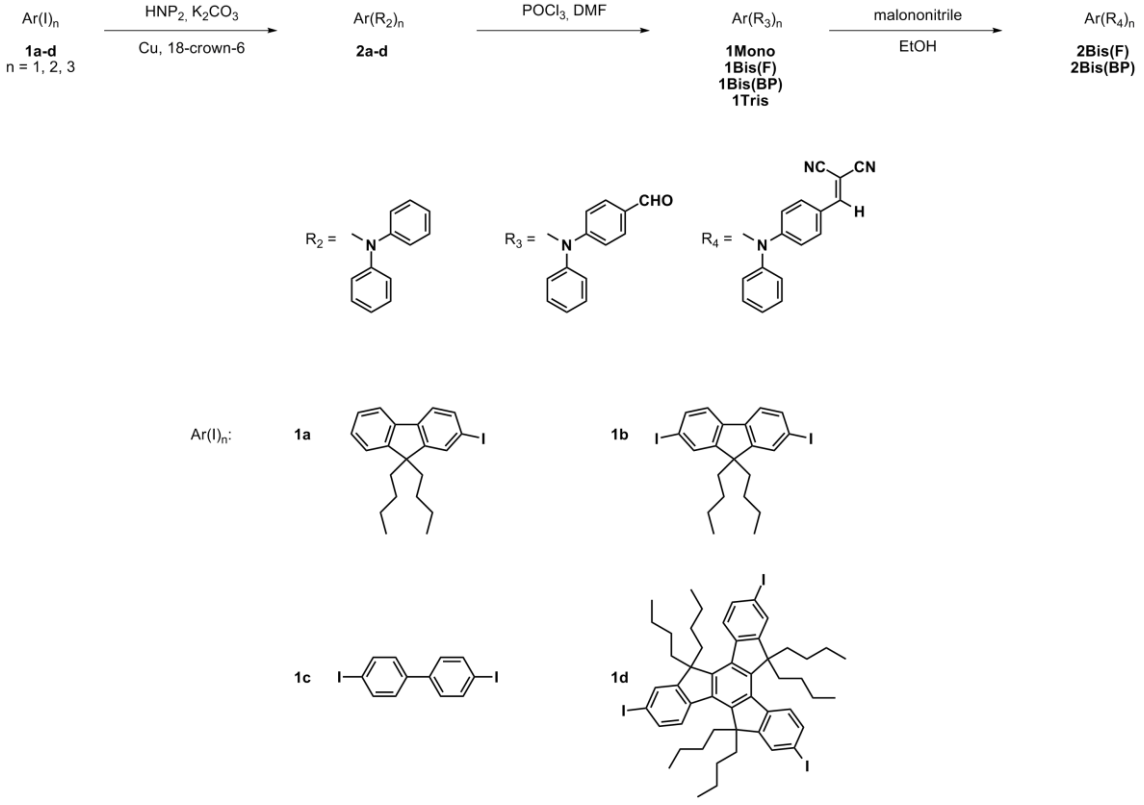

Scheme V 1. Synthetic route of the chromophores

2.1. Crystal characterization

In this paragraph are described the crystal structure obtained for the chromophores **1Bis(F)**, **2Bis(F)** and **1Tris**. As will be discussed, these molecules in the crystal packing did not display specific interactions and, thanks to the presence of hindering groups, the close π-π stacking is prevented. Thus, one can expect weak intermolecular interaction that will be an advantage for photophysical properties, when the molecule is confined in nanoparticle.

*2.1.1. Compound **1Bis(F)***

Single crystals of chromophore **1Bis(F)** were grown by slow diffusion of MeOH in a supersaturated solution of dye in THF. The compound crystallizes in a centrosymmetric monoclinic $P2_1/c$ space group.

As it can be observed in **Figure V 2a**, the two dipoles connected by the fluorene core are in antiperiplanar conformation with a torsion angle between the two CHO acceptor groups of 172.5°. It is worthy to note the planarity distortion of the fluorene π bridge of 2° between the two phenyl rings. Moreover, the two butyl chains form a cross-like structure with the core (89° the angle between the main plane of the core and the plane of the alkyl chain), which is consistent with literature[6].

The hindering groups prevent short π-π interactions, in fact among neighbor molecules one can observe a CH-π interaction between a butyl chain of a molecule and the fluorene of a chromophore forming the second layer (3.6 Å) while the distance between two fluorene cores is 7.5 Å, as displayed in **Figure V 2b**.

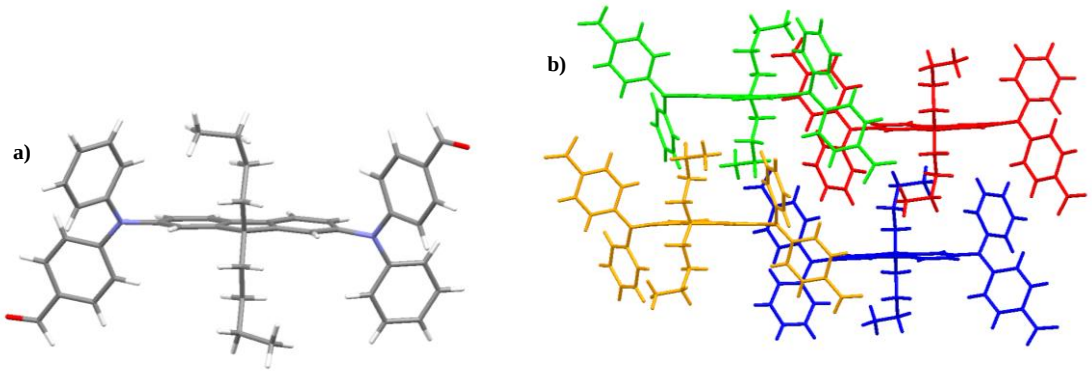

Figure V 2. a) Molecule **1Bis(F)** in general position and b) view of the crystal packing along the *b* axis

*2.1.2. Compound **2Bis(F)***

Chromophore **2Bis(F)** crystallizes in a centrosymmetric monoclinic C2/c space group, and single crystals suitable for XRD were obtained by slow diffusion of MeOH in a supersaturated solution of **2Bis(F)** in CH_2Cl_2.

As discussed before for **1Bis(F)**, also the molecule bearing DCV as acceptor group, the two dipoles are arranged in an antiperiplanar conformation with respect to the fluorene bridge, with a dihedral angle of 106°. The planarity distortion of the fluorene core is 3.6° between the two phenyl rings. As expected, the alkyl chains on the bridge are perpendicular (89°) with respect to the main plane of the π-conjugated linker.

As observed in **1Bis(F)**, the intermolecular interaction in **2Bis(F)** in crystalline state are not specific, the shortest CH-π interaction is 3.6 Å between the last methyl group of a butyl chain and the substituted phenyl group of the diphenylamine, as displayed in **Figure V 3b**.

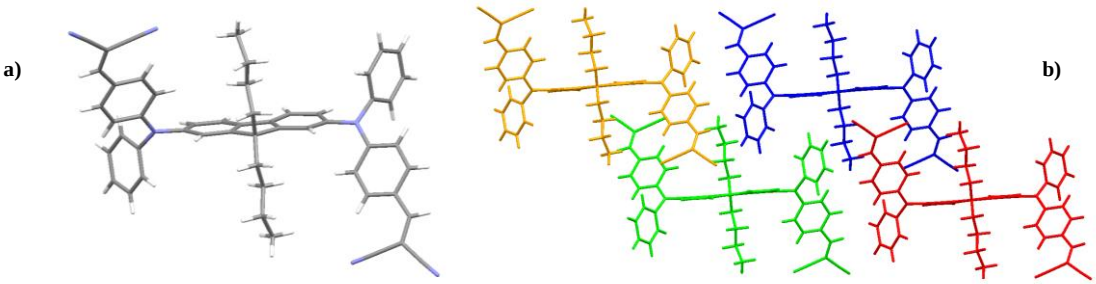

Figure V 3. a) Molecule **2Bis(F)** in general position and b) view of the crystal packing along the *b* axis

*2.1.3. Compound **1Tris***

Single crystals of **1Tris** were obtained by slow diffusion of MeOH in an oversaturated solution of the chromophore dissolved in THF. The compound crystallizes in a centrosymmetric trigonal R-3 space group.

As one can observe in **Figure V 4a-b**, the dipoles are arranged in a syn conformation with a dihedral angle between dipoles of 52°. The truxene core is distorted from planarity of 7.5° in each branch and this distortion can be attributed to the presence of the butyl chains. The hindering alkyl chains are disposed in a cross-like configuration with an angle between the main planes of 89°.

Thanks to a CH-π interaction (3.6 Å) between the alkyl chains and the truxene of a second layer, it can be observed in **Figure V 4c** the formation of a dimer. Moreover, another CH-π interaction between a phenyl ring of the diphenylamine and the truxene induces the formation of the layer of chromophores as displayed in **Figure V 4d**.

a)

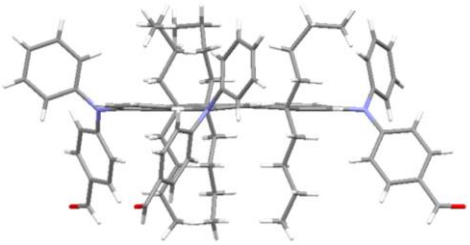

b)

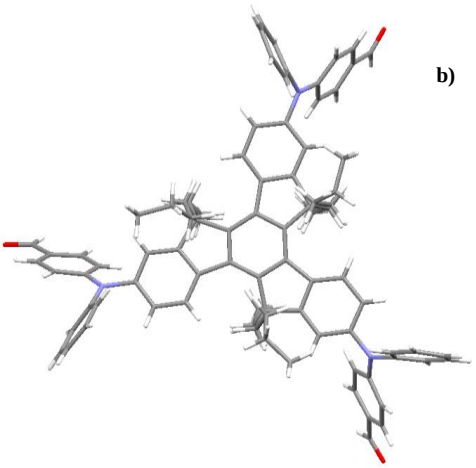

c)

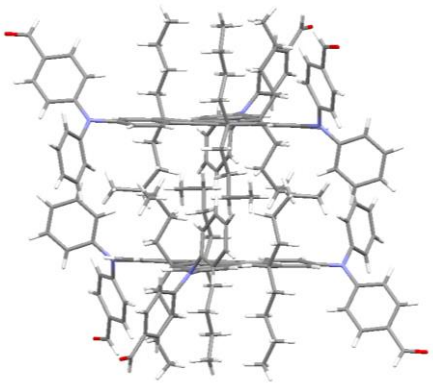

d)

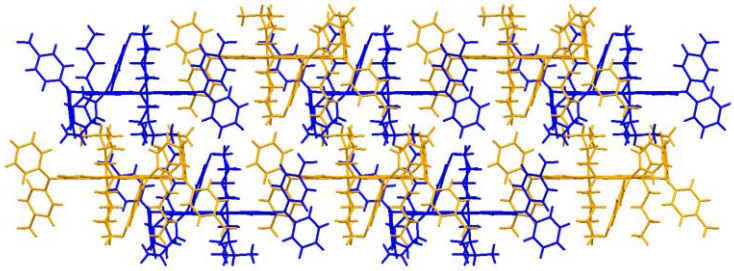

Figure V 4. Molecule **1Tris** in general position views along a) *a* axis and b) *c* axis, c) dimer and d) bi-layer in the crystal packing along *a* axis

3. Photophysical characterization in organic solutions

3.1. Linear optical properties

3.1.1. Effect of the environment

The influence of the environment on the photophysical properties was investigated by measuring both absorption and emission in organic solvent increasing the solvent polarity, from cyclohexane to dimethylsulfoxide.

As one can observe in **Figure V 5**, the absorption spectra measured for the chromophores are not affected by the solvent. Since the dipole is short and the dipolar strength is not large, this behavior was expected, suggesting that the main contribution to the ground state is given by the neutral form.

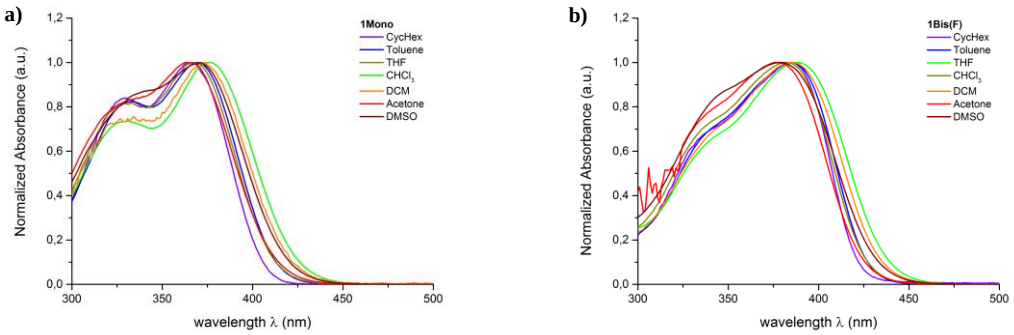

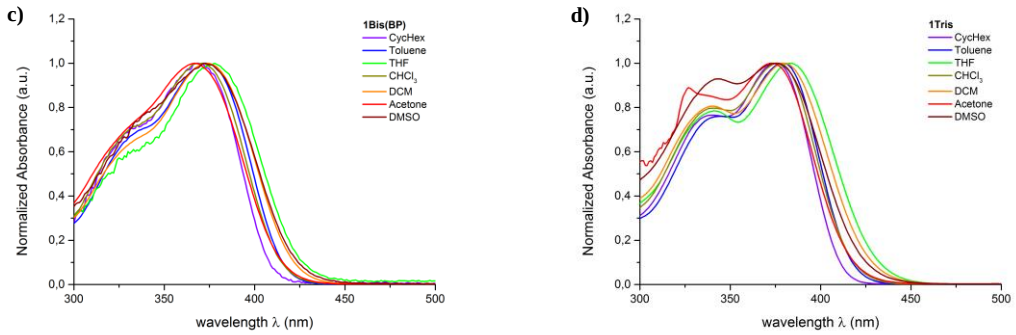

Figure V 5. Comparison between the absorption spectra measured for chromophores a) **1Mono**, b) **1Bis(F)**, c) **1Bis(BP)** and d) **1Tris**

On the other hand, an increase of the solvent polarity strongly affects the emission band inducing a marked bathochromic shift associated with a broadening of the band, from cyclohexane to DMSO (See **Figure V 6**). Interestingly, as it can be predicted that chromophores **1Mono** and **1Tris** are solvatochromic, for both dyes **1Bis** the behavior is not expected. However, the latter compounds show the typical solvatochromic behavior of standard "push-pull" chromophores undergoing an increase of dipole moment upon excitation. This is similar to what was observed for some quadrupolar chromophores that display symmetry breaking in the excited state[7-9]. This attitude can be ascribed to the presence of two "independent" dipolar subunit simply connected by a π-conjugated bridge that works only as a rigid connector.

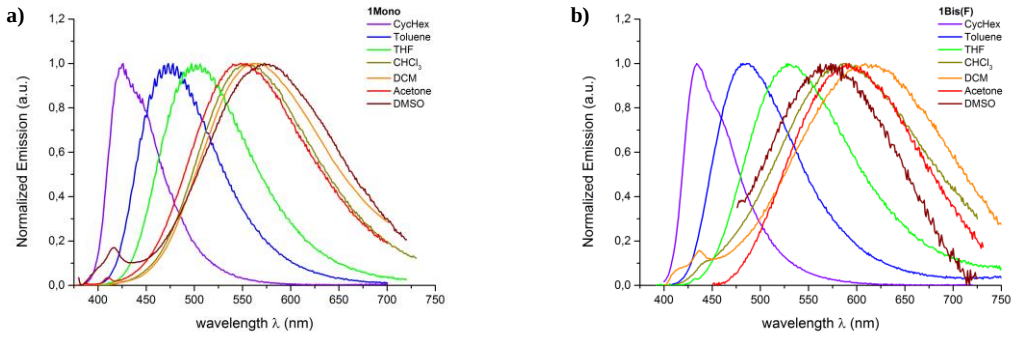

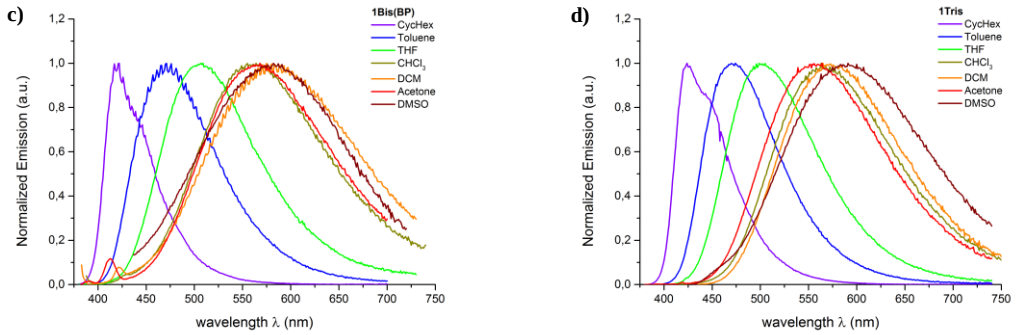

Figure V 6. Comparison between the absorption spectra measured for chromophores a) **1Mono**, b) **1Bis(F)**, c) **1Bis(BP)** and d) **1Tris**

3.1.2. Full characterization in THF solution

To study the photophysical properties of the articulated dipoles THF was used as common solvent, for a later comparison with the molecules upon nanoaggregation.

As one can observe in **Table V 1**, chromophores with CHO as acceptor group display an intense absorption band, associated with a large molar extinction coefficient (up to $9.5 \cdot 10^4$ M^{-1} cm^{-1}), that lies in the near UV spectral region. This band can be ascribed to an intramolecular charge transfer transition. As displayed in **Figure V 7a**, an increase of the number of dipolar subunits within the molecule induces a marked linear hyperchromic effect (see **Figure V 7b**), which is consistent with an additive effect. A slight bathochromic shift is observable from chromophores **1Mono** going to **1Tris** and **1Bis(F)**, this interesting effect will be discussed later in the chapter (**Paragraph 6**: Articulated dipoles: an essential state model description). Moreover, a hypsochromic shift associated with an hypochromic effect is observable by tuning the π-connector between the dipoles passing from **F** to **BP**, thanks to the fluorene that slight by increases the electron-releasing character, therefore enhancing the dipolar moment.

Tuning the acceptor group one can predict a bathochromic shift going toward stronger dipoles (**1Bis** → **2Bis**). The observed red-shift is associated with a marked hyperchromic effect (ε_{max} up to $7.8 \cdot 10^4$ M^{-1} cm^{-1}) as could be expected by increasing the dipolar strength and enhancing the probability

of the ICT transition. It is worthy to underline that a similar behavior is observed in chromophores **2Bis**, in which a rigidification of the π system (**BP** to **F**) induces an hyperchromic effect and a bathochromic shift.

Table V 1. One-photon photophysical data for chromophores in THF solution

Cpd	λ_{max}^{1PA} [nm]	ε_{max} [10^4 $M^{-1}cm^{-1}$]	λ_{max}^{em} [nm]	Φ_f	τ_1 [ns]	k_r [10^9 s^{-1}]	k_{nr} [10^9 s^{-1}]
1Mono	367	2.6	503	0.30	5.3	0.06	0.13
1Bis(F)	382	5.6	530	0.11	2.2	0.05	0.40
2Bis(F)	453	7.8	670	<0.01	/	/	/
1Bis(BP)	369	4.8	511	0.16	2.9	0.06	0.29
2Bis(BP)	448	6.8	653	<0.01	/	/	/
1Tris	376	9.5	508	0.39	5.3	0.07	0.12

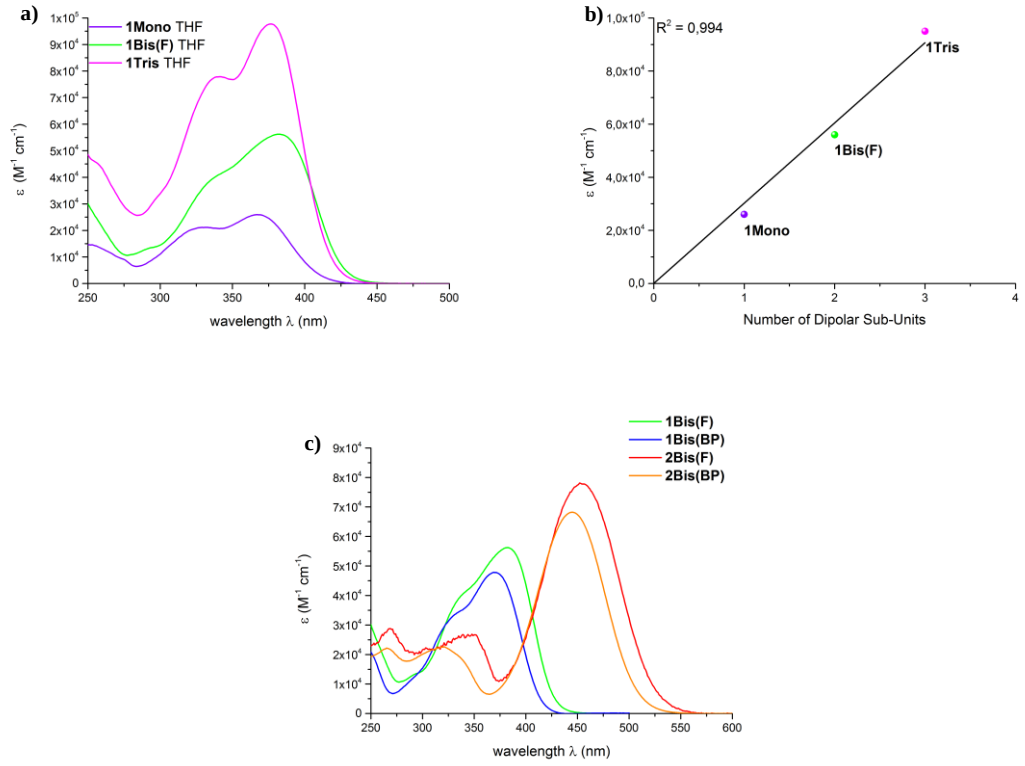

Figure V 7. Comparison between one-photon absorption spectra measured for a) **1Mono**, **1Bis(F)** and **1Tris**, c) **1Bis** and **2Bis** (**F** and **BP**), b) linear dependency of the hyperchromic effect increasing the number of dipolar subunits within the molecule (*consistent color code between the Figures in this chapter*)

Comparing chromophores bearing CHO as acceptor group one can see in **Figure V 8a** that **1Mono**, **1Bis(BP)** and **1Tris** display a good superimposition of the emission band, while **1Bis(F)** shows a red-shift. The emission bands are located in the green spectral region with medium-low fluorescence quantum yields for green emitters ranging from 0.11 (**1Bis(F)**) to 0.39 (**1Tris**). A decreasing of the luminescent properties can be observed in the quadrupolar-like chromophores **1Bis**, which can be consistent with the rotation motion of the system as non-radiative deactivation pathway. In fact, as it can be observed in **Table V 1**, the non-radiative decay rate of chromophores **1Bis** is much higher than that of **1Mono** and **1Tris**.

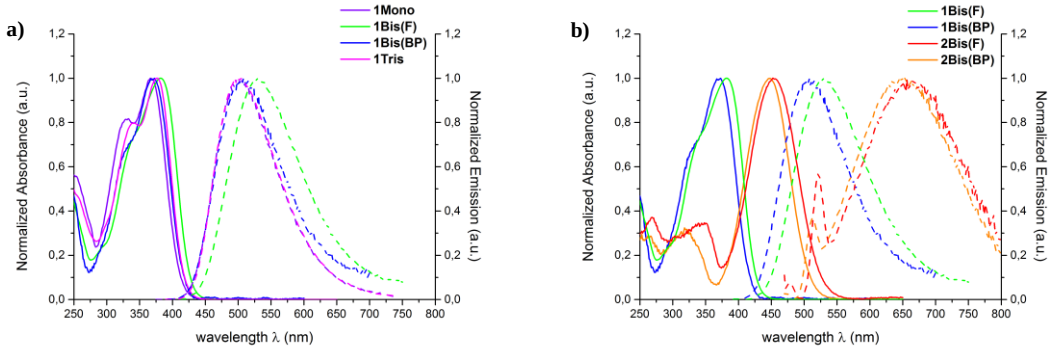

Figure V 8. Comparison between normalized absorption and emission spectra measured for a) **1Mono**, **1Bis(F-BP)** and **1Tris** and b) **1Bis** and **2Bis** (**F** and **BP**)

Similar to what was observed for absorption, the emission band is strongly affected by the tuning of the acceptor group. Indeed, replacing the aldehyde with a dicyanovinyl group induces a marked shift towards lower energies attributable to the increase of the dipolar strength. This bathochromic shift is associated with a quenching of the luminescent properties, indeed the chromophores **2Bis(F-BP)** display a Φ_f lower than 0.01. This marked decrease of the emission could be explained by the molecular motion that affects more the chromophores with dicyanovinyl group as acceptor moiety with respect to the CHO.

3.1.3. Anisotropy measurement in vitrified Me-THF

To complete the linear photophysical characterization, excitation anisotropy of chromophores **1Mono**, **1Bis(F)** and **1Tris** was measured in vitrified Me-THF in order to study the ways of depolarization that the three dyes can follow.

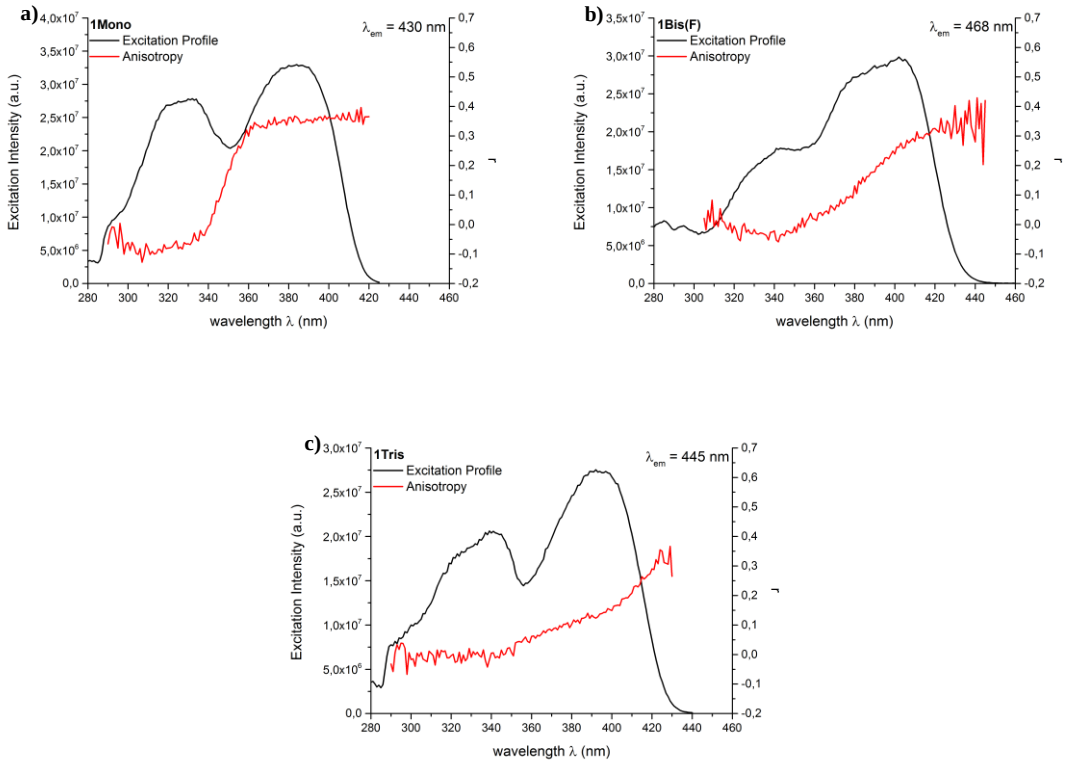

Figure V 9. Excitation anisotropy (red line) overlapped with the excitation profile (black line) measured for chromophores a) **1Mono**, b) **1Bis(F)** and c) **1Tris** in Me-THF at 77 K

The chromophore **1Mono** displays the expected behavior: when exciting inside the ICT band, the anisotropy is constant and close to 0.4 (collinear absorption and emission transition dipole moments). Anisotropy only lowers when exciting on the high-energy band, suggesting an angle of about 66° or 114° between the polarization directions of the two transitions.

More interesting are the anisotropy results for chromophore **1Bis(F)** and **1Tris**, which can be qualitatively explained by the excitonic model. Due to the small interaction between the dipoles, the

splitting between the one-exciton states is small. Nevertheless, when exciting in the blue edge of the absorption band, we mainly populate the higher-energy one-exciton state, while upon excitation in the red edge of the absorption band we mainly populate the lower-energy one-exciton state. Since emission always arises from the lowest-energy excited state, fluorescence anisotropy amounts to 0.4 upon excitation in the red edge, while it depends on the relative polarizations of the two one-exciton states when exciting in the blue edge. A similar interpretation can be given for the trimer, the decrease of anisotropy when moving the excitation wavelength from the red to the blue edge of the absorption band is faster because in this case we have three one-exciton states with different polarizations.

3.2. Non-linear optical properties

We were able to estimate the two-photon cross section of these chromophores by measuring the two-photon brightness with the 2PEF technique. Since this method is based on the emission, it was not possible to measure reliable data of chromophores **2Bis(F)** and **2Bis(BP)** in THF because of their low fluorescence quantum yield.

Table V 2. Two-photon photophysical data for chromophores in THF solution

Cpd	$2\lambda_{max}^{1PA}$ [nm]	λ_{max}^{2PA} [nm]	σ_{2max} [GM]
1Mono	734	750	103
1Bis(F)	764	740	144
1Bis(BP)	738	740	250
1Tris	752	740	225

Like for the molar extinction coefficient, also the two-photon cross section is affected by the number of dipolar subunits within the same molecule. In fact, as can be observed in **Figure V 10a**, the increase of the number of dipoles from **1Mono** to **1Tris** induces a hyperchromic effect, up to 225 GM. Anyway, contrarily to the one-photon process, the enhancement is not linear. Strikingly, chromophore **1Bis(BP)** displays a higher σ_2^{max} than the respective dye with fluorene as connector.

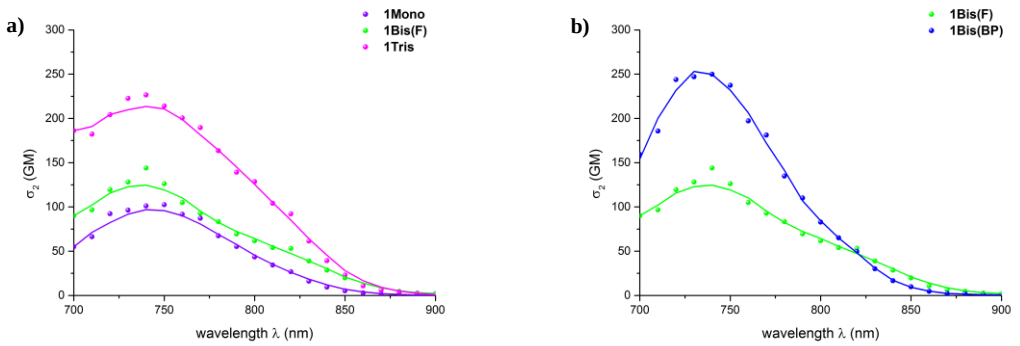

Figure V 10. Comparison between two-photon absorption spectra of a) **1Mono**, **1Bis(F)** and **1Tris**, b) **1Bis(F-BP)**

From the comparison between the responses in both processes, one can clearly observe in **Figure V 11** that the ICT transition is symmetrically allowed upon one-photon and two-photon excitation. This fact is usual for non-centrosymmetric "push-pull" chromophores, therefore it is very surprising that chromophores **1Bis(F)** and **1Bis(BP)** also follow the same behavior. This can be considered as an additional proof of the bad communication between the dipolar chromophores within the same dye.

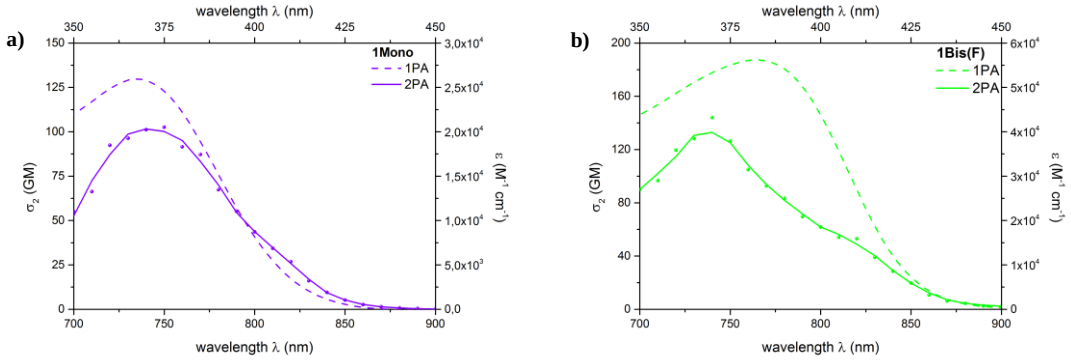

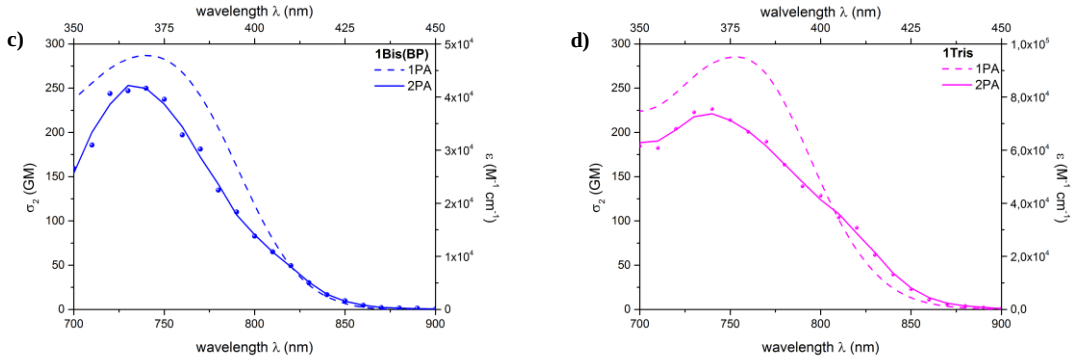

Figure V 11. Overlap between one-photon (dashed line) and two-photon (colored points and solid line) for chromophores a) **1Mono**, b) **1Bis(F)**, c) **1Bis(BP)** and d) **1Tris**

4. Photophysical characterization of FONs in water

4.1. FONs preparation and morphological characterization

To prepare organic nanoparticles with the articulated dipoles the nanoprecipitation method described in **Chapter 3** was used.

After preparation, the size and the shape of FONs were characterized by transmission electron microscopy (TEM) and confirmed by atomic force microscopy (AFM), while the surface potential was measured by zetametry. The relevant data concerning the characterization of nanoaggregates are reported in **Table V 3**.

Table V 3. Morphological and structural data

Cpd	d_{TEM} [nm]	d_{AFM} [nm]	$d_{TEM/AFM}$ [a)] [nm]	N [10^4]	ζ-potential [mV]
1Mono	73.5	66.5	70	22.8	-54
1Bis(F)	33	27	30	1.1	-68
2Bis(F)	34	36	35	1.5	-57
1Bis(BP)	60	50	55	9.6	-66
2Bis(BP)	36	48	42	3.6	-65
1Tris	44.5	51.5	48	2.8	-64

a) average diameter between TEM and AFM

As discussed in **Chapter 3**, it is not possible to predict the size and the shape of FONs depending on the chemical structure of the chromophore. Indeed if one take as example nanoobjects prepared with dyes **1Bis(F)** and **1Bis(BP)**, one can observe that the size of FONs prepared with **1Bis(BP)** is almost twice larger and there is almost one order of magnitude of difference between the number of molecules that form the nanoaggregates ($1.1 \cdot 10^4$ and $9.6 \cdot 10^4$ respectively). Moreover, the NPs presented herein display spherically shaped FONs with size ranging from 30 nm up to 70 nm.

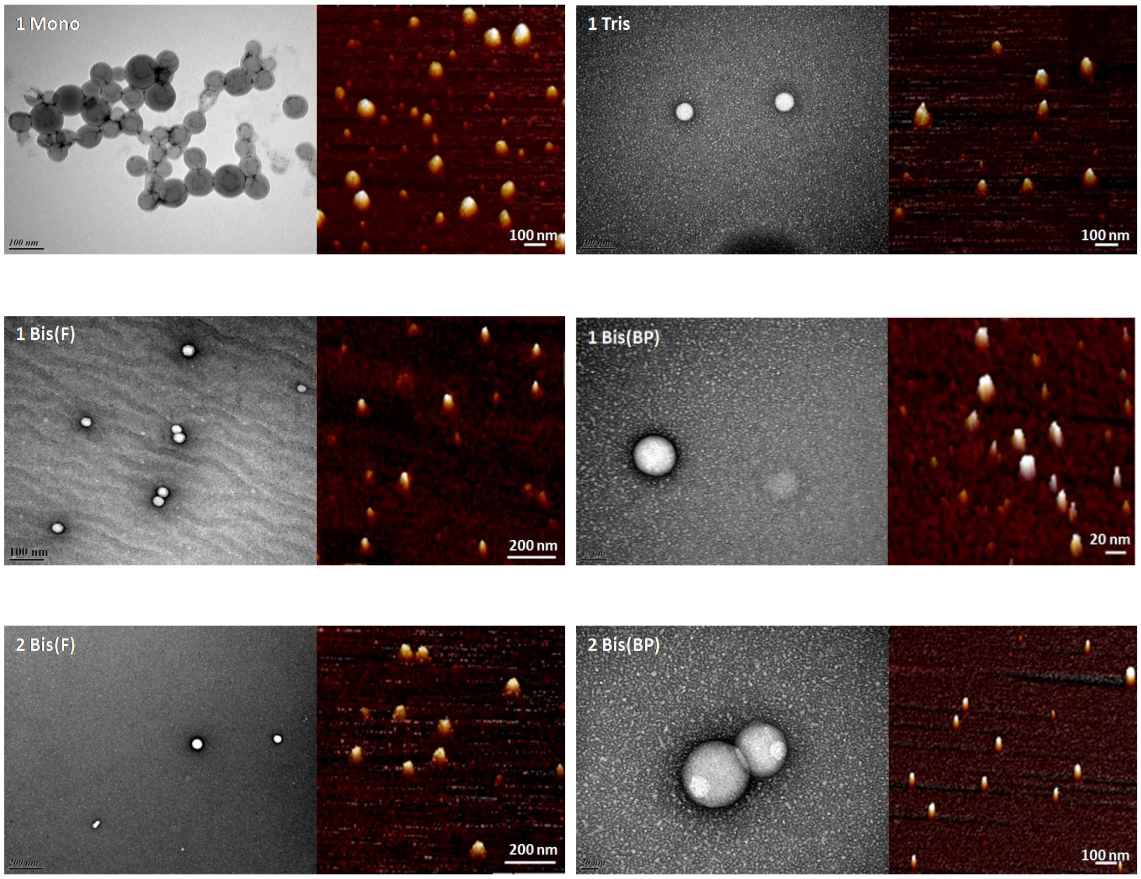

Figure V 12. TEM and AFM images of FONs prepared with the articulated dipoles presented in the chapter

4.2. One-photon characterization

After the morphological characterization, the linear optical properties of the chromophore within nanoparticles were studied.

FONs formed by chromophores bearing CHO as acceptor group display a broad absorption band located in the near UV region. A similar behavior, already discussed for the dyes in solution, is observed also upon nanoaggregation: an increase of the number of dipolar subunit inward the same molecule induces a linear hyperchromic effect (see **Figure V 13**), ascribed to an additive action.

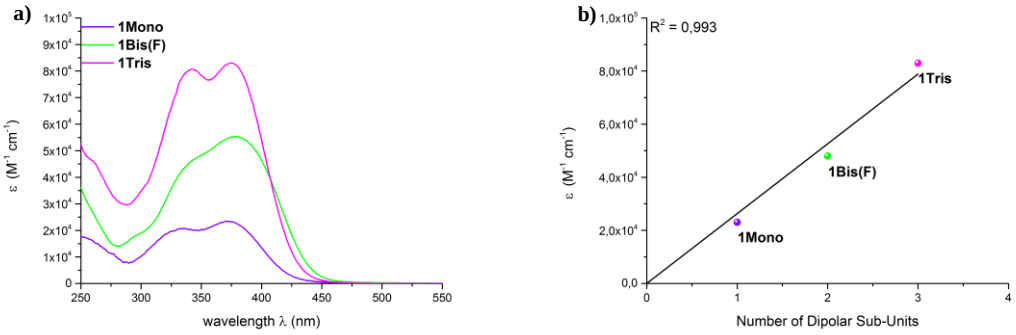

Figure V 13. Comparison between one-photon absorption spectra measured for a) **1Mono**, **1Bis(F)** and **1Tris** in FONs in water and b) linear dependency of the hyperchromic effect increasing the number of dipolar sub-units within the molecule

While FONs prepared with **1Bis(F-BP)** show an absorption band that lies in the near UV, by replacing the acceptor increasing the electron-withdrawing character, FONs **2Bis(F-BP)** display the expected bathochromic shift compared with the respective aldehydes associated with a large enhancement of the ICT transition band (see **Table V 4**). This shift towards low energies is also observable for the emission band that, from the blue-green region, shifts to the red visible region.

Table V 4. One-photon photophysical data for chromophores confined in FONs in water

Cpd	λ_{max}^{1PA} [nm]	ε_{max} [10^4 $M^{-1}cm^{-1}$]	λ_{max}^{em} [nm]	Φ_f	τ_1/τ_2 [ns]
1Mono	370	2.3	488	0.24	1.9 (0.4)/6.5 (0.6)
1Bis(F)	378	4.8	512	0.13	1.5 (0.4)/4.8 (0.6)
2Bis(F)	453	7.4	656	0.02	0.7 (0.9)/2.8 (0.1)
1Bis(BP)	370	3.7	511	0.10	1.7 (0.4)/5.5 (0.6)
2Bis(BP)	444	7.0	643	0.03	0.9 (0.8)/2.9 (0.2)
1Tris	375	8.3	499	0.20	1.6 (0.4)/5.7 (0.6)

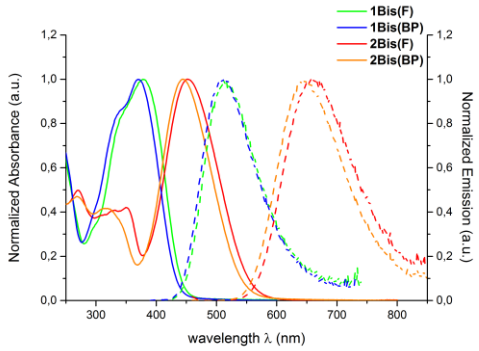

Figure V 14. Comparison between normalized absorption and emission spectra of chromophores **1Bis** and **2Bis**

Concerning the fluorescence quantum yields, one can observe from the comparison between the chromophore in THF solution and in FONs, that the aldehydes display comparable or slightly lower Φ_f, while a very small enhancement of the quantum yield is noticed upon aggregation for dyes **2Bis(F)** and **2Bis(BP)**. This phenomenon indicates that the deleterious π-π intermolecular interaction are prevented by the hindering groups present in the chemical structure of the chromophores, as well as the rotational motions are decreased by aggregation, which increase the radiative decay enhancing the emissive properties of the dyes in FONs. This interesting behavior was not observed for simple dipolar "push-pull" chromophores presented in **Chapter 3** and **Chapter 4**, thus it is a proof that the molecular arrangement of multi-dipolar chromophores upon nanoaggregation leads to a decrease of the non-radiative processes that compete with luminescence properties.

All nanoparticles display two fluorescence lifetimes: the longer one can be attributed to the fluorescence decay of the bulk, while the shorter one is ascribed to the lifetime of the chromophores that form the surface, in contact with the water environment, which leads to competitive non-radiative decays.

From the direct comparison between the chromophore in THF solution and upon nanoaggregation, one can observe in **Figure V 15** an interesting behavior: even if upon nano-confinement there is a decrease of ε_{max} (except for FONs prepared with dye **2Bis(BP)**), one can

observe a broadening of the ICT band associated with a slight hyperchromic effect towards longer wavelengths. This behavior can be ascribed to an excitonic coupling that occurs in confined environment.

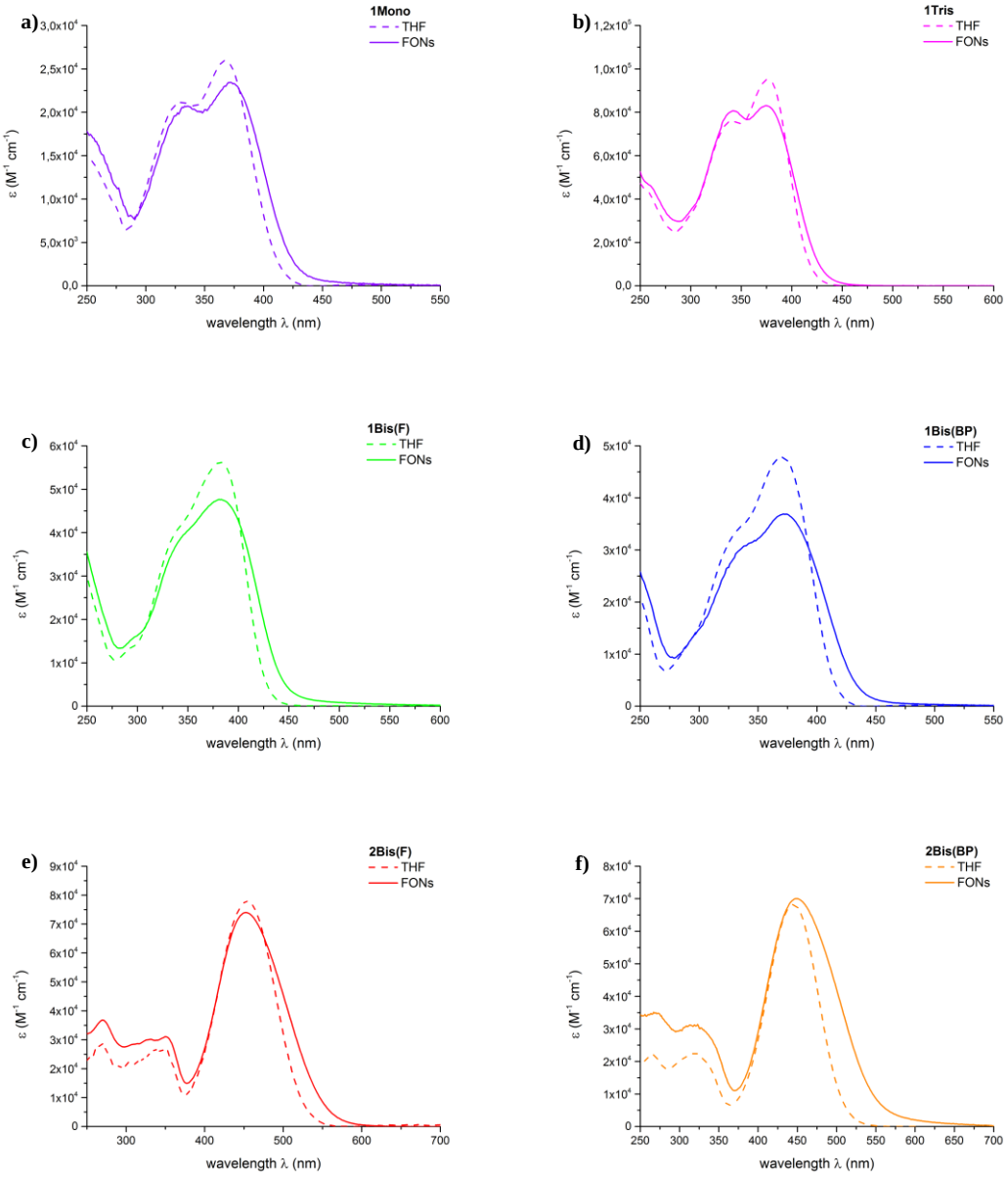

Figure V 15. Comparison between the absorption spectra measured in THF solution and FONs in water for all chromophores described in this chapter

Both the luminescent properties and the excitonic coupling observed for these chromophores upon aggregation suggest that the arrangement of dyes within the nanoparticle is not purely of J-aggregate type[10,11].

4.3. Two-photon characterization

Thanks to the enhancement of the luminescent properties of chromophores **2Bis** within FONs it was possible to estimate the two-photon cross section by measuring the TPEF on these samples and reliable data was obtained.

Table V 5. Molecular two-photon response of chromophores confined in FONs in water

Cpd	$2\lambda_{max}^{1PA}$ [nm]	λ_{max}^{2PA} [nm]	σ_2^{max} [GM]
1Mono	740	750	87
1Bis(F)	756	740	157
1Bis(BP)	740	750	222
2Bis(F)	906	940	727
2Bis(BP)	888	900	816
1Tris	750	750	130

The behavior of FONs is similar to that of the dyes in THF solution: $\lambda_{max}^{2PA} \approx 2\lambda_{max}^{1PA}$ thus the ICT transition is allowed upon both one-photon and two-photon excitation (see **Figure V 16a-b**). Since observed this behavior was also observed for nanoparticles prepared with **1Bis** and **2Bis** chromophores, it is interesting to underline that even in confined environment the communication between dipoles through fluorene or biphenyl is negligible.

The comparison of the two-photon responses of FONs prepared with **1Mono**, **1Bis(F)** and **1Tris** reveals a different behavior with respect to what was observed in solution. Moreover, the trend is also different if considering the effect upon one-photon excitation: the two-photon cross section measured upon nano-aggregation seems to be not affected by the number of dipoles within the same

molecule. Indeed, as displayed in **Figure V 16c**, FONs prepared with **1Bis(F)** show higher two-photon response than **1Tris**. We can attribute this behavior to the arrangement of chromophores within nanoparticles that produces a less polarizable environment, which is more sensitive to the two-photon excitation. Nevertheless, when the chromophores are confined in nanoparticles, the highest σ_2^{max} is also displayed by chromophore **1Bis(BP)**.

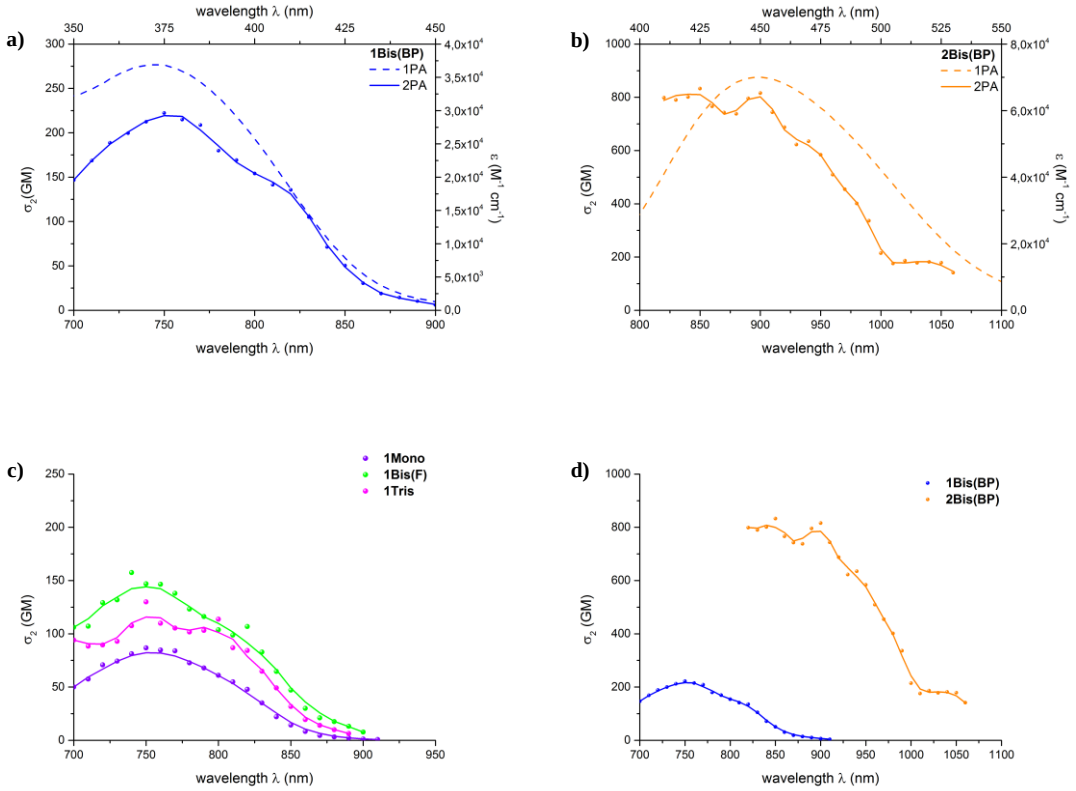

Figure V 16. Overlap between 1PA and 2PA spectra measured on FONs in water prepared with chromophores a) **1Bis(BP)** and b) **2Bis(BP)**

As expected, an enhancement of the electron-withdrawing character of the acceptor group induced a marked bathochromic shift of the absorption band, associated with a strong hyperchromic effect, as displayed in **Figure 16d**.

The 2PA band measured for the chromophore upon nano-confinement is markedly broader compared with the molecular response of the dye in THF solution. As one can observe in **Figure 16** the main trend upon aggregation is to undergo a hypochromic effect of the maximum value of cross

section, except for FONs prepared with **1Bis(F)** which exhibit higher σ_2^{max} compared with the chromophore dissolved in solution.

In spite of the decrease of the two-photon response, it is worthy to underline that the 2PA spectra of FONs display a shoulder towards low energies, suggesting an excitonic coupling. According to these observations, we can hypothesize the presence of an intermediate arrangement of chromophores within the nanoparticle that allows both transition bands.

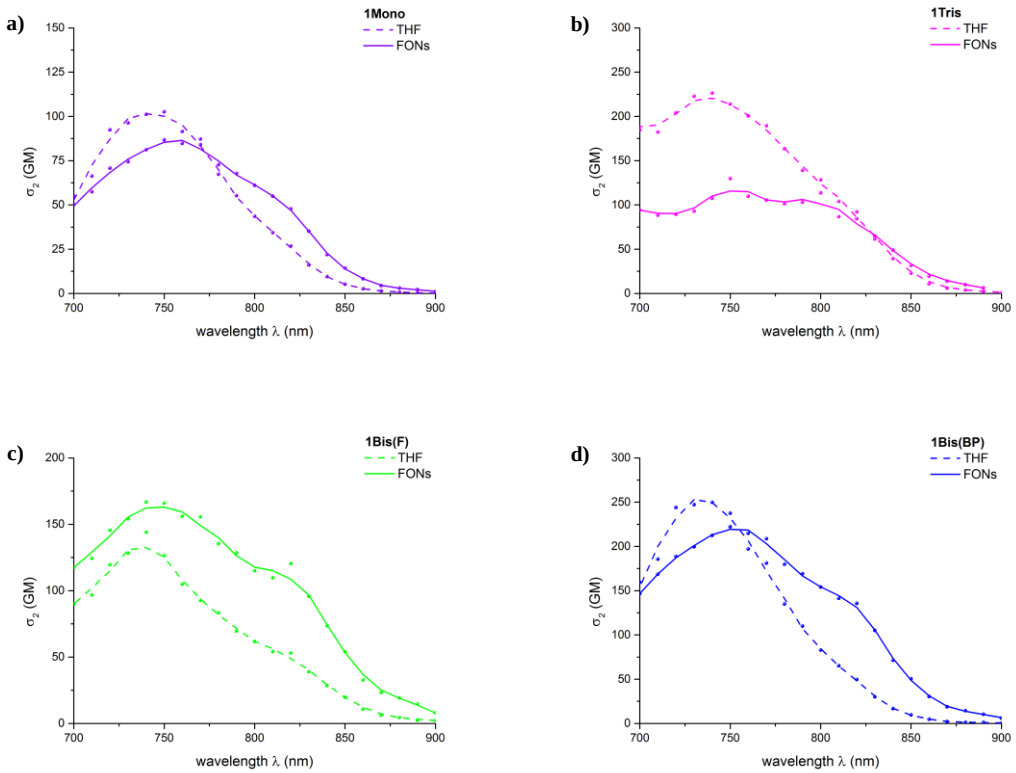

Figure V 17. Comparison between the two-photon absorption spectra measured in THF solution and FONs in water for chromophores a) **1Mono**, b) **1Tris**, c) **1Bis(F)** and d) **1Bis(BP)**.

4.4. Colloidal and structural stability overtime

To study the colloidal stability, as previously described, the evolution of both absorption and emission spectra of FONs was evaluated overtime. Thanks to their negative surface potential, ranging from -54 to -68 mV, these nanoparticles are expected to show a high colloidal stability. As one can

observe in **Figure V 18**, FONs prepared with the chromophore **1Mono** are the less stable in the period of monitoring. It can be noticed a scattering of the absorption spectra that indicates the beginning of aggregation process of nanoparticles to bigger objects. The nanoaggregates formed with the other compounds display a great colloidal stability over two weeks.

Monitoring the emission spectra, one can have an idea about the internal rearrangement of chromophores within the nanoparticles. Organic nanoparticles are formed under kinetic domain, therefore they can be considered as soft objects in which the molecules are able to rearrange their configuration toward more stable systems.

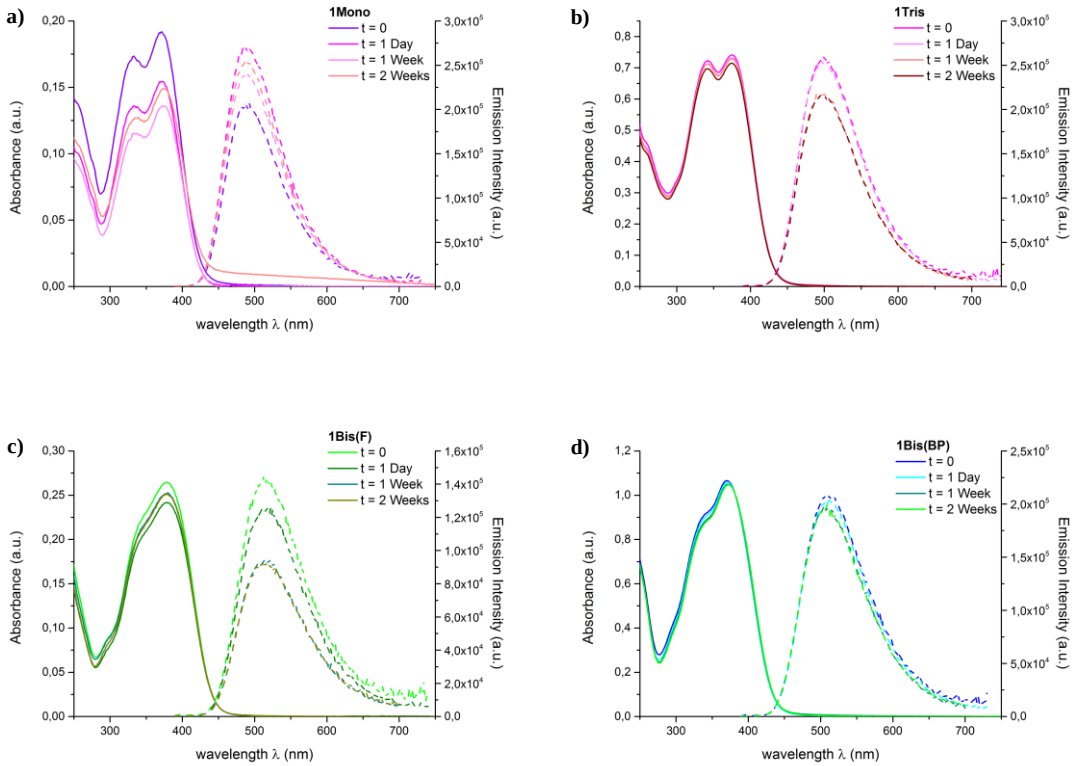

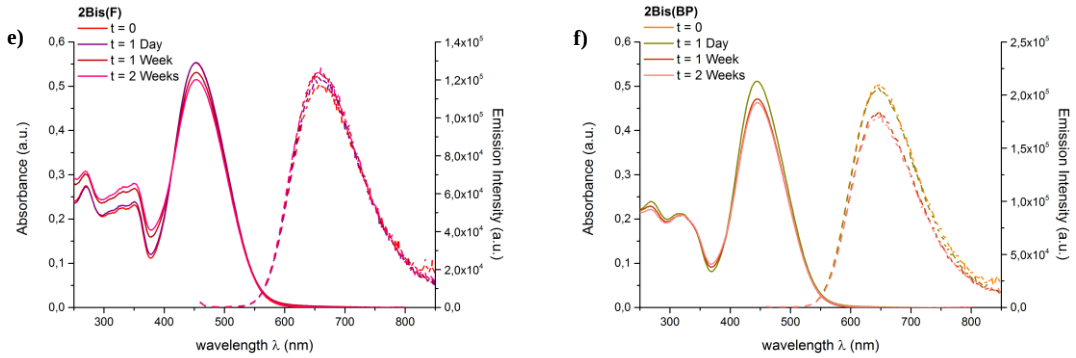

Figure V 18. Overtime monitoring of absorption and emission spectra of FONs prepared with the articulated dipoles

Sometimes the internal rearrangement that occurs during the aging of the nanoaggregates induces a decrease of the luminescence properties, as can be clearly observed for FONs prepared with chromophores **1Mono**, **1Bis(F)** and **1Tris**. Great colloidal and structural stability can be observed overtime for FONs prepared with chromophores **1Bis(BP)** and **2Bis(F)**.

5. Bioimaging and cytotoxicity of FONs

Multicolor imaging is a powerful technique in order to study complex phenomena such as protein localization[12], live cell internalization of proteins[13] or simultaneous observation of different lymphatic channels[14]. This method is based on the introduction in the bio-environment of two or more fluorescence probes and it is necessary that these markers display good overlap between the excitation spectra while they have to show different emission range in order to distinguish the different functions that are studied.

Organic fluorophores are intensively used in multicolor imaging thanks to the wide range of possible structures that can be prepared and their biocompatibility. On the other hand, their photostability and brightness in biological media are very low.

The confinement of the articulated dipoles within nano-environment induces a cooperative/additive effect that can strongly affect the brightness of FONs. Indeed, in spite of their

low fluorescence quantum yield, these nanoobjects shows giant one-photon (up to $14.8 \cdot 10^8$ M^{-1} cm^{-1}) and two-photon (ranging from 0.2 to $5.0 \cdot 10^6$ GM) brightness, as displayed in **Table V 6**, suggesting these nanoparticles as suitable tools for confocal and multiphoton imaging. Therefore, their potential application was investigated *in vitro*. In order to exploit the possibility to do multicolor imaging we chose **1Bis(BP)** as green emitting FONs and **2Bis(BP)** as red emitting FONs, and COS 7 cells as a model system.

Table V 6. Luminescence properties including one-photon and two-photon brightness of FONs in water

Cpd	λ_{max}^{1PA} [nm]	λ_{max}^{em} [nm]	$FWHM^{em}$ [10^3 cm^{-1}]	Φ_f	$\varepsilon_{max}\Phi_f$ [a)] [10^8 M^{-1} cm^{-1}]	λ_{max}^{2PA} [10^4]	$\sigma_2\Phi_f$ [a)] [10^6 GM]
1Mono	370	488	3.6	0.24	14.8	750	5.0
1Bis(F)	378	512	3.8	0.13	0.7	740	0.2
1Bis(BP)	370	511	3.9	0.10	6.1	750	2.6
2Bis(F)	453	656	3.0	0.02	0.3	900	0.4
2Bis(BP)	444	643	3.0	0.03	0.9	900	0.6
1Tris	375	499	3.7	0.20	5.5	750	0.7

a) the values of one-photon and two-photon brightness are reported taking into account the concentration of nanoparticles

Both uptake and fluorescence properties of the nanoaggregates in bio-environment (approximate 20 pM concentration of FONs) were evaluated after 8 and 20 hours of incubation by two-photon fluorescence microscopy. Strong fluorescence signal was observed after 8h of incubation, particularly for the green FONs, the red ones appeared less intense. This is in agreement with the previously determined photophysical properties of the FONs: two-photon brightness of 2.6 10^6 GM for **1Bis(BP)** and 0.9 10^6 GM for **2Bis(BP)** in confined environment. As it is displayed in **Figure V 19**, both probes are broadly distributed in the cytosol, suggesting a non-specific internalization process. Indeed their small size could lead to an uptake of the nanoparticles involving both clathrin-mediated endocytosis[15] as well as passive internalization, also due to their soft character[16,17].

The two FONs have spectral properties favorable for simultaneous multicolor fluorescence imaging: good overlap between the absorption bands, large stock shift and well separated emission bands.

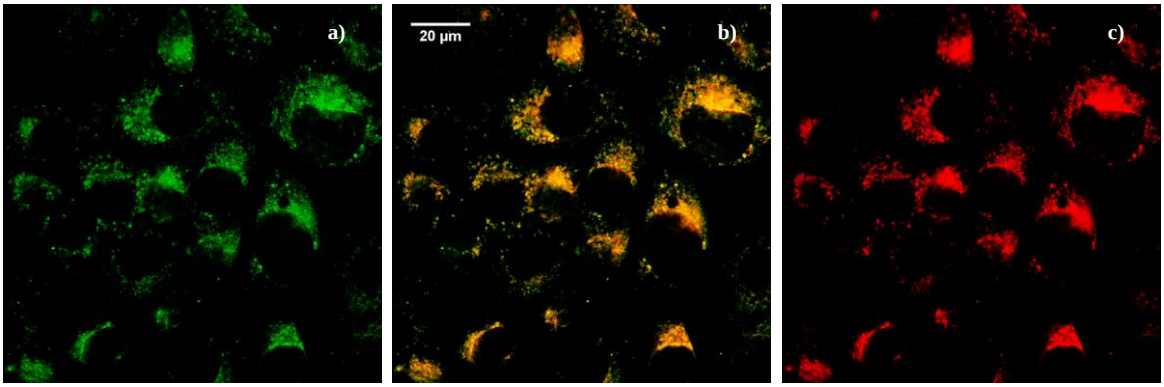

Figure V 19. Two-photon fluorescence images of COS 7 cells incubated for 20h with both FONs **1Bis(BP)** and **2Bis(BP)**; imaging conditions for a) **1Bis(BP)**: λ_{exc} = 750nm, λ_{em} = 450-550 nm and for c) **2Bis(BP)**: λ_{exc} = 900nm, λ_{em} = 600-750 nm. b) display the co-localization of both probes.

Investigating the co-localization of the two probes within the cells one can observe in **Figure V 19b** that the two FONs are fully co-localized within the cells, although the green probe is slight brighter than the red one. Thus, we provided tools for multicolor imaging in biological environments by using probes of similar characteristic (size, surface charge, composition). The targeting of biological species of interest with these nanoparticles will allow simultaneous visualization, localization and study of their interaction. It was previously shown in the hosting laboratory the potential of similar FONs for multicolor single-particles tracking in live cells[18].

In view of the potential application of the described FONs for bioimaging, we further investigated their biocompatibility. The cytotoxic effect was evaluated by MTT assay, after 24h of incubation with the COS 7 cells, as displayed in **Figure V 20**. None of the FONs proved to be toxic at the concentration used for bioimaging (approximately 20 pM), the viability of the cells being of about 100% in all conditions. The safety of these FONs as well as their photostability and high brightness indicate the great potential of these FONs in biomedical applications, including imaging and sensing.

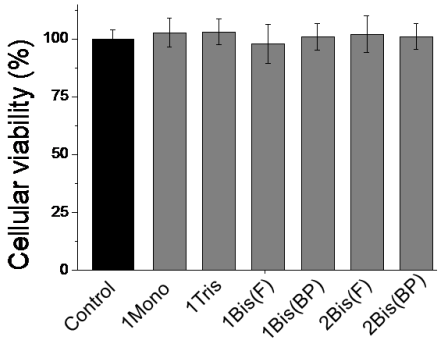

Figure V 20. Viability of COS 7 cells after 24h of incubation with the FONs, as assessed by MTT test

6. Articulated dipoles: an essential state model description

The essential state model is an interesting tool that allows to simplify the description of electronic states, choosing the main resonance structures as basis states, for the investigation of linear and non-linear optical properties in molecules that are formed from electron-releasing and electron-withdrawing end-groups connected by a π-conjugated bridge.

When dealing with dipolar dyes, the easiest description is to take into account two basis wavefunctions: the neutral and the zwitterionic resonance structures[19-22].

Illustration V 2. Representative illustration of the two basis states of a dipolar dye: the neutral $|N\rangle$ and the zwitterionic $|Z\rangle$

Both ground $|G\rangle$ and excited $|E\rangle$ state of chromophore will be linear combinations of these two basis states, depending on the strength of both the electron-withdrawing and electron-releasing moieties and on the specific structure, particularly the ability of the π-conjugated bridge to make the charge resonate. The energy gap between the two basis states is $2\,z_0$ while the mixing element is $-\sqrt{2}\,t$.

The following equations (**Eq. V 1-2**) describe the electronic Hamiltonian and its two eigenstates:

Eq V 1. $$H = \begin{pmatrix} 0 & -\sqrt{2}\,t \\ -\sqrt{2}\,t & 2\,z_0 \end{pmatrix}$$

Eq V 2. $$\begin{cases} |G\rangle = \sqrt{1-\rho}\,|N\rangle + \sqrt{\rho}\,|Z\rangle \\ |E\rangle = \sqrt{\rho}\,|N\rangle - \sqrt{1-\rho}\,|Z\rangle \end{cases}$$

The parameter ρ measures the weight of the zwitterionic state in the ground state, and thus defines its polarity. Dipolar chromophores are considered neutral in ground state when $\rho < 0.5$ and zwitterionic when $\rho > 0.5$. In the limit case in which $\rho = 0.5$, the system displays two basis states (neutral and zwitterionic) that coexist with the same weight. This case is the so-called: "cyanine limit"[23,24].

Thanks to the interesting properties observed experimentally for chromophores **1Mono**, **1Bis(F)** and **1Tris**, the idea was to describe firstly the behavior of the chromophore **1Mono** as a dipolar dye with the two-state model, then to consider the other chromophores **1Bis(F)** and **1Tris**, displayed in **Figure V 21**, as a combination of two or three dipolar units interacting *via* electrostatic interactions.

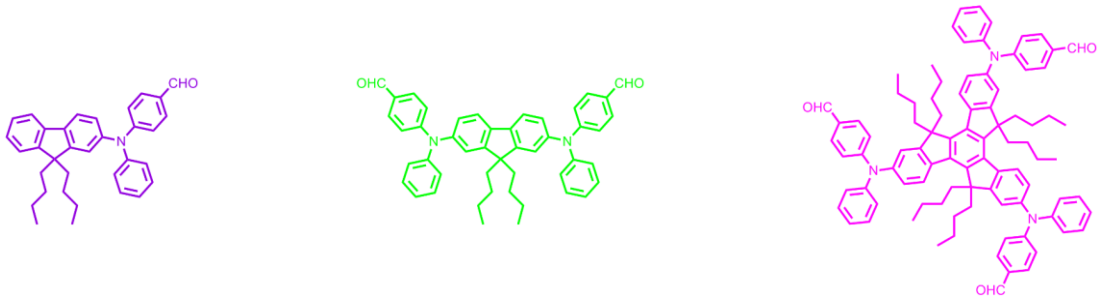

Figure V 21. Target molecules used for calculation, violet **1Mono**, green **1Bis(F)** and magenta **1Tris**

The program that I used during a period that I spent in Parma University was written by Prof. Francesca Terenziani (Università degli Studi di Parma). This program takes into account different parameters that can be divided in three parts:

- Electronic part
- Vibrational part
- Interaction with solvent

A more detailed description of the parameters used can be found in **Table V 7**.

Table V 7. Essential state model parameters

	Description	Parameter
Electronic part	Half of the energy gap between the neutral state and the zwitterionic state expressed in eV	z_0
	Mixing element of the Hamiltonian expressed in eV	$\sqrt{2}$ t
Vibrational part	Frequency of the vibration expressed in eV	ω_{vib}
	Related to the vibrational relaxation energy, is called electron-phonon coupling constant expressed in eV	g
Solvent contribution	Solvation relaxation energy expressed in eV	ε_{or}
	Linewidth of the vibronic transition expressed in eV	γ_{el}
	Permanent dipole moment of the zwitterionic state expressed in D	μ_0

To describe the system, two different approaches were used for the fitting. In the first strategy, electron-phonon coupling was considered and eight phonon states were used for each dipolar unit to reach the convergence in the calculated spectra. In the second approach, purely electronic states were used, neglecting the effects of molecular vibrations: this allowed simplifying and accelerating the calculations. In particular, for trimer **1Tris** calculations accounting for electron-phonon coupling are

too computationally costly and slow to be processed. Nonetheless, it was possible to fully describe the behavior of **1Mono** and **1Bis(F)** with the vibronic part.

6.1. Description considering the electron-phonon coupling

The essential state model is a semi-empirical method, therefore I had to fix the parameters to reproduce the previously displayed experimental data, specifically absorption and emission spectra in solvents of different polarity and the 2PA spectrum in THF. The parameters fixed correspond to a highly neutral dye, with $\rho \cong 0.05$, consistently with non-solvatochromic absorption and strongly solvatochromic emission.

Once the parameters were set for the "monomer", the idea was to keep all of the terms fixed for the "dimer" **1Bis(F)**, while adding the distance and mutual orientation of the two dipolar units.

In order to describe the intermolecular interactions in the "dimer", the following parameters are required: the length of the dipole (5.6 Å according to the crystal structure), the distance between the dipoles (9.7 Å according to the crystal structure) and the angle between the two dipoles. Concerning the angle, it was used the crystallographic torsion angle between the two dipoles: 172.5°. However, this value did not allow to obtain the correct excitation anisotropy spectrum, which could instead be well reproduced with an angle of about 110°. While the specific value of the angle has huge effects on the anisotropy spectra, allowing to have a reliable estimation of the mean mutual orientation, absorption and fluorescence spectra are slightly influenced by the specific choice of this angle. Indeed, it was verified that the spectra obtained for the angle extracted from the crystal structure, 172.5°, have negligible differences with respect to those obtained for 110°.

As written just before, we wanted to keep the values fixed for chromophore **1Mono** to reproduce the experimental data of **1Bis(F)** (see **Table V 8**). Actually we were forced to change the value of z_0 passing from **1Mono** to **1Bis(F)**, as to reproduce the slight red-shift experimentally observed in the ICT band. In fact, independently of the distance and mutual orientation of the two

dipolar subunits, the specific structure of the dimer does not allow to obtain attractive interactions between the two dipoles, so that only blue-shifts can be expected as a result of inter-chromophore interactions. The decrease of z_0 is consistent with slightly modified dipolar units, in particular a longer conjugation length.

Table V 8. Parameters used to reproduce the experimental data with good agreement

Parameters	**1Mono**	**1Bis(F)**
z_0	1.585	1.495
$\sqrt{2}$ t	0.8	0.8
ω_{vib}	0.2	0.2
g	0.215	0.215
ε_{or}	0.26 (cyclohex) 0.585 (THF) 0.855 (DCM)	0.26 (cyclohex) 0.585 (THF) 0.855 (DCM)
γ_{el}	0.04	0.04
μ_0	27.8	27.8

In **Figures V 22** is displayed the comparison of experimental and calculated spectra with respect to the solvatochromic behavior. The agreement is good, especially concerning the position and shape including inhomogeneous broadening; as one can observe the vibronic structure in cyclohexane is also well reproduced. We focused our attention on the n-π^* transition band, therefore the shoulder that can be ascribed to a π-π^* transition was not taken into account in the calculation.

Furthermore, there is a good quantitative agreement between the experimental and the calculated 1PA spectra in THF, thanks to the fact that the molar extinction coefficient follows a linear hyperchromic dependency (see **Figure V 23)**. A marked deviation is observed for the 2PA spectrum of the dimer that experimentally is less than twice the one of the monomer. This behavior is not justified in absence of strong interactions.

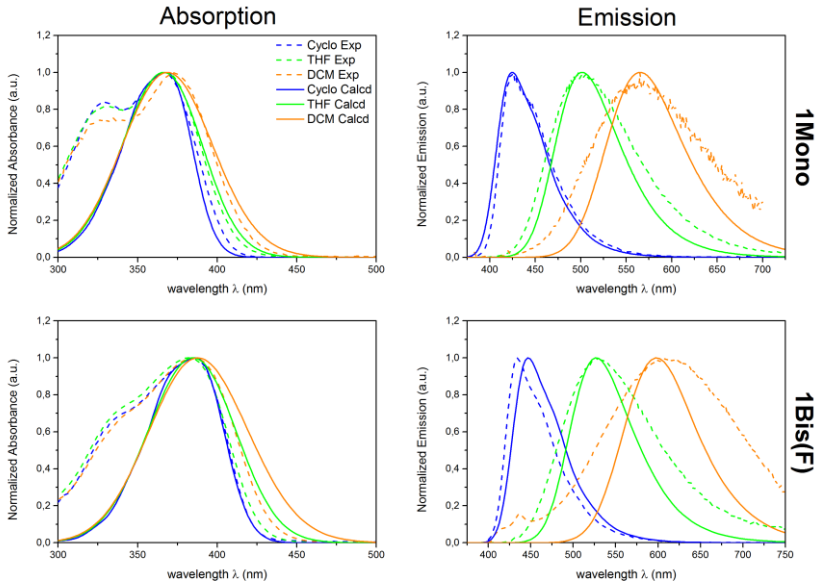

Figure V 22. Comparison between both absorption and emission spectra measured experimentally (dashed line) in solvent with different polarity and calculated with the essential state model (solid line) for chromophores **1Mono** and **1Bis(F)**

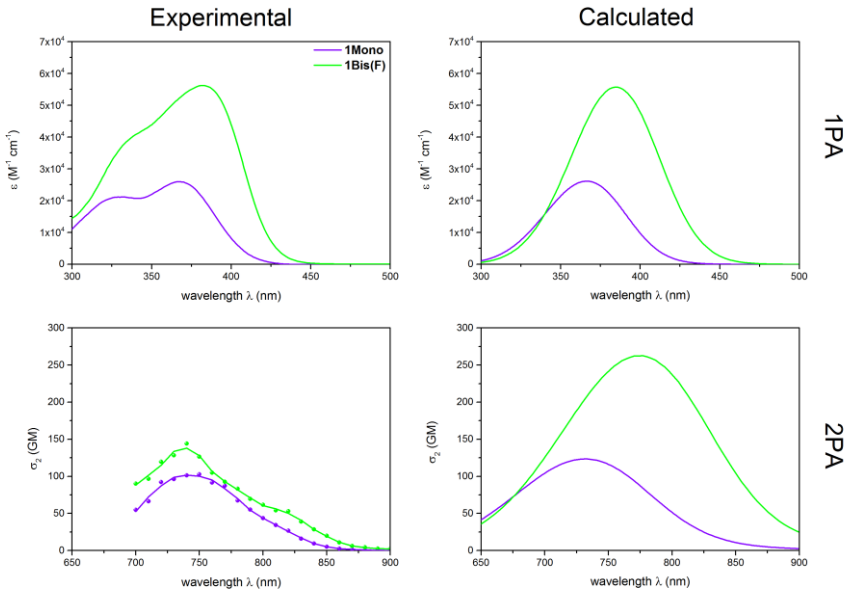

Figure V 23. Comparison between 1PA and 2PA spectra measured experimentally and calculated with the essential state model, using THF as common solvent, for chromophores **1Mono** and **1Bis(F)**

6.2. Description without considering the electron-phonon coupling

In this case too, it was necessary to optimize of the parameters for chromophore **1Mono** since we want to use this dye as prototype molecule.

For chromophore **1Bis(F)** interaction parameters were the same as previously discussed (dipole length, distance and angle), while for **1Tris** the parameters were extracted from the crystal structure: the length of the dipole is 5.6 Å, and the distance between the dipoles is 12.2 Å.

As can be observed in **Table V 9**, it was necessary to change the value of z_0 when going to dimer and trimer species, in order to reproduce the slight experimental shift observed in the absorption band.

Table V 9. Parameters used to reproduce the experimental data with good agreement

Parameters	**1Mono**	**1Bis(F)**	**1Tris**
z_0	1.55	1.485	1.505
$\sqrt{2}$ t	0.7	0.7	0.7
ω_{vib}	0.2	0.2	0.2
g	0.21	0.21	0.21
ε_{or}	0.305 (cyclohex) 0.615 (THF) 0.835 (DCM)	0.305 (cyclohex) 0.615 (THF) 0.835 (DCM)	0.305 (cyclohex) 0.615 (THF) 0.835 (DCM)
γ_{el}	0.15	0.15	0.15
μ_0	29.15	29.15	29.15

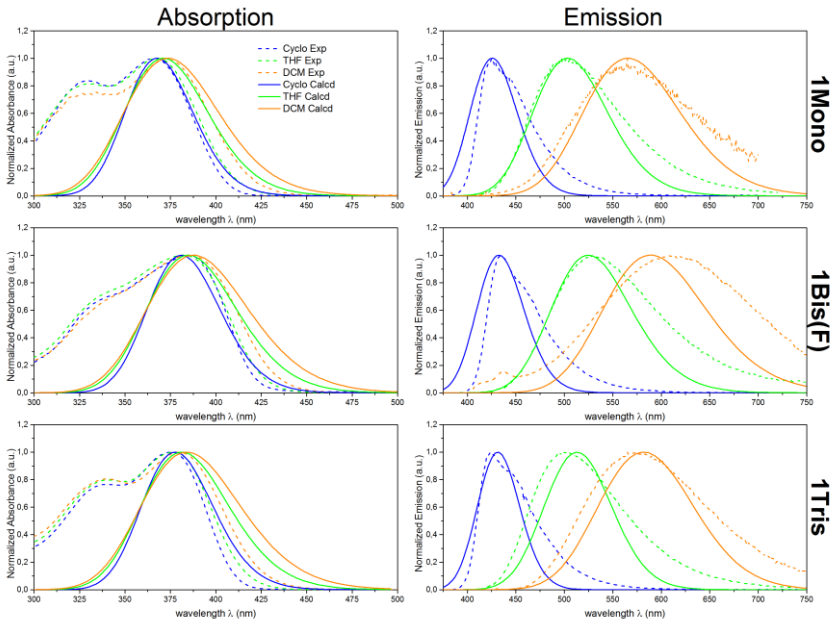

Figure V 24. Comparison between absorption and emission spectra measured experimentally (dashed line) in solvent with different polarity and calculated with the essential state model (solid line) for chromophores **1Mono**, **1Bis(F)** and **1Tris**

As displayed in **Figure V 24**, in absence of the electron-phonon coupling the spectra evidently lost the vibronic structure observed in **Figure V 22**, nevertheless the large experimental bathochromic shift is appropriately reproduced as well as the broadening of the band towards high polarity solvents.

1PA and 2PA spectra are reported in **Figure V 25** using THF as common solvent. The trend and the values upon one-photon excitation are well reproduced since the experimental hyperchromic effect is basically additive, as discussed in **Paragraph 3.1.2**. The calculated 2PA cross section displays an additive trend whereas a reduction of 2PA *per* dipolar unit is experimentally observed.

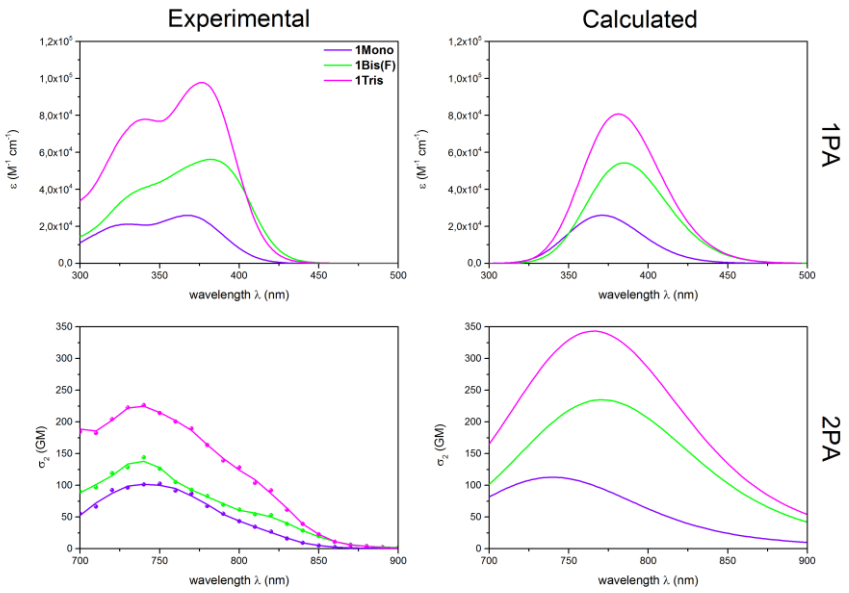

Figure V 25. Comparison between both 1PA and 2PA spectra measured experimentally and calculated with the essential state model, using THF as common solvent, for chromophores **1Mono**, **1Bis(F)** and **1Tris**

6.3. Anisotropy in vitrified Me-THF

As disclosed in **Paragraph 3.1.3**, it was possible to adequately reproduce anisotropy for dye **1Bis(F)** in glassy Me-THF using an angle of about 110° between the two dipolar units, which allows to obtain the excitation anisotropy smoothly changing from 0.4 (red edge) down to ~0 (blue edge) as displayed in **Figure V 26**. This result nicely confirms our modeling and interpretation.

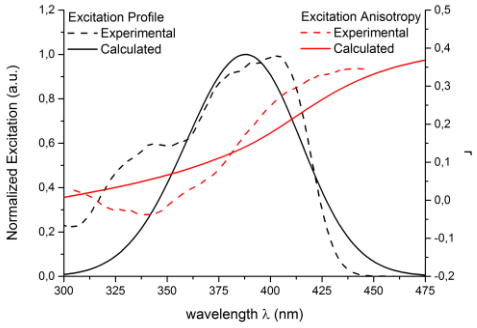

Figure V 26. Comparison between the experimental (dashed line) and the calculated (solid line) excitation profile (black) and anisotropy (red)

It is important to notice that the angle of 110° corresponds to the mean mutual orientation of the dipolar units, while a distribution of angles is possible in the sample; indeed, even if the medium is vitrified, a static disorder is present. Moreover, the absence of source of inhomogeneous broadening in our calculations forced us to increase the homogeneous linewidth of the vibronic transitions in order to obtain broad fluorescence excitation spectra at low temperature (T = 90 K, which is estimated to be the glass transition temperature of 2-MeTHF[25]).

7. Conclusions

In this chapter were discussed the linear and non-linear optical properties of a new class of multichromophoric molecules, bearing from one to three dipoles connected by rigid/semi-rigid π-conjugated bridge, in both molecular solution and nanoparticles. The changes of the photophysical properties of these chromophores were studied by enhancing the acceptor strength by tuning the electron-withdrawing end-group from CHO to DCV.

The optical characterization suggests the low/non-communication between the different subunits within the same molecule, and this hypothesis was confirmed by the essential state model calculation done in collaboration with Prof. Francesca Terenziani from Parma University.

We were able to obtain spherical nanoparticles with an average diameter ranging from 30 to 70 nm with excellent colloidal and chemical stability. Interestingly, the molecules upon aggregation display similar or even higher (**2Bis(F-BP)**) Φ_f compared with the chromophores in THF solution; moreover the prepared FONs displayed a broadening of the two-photon absorption band ascribed to a pronounced excitonic coupling that occurs in confined environment.

Despite their low fluorescence quantum yield, the FONs display large one-photon and two-photon brightness with low cytotoxic activity, evaluated through MTT test after 24h of incubation in COS7 cells.

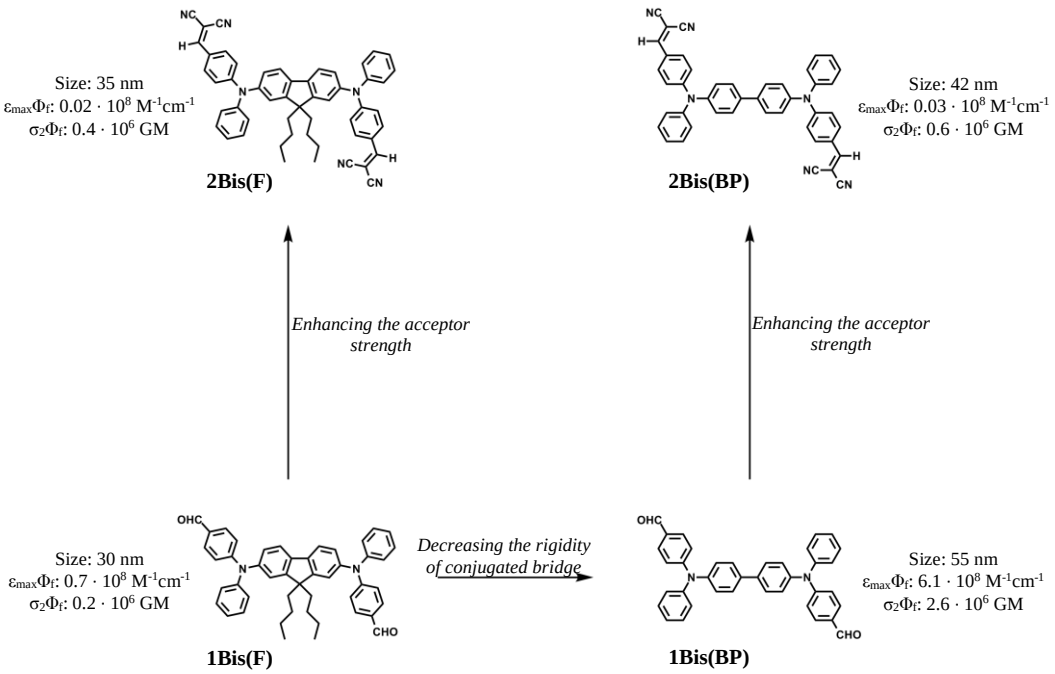

Figure V 27. Resuming flowchart of articulated dipoles confined in nanoparticles

BIBLIOGRAPHIC REFERENCES

(1) Hong, Y.; Lam, J. W. Y.; Tang, B. Aggregation-induced emission. *Chemical Society Reviews* **2011**, *40*, 5361-5388.

(2) Chen, J.; Law, C. C. W.; Lam, J. W. Y.; Dong, Y.; Lo, S. M. F.; Williams, I. D.; Zhu, D.; Tang, B. Synthesis, light emission, nanoaggregation, and restricted intramolecular rotation of 1,1-substituted 2,3,4,5-tetraphenylsiloles. *Chemistry of Materials* **2003**, *15*, 1535-1546.

(3) Luo, J.; Xie, Z.; Lam, J. W. Y.; Cheng, L.; Chen, H.; Qiu, C.; Kwok, H.; Zhan, X.; Liu, Y.; Zhu, D.; Tang, B. Aggregation-induced emission of 1-methyl-1,2,3,4,5-pentaphenylsilole. *Chemical Communications* **2001**, *0*, 1740-1741.

(4) Gierschner, J.; Lüer, L.; Milián-Medina, B.; Oelkrug, D.; Egelhaaf, H.-J. Highly emissive h-aggregates or aggregation-induced emission quenching? the photophysics of all-trans para -distyrylbenzene. *The Journal of Physical Chemistry Letters* **2013**, *4*, 2686-2697.

(5) Terenziani, F.; Morone, M.; Gmouh, S.; Blanchard‐Desce, M. Linear and two‐photon absorption properties of interacting polar chromophores: standard and unconventional effects. *ChemPhysChem* **2006**, *7*, 685-696.

(6) Destri, S.; Pasini, M.; Botta, C.; Porzio, W.; Bertini, F.; Marchiò, L. Synthesis and crystal structure and optical properties of fluorenic-core oligomers. *Journal of Materials Chemistry* **2002**, *12*, 924-933.

(7) Katan, C.; Tretiak, S.; Werts, M. H. V.; Bain, A. J.; Marsh, R. J.; Leonczek, N.; Nicolaou, N.; Badaeva, E.; Mongin, O.; Blanchard-Desce, M. Two-photon transitions in quadrupolar and branched chromophores: experiment and theory. *The Journal of Physical Chemistry B* **2007**, *111*, 9468-9483.

(8) Terenziani, F.; Painelli, A.; Katan, C.; Charlot, M.; Blanchard-Desce, M. Charge instability in quadrupolar chromophores: symmetry breaking and solvatochromism. *Journal of the American Chemical Society* **2006**, *128*, 15742-15755.

(9) Katan, C.; Terenziani, F.; Mongin, O.; Werts, M. H. V.; Porrès, L.; Pons, T.; Mertz, J.; Tretiak, S.; Blanchard-Desce, M. Effects of (multi)branching of dipolar chromophores on photophysical properties and two-photon absorption. *The Journal of Physical Chemistry A* **2005**, *109*, 3024-3037.

(10) Kasha, M.; Rawls, H. R.; El-Bayoumi, M. A. The exciton model in molecular spectroscopy. *Pure Applied Chemistry* **1965**, *11*.

(11) Würthner, F.; Kaiser, T. E.; Saha-Möller, C. R. J-aggregates: from serendipitous discovery to supra- molecular engineering of functional dye materials. *Angewandte Chemie International Edition* **2011**, *50*.

(12) Hari Shroff; Catherine G. Galbraith; James A. Galbraith; Helen White; Jennifer Gillette; Scott Olenych; Davidson, M. W.; Betzig, E. Dual-color superresolution imaging of genetically expressed probes within individual adhesion complexes. *Proceedings of the National Academy of Sciences of the United States of America* **2007**, *104*, 20308-20313.

(13) Keller, P.; Toomre, D.; Díaz, E.; White, J.; Simons, K. Multicolour imaging of post-Golgi sorting and trafficking in live cells. *Nature Cell Biology* **2001**, *3*, 140-149.

(14) Kobayashi, H.; Hama, Y.; Koyama, Y.; Barrett, T.; Regino, C. A. S.; Urano, Y.; Choyke, P. L. Simultaneous multicolor imaging of five different lymphatic basins using quantum dots. *Nano letters* **2007**, *7*, 1711-1716.

(15) Li, Y.; Shang, L.; Nienhaus, U. G. Super-resolution imaging-based single particle tracking reveals dynamics of nanoparticle internalization by live cells. *Nanoscale* **2016**, *8*, 7423-7429.

(16) Cao, Z.; Ziener, U. Synthesis of nanostructured materials in inverse miniemulsions and their applications. *Nanoscale* **2013**, *5*, 10093-10107.

(17) Yang, K.; Ma, Y.-Q. Computer simulation of the translocation of nanoparticles with different shapes across a lipid bilayer. *Nature Nanotechnology* **2010**, *5*, 579-583.

(18) Daniel, J.; Godin, A. G.; Palayret, M.; Lounis, B.; Cognet, L.; Blanchard-Desce, M. Innovative molecular-based fluorescent nanoparticles for multicolor single particle tracking in cells. *Journal of Physics D: Applied Physics* **2016**, *49*, 84002.

(19) Mulliken, R. S. Molecular compounds and their spectra, II. *Journal of the American Chemical Society* **1952**, *74*, 811-824.

(20) Painelli, A. Amplification of NLO responses: vibronic and solvent effects in push–pull polyenes. *Chemical Physics* **1999**, *245*, 185-197.

(21) Painelli, A. Vibronic contribution to static NLO properties: exact results for the DA dimer. *Chemical Physics Letters* **1998**, *285*, 352-358.

(22) Barzoukas, M.; Runser, C.; Fort, A.; Blanchard-Desce, M. A two-state description of (hyper) polarizabilities of push-pull molecules based on a two-form model. *Chemical Physics Letters* **1996**, *257*, 531-537.

(23) Mishra, A.; Behera, R. K.; Behera, P. K.; Mishra, B. K.; Behera, G. B. Cyanines during the 1990s: A Review. *Chemical Reviews* **2000**, *100*.

(24) Würthner, F.; Archetti, G.; Schmidt, R.; Kuball, H. G. Solvent effect on color, band shape, and charge‐density distribution for merocyanine dyes close to the cyanine limit. *Angewandte Chemie International Edition* **2008**, *47*, 4529-4532.

(25) Metz, D. J.; Glines, A. Density, viscosity, and dielectric constant of tetrahydrofuran between -78 and 30.degree. *Journal of Physical Chemistry* **1967**, *71*, 1158.

CHAPTER 6

RED EMITTING QUADRUPOLES

CHAPTER 6–RED EMITTING QUADRUPOLES

1. Introduction

So far, promising dipolar chromophores that, upon nanoaggregation, display interesting behaviors in terms of linear and non-linear optical properties such as red to NIR emission associated with large one-photon and two-photon brightness were presented. These properties make these nanoobjects suitable tools for bioimaging. As discussed in **Chapter 3**, the antiparallel arrangement of dipolar chromophores in confined state strongly influences the properties of FONs leading, generally, to a quenching of the luminescent properties. One possibility to prevent the typical arrangement of dipoles was discussed in **Chapter 5**, while a different way to overcome the problem of quenching upon aggregation can be the use of another class of interesting dyes: quadrupolar chromophores.

These dyes are basically symmetrical conjugated molecules bearing either two electron-releasing or two electron-withdrawing end-groups, connected with a core, that can have acceptor or donor character, through a π-conjugated bridge (**Illustration VI 1**).

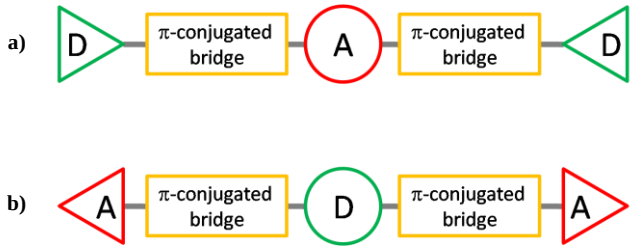

Illustration VI 1. General configuration of a) D-π-A-π-D and b) A-π-D-π-A quadrupolar chromophore

From a direct comparison between dipolar and quadrupolar chromophores, the first things to highlight, in terms of optical properties, are the selection rules. In centrosymmetric molecules the one-photon allowed transition has to be antisymmetric while the two-photon allowed transition has to reach an energetic level with the same symmetry as of the ground state, indicating that it is possible to study different excited state depending on the character of the transition (**Illustration VI 2**). On the

other hand, in non-centrosymmetric molecules the transition between the ground and the final state is allowed both upon one-photon and two-photon excitation; moreover quadrupolar chromophores, compared with the dipolar analogue, display higher two-photon cross section thanks to their periphery-to-core charge redistribution upon excitation[1-3].

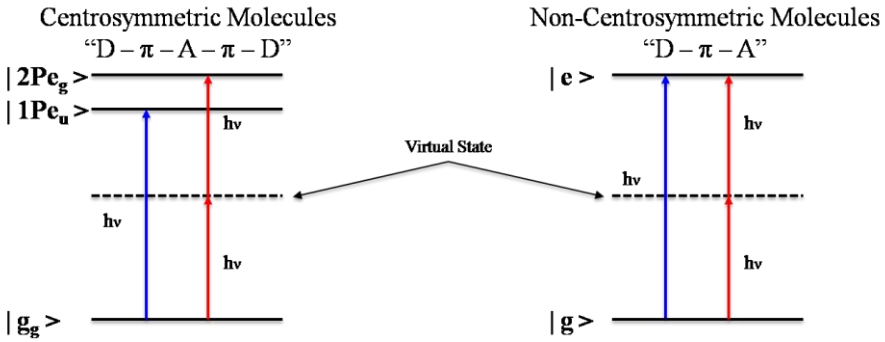

Illustration VI 2. Energy level diagrams for general centrosymmetric and non-centrosymmetric chromophores (where **|g⟩** and **|e⟩** are the ground and the excited state respectively, and the subscripted **g** and **u** are gerade and ungerade symmetry respectively).

In the last decades quadrupolar-like molecules were intensively studied[4-21], the goal is to design and synthesize quadrupolar systems with strong emission and large two-photon brightness ($\sigma_2\Phi_f$) in the red-NIR region. As discussed earlier for dipoles, also for quadrupoles the shift of both absorption (one-photon and two-photon) and emission towards lower energies depends on the end-groups and the core as well as the conjugation of the connecting bridge. Considering the same donor-acceptor couple (at least with similar strength), a longer π-conjugated path is needed to obtain strong quadrupolar red-NIR emitter, compared with dipoles. In the confined state, this may lead to a higher probability of interchromophoric interaction causing a decrease of the emissive properties.

This chapter reports a systematic study on quadrupolar chromophores, displayed in **Figure VI 1**, using triphenylamine as common donor end-group and a benzothiadiazole (BTDA) as electron-withdrawing core by either tuning the length and the conjugation of the bridge or playing with the strength of the core adding a second BTDA moiety.

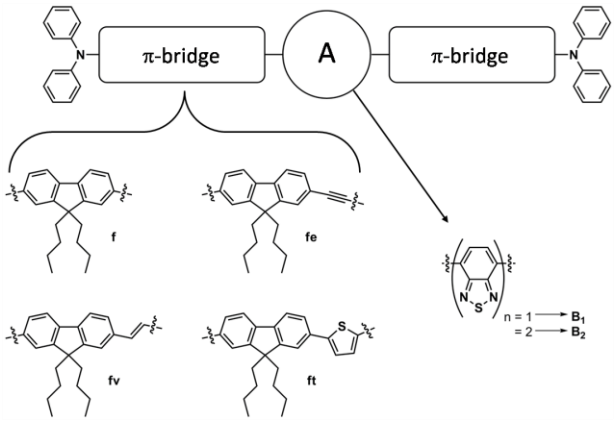

Figure VI 1. Quadrupolar D-π-A-π-D chromophores studied in this chapter

1.1. Structural characterization

*1.1.1. Compound **QfvB₁***

Single crystals of chromophore **QfvB₁** were obtained by slow diffusion of acetone layered over a supersaturated solution of the dye in DCM. The compound crystallizes in a centrosymmetric triclinic P-1 space group. Unfortunately, disordered DCM molecules present in the crystal lattice could not be refined, and thus the SQUEEZE command was applied during the resolution.

As it is possible to observe in **Figure VI 2a**, the double bonds connected to the acceptor core are in anti configuration with respect to the BTDA. The angle between the main planes formed by the two fluorenes on the two molecular branches is 66°. The alkyl chains also form a cross-like configuration with an angle of 89° as already observed in the previous chapters.

Despite the presence of hindering groups such as alkylated fluorenyl moiety and diphenyl amine, the crystal packing of this chromophore is dominated by short CH-π interactions, 3.6 Å between one alkyl chain and the fluorenyl core of a second layer, and π-π interactions of 3.5 Å between two BTDA cores of two molecules forming the dimer, **Figure VI 2b**.

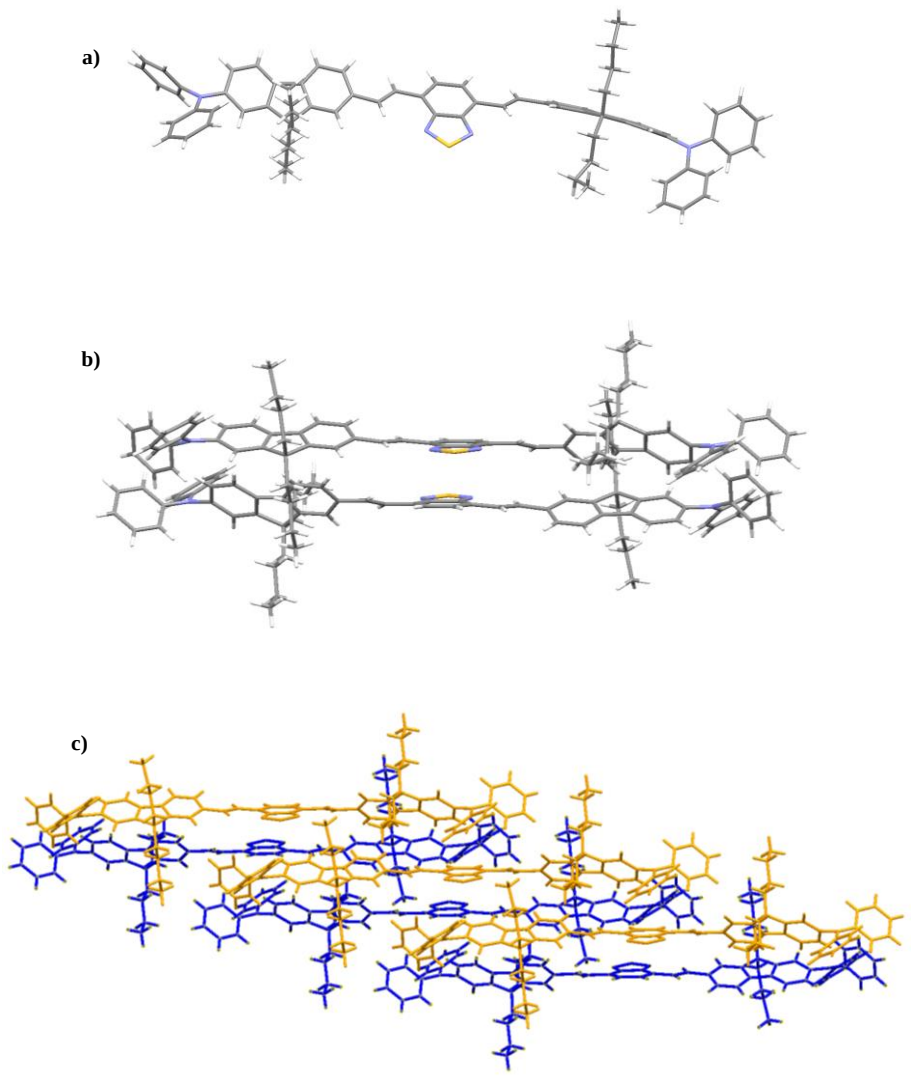

Figure VI 2. a) **QfvB$_1$** in general position, b) dimer generated by the inversion center and c) view of the crystal packing

2. Linear photophysical characterization in organic solution

For an easy comprehension, the chromophores of this chapter are compared under two different points of view: the change of the photophysical properties induces by both the π-conjugated path and a modification of the core by adding a second BTDA.

2.1. Effect of the environment

Thanks to their symmetric structure, quadrupolar molecules do not display permanent dipole moment, thus these chromophores should not be affected by any changes of the local electric field. In literature there are many examples of strong fluorescence solvatochromism indicating the existence of dipolar excited states[22-27]. This phenomenon is known as symmetry breaking: upon excitation, one branch undergoes an electronic rearrangement inducing the formation of a dipolar moment, which is strongly affected by the nature of the environment.

In **Figure VI 3**, one can observe that tuning the solvent polarity does not affect the ICT transition band indicating the neutral character of the molecules in ground state, while the environment polarity induces a marked change in the luminescent properties indicating the break of the symmetry in the excited state. One can see that all chromophores show positive solvatochromic character, as could be expected.

It is worthy to highlight the strange behavior of these chromophores in acetone. When the chromophores are dissolved in acetone, a new band appears thus the emission spectra is strongly affected, particularly it is markedly blue-shifted compared with the expectation (except for chromophore **QfvB$_1$** in **Figure VI 3b**). Unfortunately, since it was not possible to go deeper in the study due to solubility problems, one hypothesis is that probably in polar solvent (at least observed in acetone) it occurs interchromophoric interactions that lead to the unusual behavior observed.

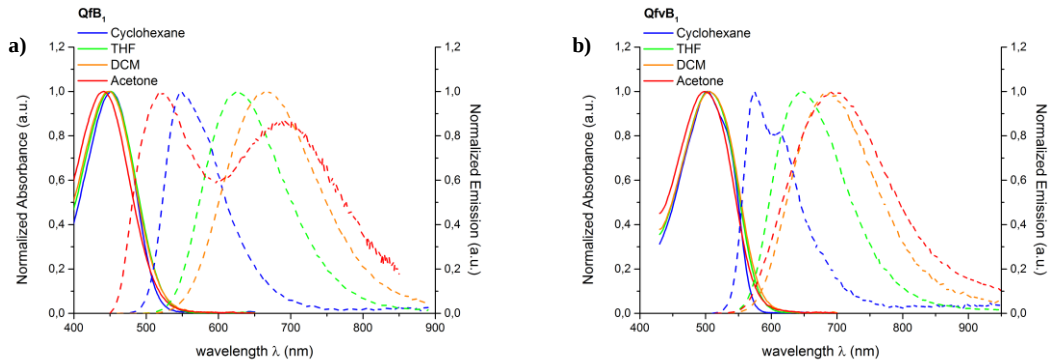

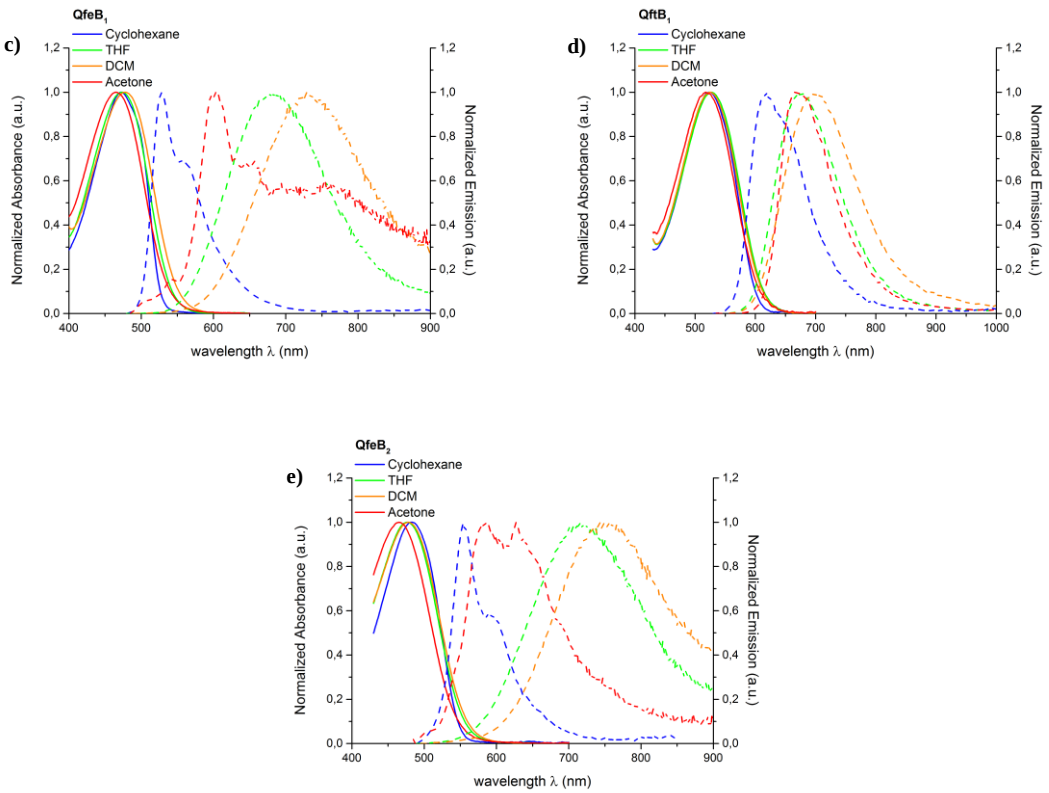

Figure VI 3. Normalized absorption and emission spectra measured in solvent of increased polarity to study the solvatochromic behavior of the quadrupolar chromophores discussed in this chapter (in the normalized absorption spectra the high energy band ascribed to π-π^* transition was cut out for clarity)

2.2. Effect of the π-conjugated bridge

In this paragraph are discussed the results obtained measuring the photophysical properties on quadrupoles by changing the π connector between the two donor end-groups and the acceptor core, in order to compare how the bridge can affect the optical behavior. We played with both the rigidity of the π system as well as the extension of the conjugation by adding an ethynyl, a vinyl or a thienyl linker to a fluorene. In **Table VI 1** are gathered the relevant data.

The absorption spectra can be clearly divided in two main bands, the more intense band is located at lower wavelength and can be ascribed to a high energy π-π^* transition, while the less intense band is red shifted and belongs to an internal charge transfer transition, the considered molar extinction coefficient is related to the ICT band. It is displayed in **Figure VI 4** that the

functionalization of the fluorene with a conjugated linker (**QfB$_1$** → **QfvB$_1$**, **QfeB$_1$** and **QftB$_1$**) leads to a bathochromic shift of the ICT band indicating the extension of electronic conjugation. As expected[8] the change of a triple bond by a double bond (**QfeB$_1$** → **QfvB$_1$**) induces a shift towards low energies linked to a marked hyperchromic effect, in line with an increase of the conjugated path. Interestingly, the replacement of a double bond by a thienyl unit leads to a bathochromic shift associated, unexpectedly, with a decrease of the molar extinction coefficient. The low aromaticity of the thienyl moiety decreases the gap between the ground and the excited state probably lowering the ICT transition.

Table VI 1. Linear photophysical relevant data

Cpd	λ_{max}^{1PA} [nm]	ε_{max} [10^4 $M^{-1}cm^{-1}$]	λ_{max}^{em} [nm]	Φ_f	τ_1 [ns]
QfB$_1$	450	2.5	628	0.64	5.15
QfvB$_1$	505	5.9	644	0.59	3.61
QfeB$_1$	474	3.9	688	0.18	2.20
QftB$_1$	528	4.5	675	0.45	3.88

The luminescence properties do not follow the trend observed for the absorption. Indeed elongating the π-conjugated bridge, from **QfB$_1$** to the other members of the class, it can be observed a bathochromic shift of the emission band, but in **Figure IV 4b** is displayed that the replacement of the ethynyl linker with the vinyl one induces an unexpected red-shift associated with a marked increase of the fluorescence quantum yield (from 0.18 to 0.59). Strikingly, the obtained chromophores, especially **QfvB$_1$** and **QftB$_1$**, display good Φ_f in the red visible region.

It can be observed a shortening of the fluorescence lifetime with passing from the chromophore with **f** as π-bridge to the elongated ones. Moreover, one can notice that the substitution of the double bond with a thienyl moiety does not affect the lifetime of the excited state, while replacing the vinyl with the ethynyl linker leads to a marked decrease of the τ_1.

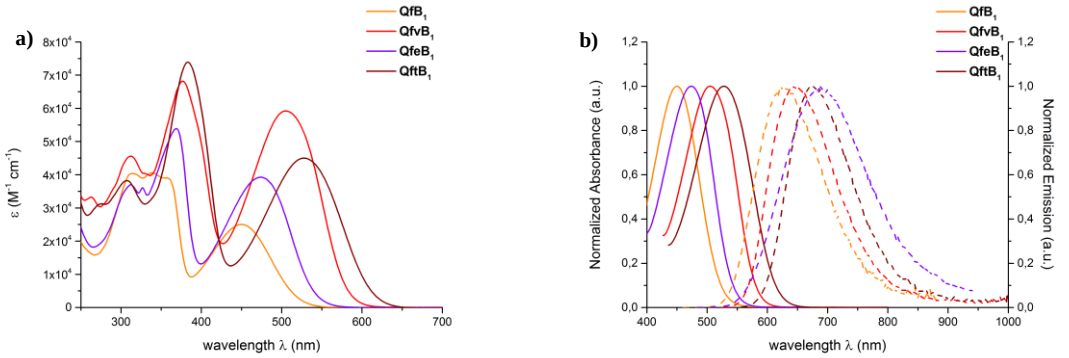

Figure VI 4. Comparison between a) one-photon absorption spectra and b) normalized absorption and emission spectra measured for the quadrupoles with different π bridge in THF solution (in the normalized absorption was cut out the higher energetic band ascribed to π-π^* transition for clarity) (*consistent color code between the figures of the chapter*)

2.3. Effect of the core

Another way to increase the charge transfer character of molecules is to try to enhance the strength of the donor or the acceptor moiety[1,2], to do so, we tried to increase the periphery to core charge transfer by adding a second electro-withdrawing group in the core of the quadrupole.

As observed in the previous paragraph, the most intense band is related to a highly energetic π-π^* transition, while the more interesting internal charge transfer band is lying at lower energies. Indeed, both chromophores display a broad ICT absorption band located in the blue spectral region. They do not show significant changes related to the addition of the second BTDA such as a shift of the ICT band or changes of the molar extinction coefficient. Probably the strengthening of the core does not affect the ground state leading in no strong differences, except a slight hypochromic effect with passing from **B_1** to **B_2**.

Table VI 2. Linear photophysical relevant data

Cpd	λ_{max}^{1PA} [nm]	ε_{max} [10^4 $M^{-1}cm^{-1}$]	λ_{max}^{em} [nm]	Φ_f	τ_1 [ns]
QfeB$_1$	474	3.9	688	0.18	2.20
QfeB$_2$	477	3.4	718	0.03	0.79

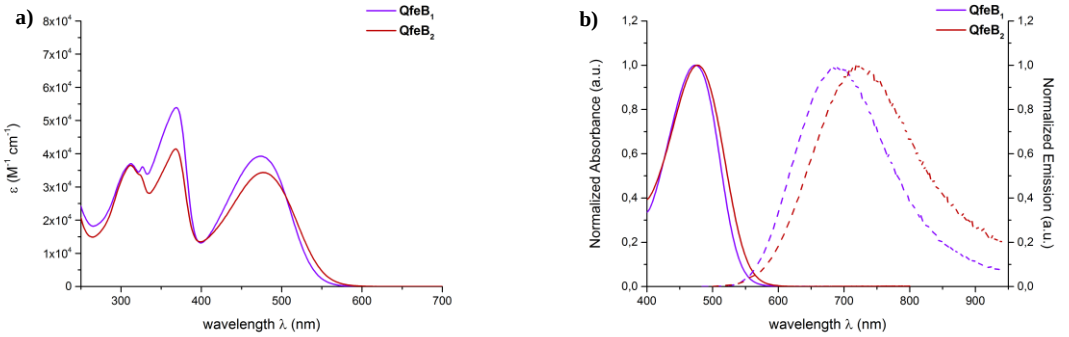

Figure VI 5. Comparison between a) one-photon absorption spectra and b) normalized absorption and emission spectra measured for the quadrupoles increase the number of benzothiadiazole in THF solution (in the normalized absorption was cut out the higher energetic band ascribed to π-π^* transition for clarity) (*consistent color code between the figures of the chapter*)

On the other hand, the addition of a second benzothiadiazole induces a slight bathochromic shift of the emission band (**QfeB$_2$** λ_{max}^{em} = 718 nm) associated with a marked decrease of the luminescence quantum yield (see **Table VI 2**). The marked shortening of the lifetime of the excited state (2.20 ns → 0.79 ns) suggests that the relaxation pathway mainly follows non-radiative decays.

3. Non-linear photophysical characterization in organic solution

Thanks to their emissive properties, we were able to evaluate the two-photon cross section of these quadrupolar chromophores by measuring the two-photon excited fluorescence. Due to their emission, from orange to NIR, the measurements were done in a range between 750 nm and 1160 using Fluorescein and Nile Red as reference chromophores[28].

3.1. Effect of the bridge

The chromophores studied in this paragraph display intense two-photon absorption spectra with the two-photon cross section ranging from 880 GM up to 2972 GM. As discussed in the introduction of the chapter, the 2PA band is markedly blue-shifted in relation with the linear ICT band, underlying that upon two-photon excitation the reached excited state is different compared with the one-photon transition.

From the comparison between the 2PA spectra displayed in **Figure VI 6e** one can clearly see that the elongation of the conjugation with an additional linker (**QfB_1** → **$QfvB_1$**, **$QfeB_1$** and **$QftB_1$**) induced a slight red-shift of the ICT band associated a marked hyperchromic effect, paralleling what was observed upon one-photon excitation. It is interesting to underline that the addition of ethynyl, vinyl or thienyl moiety in the conjugated bridge induces also the structuration of the band that cannot be observed for chromophore **QfB_1**. The substitution of the ethynyl linker with the vinyl one leads to an increase of the two-photon cross section linked to the enhancement of the conjugated character of the bridge. Moreover, the replacement of the double bond with the thienyl group induces a marked bathochromic shift of the λ_{max}^{2PA}.

Table VI 3. Non-linear photophysical relevant data

Cpd	$2\lambda_{max}^{1PA}$ [nm]	λ_{max1}^{2PA} [nm]	σ_2 [GM]	λ_{max2}^{2PA} [nm]	σ_2 [GM]
QfB_1	900	820	880	-	-
$QfvB_1$	1010	820	2972	890	2244
$QfeB_1$	948	820	2445	890	1884
$QftB_1$	1056	840	2783	890	2850

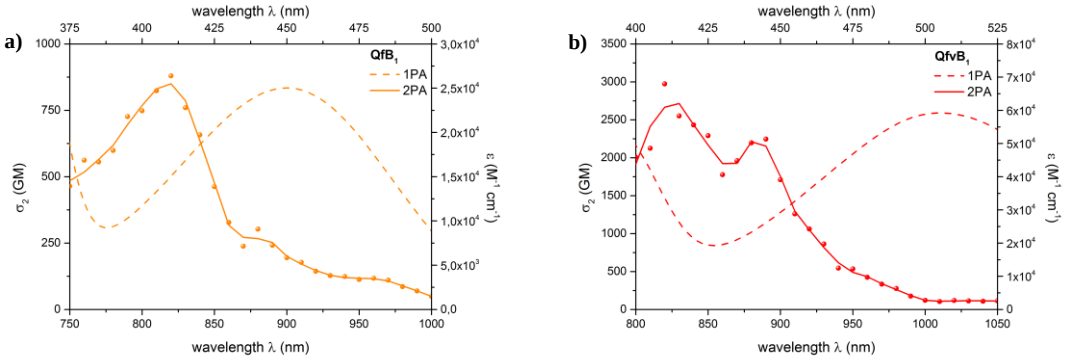

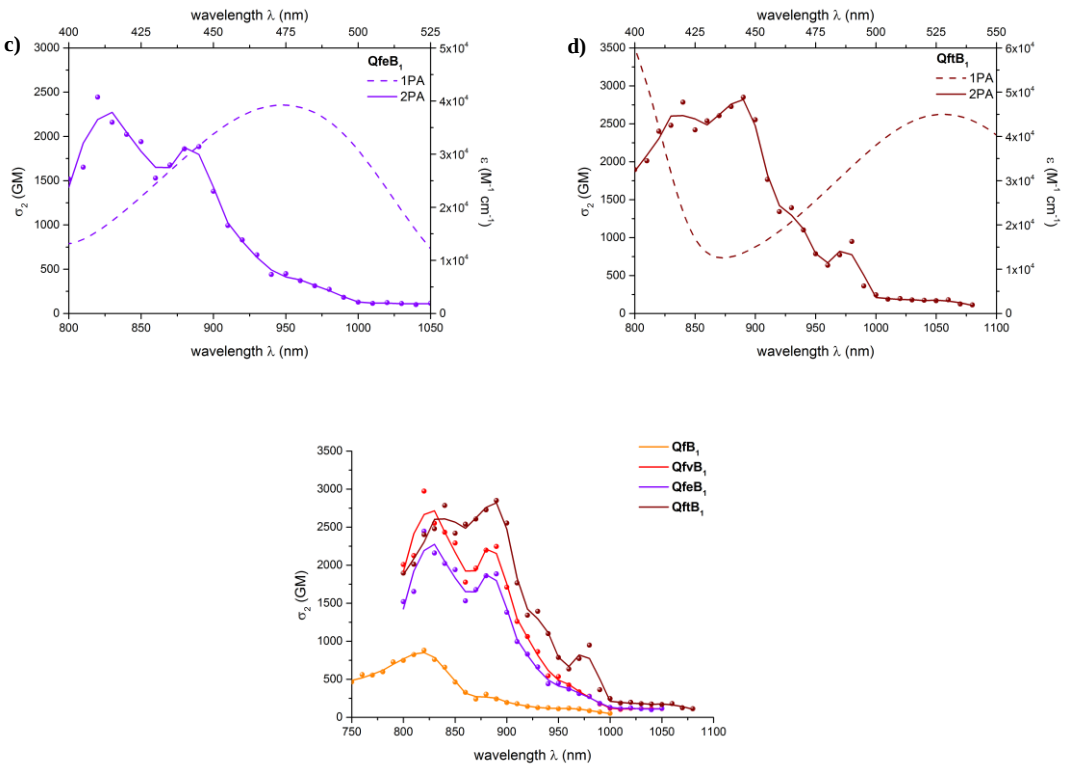

Figure VI 6. a-d) Comparison between 1PA (dashed line) and 2PA (colored point and solid line) spectra measured for chromophores by tuning the π bridge dissolved in THF solution, e) Comparison of 2PA spectra of the chromophores of the family.

3.2. Effect of the core

These chromophores display a structured intense two-photon absorption band with the maximum markedly blue-shifted compared with the double of the λ_{max}^{1PA} as expected (cf. **Paragraph 1:** Introduction). Interestingly, in both 2PA spectra is visible a shoulder located at low energies that can be ascribed to the one-photon allowed transition. The addition of the second BTDA in the core of the molecules does not affect the absorption band in terms of shift, but it is interesting to underline the unexpected decrease of the σ_2 at λ_{max}^{2PA} measured passing from **B1** to **B2**, while is observable a slight hyperchromic effect at low energies. The latter behavior is probably related to the one-photon allowed transition more pronounced in the chromophore with double core.

Table VI 4. Non-linear photophysical relevant data

Cpd	$2\lambda_{max}^{1PA}$ [nm]	λ_{max1}^{2PA} [nm]	σ_2 [GM]	λ_{max2}^{2PA} [nm]	σ_2 [GM]
QfeB$_1$	948	820	2445	890	1884
QfeB$_2$	954	820	1740	890	1600

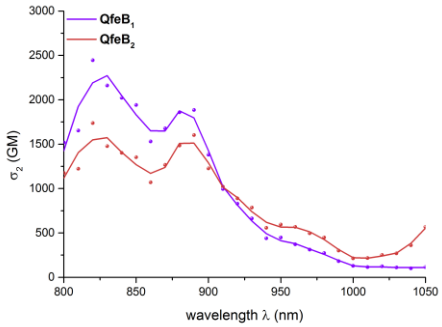

Figure VI 7. Comparison between two-photon absorption spectra measured for chromophores **QfeB$_1$** and **QfeB$_2$** in dissolved THF

4. FONs preparation and morphological characterization

The nanoparticles were prepared with the already described nanoprecipitation method. The size and the shape of the obtained nanoaggregates were evaluated using the transmission electron microscopy (TEM), while the surface potentials were measured by zetametry. In **Table VI 5** are gathered the relevant data concerning the FONs.

Table VI 5. Morphological and structural relevant data

Cpd	d_{TEM} [nm]	N [10^4]	ζ-potential [mV]
QfB$_1$	52	4.9	-67
QfvB$_1$	26	0.5	-64
QfeB$_1$	39	1.7	-74
QftB$_1$	57	4.9	-70
QfeB$_2$	19	0.2	-66

The prepared FONs display a spherical shape with a diameter size ranging from 19 nm to 57 nm. Since the nanoparticles are spherical, one can assume an internal disorder, and so no specific interactions should occur between neighbor chromophores. Furthermore, as widely discussed earlier in the manuscript, the number of chromophores *per* nanoparticles is an important data in order to evaluate the overall brightness of the nanoobject and this number is directly related to both the size of the nanoparticles and the molar weight of the molecule.

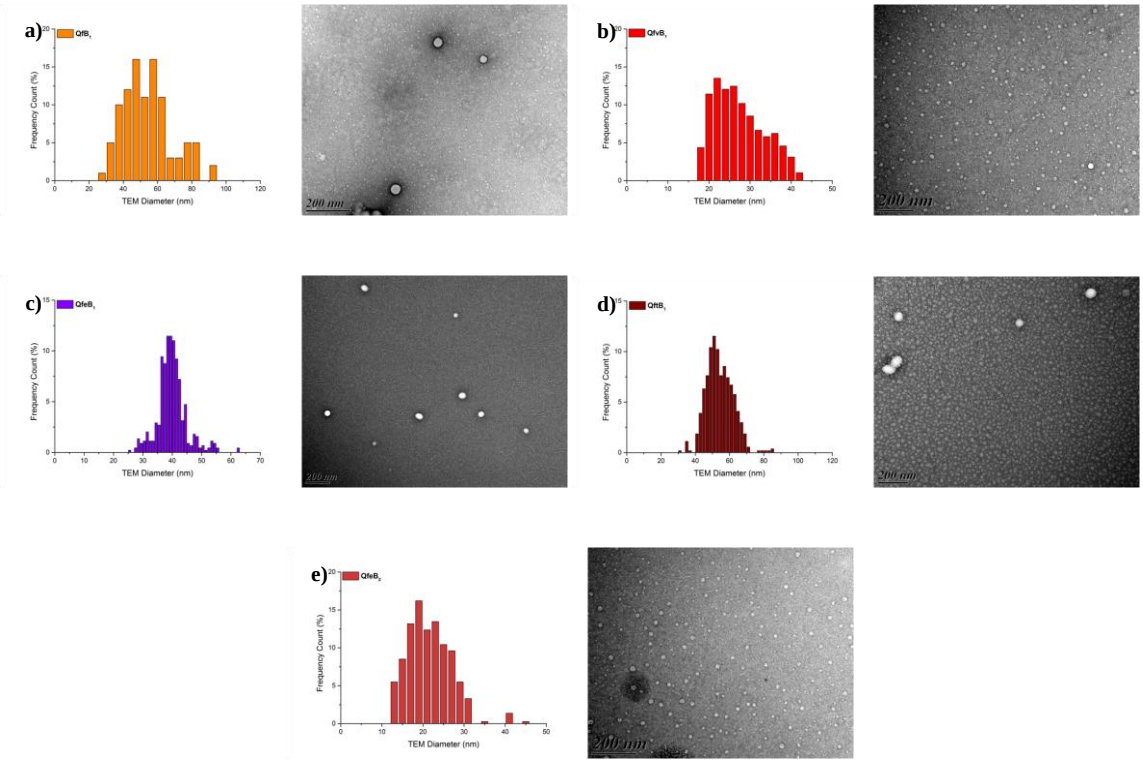

Figure VI 8. Size distribution (left panel) and TEM image (right panel) of FONs prepared with a) **QfB$_1$**, b) **QfvB$_1$**,c) **QfeB$_1$**,d) **QftB$_1$** and e) **QfeB$_2$**.

5. Linear and non-linear optical characterization of FONs

The next step, after the preparation of FONs was to study their photophysical properties in order to see if these nanoobjects can be used as probes in bioimaging. Also in this paragraph the description will be divided taking into account the conjugated path and the strength of the core.

5.1. Effect of the π-conjugated bridge

5.1.1. One-photon characterization

Following the trend observed for these chromophores in solution, the elongation of the conjugation also induces a bathochromic shift of the absorption band upon nanoaggregation. Concerning the molar extinction coefficient, we have a parallel behavior: a marked hyperchromic effect from **QfB$_1$** to **QfeB$_1$** and then to **QfvB$_1$**, while we observed a decrease of the ε_{max} by replacing the vinyl linker with a thienyl moiety.

Table VI 6. Linear photophysical relevant data

Cpd	λ_{max}^{1PA} [nm]	ε_{max} [10^4 $M^{-1}cm^{-1}$]	λ_{max}^{em} [nm]	Φ_f	τ_1 [ns]
QfB$_1$	458	2.7	600	0.32	2.4 (0.3) 5.4 (0.7)
QfvB$_1$	505	9.5	650	0.09	4.5 (0.1) 1.6 (0.7) 0.58 (0.2)
QfeB$_1$	477	3.1	621	0.04	4.6 (0.4) 1.0 (0.3)
QftB$_1$	534	4.9	690	0.08	17.5 (0.3) 1.1 (0.5) 2.4 (0.5)

Comparing the quadrupoles in both solution and confined environment one can see, in **Figure VI 9**, an hyperchromic effect displayed upon nanoaggregation, except for **QfeB$_1$**, indicating a cooperative effect between the neighbor chromophores within the nanoparticle. Moreover, one can observe a broadening of the ICT band that can be ascribed to an excitonic coupling after nanoconfinement. The excitonic coupling is more pronounced in FONs **QfvB$_1$**, in fact one can see the formation of a shoulder suggesting an intermediate molecular arrangement between the two limit: J and H aggregates[29].

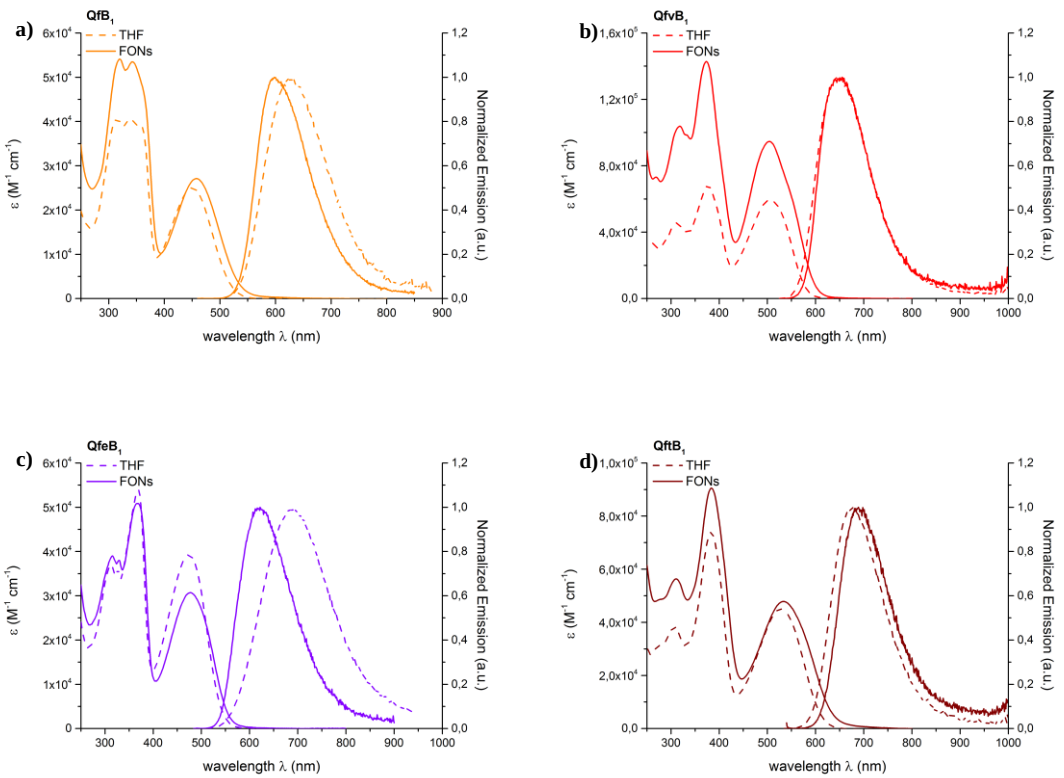

Figure VI 9. Comparison between one-photon absorption spectra and normalized emission measured for chromophores a) **QfB$_1$**, b) **QfvB$_1$**,c) **QfeB$_1$**,d) **QftB$_1$** in both THF solution and FONs in water.

In **Figure VI 10** is displayed the comparison between the emission spectra measured for the quadrupoles in confined environment. Contrarily to what was observed for the chromophores in solution, the FONs follow the trend observed in absorption. With extending the conjugation, there is a shift of the emission band towards low energies. Playing on the π-conjugated bridge we were able to obtain FONs with emission ranging from orange to deep red with strikingly good fluorescence quantum yield (from 0.32 for **QfB$_1$** to 0.04 for **QfeB$_1$**) even if a luminescence quenching can be observed upon aggregation. Interestingly, the values of Φ_f do not follow the same tendency as the emission band, in fact the nanoaggregates prepared with **QfeB$_1$** were weakly emissive. This behavior is probably due to intermolecular interactions, indeed the rigidity of the π-conjugated bridge could promote stronger π-π stacking that leads to a decrease of the luminescence properties. From a direct comparison between the emissions band measured in THF solution and in FONs in water one can see that the chromophores do not display the same behavior, depending on the chemical structure, the

emission of FONs can be blue-shifted, similar or red-shifted compared with the band measured in THF solution. Since the chromophores are solvatochromic, the behavior of the molecules within the nanoparticle suggests that the polarity of the environment of chromophore **QfvB$_1$** (**Figure VI 9b**) is comparable to that measured in THF solution, while chromophore **QfeB$_1$** (**Figure VI 9c**) encounters an environment upon nanoconfinement less polar than THF.

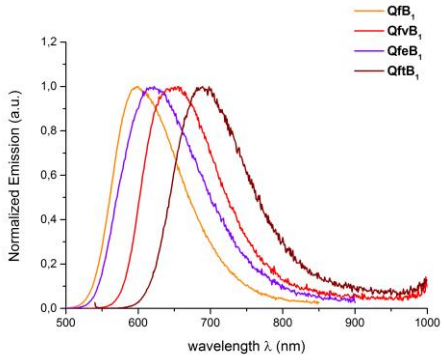

Figure VI 10. Normalized emission spectra of the quadrupolar chromophores upon nanoaggregation

5.1.2. Two-photon characterization

Within nanoparticles, the molecules have a similar behavior than that already observed in solution: as expected, when the molecules are confined in nano-environment, the excited state reached with the non-linear process is different compared with the one reached upon one-photon excitation.

Contrarily to what was observed in one-photon absorption, the comparison between the spectra measured for the quadrupoles in THF solution and in FONs in water did not show the cooperative effect that enhance the two-photon cross section at the maximum wavelength, except for nanoparticles prepared with **QfB$_1$**. However, all the dye within nanoparticles display a broadening of the absorption band with the formation of a shoulder (marked for **QfeB$_1$** and **QftB$_1$**), towards low energies, suggesting the excitonic coupling also observed in the linear process. Moreover, the comparison also shows that the sub-bands of the 2PA spectra are well superimposed between solution

and nanoparticles, but with relative intensity changes: typically the most intense band for the nanoconfined quadrupole is red-shifted with respect to the chromophore in THF.

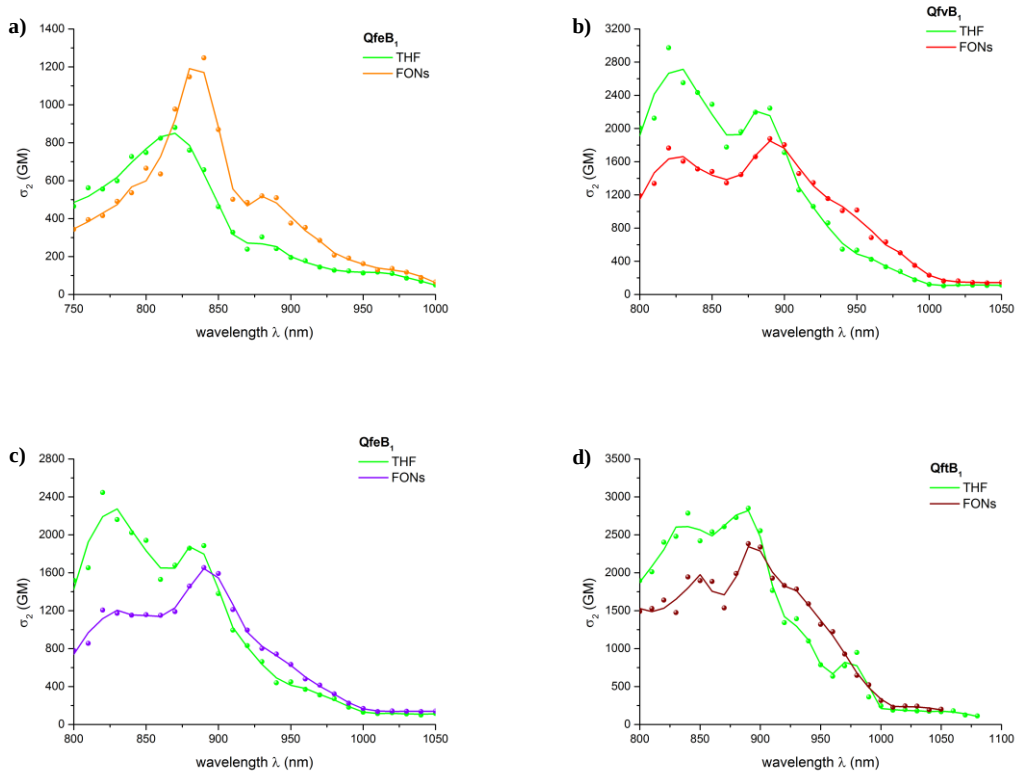

Figure VI 11. Comparison between the 2PA spectra measured for the quadrupoles in both THF solution (green colored point and solid line) and FONs in water (colored point *consistent color code between the figures*)

Table VI 7.

Cpd	$2\lambda_{max}^{1PA}$ [nm]	λ_{max1}^{2PA} [nm]	σ_2 [GM]	λ_{max2}^{2PA} [nm]	σ_2 [GM]
QfB1	916	840	1247	880	519
QfvB1	1010	820	1764	890	1877
QfeB1	954	820	1210	890	1650
QftB1	1068	840	1945	890	2383

5.2. Effect of the core

5.2.1. One-photon characterization

By increasing the electron withdrawing character of the core, we can observe the same trend as for the chromophores in solution. In **Figure VI 12a** a hypochromic effect it can be noticed after the addition of the second BTDA in the core, associated with a slight red-shift of the ICT band. Moreover, a decrease of the molar extinction coefficient it can be observed upon nanoconfinement for chromophore **QfeB$_2$**, as observed previously for the quadrupole with one BDTA (**Figure VI 12b** and **Figure VI 9c** respectively).

Table VI 8. Linear photophysical relevant data

Cpd	λ_{max}^{1PA} [nm]	ε_{max} [10^4 $M^{-1}cm^{-1}$]	λ_{max}^{em} [nm]	Φ_f	τ_1 [ns]
QfeB$_1$	477	3.1	621	0.04	4.6 (0.4) 1.0 (0.3) 17.5 (0.3)
QfeB$_2$	484	2.8	652	0.03	4.8 (0.4) 0.9 (0.3) 17.8 (0.3)

Concerning the luminescent properties, increasing the number of electron acceptor moieties in the core of the quadrupole induces a bathochromic shift but, interestingly, the fluorescence quantum yield is not affected. On the other hand, comparing **QfeB$_2$** in both THF solution and FONs in water displayed in **Figure VI 12b**, one can see that the nanoconfinement leads to an hypsochromic shift of the emission band but, remarkably, the FONs prepared do not display the quenching observed for all the other chromophores of the series.

As reported in **Table VI 8** both dyes in confined environment display three lifetimes in the same range, indicating that, in addition with the two "classical" lifetimes measured for the chromophores in the core and in the shell, these two dyes form upon aggregation a third emissive system that is probably related to a particular arrangement of molecules organized in a short range, which display a long lifetime in the range of 17 ns (see **Table VI 8**).

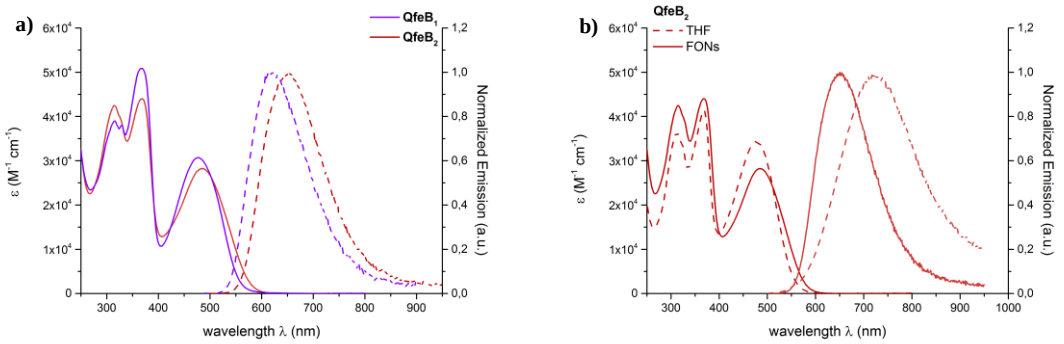

Figure VI 12. a) Comparison between absorption and normalized emission spectra of the FONs prepared with **QfeB$_{1\text{-}2}$**; b) Comparison between one-photon absorption spectra and normalized emission measured for chromophore **QfeB$_2$** in both THF solution and FONs in water

5.2.2. Two-photon characterization

The molecules upon nanoconfinement and the one dissolved in organic solvent display similar properties. Indeed, as shown in **Figure VI 13a**, the maximum wavelength of the two-photon absorption spectra is markedly blue-shifted compared with twice λ_{max}^{1PA}, indicating that, even in nanoparticles, the excited state reached upon two-photon excitation is not the one reached after the absorption of one photon.

Table VI 9. Non-linear photophysical relevant data

Cpd	**$2\lambda_{max}^{1PA}$ [nm]**	**λ_{max1}^{2PA} [nm]**	**σ_2 [GM]**	**λ_{max2}^{2PA} [nm]**	**σ_2 [GM]**
QfeB$_1$	954	820	1210	890	1650
QfeB$_2$	968	820	1140	900	1320

It can be noticed in **Figure VI 13b** that the addition of a second BTDA in the core induces a weak hypochromic effect does not affecting significantly the absorption band.

From a direct comparison between the two-photon absorption spectra measured for the chromophore **QfeB$_2$** in both THF solution and FONs in water displayed in **Figure VI 13c**, one can see that both spectra show a structured band and it is interesting to highlight that the relative intensities of

both sub-bands is different, specifically the most intense band measured in FONs correspond to the less intense band measured for the dye in THF, causing a bathochromic shift of the λ_{max}^{2PA}. Moreover, It is worthy to underline that with passing from molecular solution to nanoconfinement a pronounced shoulder appears at low energies, suggesting an excitonic coupling upon aggregation.

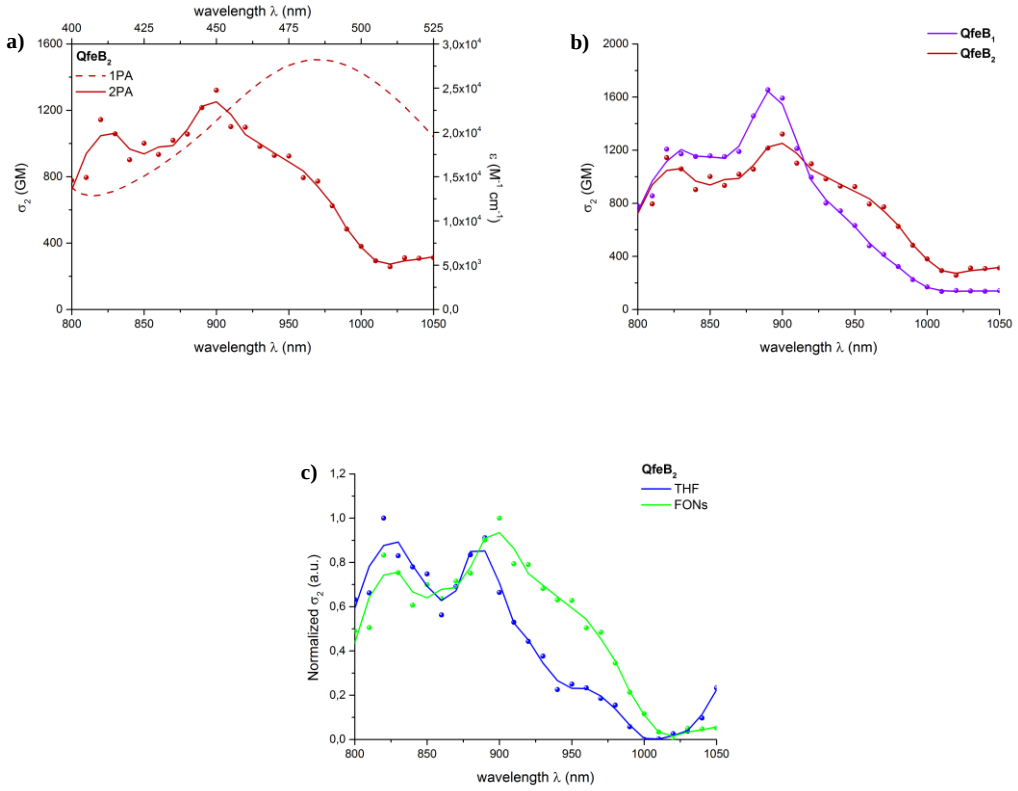

Figure VI 13. a) Overlap between one-photon absorption (dashed line) and two-photon absorption (solid line and colored points) measured for chromophore **QfeB$_2$** in confined environment; comparison between 2PA spectra measured on FONs **QfeB$_{1\text{-}2}$** and c) comparison between normalized 2PA spectra measured for **QfeB$_2$** in both THF solution and FONs in water

6. Biological studies

As widely discussed in the previous chapters, the confinement of a large number of chromophores in nanoparticles induces additive/cooperative effects that lead to high one-photon and two-photon brightness. We were able to test the nanoparticles prepared with **QfvB$_1$** and **QfeB$_2$** in COS7 cells in order to study their ability of internalization and their luminescent properties in

bioenvironment. The images were taken after 24h of incubation of the FONs in cells using DAPI as label of nuclei.

Table VI 10. Luminescence properties including one-photon and two-photon brightness of FONs in water

Cpd	λ_{max}^{1PA} [nm]	λ_{max}^{em} [nm]	$FWHM^{em}$ [10^3 cm^{-1}]	Φ_f	$\varepsilon_{max}\Phi_f$ a) [10^8 M^{-1} cm^{-1}]	λ_{max}^{2PA} [nm]	$\sigma_2\Phi_f$ a) [10^6 GM]
QfB_1	458	600	5.2	0.32	4.2	840	19.4
$QfvB_1$	505	650	4.4	0.09	0.4	890	0.9
$QfeB_1$	477	621	4.9	0.04	0.2	890	1.1
$QftB_1$	534	690	4.2	0.08	1.9	890	9.3
$QfeB_2$	484	652	5.3	0.03	0.01	900	0.07

a) the values of brightness (both one-photon and two-photon) are considered using the concentration of nanoparticles

In **Figure VI 14-15** are displayed the experiment of one-photon microscopy (**a-c**) and two-photon microscopy (**d-f**) using as probes the FONs prepared with **$QfvB_1$** and **$QfeB_2$** respectively, underlying that these nanoparticles are suitable for both techniques.

It is worthy to highlight that, contrarily to what was observed in **Chapter 5** for FONs prepared with chromophores **1Bis(BP)** and **2Bis(BP)**, in this case the nanoparticles are not broadly distributed in the cytosol but seem to be located in particular compartments close to the nucleus.

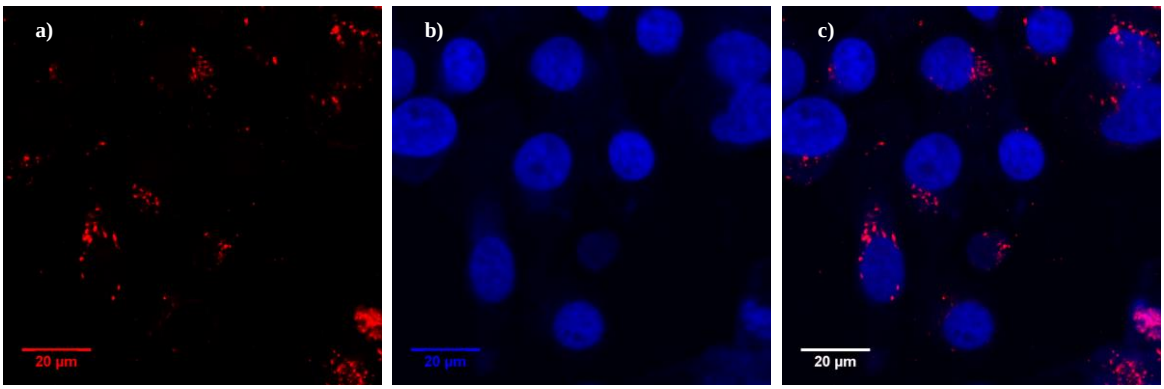

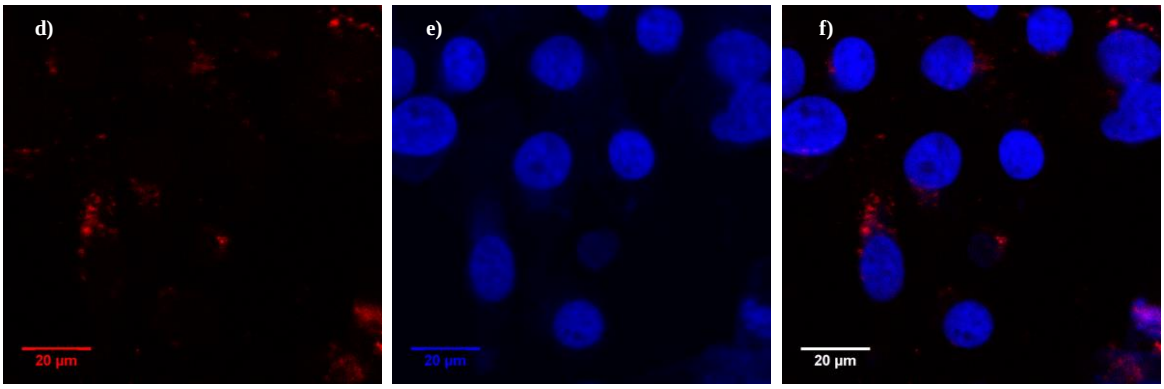

Figure VI 14. COS 7 cells incubated for 24h with FONs **QfvB$_1$** and stained with DAPI to label the nuclei a) λ_{exc} = 514 nm and λ_{em} = 600-750 nm; b) λ_{exc} = 405 nm and λ_{em} = 460-475 nm; c) co-localization; d) λ_{exc} = 890 nm and λ_{em} = 600-750 nm; e) λ_{exc} = 405 nm and λ_{em} = 460-475 nm; f) co-localization. [FONs] ≈ 15 pM

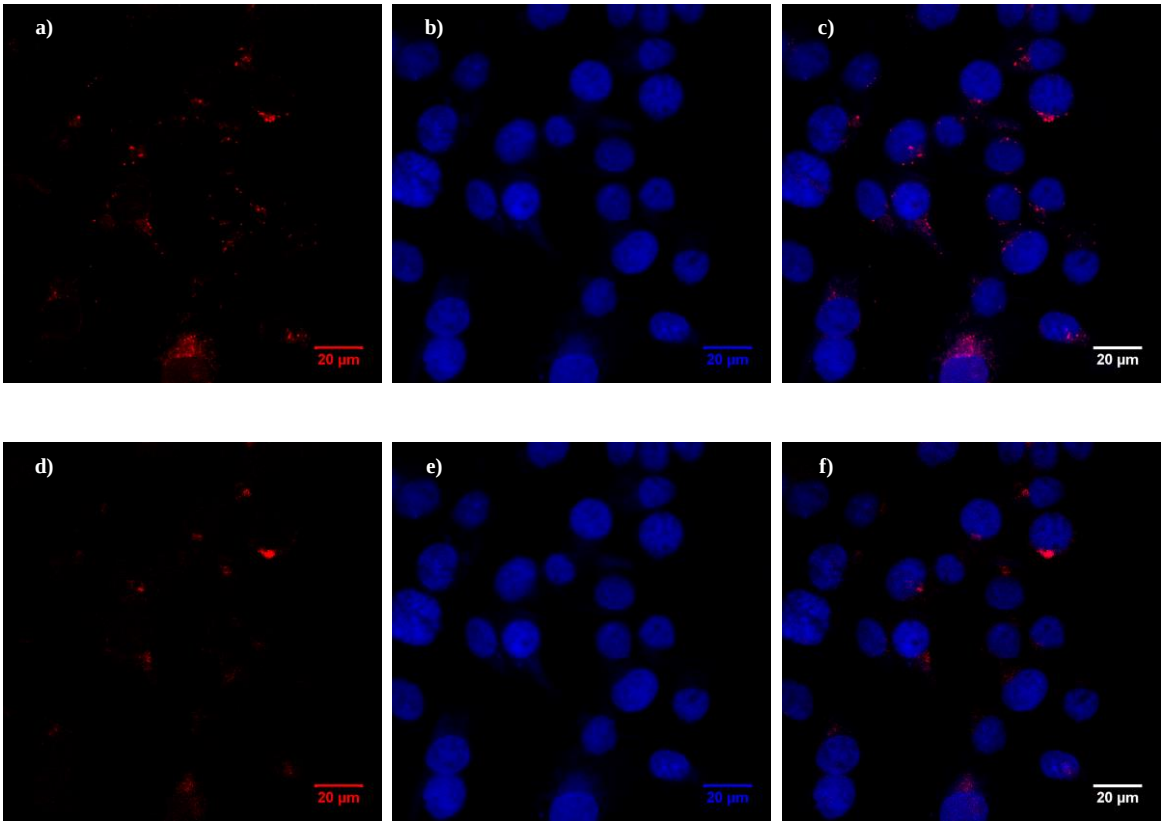

Figure VI 15. COS 7 cells incubated for 24h with FONs **QfeB$_2$** and stained with DAPI to label the nuclei a) λ_{exc} = 488 nm and λ_{em} = 600-750 nm; b) λ_{exc} = 405 nm and λ_{em} = 460-475 nm; c) co-localization; d) λ_{exc} = 900 nm and λ_{em} = 600-750 nm; e) λ_{exc} = 405 nm and λ_{em} = 460-475 nm; f) co-localization. [FONs] ≈ 15 pM

Moreover, we evaluated the biocompatibility of these FONs by checking their cytotoxic activity by MTT assay after 24h and 48h of incubation. As displayed in **Figure VI 16** these FONs proved to be non-toxic even after 48h of incubation. This property in addition with the high brightness observed in biological media make these nanoobjects good candidate for applications as potential biomedical probes.

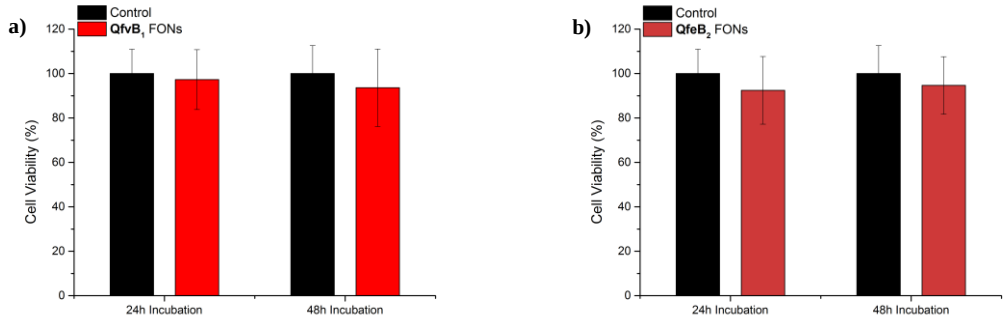

Figure VI 16. Viability of COS 7 cells after 24h and 48h of incubation with FONs prepared with a) **QfvB$_1$** and b) **QfeB$_2$**

7. Conclusions

In this chapter were discussed the optical properties of new red-emitting quadrupolar dyes in both molecular solution and nanocolloidal suspension. The tuning of the photophysical properties was obtained by playing on the length and rigidity of the π connector between the two donor end-groups and the benzothiadiazole acceptor core, as well as by increasing the electron-withdrawing character of the core adding a second BTDA moiety.

The comparison between the photophysical properties measured in solution and nanoparticles suggest that upon nanoconfinement the arrangement of the molecules induces a general hyperchromic effect of both molar extinction coefficient and two-photon cross section, indicating an excitonic coupling behavior.

Thanks to the large brightness upon both one and two-photon absorption, and the emission in the biological transparency window of these nanoparticles it was possible to use them in bioenvironment as fluorescent probes, where they showed low cytotoxic activity.

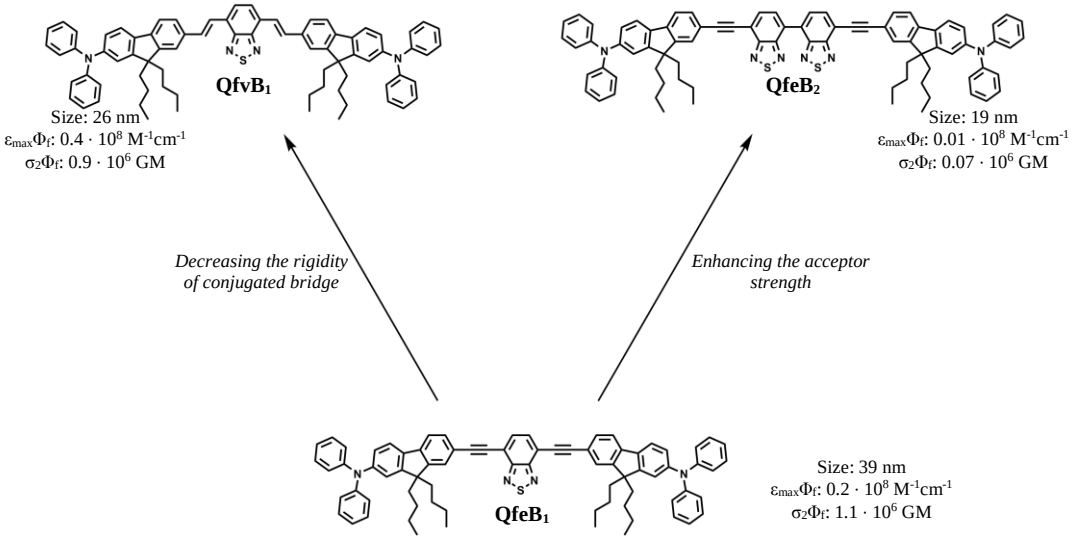

Figure VI 17. Resuming flowchart of some chromophores, described in this chapter, in FONs in water

BIBLIOGRAPHIC REFERENCES

(1) Terenziani, F.; Katan, C.; Badaeva, E.; Tretiak, S.; Blanchard‐Desce, M. Enhanced two‐photon absorption of organic chromophores: theoretical and experimental assessments. *Advanced Materials* **2008**, *20*, 4641-4678.

(2) Pawlicki, M.; Collins, H. A.; Denning, R. G.; Anderson, H. L. Two‐photon absorption and the design of two‐photon dyes. *Angewandte Chemie International Edition* **2009**, *48*, 3244-3266.

(3) Collini, E.; Carlotto, S.; Ferrante, C.; Bozio, R.; Polimeno, A.; Bloino, J.; Barone, V.; Ronchi, E.; Beverina, L.; Pagani, G. A. Multipolar symmetric squaraines with large two- photon absorption cross-sections in the NIR region. *Physical Chemistry Chemical Physics* **2011**, *13*, 12087-12094.

(4) Kim, O.-K.; Lee, K.-S.; Woo, H.; Kim, K.-S.; He, G. S.; Swiatkiewicz, J.; Prasad, P. N. New class of two-photon-absorbing chromophores based on dithienothiophene. *Chemistry of Materials* **2000**, *12*, 284-286.

(5) Reinhardt, B. A.; Brott, L. L.; Clarson, S. J.; Dillard, A. G.; Bhatt, J. C.; Kannan, R.; Yuan, L.; He, G. S.; Prasad, P. N. Highly active two-photon dyes: design, synthesis, and characterization toward application. *Chemistry of Materials* **1998**, *10*, 18631874.

(6) He, G. S.; Reinhardt, B. A.; Bhatt, J. C.; Dillard, A. G.; Xu, G. C.; Prasad, P. N. Two-photon absorption and optical-limiting properties of novel organic compounds. *Optics Letters* **1995**, *20*, 435.

(7) Rouxel, C.; Charlot, M.; Mir, Y.; Frochot, C.; Mongin, O.; Blanchard-Desce, M. Banana-shaped biphotonic quadrupolar chromophores : from fluorophores to biphotonic photosensitizers. *New Journal of Chemistry* **2011**, *35*, 1771-1780.

(8) Mongin, O.; Porrès, L.; Charlot, M.; Katan, C.; Blanchard-Desce, M. Synthesis, fluorescence, and two-photon absorption of a series of elongated rodlike and banana-shaped quadrupolar fluorophores: a comprehensive study of structure-property relationships. *Chemistry* **2007**, *13*, 1481-1498.

(9) Charlot, M.; Izard, N.; Mongin, O.; Riehl, D.; Blanchard-Desce, M. Optical limiting with soluble two-photon absorbing quadrupoles: Structure–property relationships. *Chemical Physics Letters* **2006**, *417*, 297-302.

(10) Werts, M. H. V.; Gmouh, S.; Mongin, O.; Pons, T.; Blanchard-Desce, M. Strong modulation of two-photon excited fluorescence of quadripolar dyes by (de)protonation. *Journal of the American Chemical Society* **2004**, *126*, 16294-16295.

(11) Blanchard-Desce, M. Molecular engineering of NLO-phores for new NLO microscopies. *Comptes Rendus Physique* **2002**, *3*, 439-448.

(12) Ventelon, L.; Moreaux, L.; Mertz, J.; Blanchard-Desce, M. Optimization of quadrupolar chromophores for molecular two-photon absorption. *Synthetic Metals* **2002**, *127*, 17-21.

(13) Barzoukas, M.; Blanchard-Desce, M. Molecular engineering of push–pull dipolar and quadrupolar molecules for two-photon absorption: A multivalence-bond states approach. *The Journal of Chemical Physics* **2000**, *113*, 3951.

(14) Ventelon, L.; Blanchard-Desce, M.; Moreaux, L.; Mertz, J. New quadrupolar fluorophores with high two-photon excited fluorescence. *Chemical Communications* **1999**, 2055-2056.

(15) Beverina, L.; Salice, P. Squaraine compounds: tailored design and synthesis towards a variety of material science applications. *European Journal of Organic Chemistry* **2010**, *2010*, 1207-1225.

(16) Albota, M.; Beljonne, D.; Brédas, J. L.; Ehrlich, J. E.; Fu, J. Y.; Heikal, A. A.; Hess, S. E.; Kogej, T.; Levin, M. D.; Marder, S. R.; McCord-Maughon, D.; Perry, J. W.; Röckel, H.; Rumi, M.; Subramaniam, G.; Webb, W. W.; Wu, X. L.; Xu, C. Design of organic molecules with large two-photon absorption cross sections. *Science* **1998**, *281*, 1653-1656.

(17) Zhang, Y.; Kim, B.; Yao, S.; Bondar, M. V.; Belfield, K. D. Controlled Aggregation and enhanced two-photon absorption of a water-soluble squaraine dye with a poly(acrylic acid) template. *Langmuir* **2013**, *29*, 11005-11012.

(18) Yao, S.; Belfield, K. D. Two‐photon fluorescent probes for bioimaging. *European Journal of Organic Chemistry* **2012**, *2012*, 3199-3217.

(19) Daniel, J.; Godin, A. G.; Palayret, M.; Lounis, B.; Cognet, L.; Blanchard-Desce, M. Innovative molecular-based fluorescent nanoparticles for multicolor single particle tracking in cells. *Journal of Physics D: Applied Physics* **2016**, *49*, 84002.

(20) Li, H.; Daniel, J.; Verlhac, J. B.; Blanchard‐Desce, M.; Sojic, N. Bright electrogenerated chemiluminescence of a bis‐donor quadrupolar spirofluorene dye and its nanoparticles. *Chemistry - A European Journal* **2016**, *22*, 12702-12714.

(21) Daniel, J. Nano outils moléculaires biphotoniques pour le vivant. Université de Bordeaux, 2015.

(22) Kelley, A.; Shoute, L. C. T.; Blanchard-Desce, M.; Bartholomew, G. P.; Bazan, G. C. Resonance raman, hyper-raman, and hyper-rayleigh depolarization ratios and symmetry breaking in solution. *Molecular Physics* **2006**, *104*, 1239-1247.

(23) Terenziani, F.; Painelli, A.; Katan, C.; Charlot, M.; Blanchard-Desce, M. Charge instability in quadrupolar chromophores: symmetry breaking and solvatochromism. *Journal of the American Chemical Society* **2006**, *128*, 15742-15755.

(24) Carlotti, B.; Benassi, E.; Spalletti, A.; Fortuna, C. G.; Elisei, F.; Barone, V. Photoinduced symmetry-breaking intramolecular charge transfer in a quadrupolar pyridinium derivative. *Physical Chemistry Chemical Physics* **2014**, *16*, 13984-13994.

(25) Carlotti, B.; Benassi, E.; Fortuna, C. G.; Barone, V.; Spalletti, A.; Elisei, F. Efficient excited ‐ state symmetry breaking in a cationic quadrupolar system bearing diphenylamino donors. *ChemPhysChem* **2016**, *17*, 136-146.

(26) Dereka, B.; Rosspeintner, A.; Krzeszewski, M.; Gryko, D. T.; Vauthey, E. Symmetry-breaking charge transfer and hydrogen bonding: toward asymmetrical photochemistry. *Angewandte Chemie International Edition* **2016**, *55*, 15624-15628.

(27) Dozova, N.; Ventelon, L.; Clermont, G.; Blanchard-Desce, M.; Plaza, P. Excited-state symmetry breaking of linear quadrupolar chromophores: A transient absorption study. *Chemical Physics Letters* **2016**, *664*, 56-62.

(28) Makarov, N. S.; Drobizhev, M.; Rebane, A. Two-photon absorption standards in the 550-1600 nm excitation wavelength range. *Optics Express* **2008**, *16*, 4029.

(29) Würthner, F.; Kaiser, T. E.; Saha-Möller, C. R. J-aggregates: from serendipitous discovery to supra- molecular engineering of functional dye materials. *Angewandte Chemie International Edition* **2011**, *50*.

CHAPTER 7

GENERAL CONCLUSION

CHAPTER 7–GENERAL CONCLUSION

This manuscript can be inserted in the wide topic, very active nowadays, towards the achievement of new bright probes suitable for imaging in biological media. I focused my work in the design,the synthesis and the photophysical studies of new chromophores for the further preparation of full organic fluorescent organic nanoparticles (FONs). The work presented in this Thesis show four different classes of new chromophores with tunable photophysical properties, specifically with tunable emission that cover the visible range towards NIR region: neutral dipoles (**Chapter II** and **III**), charged dipoles (**Chapter IV**), articulated dipoles (**Chapter V**) and quadrupoles (**Chapter VI**).

I demonstrate that a careful molecular design leads to chromophores with expected properties, preventing strong molecular interaction, deleterious for the emissive properties, and improving the colloidal and structural stability of the nanoobjects prepared. Moreover, was displayed an additional/cooperative effect of the chromophores upon nano-confinement, leading to large molar extinction coefficients as well as large two-photon cross section of FONs.

Comparing these nanoparticles with the commercially available chromophores[1] or nanoobjects[2,3] it can be noticed that the prepared FONs display at least one order of magnitude higher brightness (one-photon brightness: QDs $\approx 10^5$ M^{-1} cm^{-1}; Carbon Nanodots $\approx 10^3$ M^{-1} cm^{-1}; Nanodiamonds $\approx 10^7$ M^{-1} cm^{-1}; Alexa 647 $\approx 10^5$ M^{-1} cm^{-1}; two-photon brightness: QDs $\approx 10^4$ GM).

The final purpose is to use these systems in biological environment for either one-photon or two-photon microscopy. Since some of the FONs display large one- and two-photon brightness associated with an emission in the red/NIR region, which falls in the biological transparency window, it is possible to use these nanoparticles in bioimaging using COS7 cells as bio-environment. The nice results obtained open new perspective for future works such as the functionalization of these nanoobjects in order to target specifically some organelles of the cells for theranostic purposes.

Concluding I will not say that one class of studied FONs is better than the others in terms of properties, thus this following flowchart would be an overview of the most promising nanoparticles for biological applications.

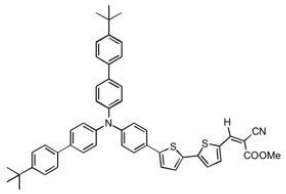

D3'c

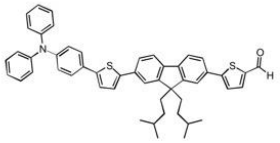

D1'''a

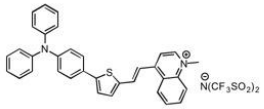

DIq$^+$

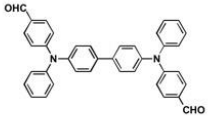

1Bis(BP)

2Bis(BP)

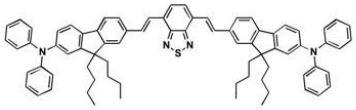

QfvB$_1$

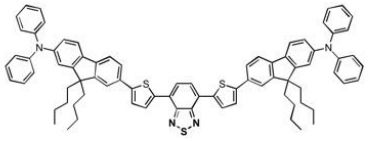

QftB$_1$

Cpd	d_{TEM} [nm]	ζ-potential [mV]	λ_{max}^{1PA} [nm]	λ_{max}^{em} [nm]	Φ_f	$\varepsilon_{max}\Phi_f$ a) [$10^8 M^{-1} cm^{-1}$]	λ_{max}^{2PA} [nm]	$\sigma_2\Phi_f$ a) [10^6 GM]
D3'c	32	-73	499	702	0.04	0.1	1050	0.2
D1'''a	34	-73	409	557	0.035	0.3	730	0.4
DIq$^+$	82	+54	553	830	0.002	0.22	-	-
1Bis(BP)	55	-66	370	511	0.10	6.1	750	2.6
2Bis(BP)	42	-65	444	643	0.03	0.9	900	0.6
QfvB$_1$	26	-64	505	650	0.09	0.4	890	0.9
QftB$_1$	57	-70	534	690	0.08	1.9	890	9.3

a) One-photon and two-photon brightness are considered taking into account the concentration of FONs

(1) Johnson, I.; Spence, M. T. Z.: *The Molecular Probes Handbook*; 11th ed.; Life Technologies, 2010.

(2) Reineck, P.; Francis, A.; Orth, A.; Lau, D.; Nixon‐Luke, R.; Rastogi, I.; Razali, W.; Cordina, N.; Parker, L.; Sreenivasan, V.; Brown, L.; Gibson, B. Brightness and Photostability of Emerging Red and Near‐IR Fluorescent Nanomaterials for Bioimaging. *Advanced Optical Materials* **2016**, *4*, 1549-1557.

(3) Larson, D. R.; Zipfel, W. R.; Williams, R. M.; Clark, S. W.; Bruchez, M. P.; Wise, F. W.; Webb, W. W. Water-Soluble Quantum Dots for Multiphoton Fluorescence Imaging in Vivo. *Science* **2003**, *300*, 1434-1436.

ABBREVIATIONS

- AFM = atomic force microscopy
- BTDA = benzothiadiazole
- CHO = aldehyde
- DAPI = 4',6'-diethylamidino-2-phenylindole
- DETB = 1,3-Diethyl-2-thiobarbiturate
- FONs = fluorescent organic nanoparticles
- FWHM = full width at half maximum
- IC = internal conversion
- ICT = intramolecular charge transfer
- ISC = intersystem crossing
- NIR = near infrared
- NLO = non-linear optics
- ONPs = organic nanoparticles
- TEM = transmission electron microscopy
- TPEF = two-photon excited fluorescence
- 2PA = two-photon absorption
- 2PM = two-photon microscopy

TARGET MOLECULES

Chapter 2-3

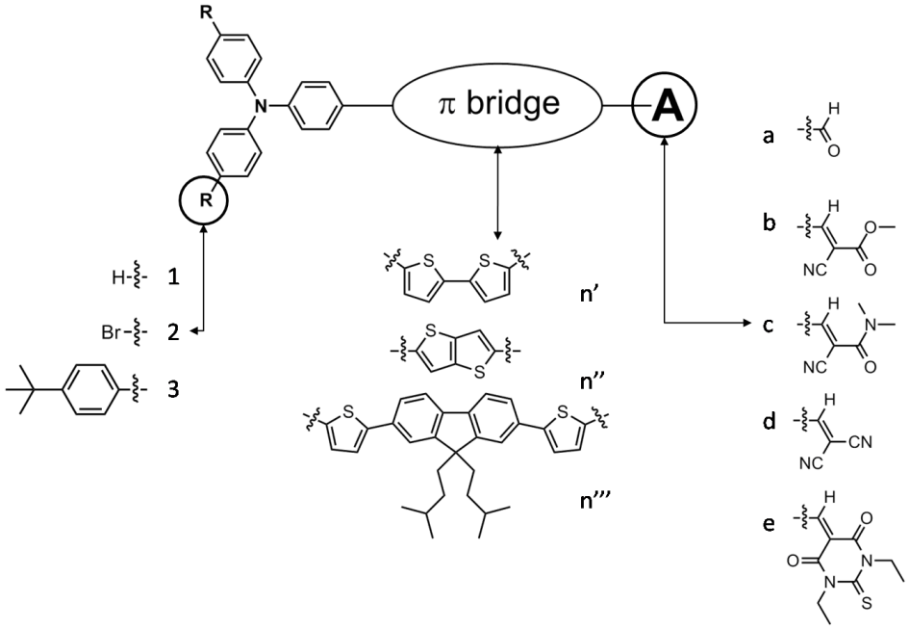

Chapter 4

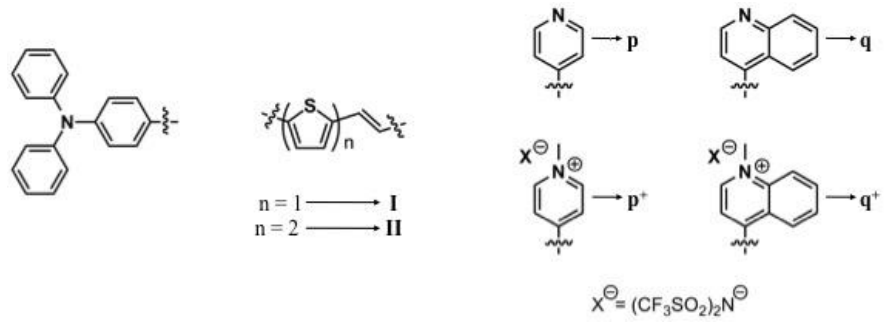

Chapter 5

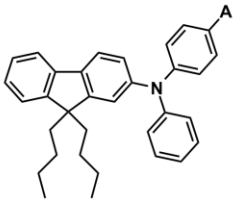

1Mono: A = CHO

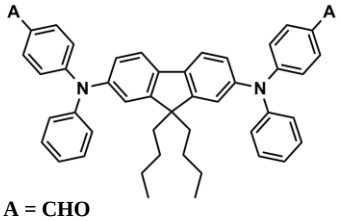

1Bis(F): A = CHO
2Bis(F): A = CH=C(CN)$_2$

1Bis(BP): A = CHO
2Bis(BP): A = CH=C(CN)$_2$

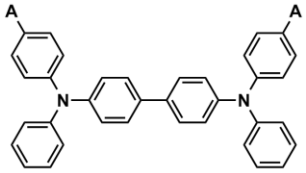

1Tris: A = CHO

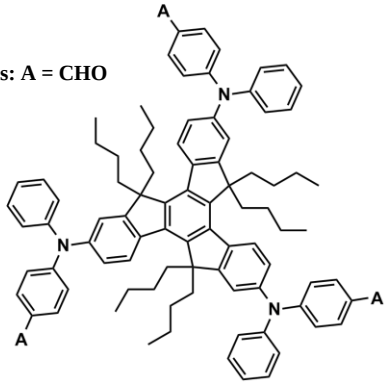

Chapter 6

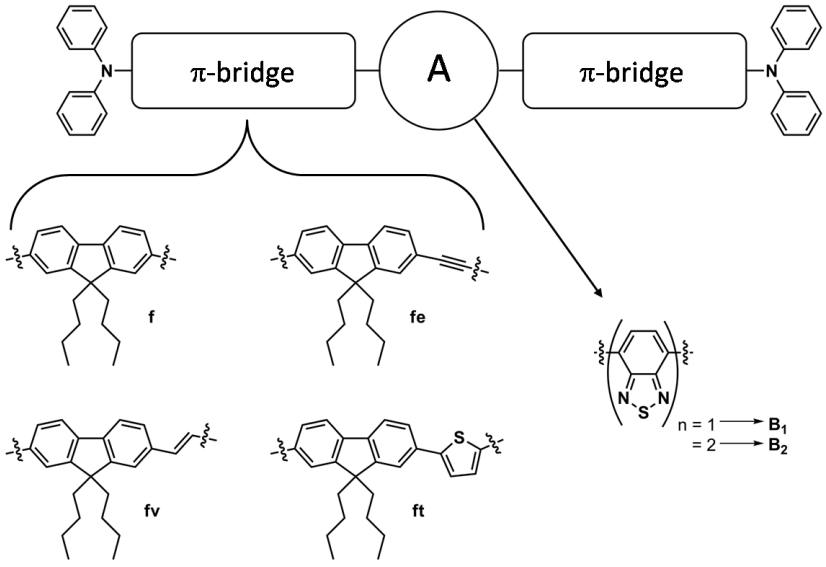

EXPERIMENTAL PART

EXPERIMENTAL PART

1. Materials and methods

1.1. Synthesis

Commercially available reagent (purchased from Aldrich, Alfa Aesar and TCI) were used without further purification. Dry solvents were distilled from the appropriate drying reagents immediately before use. Compounds already described in the literature were characterized by ^{1}H NMR spectra and melting points and compared to reported data. All air- or water-sensitive reactions were carried out under argon. Column chromatography was performed using Fluka silica gel Si 60 (40-63 µm, 230-400 mesh).

1.2. Chemical characterization

Melting points were determined in a STUART SMP 10 digital melting point instrument. Infrared spectra were measured on a Perkin Elmer Spectrum 100 Optica. ^{1}H and ^{13}C NMR spectra were recorded on a Bruker Advance III 200 (400) spectrometer at 200 (400) MHz and 50 (100) MHz respectively. Mass spectra were performed by the CESAMO (Bordeaux, France). X-ray diffraction measurements on single crystals **D1'b**, **D1'c** and **D2'b** were performed on a Bruker APEX II diffractometer at CESAMO platform (Bordeaux, France), while measurement on single crystals **1D'''a**, **1Bis(F)**, **2Bis(F)**, **1Tris**, **QfvB$_1$** and **QfeB$_1$** were performed on a FR-X Rigaku diffractometer at IECB (Bordeaux, France). The structures were solved with SHELXS97 and refined by a full-matrix least-squares method on F^2 using SHELXL-97[1]. All non-hydrogen atoms were refined with anisotropic displacement parameters. Hydrogen atoms were placed at calculated positions using suitable riding models. Their positions were constrained relative to their parent atom using the appropriate HFIX command in SHELXL-97. Additional disordered solvent molecules were found in the lattice of **1D'c** (THF) and **QfvB$_1$** (DCM), unfortunately they could not be refined and thus the SQUEEZE command was applied.

1.3. Nanoparticles characterization

TEM was carried out using a HITACHI H7650. The copper grid coated with a carbon membrane was pretreated using the Glow discharge technique to yield positively charged hydrophilic carbon surface to allow stronger interaction between the sample and the grid itself and thus easier imaging. One droplet of the dilute aqueous suspension was deposited on the grid and the excess liquid was dried off with a paper. A staining procedure using uranyl acetate was then used to enhance the contrast. AFM analysis, 20 µl of suspension of FONs was deposited onto freshly cleaved mica disks and left to dry at room temperature. A Bruker's Dimension Icon®, Atomic Force Microscope operated in peak force mode, available at SIV-ISM (Bordeaux) was used. ScanAsyst-Air (Bruker) probes were employed, with a set point of 500 pN and the scan rate 0.250 Hz. The images were processed with NanoScope Analysis 1.5 program. Zeta-potential analysis was performed with the same instrument, 20 measurements were realized for each sample according to a predefined operating procedure. The global concentration of the dye in the FONs suspension was determined by taking an aliquot of the suspension, which was further lyophilized then dissolved in the same volume of $CHCl_3$. The concentration was then derived from the absorbance and the value of the molar extinction coefficient in $CHCl_3$ by using the Lambert-Beer law.

1.4. Photophysical characterization

All photophysical studies have been performed with freshly prepared air-equilibrated solutions at room temperature (298 K). UV/Vis absorption spectra were recorded on a Jasco V-670 spectrophotometer. Steady-state measurements were carried out on a Fluoromax-4 spectrofluorometer and time resolved fluorescence measurements were carried out on a Fluorolog spectrofluorometer. The emission spectra were corrected for the wavelength-sensitivity of the detection unit, and they were obtained under excitation at the wavelength of the absorption maximum. Fluorescence quantum yields of dilute dye solutions and of the FONs suspensions were measured according to literature procedures[2,3] using DCM (Φ = 0.437 in EtOH, λ_{exc} = 443 nm), Nile Blue (Φ = 0.27 in EtOH, λ_{exc} =

200-610 nm range), Cresyl Violet (Φ = 0.54 in MeOH, λ_{exc} = 570 nm), Indocyanine Green (Φ = 0.11 in DMSO λ_{exc} = 678 nm), Rhodamine-6G (Φ = 0.94 in EtOH, λ_{exc} = 488 nm) or Fluorescein in NaOH 0.1 M (Φ = 0.9 in NaOH 0.1 M, λ_{exc} = 474 nm) depending on the emission range[4]. The reported fluorescence quantum yield values obtained via this method are within ± 0.005. In Eq. 1 is displayed the equation used to calculate the Φ_f of the sample taking into account the refraction index *n*, the absorbance *A* and the integral of the emission *I*.

Eq 1. $$\Phi_{fs} = \Phi_{fr} \cdot \frac{n_s^2}{n_r^2} \cdot \frac{1-10^{-A_r^{\lambda exc}}}{1-10^{-A_s^{\lambda exc}}} \cdot \frac{\int_0^\infty I_{fs}\,(\lambda_{exc},\ \lambda_f)\ d\lambda_f}{\int_0^\infty I_{fr}\,(\lambda_{exc},\ \lambda_f)\ d\lambda_f}$$

Fluorescence decays were measured in a time-correlated single photon counting (TCSPC) configuration, under excitation from a NanoLED (370 nm, 455 nm or 570 nm). The instrument response was determined by measuring the light scattered by a Ludox® suspension. The lifetime values were obtained from the deconvolution fit analysis of the decays profiles; the quality of the fits was judged by the reduced χ^2 value ($0.9 < \chi^2 < 1.1$). The reported lifetimes are within ± 0.1 ns.

Anisotropy measurements were carried out on a Fluorolog spectrofluorometer using triacetin at 20°C (293.15 K) or on a Fluoromax-3 using 2-MeTHF at -203.15°C (70 K)

Two-photon absorption cross sections (σ_2) were determined from the two-photon excited fluorescence (TPEF) cross sections ($\sigma_2\Phi$) and the fluorescence quantum yield (Φ). TPEF cross sections were measured relative to Fluorescein in 0.01 M aqueous NaOH in the 680-1000 nm spectral range and relative to Nile Red in DMSO in the 1000-1160 nm spectral range, using the method described by Xu and Webb[5] and the appropriate solvent-related refractive index corrections. The quadratic dependence of the fluorescence intensity on the excitation power was checked at all wavelengths. Measurements were conducted using an excitation source delivering fs pulses. This allows avoiding excited-state absorption during the pulse duration, a phenomenon, which has been shown to lead to overestimated two-photon absorption cross-section values. To scan the 680-1080 nm range, a Nd:YVO4-pumped Ti:Sapphire oscillator was used generating 140 fs pulses at a 80 MHz rate.

To span the 1000–1200 nm range, an OPO (PP-BBO) was added to the setup to collect and modulate the output signal of the Ti:Sapphire oscillator. The excitation was focused into the cuvette through a microscope objective (10X, NA 0.25). The fluorescence was detected in epifluorescence mode via a dichroic mirror (Chroma 675dcxru) and a barrier filter (Chroma e650sp-2p) by a compact CCD spectrometer module BWTek BTC112E. Total fluorescence intensities were obtained by integrating the corrected emission. The experimental uncertainty of the absorption cross-section values determined from this method has been estimated to be ±10%.

1.5. Cellular imaging and cytotoxicity

For the fluorescence imaging experiments, COS 7 cells were cultured on glass disks, using DMEM supplemented with 10% Fetal Calf Serum, as culture medium. When the cells reached 30% confluence, the FONs were added to the culture medium at a final concentration of dye of 1 µM (equivalent to a nM concentration of nanoparticles). After 8h of incubation, the cells were abundantly washed with PBS, fixed with 4% para-formaldehyde and mounted using a Fluoromount™ media (Sigma). The fluorescence imaging was performed at Bordeaux Imaging Center using a Leica DM6000 confocal microscope. For the co-localization experiments, the cells were incubated simultaneously with both FONs, at equimolar concentration (final concentration in chromophore of 1µM).

For the toxicity test, cells were pleated in 96 wells culture plate and grown in DMEM culture medium until approximately 80% confluence. At this point, the culture medium was replaced by a new one, enriched with FONs at a final concentration of dye of 1µM. The cytotoxicity was determined after 24h of incubation with the FONs by MTT assay based on the conversion of tetrazolium salt (MTT) into a purple formazan product, using the iMark™ microplate reader (BioRAD).

2. Synthesis

2.1. Synthesis of chromophores D1'a-d, D2'a-d and D3'a,c-d

The synthesis of the chromophore **D1'a** was carried out optimizing a literature reported procedure[6], while chromophores **D2'a** and **D3'a** were prepared according to an earlier described pathway[7].

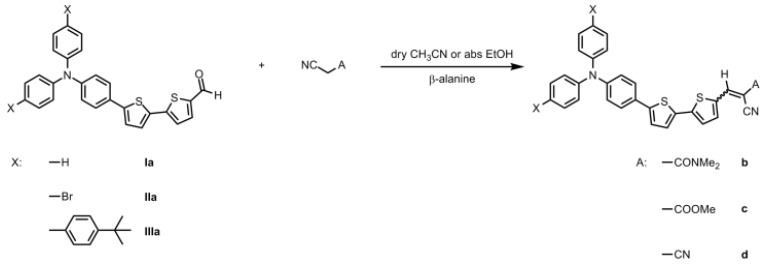

Scheme ExpPart 1. General reaction followed for the synthesis of chromophores **D1'a-d**, **D2'a-d** and **D3'a,c-d**

General method of Knoevenagel condensation

α-acid derivatives (1.25 eq.), the corresponding aldehyde (1 eq.) and β-alanine (catalytic amount) were dissolved under Ar in absolute EtOH (or dry CH_3CN for **D1-3'c** compounds) and refluxed overnight. The reaction mixture was cooled down to RT and the solid was filtrated over Buchner and dried under vacuum to yield the corresponding product.

2-cyano-3-[5'-[4-(diphenylamino)phenyl][2,2'-bithiophen]-5-yl]-*N,N'*-dimethylacrylamide (D1'b): Following the general procedure using **D1'a** as aldehyde and *N,N'*-dimethylcyanoacetamide as α-acid derivatives to yield compound **D1'b** as a bright red solid (yield = 62%).

Monocrystals suitable for X-ray diffraction were obtained by slow evaporation of a toluene solution.

Melting Point: degradation over 125°C

^{1}H NMR (200 MHz, DMSO-d6): 8.03 (s, 1H,); 7.77 (d, J = 4Hz, 1H); 7.62–7.49 (m, 5H); 7.46 (d, J = 4Hz, 1H); 7.37–7.29 (m, 4H); 7.12–7.04 (m, 6H); 6.93 (d, J = 8Hz, 2H); 3.02 (br, 6H) ppm.

^{13}C NMR ($CDCl_3$, 50 MHz) 164.0, 148.0, 147.3, 146.1, 145.7, 145.2, 137.6, 134.5, 134.1, 129.4, 127.2, 127.1, 126.6, 124.8, 123.6, 123.5, 123.3, 123.2, 116.8, 100.5, 38.1, 35.5 ppm.

FTIR (ATR): ν (CH_{arom}/HC=C) 3070 cm^{-1}; ν ($N(CH_3)_2$) 2917 cm^{-1}; ν (C≡N) 2198 cm^{-1}; ν (C=O) 1637 cm^{-1}.

HRMS (m/z) [M]calcd for $C_{32}H_{25}N_3OS_2$: 531.14390, found: 531.14600.

Methyl-2-cyano-3-[5'-[4-(diphenylamino)phenyl][2,2'-bithiophen]-5-yl]acryate (D1'c): Following the general procedure using **D1'a** as aldehyde and methylcyanoacetate as α-acid derivatives to yield compound **D1'c** as a bright red solid (yield = 80%).

Monocrystals suitable for X-ray diffraction were obtained by slow evaporation of a THF solution.

Melting Point: degradation over 178°C.

^{1}H NMR (200 MHz, DMSO-*d6*) 8.55 (s, 1H); 8.03 (d, J = 4Hz, 1H); 7.64–7.58 (m, 4H); 7.48 (d, J = 4Hz, 1H); 7.37–7.29 (m, 4H); 7.09–7.04 (m, 6H); 6.97 (d, J = 8Hz, 2H); 3.82 (s, 3H) ppm.

^{13}C NMR ($CDCl_3$, 50 MHz) 163.6, 148.2, 148.1, 147.2, 146.9, 146.4, 139.5, 133.8, 133.7, 129.4, 127.7, 126.9, 126.6, 124.9, 124.0, 123.6, 123.4, 123.0, 116.2, 96.7, 53.2 ppm.

FTIR (ATR): ν (CH_{arom}/HC=C) 3080 cm^{-1}; ν ($O(CH_3)$) 2950 cm^{-1}; ν (C≡N) 2210 cm^{-1}; ν (C=O) 1724 cm^{-1}.

HRMS (m/z) [M]calcd for $C_{31}H_{22}N_2O_2S_2$: 518.11227, found: 518.11021.

2-[[5'- [4-(diphenylamino)phenyl] [2,2'-bithiophen] -5-yl] methylene] malononitrile (D1'd): Following the general procedure using **D1'a** as aldehyde and malononitrile as α-acid derivatives to yield compound **D1'd** as a dark red solid (yield = 39%).

Melting Point: 183°C

^{1}H NMR (200 MHz, DMSO-*d6*) 8.61 (s, 1H); 7.90 (d, J = 4Hz, 1H); 7.69 (d, J = 8Hz, 2H); 7.65 (d, J = 8Hz, 2H); 7.51 (d, J = 4Hz, 1H); 7.37–7.30 (m, 4H); 7.13–7.04 (m, 6H); 6.97 (d, J = 8Hz, 2H) ppm.

3-[5'-(4-(bis(4-bromophenyl)amino)phenyl)2,2'-bithiophen-5-yl]-2-cyano-*N,N'*-dimethylacrylamide (D2'b): Following the general procedure using **D2'a** as aldehyde and *N,N'*-dimethylcyanoacetamide as α-acid derivatives to yield compound **D2'b** as a bright red microcrystals (yield = 88%).

Monocrystals suitable for X-ray diffraction were obtained by slow evaporation of a CH_2Cl_2 solution.

Melting Point: 148°C.

^{1}H NMR (200 MHz, DMSO-d6) 8.04 (s, 1H); 7.78 (d, J = 4Hz, 1H); 7.64 (d, J = 8Hz, 2H); 7.57–7.46 (m, 7H); 7.05–6.97 (m, 6H); 3.02 (br, 6H) ppm.

FTIR (ATR): ν (CH_{arom}/HC=C) 3065 cm^{-1}; ν ($N(CH_3)_2$) 2964 cm^{-1}; ν (C≡N) 2198 cm^{-1}; ν (C=O) 1634 cm^{-1}.

HRMS (m/z) [M]calcd for $C_{32}H_{23}Br_2N_3OS_2$: 686.96493, found: 686.96550.

Methyl-3-[5'-[4-bis(4-bromophenyl)amino)phenyl)-2,2'-bithiophen-5-yl]-2-cyanoacryate (D2'c): Following the general procedure using **D2'a** as aldehyde and methylcyanoacetate as α-acid derivatives to yield compound **D2'c** as bright red solid (yield = 81%).

Melting Point: 226°C.

^{1}H NMR (200 MHz, DMSO-*d6*) 8.55 (s, 1H); 8.03 (d, J = 4Hz, 1H); 7.68–7.59 (m, 4H); 7.54–7.46 (m, 5H); 7.05–6.98 (m, 6H); 3.82 (s, 3H) ppm.

^{13}C NMR (75 MHz, $CDCl_3$) 147.84, 147.07, 146.49, 145.95, 134.18, 133.97, 132.58, 128.14, 127.69, 126.87, 126.00, 124.09, 123.80, 116.30, 116.18, 53.23.

FTIR (ATR): ν (CH_{arom}/HC=C) 3025 cm^{-1}; ν ($O(CH_3)$) 2948 cm^{-1}; ν (C≡N) 2214 cm^{-1}; ν (C=O) 1721 cm^{-1}.

HRMS (m/z) [M] calcd for $C_{31}H_{20}Br_2N_2O_2S_2$: 673.93329, found: 673.93211.

2-[[5'-(4-(bis(4-bromophenyl)amino)phenyl)-2,2'-bithiophen)-5-yl]methylene]malononitrile (D2'd): Following the general procedure using **D2'a** as aldehyde and malononitrile as α-acid derivatives to yield compound **D2'd** as a deep purple solid (yield = 96%).

Melting Point: 224°C.

^{1}H NMR (200 MHz, DMSO-*d6*) 8.61 (s, 1H); 7.89 (d, J = 4Hz, 1H); 7.70–7.63 (m, 4H); 7.55–7.46 (m, 5H); 7.04–6.98 (m, 6H) ppm.

^{13}C NMR ($CDCl_3$, 50 MHz) 150.1, 149.5, 147.3, 147.2, 145.9, 140.3, 133.6, 133.2, 132.6, 128.5, 127.8, 126.9, 126.1, 124.2, 123.9, 123.6, 116.4, 114.4, 113.5, 75.7 ppm.

FTIR (ATR): ν (CH_{arom}/HC=C) 3021 cm^{-1}; ν (C≡N) 2210 cm^{-1}.

HRMS (m/z) [M] calcd for $C_{30}H_{17}Br_2N_3S_2$: 640.92306, found: 640.91988.

Methyl-3-[5'-(4-(bis-(4'-*tert*-butylbiphenil-4-yl)amino)phenyl)-2,2'-bithiophen-5-yl]-2-cyanoacryate (D3'c): Following the general procedure using **D3'a** as aldehyde and methylcyanoacetate as α-acid derivatives to yield compound **D3'c** as dark red solid (yield = 78%).

^{1}H NMR (300 MHz, $(CD_3)_2CO$-*d6*): 8.46 (s, 1H); 7.98 (d, J = 3.9 Hz, 1H); 7.72–7.60 (m, 11H); 7.55–7.49 (m, 6H); 7.24 (d, J = 8.3 Hz, 4H); 7.18 (d, J = 8.4 Hz, 2H); 2.80 (s, 3H); 1,36 (s, 18H).

^{13}C NMR (75 MHz, $CDCl_3$) 163.61, 150.04, 146.11, 137.61, 136.15, 133.84, 133.80, 127.89, 127.76, 127.23, 126.71, 126.40, 125.75, 124.88, 124.01, 123.48, 34.55, 31.39.

FTIR (ATR): ν (CH_{arom}/HC=C) 3085 cm^{-1}; ν ($O(CH_3)$) 2948 cm^{-1}; ν (C≡N) 2210 cm^{-1}; ν (C=O) 1724 cm^{-1}.

HRMS (m/z) [M] calcd for $C_{51}H_{46}N_2O_2S_2$: 782.30007, found: 782.29934.

2-[[5'-(4-(bis-(4'-*tert*-butylbiphenil-4-yl)amino)phenyl)-2,2'-bithiophen)-5-yl] methylene] malononitrile (D3'd): Following the general procedure using **D3'a** as aldehyde and methylcyanoacetate as α-acid derivatives to yield compound **D3'd** as dark grey (yield = 83%).

Melting Point: 205°C.

^{1}H NMR (400 MHz, $CDCl_3$): 7.74 (s, 1H), 7.62 (d, J = 4 Hz, 1H), 7.49–7.54 (m, 10H), 7.46 (d, J = 8.3 Hz, 4H), 7.40 (d, J = 4 Hz, 1H), 7.26 (d, J = 4 Hz, 1H), 7.23 (d, J = 4 Hz, 1H), 7.22 (d, J = 8.3 Hz, 4H), 7.16 (d, J = 8.3 Hz, 2H), 1.36 (s, 18H) ppm.

^{13}C NMR ($CDCl_3$, 100 MHz) 150.3, 150.2, 149.9, 148.4, 148.0, 146.2, 140.4, 137.7, 136.7, 136.5, 133.3, 133.2, 128.7, 128.1, 127.1, 127.0, 126.6, 125.9, 125.2, 124.2, 123.9, 123.6, 114.6, 113.8, 34.7, 31.6 ppm.

FTIR (ATR): ν (CH_{arom}/HC=C) 3025 cm^{-1}, ν (C≡N) 2220 cm^{-1}.

HRMS (m/z) [M] calcd for $C_{50}H_{43}N_3S_2$: 749.28984, found: 749.28866.

2.2. Synthesis of chromophore D1‴a

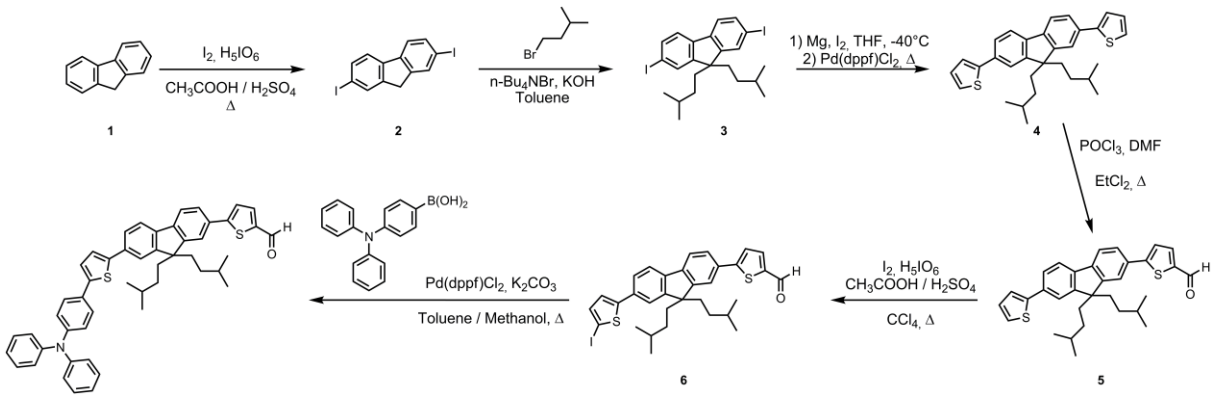

Scheme ExpPart 2. Multistep synthetic route follone to synthesize chromophore **D1‴a**

<u>2,7–diiodo 9H fluorene (2)</u>: Fluorene (**1**) (0.12 mol, 1 eq.), 100 mL of acetic acid, 2.8 mL of sulfuric acid and 7 mL of distilled water, were added in a round bottom flask and the temperature was increased to 75°C under stirring. After the dissolution of fluorene, at the reaction mixture were added iodine (0.063 mol, 1 eq.) and periodic acid (0.031 mol, 0.52 eq.) and the reaction was stirred for 1h. When the time was over another amount of iodine (0.063 mol, 1 eq.) and periodic acid (0.031 mol, 0.52 eq.) were added to the reaction mixture with 100 mL of acetic acid, and the reaction was kept at 75°C under stirring. After the 2nd hour of reaction, the temperature was slowly cooled to RT and filtered over Buchner. The solid was mixed with dichloromethane and a saturated solution of NaS_2O_3

in an Erlenmeyer flask and was stirred for 1h neutralizing the I_2 in excess. The mixture was filtered and the solid washed with dichloromethane and dried at 85°C overnight. A brown solid was obtained (yield = 63%).

Melting Point = 152°C;

^{1}H-NMR (300 MHz, $CDCl_3$): 7.89 (s, 1H); 7.72 (d, 1H, J = 8Hz); 7.51 (d, 1H, J = 8Hz); 3.86 (s, 1H) ppm.

2,7–diiodo–9,9–diisopentyl 9H fluorene (3): In a solution of KOH (0.189 mol in 15 mL of water) was added n-Bu_4NBr (3.75 mmol, 0.2eq.) and the mixture was stirred at RT for 15 minute. When the time was over, at the reaction mixture were added **2** (19.3 mmol, 1 eq.), 1-bromo-3-methylbutane (115 mmol, 6 eq.) and 20 mL of toluene. The mixture was stirred at 65°C for 2h, then it was cooled down to RT and left reacts for 24h more. The reaction was quenched with water and extracted with dichloromethane. The organic phase was dried under reduced pressure. The crude was purified by a column chromatography (SiO_2, petroleum ether). A dark olive solid was isolated (yield = 46%).

Melting Point = 155°C

^{1}H-NMR (300 MHz, $CDCl_3$): 7.67 (d, J = 7.9 Hz, 4H); 7.42 (d, J = 7.9 Hz, 2H); 1.92 (m, 4H); 1.31 (m, 2H); 0.72 (d, J = 6.6 Hz, 12H); 0.49 (m, 4H) ppm.

2,2'–(9,9–diisopentyl 9H fluorene–2,7 diyl) dithiophene (4): In a Schlenk flask were insert Mg (8.14 mmol, 4.55 eq.), one crystal of iodine and 32 mL of dry THF, under Ar. While stirring the temperature was decreased at -40°C, at the mixture were added dropwise bromothiophene (8.14 mmol, 4.55 eq.) and the reaction was left at -40°C for 1h30. In the meanwhile in another Schlenk flask were introduced **3** (1.79 mmol, 1 eq.) and $Pd(dppf)Cl_2$ (0.054 mmol, 0.03 eq.). After 1h30 the solution of

the first flask were added under Ar in the second flask and the reaction was left in reflux for 48h. The reaction was quenched with ice and extract with diethyl ether. The organic phase was dried under reduced pressure. The crude was purified by a recrystallization in cyclohexane. A white solid was isolated (yield = 88%).

Melting Point = 138-139°C.

^{1}H-NMR (300 MHz, $CDCl_3$): 7.72 (d, J = 7.9 Hz, 2H), 7.65 (dd, J^1 = 1.6 Hz, J^2 = 7.9 Hz, 2H), 7.61 (d, J = 1.6 Hz, 2H), 7.42(dd, J^1 = 1.1 Hz, J^2 = 3.6 Hz, 2H) ,7.33(dd, J^1 = 1.1, J^2 = 5.1 Hz, 2H), 7.16(dd, J^1 = 3.6 Hz, J^2 = 5.1 Hz, 2H), 2.09 (m, 4H), 1.35 (m, 2H), 0.74 (d, 6.6 Hz, 12H), 0.62(m, 4H) ppm.

^{13}C-NMR ($CDCl_3$, 100 MHz): 151.63, 145.24, 140.33, 133.33, 128.12, 125.05, 124.57, 122.91, 120.136(2C), 55.07, 38.31, 32.57, 28.28, 22.42 ppm.

5–(9,9–diisopentyl–7–(thiophene–2–yl) 9H fluorene–2–yl)–thiophene–2–carbaldehyde (5): 8 mL of dichloroethane were added under Ar to **4** (1.48 mmol, 1 eq.), $POCl_3$ (2.97 mmol, 2 eq.) and distilled DMF (12 mmol, 8 eq.) at 0°C. The reaction mixture was warmed to RT and stirred for 4h, then it was heated up to reflux for 20h. The reaction was quenched with the addition of 45 mL of a saturated solution of sodium acetate. The crude was extracted with dichloromethane, and then concentrated under reduced pressure. The crude was purified by recrystallization in iPrOH. A yellow-green crystals were isolated (yield = 42%).

Melting Point = 161-162 °C.

^{1}H-NMR (400 MHz, $CDCl_3$): 9.93 (s,1H), 7.78 (d, J = 4Hz, 1H), 7.75 (d, J = 7.9Hz, 1H), 7.73 (d, J = 7.9Hz, 1H), 7.70 (dd, J^1 = 1.6 Hz, J^2 = 7.9 Hz, 1H), 7.66 (dd, J^1 = 1.6 Hz, J^2 = 7.7 Hz, 1H), 7.64 (d, J = 1.6 Hz, 1H), 7.59 (d, J = 1.6 Hz, 1H),), 7.49 (d, J = 4 Hz, 1H),7.41 (dd, J^1 = 1 Hz, J^2 = 3.6 Hz, 1H),

7.33 (dd, J^1 = 1 Hz, J^2 = 5.1 Hz, 1H), 7.16 (dd, J^1 = 3.6 Hz, J^2 = 5.1 Hz, 1H), 2.07 (m, 4H), 1.33 (m, 2H), 0.72 (d, 6.6Hz, 12H), 0.58 (m, 4H) ppm.

^{13}C-NMR (CDCl3, 50 MHz): 182.72, 155.20, 151.91, 151.88, 144.95, 142.36, 142.04, 139.70, 137.53, 134.00, 131.79, 128.16, 125.63, 125.17, 124.83, 123.84, 123.14, 120.60, 120.54, 120.36, 120.16, 55.18, 38.19, 32.57, 28.21, 22.38 ppm.

5–(7–(5–iodothiophene–2–yl)–9,9–diisopentyl 9H fluorene–2–yl)thiophene–2–carbaldehyde (6): In a round bottom flask were added 200 µL of water, 300 µL of acetic acid, 6.6 µL of sulfuric acid, **5** (0.206 mmol, 1 eq.) and periodic acid (1.44 mmol, 7 eq.) under stirring. In the meanwhile a solution of iodine (0.206 mmol, 1 eq.) in 1.1 mL of carbon tetrachloride was prepared and added dropwise to the reaction mixture. The temperature was increased to 80°C for 1h, then was cooled to RT and the reaction was kept under stirring overnight. The reaction mixture was neutralized with a saturated solution of $NaHCO_3$ and extracted with dichloromethane. The organic phase was washed with a saturated solution of $Na_2S_2O_3$ and dried under reduced pressure. Yellow-green crystals were obtained after recrystallization from iPrOH (yield = 74%).

Melting Point = 168-169 °C.

^{1}H-NMR (300 MHz, $CDCl_3$): 9.93 (s, 1H), 7.79 (d, J = 4 Hz, 1H), 7.72 (m, 3H), 7.64 (d, J = 1.5 Hz, 1H), 7.55 (dd, J^1 = 1.6 Hz, J^2 = 7.9 Hz, 1H), 7.50 (d, J = 1.6 Hz, 1H), 7.49 (d, J = 4Hz, 1H), 7.28 (d, J = 3.6 Hz, 1H), 7.08 (d, J = 3.6 Hz, 1H), 2.06 (m, 4H), 1.33 (m, 2H), 0.71 (d, J = 6.6 Hz, 12H), 0.56 (m, 4H) ppm.

^{13}C-NMR ($CDCl_3$, 75 MHz): 182.75, 155.09, 151.99, 151.96, 150.93, 142.36, 142.13, 140.18, 138.02, 137.55, 133.09, 132.00, 125.70, 124.8, 124.56, 123.93, 12.65, 120.62, 120.49, 119.99,72.34, 55.23, 38.17, 32.59, 28.22, 22.39 ppm.

5–(7–(4–(diphenylamino)phenyl)thiophene–2–yl)–9,9–diisopentyl 9H fluorene–2–yl)thiophene–2–carbaldehyde (D1‴a): 6 (0.153 mmol; 1 eq.), 4-(diphenylamino)phenylboronic acid (0.184 mmol; 1.2 eq.), K_2CO_3 (0.383 mmol; 2.5 eq.) and Pd(dppf)Cl_2 ($7.65 \cdot 10^{-3}$ mmol; 0.05 eq.) were placed in a Schlenk flask with a stirring bar. After drying with a mechanical pump, 10 mL of 1/1 mixture toluene/Methanol degased with Ar were added in the flask. The temperature was increased to 85°C and kept for 24h. After slow cooling to RT, the reaction mixture was filtered over celite and washed with dichloromethane. The filtrate was evaporate under reduced pressure. The crude was purified with chromatography column (SiO_2, dichloromethane/petroleum ether, 70/30), the dark yellow powder was recrystallized from acetone. A bright yellow microcrystalline powder was isolated (yield = 60%).

Monocrystals suitable for X-ray diffraction were obtained by slow diffusion of pentane layered over a solution of CH_2Cl_2.

Melting Point = 161-162 °C.

^{1}H-NMR (300 MHz, $CDCl_3$): 9.93 (s, 1H); 7.79 (d, J = 4 Hz, 1H); 7.74 (m, 3H) 7.64 (m, 1H); 7.60 (m, 1H); 7.54 (d, J = 8.8 Hz, 2H); 7.50 (d, J = 3.8 Hz, 1H); 7.38 (d, J = 3.8 Hz, 1H); 7.32 (m, 4H); 7.26 (d, J = 3.8 Hz, 1H); 7.18 (m, 3H); 7.15 (m, 2H); 7.12 (m, 3H); 7.06 (m, 1H); 2.08 (m, 4H); 1.34 (m, 2H); 0.73 (d, J = 6.8 Hz, 12H); 0.58 (m, 4H) ppm.

^{13}C NMR (75 MHz, $CDCl_3$): 182.71, 155.21, 151.88, 147.57, 147.45, 147.36, 143.61, 143.17, 142.38, 141.99, 139.57, 137.54, 133.98, 131.72, 129.34, 129.27, 128.29, 126.43, 126.38, 125.62, 124.69, 124.57, 124.07, 123.81, 123.62, 123.20, 123.17, 123.02, 120.57, 120.54, 120.31, 119.63, 77.23, 55.15, 38.20, 32.55, 28.21, 22.39, 22.36.

HRMS (m/z) [M]calcd for $C_{50}H_{47}N_1O_1S_2$: 741.30991, found: 741.31082

3. Crystallographic data

3.1. Dipolar chromophores

Cpd	D1'b	D1'c	D2'b	D1'''a
Space group	P 2_1/c	C 2	P 2_1/n	P 2_1/c
Cell length	a = 18.8153 (7) b = 8.7012 (3) c = 16.5157 (7)	a = 17.8098 (16) b = 7.2828 (6) c = 20.9176 (19)	a = 7.2850 (2) b = 36.5610 (3) c = 12.0100 (9)	a = 21.720 (6) b = 9.403 (3) c = 20.647 (5)
Cell angles	α = 90 β = 98.113 (2) γ = 90	α = 90 β = 96.588 (3) γ = 90	α = 90 β = 96.778 (1) γ = 90	α = 90 β = 107.007 (5) γ = 90
Cell volume	2676.82	2695.21	3176.47	4032.40
R-factor (%)	3.46	5.12	5.14	5.19
Density	1.319	1.278	1.531	1.222

3.2. Articulated dipoles

Cpd	1Bis(F)	2Bis(F)	1Tris
Space group	P 2_1/c	C 2/c	R-3
Cell length	a = 15.2311 (3) b = 11.4426 (2) c = 20.5705 (14)	a = 11.1243 (2) b = 14.9629 (3) c = 25.5681 (18)	a = 24.50 (3) b = 24.50 (3) c = 31.71 (6)
Cell angles	α = 90 β = 93.360 (7) γ = 90	α = 90 β = 97.586 (7) γ = 90	α = 90 β = 90 γ = 120
Cell volume	3578.93	4218.61	16483
R-factor (%)	/	5.52	5.14
Density	/	1.204	0.763

3.3. Red emitting quadrupoles

Cpd	QfvB$_1$
Space group	P -1
Cell length	a = 13.2049 (2) b = 15.3857 (3) c = 17.0773 (3)
Cell angles	α = 69.232 (2) β = 82.932 (1) γ = 76.355 (2)
Cell volume	3151.42
R-factor (%)	5.12
Density	1.223

BIBLIOGRAPHIC REFERENCES

(1) Sheldrick, G. M.: SHELXLT. version 6.12 ed.; Bruker Analytical X-Ray Systems, Madison, 2000.

(2) Würth, C.; Grabolle, M.; Pauli, J.; Spieles, M.; Resch-Genger, U. Relative and absolute determination of fluorescence quantum yields of transparent samples. *Nature Protocols* **2013**, *8*, 1535-1550.

(3) Resch-Genger, U.; Rurack, K. Determination of the photoluminescence quantum yield of dilute dye solutions (IUPAC Technical Report). *Pure and Applied Chemistry Pure Appl. Chem.* **2013**, *85*, 2005-2013.

(4) Brouwer, A. M. Standards for photoluminescence quantum yield measurements in solution (IUPAC Technical Report). *Pure and Applied Chemistry* **2011**, *83*, 2213-2228.

(5) Xu, C.; Webb, W. W. Measurement of two-photon excitation cross sections of molecular fluorophores with data from 690 to 1050 nm. *Journal of Optical Society of America B* **1996**, *13*.

(6) Khanasa, T.; Jantasing, N.; Morada, S.; Leesakul, N.; Tarsang, R.; Namuangruk, S.; Kaewin, T.; Jungsuttiwong, S.; Sudyoadsuk, T.; Promarak, V. Synthesis and Characterization of 2D‐D‐π‐A‐type organic dyes bearing bis (3,6‐di‐tert‐butylcarbazol‐9‐ylphenyl) aniline as donor moiety for dye‐sensitized solar cells. *European Journal of Organic Chemistry* **2013**, *2013*, 2608-2620.

(7) Genin, E.; Gao, Z.; Varela, J. A.; Daniel, J.; Bsaibess, T.; Gosse, I.; Groc, L.; Cognet, L.; Blanchard‐Desce, M. "Hyper‐bright" near‐infrared emitting fluorescent organic nanoparticles for single particle tracking. *Advanced Materials* **2014**, *26*, 2258-2261.